October 2019

DIETARY OLIGOSACCHARIDES ARE DIFFERENTIALLY METABOLIZED BY COMMENSAL MICROBIOTA WITHIN IN VITRO MODEL SYSTEMS

Ezgi Özcan

DIETARY OLIGOSACCHARIDES ARE DIFFERENTIALLY METABOLIZED BY COMMENSAL MICROBIOTA WITHIN *IN VITRO* MODEL SYSTEMS

A Dissertation Presented

by

EZGI ÖZCAN

Submitted to the Graduate School of the

University of Massachusetts Amherst in partial fulfillment

of the requirements for the degree of

DOCTOR OF PHILOSOPHY

September 2019

Department of Food Science

DIETARY OLIGOSACCHARIDES ARE DIFFERENTIALLY METABOLIZED BY COMMENSAL MICROBIOTA WITHIN *IN VITRO* MODEL SYSTEMS

A Dissertation Presented

by

Ezgi Özcan

Approved as to style and content by:

_____
David A. Sela, Chair

_____
Matthew D. Moore, Member

_____
Carrie-Ellen Briere, Member

_____
Eric A. Decker, Department Head
Department of Food Science

ACKNOWLEDGMENTS

First and foremost, I would like to express my sincere gratitude to my advisor, Dr. David A. Sela, for his guidance, encouragement, motivation and continuous support throughout not just my research but also my career. I appreciate his advice with immerse knowledge on both experiment and writing phase of my dissertation. It is my great honor to work in Sela Lab with great colleagues.

My sincere thanks also go to my committee members, Dr. Matthew Moore and Dr. Carrie-Ellen Briere to devote their time and effort for my dissertation with their insightful guidance and support. Moreover, I am very grateful for the financial support by Ocean Spray Inc, during my graduate study.

I would like to give many thanks to all my previous and present lab mates, especially Dr. Asha Rani, Xiaomeng You, Korin Albert, Yang Lyu, Liv Dedon, Shuqi Li, Margaret Hilliard, Michelle Rozycki, Timothy Yeung, Anna Kundman, Giovanna Camacho, Elif Üçok for their precious friendship, support and encouragement. It is great pleasure to work with them and learn from them. Many thanks to Cindy Kane for her technical assistance and help provided to me and other lab members. Furthermore, I will always appreciate the support of all of Food Science faculty, staffs and students, especially Fran Kostek, Deby Lee, David Prodanas, Stacy Apostolou and Mary Bell.

I would like to thank to my dear friends, Antonia Carcelen, Bilgesu Sümer, Benjamin Nolan, Sarah Tanzi, Claudia Morales, Jyoti Iyer, Swati Birla, Helin Unal, Leslie Edwards Davis, Begüm Topçuoğlu, Susanne Westerhoff-Uprety, Candice Travis, Katty Alhayek, Basileus Zeno, Eric Sippert, Tyler Novaichick, Zeyno Ustun, Omid Shekari, Candan Turkkan, Canan Cevik, Trisha Zintel and Gizem Özan for their precious friendship,

motivation, physical and emotional support, intellectual scholarship and international solidarity.

Last but not least, I would like to express my gratitude to my lovely family, especially my parents Gülten Özcan and Meriç Özcan, my sister Özgen Özcan Tarıkcı, my aunts Sevil Can and Selma Türkmenoğlu, my brother-in-laws Hasan Can, Levent Tarıkcı, my cousins Gizem and Sinem Türkmenoğlu and my niece Duru Tarıkcı for their strong backing, patience and unconditional love. Thanks to all the people who have helped and loved me and all the women who inspired me in my life.

ABSTRACT

DIETARY OLIGOSACCHARIDES ARE DIFFERENTIALLY METABOLIZED BY COMMENSAL MICROBIOTA WITHIN *IN VITRO* MODEL SYSTEMS

SEPTEMBER 2019

EZGI ÖZCAN

B.S., MIDDLE EAST TECHNICAL UNIVERSITY, TURKEY

M.S., YEDITEPE UNIVERSITY, TURKEY

Ph.D., UNIVERSITY OF MASSACHUSETTS, AMHERST, MA

Directed by: Professor David A. Sela

Our diet contains indigestible carbohydrates that are available for microbial metabolism within the gastrointestinal tract. These carbohydrate sources are oligosaccharides found in plants and human milk. Oligosaccharide utilization phenotypes are often consistent with the ecological niche that microbes occupy (e.g. adult gut, infant gut, plants). This study represents an in-depth metabolic analysis for utilization of human milk oligosaccharides (HMOs) including lacto-N-tetraose (LNT) and lacto-N-neotetraose (LNnT), and cranberry oligosaccharides (i.e. xyloglucans) within *in vitro* modeled systems. These model systems include microplate systems for pure cultures as well as an adapted bioreactor system to mimic microbial interactions within the gut.

Infant-colonizing *Bifidobacterium longum* subsp. *infantis* (*B. infantis*) metabolized both LNT and LNnT that vary by a single glycosidic linkage with inefficient metabolism

resulting in increased formate production. The utilization of LNT and LNnT varied by strain. The strain-variant metabolism was also observed during pooled HMO utilization.

The differential HMO metabolism of *B. infantis* is of interest in terms of microbe-microbe interactions within in the infant gut. A modeled microbe-microbe interaction was conducted by supplementing *B. infantis* to the infant fecal derived modeled microbiomes. Depending on the microbial composition to be used for modeled microbiomes, LNT and LNnT metabolism differed. Moreover, *B. infantis* addition to the modeled microbiomes shifted complex microbial metabolism during LNnT towards formate production and transformed microbial structure towards *Clostridium* spp. as well as butyrate producers.

Plant-based foods also contain bioactive compounds that are impervious to host digestion but modulate the gut microbiome. Xyloglucans are oligosaccharides found in plant cell walls in cranberries. The phylogenetic near-neighbor *B. longum* subsp. *longum* (*B. longum*), isolated from the infant gut, was capable of utilizing xyloglucans, resulting in formate production. Probiotic *Lactobacillus plantarum* also utilized cranberry xyloglucans to a greater extent than bifidobacterial strains. Interestingly, crude cranberry extracts that contain additional molecules stimulated bacterial growth. Thus, we hypothesized that secondary products, e.g. polyphenols from cranberries, with oligosaccharides might synergistically impact on *L. plantarum* physiology. This strain deployed differential metabolic response to proanthocyanidins (PACs) from cranberries depending on the carbohydrate source. In summary, this study characterizes the structure-function relationships between dietary oligosaccharides and bifidobacteria, lactobacilli, and within the microbiome.

TABLE OF CONTENTS

Page

LIST OF TABLES

LIST OF FIGURES

CHAPTER 1

IN VITRO MODELS OF HOST-MICROBIAL INTERACTIONS WITHIN THE GASTROINTESTINAL TRACT

Ezgi Özcan[1], Rachel Levantovsky[1,2], and David A. Sela[1,3]

[1]Department of Food Science, University of Massachusetts, USA

[2]Commonwealth Honors College, University of Massachusetts, USA

[3]Department of Microbiology & Physiological Systems and Center for Microbiome Research, University of Massachusetts Medical School, Worcester, MA.

1.1 The human gastrointestinal tract

The human gastrointestinal tract (GIT) refers to the anatomical features and organs that are linked sequentially and participate in the digestion and absorption of nutrients and water. The adult GIT is approximately 1.5 m in length and supports a volume of 500 mL, and often contains 200 g of solid content [1]. Beginning with the oral cavity and esophagus, the GIT progresses through the stomach and into the small and large intestine, ending at the rectum. The term "gut" is often used colloquially to describe the entire GIT, and particularly the colon proper. Food moves through the colon more slowly compared to the upper GIT, which is aided by peristaltic movements [1]. Colonic digesta consists of exogenous dietary molecules in addition to microbial cells which are estimated to contribute to 50% of the total mass [1]. Therefore, microbial metabolic processes that occur within the gut contribute to host homeostasis in a significant fashion. On the average, the

nutrient content that reaches the colon from the small intestine is about 20-60 g/day carbohydrates (i.e. polysaccharides) and 5-20 g protein [2].

The human colon is segregated into three primary anatomical sites, termed the proximal, transverse, and distal colon. In the proximal region, saccharolytic fermentation proceeds due to high concentrations of non-digestible carbohydrates that colonizing microbiota utilize. As a result, short chain fatty acids (SCFA) are secreted by microbes which decreases the local pH to 5-6 and promotes rapid bacterial growth [3]. As the digesta transits to the transverse colon, fermentable carbohydrates decrease to coincide with less microbial acid production to promote an environment that approaches neutral pH [4]. In the distal colon, microbial proteolysis rapidly results in the production of ammonia, amines, phenols, thiols, and indoles in addition to other metabolites including SCFAs [5, 6]. As available substrates change across the length of the colon, the microbial communities and their inherent metabolic function are somewhat distinct in these environments [5, 7].

The human gut is colonized by bacteria and archaea in quantities of up to 10^{12} cells per gram [2, 3, 8]. The development or microbial succession within the mammalian gut shares an evolutionary relationship with milk and soluble factors delivered within [9]. In newborn infants that are breastfed, bifidobacterial populations often dominate the microbiome due their ability to utilize human milk oligosaccharides [10–12]. Post-weaning, gut microbial community diversity is influenced by their host's nutrition and genotype [8, 13–15]. This is in addition to environmental factors such as antibiotic and other exposures. The impact of diet on guiding the microbial community has been studied in comparing children from Europe and Burkina Faso [16] as well as other human and animal studies [17–22].

The human gut may host up to 1200 microbial species within the microbiome [23, 24], with several bacterial phyla that are consistently represented including Actinobacteria, Firmicutes, Bacteroidetes, Proteobacteria, Fusobacteria, and Verrucomicrobia. Of these, Bacteroidetes and Firmicutes are typically dominant and comprise up to 90% of the GIT microbiota [25–28]. The diversity within microbial communities is influenced by host diet and genotype among other host-microbial interactions and microbe-microbe interactions [19, 25, 29]. Microbial species that colonize the mature human gut are facultative anaerobes or strict anaerobes [30]. In addition to maintaining an anaerobic environment, studying GIT microbial ecosystems often requires culture-dependent approaches.

Accordingly, some bacteria require complex cultivation requirements that are not well understood or are impossible to recapitulate in the laboratory. For example, some bacteria require the metabolic activities of heterologous species or hosts to provide essential molecules [31]. Since culturing-based approaches require optimal viability within the growth media of choice, it often underestimates bacterial diversity or biases the representation. This is often referred to as the "great plate count anomaly"[32]. In response, culture-independent approaches are often deployed to determine the phylogenetic diversity present in the gut from fecal community extracts [28, 33–35]. This includes massively parallel sequencing of the small subunit ribosomal RNA (16s) gene to enable the identification of uncultivable species. Accordingly, the community composition could be characterized in previously unprecedented resolution [36, 37]. Shotgun metagenomics of total community DNA allows the classification of the genetic functional capacity of the microbiome. This is coupled with other system-level approaches such as metatranscriptomics to infer the gene expression profile of the community, as well as

metabolomics to characterize metabolite production within the gut [38–41]. These methods have been used in large consortium-level collaborations such as the European Metagenomics of Human Intestinal Tract (MetaHIT) and the US Human Microbiome Project (HMP) [42–44]. Regardless of taxonomic diversity within one's microbiome, the core functions of their community remains similar in healthy subjects [27, 41]. This functional redundancy is a consistent theme that has emerged in the study of the human microbiome.

The gut microbiota extract energy and nutritive molecules from dietary components that are otherwise impervious to host digestion. This leads to the production of metabolites such as SCFAs, vitamins and amino acids to be utilized in host metabolism. Microbial metabolic activity is influenced by both endogenous factors (e.g. secreted mucins, bile, enzymes, immune cells) and exogenous factors (e.g. diet, xenobiotics, environmental exposures). Specific carbohydrates that are encountered by the gut microbiota include resistant starch, non-starch polysaccharides, milk oligosaccharides, plant cell wall oligosaccharides, non-digestible oligosaccharides (fructo-oligosaccharides (FOS), galactooligosaccharides (GOS) and inulin) [45–54]. In addition to carbohydrates, proteins and peptides released during digestion could also interact with microbial communities established along the length of the GIT [55–57]. Phenolic-based compounds participate in reciprocal interactions with the microbiota, as they are transformed by the community metabolism [58]. The interactions of phenolics with the gut microbiota may dictate the function of these dietary molecules as well as their bioavailability. Often these phenolic compounds are transformed *in vivo* and may modulate the gut microbiota to promote health benefits for the host [59–64]. Several studies have been performed to elucidate the complex

interactions between dietary polyphenolics and gut microbiota [65–69]. In order to utilize these dietary molecules, microbes have evolved an assortment of enzyme systems to degrade molecules both extracellularly and within intracellular compartments following transport [70–73].

Microbial metabolism in the gut is not restricted to linear pathways, or bound by the cellular envelope. Microbes compete for substrates, with metabolites secreted by one member often utilized by a secondary taxon [74]. Syntrophic metabolism is extended towards interactions with their host. Among other activities, microbial SCFAs (i.e. acetate, propionate, butyrate, formate) provide an energy source for specific host tissues including butyrate utilization by gut enterocytes [75, 76]. In addition, SCFAs interact with the immune cells that further regulates the microbiome [77, 78]. Along these lines, dietary phenolic derivatives may have local or systemic anti-inflammatory activity in the host [79–81]. Moreover, proteolytic catabolism may lead to the formation of toxic compounds such as ammonia and amines, both of which have been linked to colon cancer [82].

Since the gut microbiome is composed of both commensal and potentially opportunistic pathogens, analysis of microbial ecosystems in aggregate is required to test scientific hypotheses to ultimately be applied in maintaining a healthy gut state. Thus *in vitro* systems to model complex community interactions have been innovated to study associated scientific questions.

1.2 The current state of *in vitro* model systems to model gut ecosystems

In vitro systems enable the investigation of microbial communities and their respective functions by modeling microbial ecology and the interface with host physiology. This could include single or multiple bioreactors that are seeded by fecal inocula or defined

communities (e.g. 8 bacterial species) [3]. Parameters are manipulated to reflect GIT physiology and include temperature, pH, oxygen tension, and substrates introduced to the system at defined intervals and flow rates. These systems vary by experimental approach and differ by inoculation, transit/resident time, and the specific bioreactors.

In vitro models are preferred in many instances, as *in vivo* studies are expensive and require special facilities to maintain animals or interact with human subjects in an ethical manner. For the latter, access to the internal anatomy of human subjects is prohibitively restricted, thus most studies focus on analyzing fecal excreta [3]. This is a limitation for investigations of other GIT sites beyond the distal colon. Moreover, nutritional interventions require a controlled diet over extended time intervals, and sufficient participants who must comply with inconvenient study parameters. In contrast, *in vitro* studies are not restricted by similar ethical constraints, are often cost effective, and enable mechanistic studies. A strong argument for their use is to allow pre-clinical hypothesis testing prior to *in vivo* trials with human and animal subjects.

Other advantages for *in vitro* models include facile sampling across time with strict control of variables. Some models allow parallel experiments to account for inter-community variation while measuring several outcomes simultaneously. The accumulation of microbial metabolites allows for cross-sectional and time course studies and access to molecular markers that would otherwise be rapidly sequestered *in vivo*.

There are, however, limitations to *in vitro* experimental systems in comparison to *in vivo* approaches. Fecal inocula does not fully model the spatial complexity of microbial ecosystems along the GIT [83]. Moreover, reproducibility and stability is a challenge to

establishing an informative *in vitro* model. The priority lies in managing the inoculation and colonization efficiency of fecal microbiota, both qualitatively and quantitatively.

The reproducibility and stability of modeled microbiomes has been evaluated using various approaches [83–92]. The HITChip microarray analysis and next-generation sequencing (NGS) has been employed to test the stability of *in vitro* microbiomes [83, 89]. These approaches enable characterization of microbial succession with great precision. As sequencing technologies improve, taxonomic discrimination is enhanced with NGS approaches rapidly ascending to the tool of choice [83].

Experimental reproducibility is a concern often cited with these approaches. There is evidence that the initial fecal inocula must be fresh to reduce errors in composition due to freeze-induced bias [93]. Another approach is to pool fecal specimens from multiple donors to approximate a stable microbial community, albeit theoretical or otherwise ideal [83]. This approach may inadvertently lead to artifacts resulting from inter-microbial interactions that do not occur *in vivo* [3]. Inoculation with recently acquired of fecal samples is generally preferred for batch culture systems used in short-term studies [94].

1.3 Batch culture systems to model the gut microbial consortium

Batch culture typically involves small reactor vessels (i.e. 70-1000 ml) inoculated with either axenic cultures or a mixed community that is allowed to grow in a medium for a short period of time (e.g. 72 hours) with regular sampling [3, 94]. These are either closed or fed-batch bioreactor systems that are maintained under anaerobic conditions by sparging with oxygen-free gas (usually nitrogen). Closed systems are used to model a single component of the human gut, such as the distal colon but other sites have been developed as well [3, 94]. A common use of batch models is to measure the response to a given

treatment or perturbation to dominant populations maintained within the simple system [3, 94, 95]. Although this may not represent the full functional potential of the community it permits investigation of simplified mechanistic relationships. In general, batch systems are seeded with fecal inocula perform well for initial characterizations of inter-individual variation in community metabolism [96]. These systems are tractable for many research groups, cost-effective, and operate well when large amounts of substrates and seed microorganisms are available [3, 94]. Batch models are typically stirred continuously to promote homogeneity, sparged with nitrogen to reduce oxygen tension, with pH and temperature controlled throughout the experimental cycle.

Batch culture systems to represent the GIT are made up small volume of reactor vessels in order to represent the typical volumetric space of GIT. It also points out a scientific shift from commonly used fermentation experiments to *in vitro* gut model systems. Additionally, it is important to validate the usage of model systems.

Batch culture systems have been developed to investigate carbohydrate catabolism and the interactions of modeled GIT communities with other exogenous factors [97, 98]. This includes both prebiotics and probiotics that are believed to influence host physiology by influencing endogenous microbiota [99–103]. In 1992, Macfarlane and colleagues investigated the fermentation within different regions of the GIT using contents harvested from sudden death victims [5]. *In vitro* fermentations were conducted in 70 ml capacity serum bottles gassed with argon and incubated at 37°C anaerobically in an orbital shaker using 10 % (w/v) fecal slurries. Interestingly, the secretion of fermentative end products correlated with variations in the donors. Although in general, SCFAs, lactate, and ethanol concentrations were higher in the ascending colon whereas protein fermentation products

such as ammonia and phenolic compounds increased in the descending colon. In 1993, Wang and Gibson [104] investigated oligofructose and inulin utilization in an *in vitro* fermentation by *Bifidobacterium* and *Clostridium* spp. in a 280 ml volume fermentation vessels which were run for 48 h at 37°C and pH of 7.0. They were sparged with oxygen-free nitrogen and continuously stirred using 5% fecal slurries collected from 6 individuals. These were prepared freshly by homogenizing in anaerobic phosphate buffer. Thus it was determined that oligofructose and inulin are utilized by intestinal commensals as SCFA coincides with the increase in specific beneficial populations and reduces *Escherichia coli* and *Clostridium perfringens*. This Gibson model has been replicated in several additional studies to be discussed in subsequent sections.

Phenolic biotransformation within the human gut has been modeled in batch culture systems. Microbial metabolism of anthocyanins and quercetin were conducted either in head-space bottles or large-scale fermenters under controlled temperature, pH, and oxygen concentration [105, 106]. In 2008, Tzounis and colleagues [107] developed a batch culture model similar to the Gibson system with 300 mL vessels under expected conditions within the gut. Afterward, this model was used in several studies of flavanol and anthocyanin metabolism transformed by colonic microbiota and assessed by metabolite and microbial profiling using liquid chromatography (HPLC) and fluorescent in situ hybridization (FISH), respectively [108–110]. Flavanol and anthocyanin phenolics are degraded by gut microbiota, with products increasing the populations of *Bifidobacterium* and *Eubacterium* reflecting the potential enriching activity of precursor phenolics. Several static batch colonic fermentation models were developed to investigate flavonol and phenolic acid degradative pathways [96, 111–113].

Two batch systems were prepared with phosphate-buffered saline (PBS, oligotrophic) and basal culture medium (BCM, eutrophic) and seeded with fecal inoculum to characterize the response of the modeled community to a prebiotic formulation of GOS and guar gum [114]. As a result, significant shifts within specific populations receiving treatment were observed in the pyrosequencing community analysis.

Despite frequent use of batch culture fermentation systems, models have limitations related to over-simplification of the ecosystem being modeled in the absence of the host physiology. Moreover, accumulation of toxic compounds and substrate diminishment may restrict microbial activity as the system will not achieve steady-state equilibrium [115]. A simple *in vitro* batch culture fermentation study conducted in multiple labs illustrates limitations of the batch culture systems [99]. Accordingly, dietary fiber was fermented within several laboratories with outcomes varying in terms of the rate of substrate degradation as well as the amount of SCFAs produced. It was concluded that the most significant potential source of variation is the fecal inoculum in *in vitro* models. Thus batch systems are typically appropriate for short-term resident times with continuous, semi-continuous, and dynamic model systems used in more complex models.

1.4 Continuous systems to model the human GIT

Continuous model systems contain multiple chemostats used in long-term studies with constant provision of substrates and removal of toxic compounds under defined parameters. In general, optimal conditions for microbial growth may be achieved at steady-state conditions unless experimental goals dictate otherwise. Chemostat conditions reflect distinct parts of the human GIT and often consist of the proximal, transverse, and distal colon [3]. Environmental conditions are simulated including substrate retention time and

may involve modeling peristaltic movements. Continuous model systems are appropriate for studies that require longer response measurements to a given treatment or perturbation. Important considerations in designing these experimental schemes include maintaining physiological concentrations of metabolites and relative concentrations of microbial populations to reflect fermentation rates of substrates and interactions between microbes [86]. Often *in vitro* models are constrained by maintaining stable communities of microbes to model *in vivo* states. Stabilization requires a period of adaptation to the simulated environment that involves microbial interactions within this unique environment. This is often not considered in batch culture models due to shorter resident times. However, in continuous models the adaptation period must be addressed. The validation of the stability of these systems was tested using culture-independent techniques [87, 89].

An early semi-continuous system was developed by Miller and Wolin in a glass vessel to maintain 500 ml of stirred anaerobic culture over 81 days [116]. Fermentation was initiated with 156 g of freshly collected feces diluted in 200 ml of solution containing sodium bicarbonate, urea, hemin, casein and a vitamin mixture. The microbial community was left to stabilize for 18 days before a suspension of dietary material was added derived from various fruits and vegetables. Sodium deoxycholate represented bile salts and mixed with nutrient suspensions to be pumped into the fermentation vessels once or twice daily. In the same year, Veillux and Rowland developed a 2 stage continuous reactor to simulate the distal part of the rat intestine [117]. Two-stage cultures were connected in series with sterile media added to the first stage. The continuous system was run in a volume of 600 ml in an agitated, temperature, and pH-controled fermenter and continuously flushed at a rate of 0.5 l/min. The medium reservoir was held under anaerobic conditions and agitated

to ensure a homogenous distribution of the components and pumped continuously. Fecal suspensions were homogenized shortly after acquisition and allowed to stabilize for 12 h before culture medium addition. These model systems were developed based on a number of assumptions. The first is that most microbial growth and metabolism occurs immediately after ileal fluid entry into the colon and prior to water removal that concentrates substrates. Another assumption is the use of fecal communities is representative of the colonic microbial community. Furthermore, the high concentration of insoluble carbohydrates in dietary substrates in the study is predicted to evade digestion in the stomach and small intestine. These assumptions are necessary in order to simplify the system in these *in vitro* systems. Regardless, the metabolite and microbiological profile was found to be consistent between the model and *in vivo* systems.

A three stage continuous system was developed by the Gibson group to investigate the influence of mucin on sulfate reduction and methanogenesis by mixed populations of human gut microbiota [118]. This three-stage continuous culture system was inoculated with 20 % (w/v) of feces in an anaerobic sodium buffer and maintained under controlled conditions for 120 days. A mixture of polysaccharides and proteins were added as carbon and nitrogen sources respectively. The vessels operating volumes (0.3, 0.5, and 0.8 liter) and pH (6.0, 6.5 and 7.0) reflected the physiological characteristics of the colon. Porcine gastric mucin was added to the first vessel after 48 days, with microbial degradation allowed to proceed for 22 days until the mucin was replaced by distilled water. As a result, the mucin was extensively hydrolyzed which stimulated volatile fatty acid production. Mucin participated in sulfate-reduction, however methanogenesis was the major route for the disposal of electrons in the absence of mucin. Of primary interest, this study modeled

competition between sulfate-reducers bacteria and methanogens over a limited nutrient source.

In another approach, a three-stage continuous system was developed to test the effects of retention time of various organic carbon and nitrogen sources on the community ecology and metabolism of gut microbes [7]. This system consisted of three vessels simulating the ascending, transverse, and distal colon by judiciously dictating pH, temperature, operating volumes, and retention time. Since fecal extracts do not reflect the community structure in the proximal colon, the researchers used content harvested from four sudden death victims. Operating volumes of the three vessels were set as 0.22, 0.32 and 0.32 L and pH was maintained at 5.5, 6.2, and 6.8 under automated control. The environmental conditions sought to recapitulate the spatial, temporal, nutritional, and physicochemical characteristics encountered by gut microbiota. The first vessel (V1) was fed with culture media containing polysaccharides, proteins, vitamins, and salts under anaerobic conditions. The three stages were continuously linked, and the vessels were inoculated with 100 ml of 20% (w/v) fecal slurry. The system was equilibrated overnight and allowed to achieve steady state after at least 336 h assessed by monitoring SCFA production. The retention time for each vessel was determined as the reciprocal of dilution rate and evaluated by comparing the chemical and biological characteristics of the fecal suspensions from donors.

Further advances to the development of the 3 stage *in vitro* model were made to investigate fermentation of dextran, oligodextran, and maltodextrin by human gut microbiota [4]. In this approach, a cascade of three fermenters inoculated with 10 % (w/v) freshly collected and homogenized fecal slurry were linked in series, with operating

volumes of 250, 250 and 300 ml, and pH values of 5.5, 6.2 and 7.1 under continuous stirring and anaerobic conditions. Vessel 1 simulated the acidic conditions and rapid bacterial growth in response to high substrate availability that are experienced in the proximal colon. In contrast, vessel 3 was maintained at a neutral pH and with limited substrates to model conditions in the distal colon. In total the retention time was 60 hours which was selected according to previous three stage continuous models validated for retention time [7]. Oligodextran IV was shown to enrich for bifidobacteria and lactobacilli with steady-state populations achieving higher densities in all three vessels. However, substrate utilization varied among the three stages of the colonic model. Whereas dextran is a suitable growth substrate for bifidobacteria and lactobacilli in the proximal colon (Vessel 1), maltodextrin was used as the carbohydrate source for both bacterial groups in Vessel 3. Recently, a similar system was used to model the effects of the antibiotic rifaximin on the colonic microbiota of patients with Crohn's disease [119]. Interestingly, rifaximin promoted the relative abundance of *Bifidobacterium*, *Atopobium*, and *Faecalibacterium prausnitzi* that was confirmed using fluorescent *in situ* hybridization (FISH), quantitative PCR, and other culture-independent methods. The coinciding shift in microbial metabolism was observed with ^{1}H-NMR and solid phase microextraction coupled with gas chromatography/mass spectrometry. Accordingly, SCFAs, propanol, decanol, nonanone, and aromatic organic compounds were increased, and ethanol, methanol and glutamate were decreased. In addition, wheat dextrin soluble fiber influenced the composition and metabolic activity of the gut microbiota in this model as measured by 16S rRNA-based FISH and gas chromatography [120]. Wheat dextrin fermentation significantly increased production of acetate (vessels 2 and 3) and propionate (vessel 3), coinciding with a significant increase

in key butyrate-producing bacteria assigned to clostridial cluster XIVa and the genus *Roseburia*.

Another three stage continuous model was developed and termed GIS2 (gastrointestinal simulation) to study the effects of a probiotic product (i.e. PROEXO) on the modeled infant gut microbiota [121]. This three-stage system consists of three Duran bottles (1,000 ml capacity) and maintained at pH values of 5.5, 6.2 and 6.3. Culture media and the substrate which functions as both a probiotic and prebiotic were introduced to the first vessel to be pumped to vessel 2 and 3. The model was seeded by fecal samples obtained from healthy infants of 6 months and stabilized after an initial period of 10 days assessed by culture-dependent quantification. In this system, polysaccharides present in the tested product enriched the lactic acid bacteria in the modeled ascending colon.

A four stage, semi-continuous colonic model system (i.e. EnteroMix human colon simulator) was developed to model the effects of lactose on the growth and fermentation dynamics of colonic microbiota [122]. This system contains four glass vessels connected in sequence, with conditions adjusted to represent each compartment of the human colon under anaerobic conditions. pH values were maintained at 5.5, 6.0, 6.5 and 7.0 from the ascending colon towards the distal colon. The system was run in parallel with six treatment and three baseline simulations using the same fecal inoculum preconditioned at 37°C for 24 h, anaerobically. The microbial density was adjusted from vessel 1 to vessel 4. Lactose was initially dissolved in sterile simulator medium, which mimics the contents of the human ileum and was semi continuously fed to the first vessel. Microbial populations and metabolite (SCFA) profiling were monitored by flow cytometry and HPLC. In a subsequent study, the effects of polydextrose and xylitol were investigated in the

EnteroMix four-stage colon model [123]. While polydextrose degradation leads to higher concentrations of all SCFA, especially acetate and propionate, xylitol degradation increased the concentration of butyrate in the medium. This was attributed to population shifts of *Bifidobacterium* and *Lactobacillus*. In addition, this model was used to study the effects of xylo-oligosaccharides on bifidobacteria in the human colon [124]. Interestingly, xylo-oligosaccharides were preferred by *Bifidobacterium lactis* strains and lactitol by lactobacilli in this four stage *in vitro* model, whereas galacto-oligosaccharides, fructo-oligosaccharides and gentiobiose were preferred by a larger group of microbes.

Molly and colleagues developed a novel model that was termed the simulated human intestinal microbial system (SHIME) [125]. This is a five-stage bioreactor system consisting of a large intestine phase that encompasses three bioreactors, and is fed by a small intestine reactor 1 and 2 (duodenum/jejunum and ileum) simulated by a two-step fill and draw system. This system was based on the presence of indicator bacterial groups, volatile fatty acids, enzymatic activities (e.g. α- galactosidase β-galactosidase, α-glucosidase, β-glucosidase, β -xylosidase), and headspace gases. The first substrates tested in the SHIME system included dietary carbohydrates such as arabinogalactan, xylan, pectin, dextrin and starch. In addition, SHIME has been deployed to model microbial activity in the GIT in separate operations [126]. Each reactor vessel was designed with eight ports for medium transfer, sampling of the liquid phase and headspace gases, pH-electrode, pH-control (acid and base) and for flushing of the headspace. Pumps were used to transfer the reactor contents between the successive vessels. Media containing polysaccharides were introduced to the first vessel semi-continuously (3 times a day) and two hours after first feeding, pancreatic juice supplemented with bile (pancreas acetone

powder dissolved in NaHCO) was added to reactor vessel 1 to simulate the conditions in dueodenum/jejunum. In order to model the GIT, stool specimens (10 % w/v) from eight healthy individuals were fed into reactor vessels 3-4-5 (caecum and ascending colon, transverse colon, descending colon) [126]. Validation of the SHIME system was performed by analyzing a number of microbial activities, degradation of four polysaccharides and direct enumeration of bacteria by plate count [125, 126]. A validation of a model system is generally performed on the available data in literature by comparing the outcomes with *in vivo* clinical trials. Additionally, validation also requires the reproducibility, stability and consistency within the same system. Not much sufficient information is available in literature for every model system validation that is used *in vitro* experiments. From scientific perspective, it was assumed that the validation of a system had done before the related outcomes for the treatment were established.

SHIME has been employed in several applications since its initial development. In 1999, Alander and colleagues tested six stages of SHIME for screening and selection of five probiotic strains (*Lactobacillus plantarum*, two strains of *Lactobacillus paracasei* subsp. *paracasei*, *Lactobacillus rhamnosus* and *Bifidobacterium* sp.) [127]. In this study, they developed a SHIME reactor consisting of five closed vessels in series to which a sixth reactor was added (simulating the stomach). Stabilization of probiotic strains required a 7-day pre-treatment period, followed by a 7-day inoculation period during which the supplement was added daily. A 2-week post-treatment washout period was included. The impact of the strains on the composition of modeled gut microbiota and its metabolic activities (production of lactic acid and SCFA) were measured by plate count enumeration and gas chromatography coupled with flame ionization detector. Accordingly, lactic acid

increased in the SHIME probiotics were added as well as the relative increase in lactobacilli and bifidobacteria. Interestingly, SCFA profile remained somewhat static. Members of the enterobacteriaceae and clostridia decreased markedly during the intervention, while enterococci tended to increase post-treatment. This suggests that the positive effects attributed to probiotic treatment are reversible.

The effects of a synbiotic mixture of *Lactobacillus acidophilus* and fructo-oligosaccharides (FOS) were also tested in a six stage version of SHIME [128]. Alterations to the microbial community structure and their metabolic activity were monitored by culture-dependent methods and assayed for β-galactosidase and β-glucuronidase activity. These experimental conditions were similar to those performed by Alander and colleagues including pretreatment (10 days), treatment (addition of probiotic strains and FOS; 17 days) and post-treatment (10 days) [127]. To avoid the deleterious effects of stomach acid on the integrity of the synbiotics, the treatment feeding started from the second set of vessels. The addition of the synbiotic product increased the bifidobacterial population and production of butyric and propionic acid.

A synbiotic mixture of *Lactobacillus* GG and fermented oat bran was introduced to a modeled gut microbiome in a six-stage SHIME system [129]. This system diverges from the canonical SHIME model [128] as the model stomach and small intestine vessels were fed semi-continuously. Accordingly, pre-feeding occurred for 8-10 days, feeding totaled 12 days, and post-feeding lasted for 19 days. Lactic acid bacteria, bifidobacteria, enterobacteria and clostridia were enumerated by culture-dependent methods. It was concluded that *Lactobacillus* GG may colonize in the human gut for several weeks with the fermented oat bran enriching bifidobacteria and the production of several desirable

metabolites. However, one limitation of the SHIME model is that lack of absorption led to an overestimation of digesta constituents that reached the colon [128, 129].

Possemiers and colleagues [87] employed 5-stage SHIME (stomach, small intestine, and three colonic phases) to produce a stable bacterial community for 27 days. The microbiome members were quantified by enumeration of total aerobes and anaerobes, total coliforms, and other targeted groups by culture-dependent methods and PCR-DGGE. SCFAs and ammonium in the reaction vessels were monitored by gas chromatography coupled with flame ionization and as a released of ammonia to determine the metabolic activity of the microbial community. Microbiome stability was achieved after two weeks, while metabolic activity required three weeks to achieve stead-state.

In another application of the five-stage SHIME system, the prebiotic potential of inulin that varied by degrees of polymerization was evaluated [90, 130]. Moreover, the SHIME system was used to screen for prebiotic sources from soy germ and to model potential alterations in the microbial ecology of the human colon [131, 132]. In 2009, the prebiotic potential of arabinoxylan oligosaccharides and inulin was evaluated in a TWIN-SHIME system which is two systems run in parallel to compare treatments simultaneously [133]. This enables real time inline monitoring of oligosaccharide hydrolysis and the production of marker metabolites in parallel. Microbial colonization was developed in TWIN-SHIME that was simultaneously inoculated with the same human fecal seed. The microbial diversity was assessed with a high-resolution phylogenetic microarray: the human intestinal tract chip (HITChip) [134]. This model was found to be reproducible in SHIME units and resulted in highly diverse microbial communities that were colon region specific, with the proximal regions harboring saccharolytic microbes (e.g., *Bacteroides*

spp. and *Eubacterium* spp.) and the distal regions harboring mucin-degrading microbes (e.g., *Akkermansia* spp.). Subsequently, the TWIN-SHIME system was used to evaluate the microbial metabolism of red wine and black tea extracts [65].

In another effort to model an interaction between food constituents and gut microbiota, the TWIN-SHIME system was used in conjunction with key dietary polyphenols [135]. Ingestion of polyphenols might influence health through absorption, as well as interactions with resident gut microbiota. Accordingly, black tea and a red wine grape extract (RWGE), both contain complex dietary polyphenols and influence the microbiome structure and function. This was measured by both culture-independent and –dependent methods and gas chromatography. Pyrosequencing of community phylogenetic markers indicated that the Firmicutes:Bacteroidetes ratio was altered in the presence of polyphenolic extracts. Moreover, black tea stimulated *Klebsiella*, enterococci and *Akkermansia* and reduced bifidobacteria, *B. coccoides*, *Anaeroglobus* and *Victivallis*. Likewise, RWGE promoted growth of *Klebsiella, Alistipes, Cloacibacillus, Victivallis* and *Akkermansia* while bifidobacteria, *B. coccoides, Anaeroglobus, Subdoligranulum* and *Bacteroides* were decreased. In addition, the effects of cranberry and grape seed polyphenols were tested on a similarly modeled microbial community in SHIME [136]. Finally, a single strain of *Lactobacillus plantarum* IFPL935 was evaluated for their ability to metabolize a polyphenolic red wine extract by monitoring phenolic derivatives using UPLC–ESI-MS/MS and community changes using qRT-PCR [137].

Currently, next-generation sequencing (NGS) beyond pyrosequencing is commonly used to determine to measure phylogenetic diversity of modeled gut microbiota. These techniques have been particularly valuable in prebiotic studies [138]. As an example,

fructo-oligosaccharides and inulin were introduced to a model community in SHIME and the microbial communities assessed by Illumina sequencing [139].

In addition to simulations of the GIT, a multi-compartmental dynamic computer-controlled system for the stomach and small intestine (TIM-1, TNO intestinal model) was developed [140]. A similar system to simulate the large intestine with peristaltic mixing, and the dynamic absorption of fermentation products and water (TIM-2) was developed as well [86]. The TIM-2 was engineered to host the relatively high concentrations of microbes to model *in vivo* conditions. Moreover, hollow-fiber membranes were included inside the reactor compartments to simulate absorption of water and dialysis of metabolites. In this system, a dense chyme model is mixed and transported to the tubular loop-shaped segment with movement to mimic peristalsis where the colonic fermentation occurs. Water and SCFAs were removed from the system to obtain the desired cell density, which provides an advantage over batch culture systems. The TIM-2 system contains four glass units, all connected and each with flexible inner walls to permit peristaltic movements by controlling the hydraulic pressure to circulate the chyme through the loop-shaped system. The tubular shape of the model lumen prevents blockage or obstipation. The water activity of the luminal content is maintained via absorption controlled by a level sensor, and the system is kept anaerobic reflecting conditions in the proximal part of the large intestine. In addition to metabolite removal, the TIM-2 system also maintains metabolite concentrations through controlling the dilution rate and providing a limited amount of substrates. In addition, TIM-2 models the proximal colon, as most carbohydrate fermentation occurs in this region allowing for the mechanistic study of the transformation and bioactivity of exogenous molecules [92]. Accordingly, the TIM-2 system was used to model the effects of lactulose

on the composition of anaerobic bacterial groups within an intestinal microbial community by plate counting and SCFA production by gas chromatography [92]. The TIM-2 model has been used in a variety of experiments to model host-microbial interactions and diet-microbial interactions This includes investigating bacterial metabolism of black tea polyphenols [141], the diversity of glucose fermenting microbiota [142], phylogenetic analysis of starch fermenting bacteria [143], and the effects of inulin (degree of polymerization = 3-25) on the metabolic activity of modeled gut microbiota in the presence of *Clostridium difficile* [144].

In an effort to benchmark the performance of the SHIME and TIM-2 systems, the models were compared in parallel characterizations of the fermentation patterns of arabinoxylan and inulin [145]. This revealed similar effects for arabinoxylan and inulin on structure and function of the modeled microbiome in both models. In the TIM-2 model, ten fecal samples were pooled and stabilized for 16 h prior to the addition of either inulin or arabinoxylan in three days. In contrast, the microbial ecosystem in the SHIME model was derived from a single fecal suspension that was stabilized for 14 days with inulin or arabinoxylan introduced for 21 days. Both *in vitro* systems exhibited an increase in propionate and butyrate in response to a given substrate. Furthermore, arabinoxylan enriched *Bifidobacterium longum* in the modeled community, whereas inulin stimulated populations of *Bifidobacterium adolescentis*.

In addition to previously described models, the dynamic SIMulator of the GastroIntestinal tract (SIMGI) was innovated to simulate operations of digestion and fermentation [146]. This system incorporates three-stage culture reactors to model the ascending, transverse, and descending colon. In addition, the SIMGI model includes a

gastric compartment that simulates peristaltic mixing and a dedicated reactor to simulate the small intestine. Most *in vitro* gut model systems were engineered to simulate either the upper GIT or the colon [86, 125, 140, 145]. Thus the SIMGI model represents an advance compared to previous models as this fully computer-controlled, multi-compartmental system allows joint or independent simulation of gastric and colonic processes. The stomach compartment is comprised of two transparent, rigid, methacrylate plastic modules covering a reservoir of flexible silicone walls. The gastric content is mixed by peristaltic movements created by pumping thermostated water into a jacket between the plastic modules and the flexible reservoir. Beyond mimicking peristalsis, water movement is used to maintain temperature of the gastric compartment. The initial food intake is mixed with gastric electrolytes and enzymes in the stomach compartment. The other four vessels, representing the small intestine and the three distinct colonic regions, are magnetically stirred, continuous flushed by nitrogen and pH and temperature controlled, and connected sequentially through pipes and peristaltic pumps. The succession and stability of the microbial community was evaluated by PCR-DGGE and quantitative PCR in this particular study.

Recently, a high-throughput continuous-flow system was developed to allow microbial community dynamics to be examined in minibioreactor arrays (MBRA) [83, 147]. The MBRA was designed in continuously stirred six reactors, with a working volume of 15 ml to operate under an atmosphere of 5% CO_2 -5% H_2 -90% N_2 at 37°C in a heated anaerobic chamber. To simulate microbial community, pooled fresh fecal samples were mixed in anaerobic phosphate buffer, inoculated in 5 % (w/v) in each bioreactor and stabilized for 72 h. This MBRA system was used to describe community differences

between epidemic and non-epidemic *Clostridium difficile* infections which is a common cause of severe cases of antibiotic-associated diarrhea (AAD) [147]. In this study, the *tcdA* gene was used to quantify *C. difficile* invasion and 16S rRNA amplicon sequencing was used to profile microbiome diversity in the presence of *C. difficile* and antibiotic treatment. Interestingly, clinical strains outcompeted the other strains in the presence of complex microbiota.

1.5 Mucus-immobilized models of the gut

Mucosal microbiota are difficult to study *in vivo* as human intervention studies are typically restricted to observations on fecal samples. Microbes do not typically interact with the host epithelia and are instead found within the mucin layer secreted by goblet cells [148–151]. Bacteria that reside in the mucosal gel layer contribute to inhibiting pathogenic epithelial invasion, either by excreting antimicrobial molecules or competing for adhesion sites [148]. Model systems that incorporate mucosal immobilization are used to study interactions between luminal and mucosal microbiota. Models that simulate dynamic interactions that occur with long-term residence times typically do not address the mucosal environment and may restrict their predictive power.

Immobilized mucus systems utilizing cell immobilization in anaerobic continuous-flow cultures for modeling the GIT were first established in the Lacroix model [152]. Thereafter, the model was used for the immobilization of infant fecal microbiota in *in vitro* gut fermentation model system by Cinquin et al [153]. The system is predicated on a three-stage bioreactor that models immobilization of mucosal microbiota with xanthan-gellan gum beads to simulate bacterial cells entrapped in fibrous particles or forming biofilms on the intestine epithelium [152]. Bacteria isolated from infant feces were immobilized in

xanthan-gellan gum beads using a two-phase dispersion process previously described for the immobilization of lactic acid bacteria in kappa-carrageenan/locust bean gum gel beads [154]. This is done in order to study the compositional changes in the microbial ecosystem over a long time period of fermentation. The medium was formulated to approximate the carbohydrate:nitrogen ratio present in infant chyme, with the bile salt concentrations reduced to the levels of secretion observed in infants. This model has several improvements including growing bacteria within biofilm structures, achieving high cell density in gel beads, maintaining community stability, protection of sensitive bacterial taxa from shear stress, prevention of washout and loss of less competitive bacteria. Based on these characteristics, a model with immobilized fecal bacteria was developed to simulate intestinal *Salmonella* infections and long-term shedding in children was developed [155].

In order to model sessile gut bacteria populations, a single stage chemostat could house mucin beads to encourage microbial adhesion encased within a dialysis membrane [88]. Water and metabolites are removed by osmosis and diffusion respectively using polyethylene glycol (PEG) and the media is maintained under anaerobic conditions. This model system supports the growth of bacteria associated with mucin beads and planktonic bacteria in the culture medium. Distinct differences were observed between the biofilm fermenter system and traditional chemostats including microbial populations and their secreted metabolites.

Recently, a chemostat gut model was developed and validated to model planktonic and sessile states of colonic bacteria in biofilm formation associated with *Clostridium difficile* infections (CDI), [156]. In this model, macroscopic biofilms were facilitated with 18 glass rods inserted into the biofilm vessel, positioned to ensure the sampling portion of

the rod extended across the liquid/gas interface to simulate CDI. Rods were affixed to the lid under an anaerobic environment with the vessel modified to encourage an even distribution of gas flow across the rods. The continuous chemostat model was inoculated with a pooled human fecal emulsion. Planktonic and sessile bacterial populations were enumerated culturing methods and *C. difficile* toxin production was monitored using a Vera cell cytotoxicity assay Interestingly, *C. difficile* spores preferentially persisted within biofilm structures.

The SHIME model has been adapted to simulate surface attached mucosal microbes (M-SHIME) [157]. Two SHIME units used in parallel (i.e. Twin-SHIME) were inoculated with luminal microbes (i.e. luminal-SHIME or L-SHIME), along with mucin-enveloped microcosms to the ascending colon model vessel for a mucosal environment (i.e. mucosal-SHIME or M-SHIME). In order to achieve a representative mucosal surface in the M-SHIME, microcosms were created with mucin-encapsulated suspensions. Mucin-adhesion assays were performed to track the succession of the community in addition to typical microbiological assays. The study reported *Lactobacillus mucosae* and *Pediococcus acidilactici* were both present in the modeled lumen, though *L. mucosa was* strongly enriched in the mucosal phase due to a specific mucus binding (mub) protein. In addition, *Lactobacillus rhamnosus* GG specifically colonized mucus upon inoculation.

The Polyfermentor Intestinal Model (PolyFermS) was developed to study the ecological distribution of intestinal microbiota [158]. In this model, the proximal colon is simulated in the primary reactor containing fecal microbiota from healthy children immobilized in gel beads. The reactor continuously inoculates a set of parallel second stage reactors referred to as an inoculum reactor (IR). This is to enhance reproducibility, by

allowing testing of the same complex microbiota in parallel reactions. A single reactor serves as intra-model control for assessing system stability. The PolyFermS system favors stable microbial compositions and metabolite production consistent with bacterial activity reported *in vivo*. The intestinal communities were validated as stable communities using HITChip microarray analysis and metabolic activity over a 38-day culture were observed at ratios similar feces of healthy donors. Enhanced butyrate production at the expense of acetate in inoculum reactors were detected, which was accompanied by a donor-specific reorganization of the reactor community. This suggests a metabolic adaptation and induction of community-specific lactate or acetate cross-feeding pathways in response to varying pH conditions. In addition, the PolyFermS was used to model fermentation that occurs in the gut of elderly individuals [159]. Three platforms were deployed to conduct this study. The first vessel system was in three-stages to emulate the proximal, transverse, and distal colon similar to adult gut microbiota previously validated in infant and child microbiota fermentation in the Lacroix model. Vessel systems two and three were based on the PolyFermS composed of an IR that was seeded with immobilized fecal microbiota and used to continuously inoculate second-stage reactors in parallel. The modeled gut microbial diversity and metabolite production was monitored using qRT-PCR, pyrosequencing, and HPLC [159].

In addition to human GIT models, PolyFermS was utilized to simulate the conditions of the porcine proximal colon [160]. This was composed of a first-stage IR seeded with immobilized fecal porcine microbiota and used to inoculate (10% v/v) five second-stage reactors, with all reactors fed fresh media with carbohydrate and protein concentrations to closely mimic the ileal chyme found in pigs. First, the IR was operated

in batch mode to colonize the fecal beads and the nutritive medium was replaced by fresh medium every 12 hours. After colonization, continuous operation in IR was initiated, followed by a stabilization period of 5 days before connection to CR (control reactor) and TR1-4 (treatment reactors). The entire two-stage system was then stabilized for another 5 days. Thus, the model provides a tool for efficient, reproducible and cost- effective screening of environmental factors, such as dietary additives, on colonic fermentation.

1.6 Models to simulate complex host-microbial interactions

Canonical bioreactor systems such as those described previously are ideal for studying single microbial species and inter-microbial interactions. However, they do not fully account for all features of the human GIT that add complexity to host-microbial interactions. While iterations of these models have been developed in order to achieve accurate simulations of the human GIT, *in vitro* bioreactor modeling systems typically do not account for the three-dimensional architecture of the colon. The colonic walls present intricate patterns of epithelial invaginations. Whereas conventional bioreactors mimic luminal conditions, including pH, gas content, and temperature, direct microbial-epithelial interactions cannot be simulated in such systems. Furthermore, it is difficult to model the planktonic and sessile phases, as they exist *in vivo*, despite development of mucosal systems. This is not representative of the complex interplay between the host epithelia and commensal microbes that reciprocally interact.

As *in vitro* model systems have evolved to include peristaltic movement and fluid flow under constant parameters, there have been efforts to develop systems to bridge the three-dimensional gap. One solution to this concern is the recent development of an approach referred to as “gut-on-a-chip” [161]. The general setup of the gut-on-a-chip is a

small chamber made of a flexible polymer with several microchannels traversing its length. Upper and lower channels of the same dimensions, 150 μm high by 1000 μm wide, are separated by a porous layer of the same flexible polymer, and this membrane is then coated with an extracellular matrix solution, typically containing collagen of mammalian origin. The channels are connected to both a vacuum source and a source of fluid medium, both of which can be manipulated to achieve the desired flow rate and peristaltic simulation. A common epithelial cell line such as Caco-2 are deposited on the top surface of the polymer membrane using a syringe and maintained in culture. The cells are deposited at a density of $1.5x10^5$ cells/cm^2, and have been observed to adhere to the membrane in 30 minutes, and form inter-cellular adhesions in one hour. Once the Caco-2 cells have formed attachments, culture medium is perfused through the channels with enough shear stress to ensure that any superimposed cells or cell aggregates are washed away, and only a monolayer remains.

Prior to the development of gut-on-a-chip, complex host-microbial interactions were best performed in animal studies. Not only these studies are costly, they may also require dedicated resources, such as gnotobiotic centers, and come with ethical concerns inherent to working with live animals. Gut-on-a-chip does not present any ethical concerns, as human cell lines are a widely distributed and available. Also, interactions between human gut microbiota and the cells may better reflect *in vivo* interactions over time. Microbial viability under these experimental conditions was determined through assays of enzymatic activity, and the level of activity remained comparable to those observed *in vivo* [161].

Most significantly, however, is how accurately the gut-on-a-chip model emulates intestinal physiology, including response to laminar flow, peristalsis, and cell morphology. While other models of planar epithelium have been previously utilized, the gut-on-a-chip promotes the three-dimensional arrangement of epithelium observed *in vivo*. Multiple factors of the model's design work in conjunction to shape the cells in villus-like structures. These influences include the shear stress of laminar fluid flow, mechanical strain, and cyclic strain.

In the static system, the Caco-2 monolayer lies flat, and does not undergo any dynamic changes in cell structure or arrangement regardless of shear stress or mechanical strain. On the contrary, when cells on the gut-on-a-chip membrane were exposed to a shear stress of 0.02 dyne/cm^2 an obvious directionality was observed. The cells grew to a columnar shape and height of 30-40 μm, the expected characteristics of epithelium in a healthy human large intestine [161]. Forces of laminar flow that epithelial cells experience *in vivo* are effectively represented in this system, and results indicate their important role in cellular morphology. In addition to the spontaneous formation of a columnar cell shape, when the same levels of laminar flow are maintained for a longer period of time, in the presence of cyclic strain, the monolayer also began to spontaneously fold. Through histology, the folds were confirmed to mimic the natural villi, comprised of columnar epithelium, that line the colon, thus achieving a model of the barrier environment that much of the gut microbiome inhabits.

The effects of mechanical stress and cyclic stress were also experimentally determined, and while the phenomena did not directly affect the formation of villi from the cellular monolayer, both of these stressors are critical to simulate peristaltic motion that

occurs *in vivo*. Peristalsis is also involved with dictating whether a model system could withstand strain similar to the host organism, and how this may interact with microbial commensals. Classic static epithelial monolayers do not mimic the degree of permeability observed in the human gut. However, the introduction of peristaltic, cyclic strain to the gut-on-a-chip system led to a four-fold increase of monolayer permeability, without compromising the integrity of the tight junctions [161]. Barrier integrity continued to be measured in the presence of bacteria, and was determined to increase over time as the epithelial and microbial cells interacted. This supports previously reported findings that "probiotic" strains promote the health of intestinal epithelium and enhance its barrier function [161, 162].

Gut-on-a-chip performs well in studies of complex microbial communities, such as those derived from human fecal samples. Specific analytical platforms have been created in conjunction with microarray technologies to assess mass quantities of phylogenetic information [162]. In addition, massively parallel sequencing could now be applied towards analyzing data from 454-pyrosequening of a variable region of the 16srRNA gene [162].

Overall, the gut-on-a-chip *in vitro* model holds a great deal of promise for studying host-microbial interactions that take place in the human colon. Due to their representation of colonic forces, including strain and flow, epithelial cell morphology, and barrier strength and permeability, these models provide a degree of accurate mimicking of colonic physiology and microbial interactions at the epithelial barrier.

1.7 Gastric-small intestine model systems

Although the majority of microbes colonize the large intestine, other GIT segments are relevant to health outcomes. Accordingly, modeling the colon in the absence of the upper GIT does not represent the harsh barriers experienced by food and microbes once consumed or delivered.

Modeling the stomach and small intestine requires maintenance of proper pH in both simulated organs (2 in the stomach, 6-7.4 in the small intestine) [140, 163]. Besides pH, modeling the proper composition of gastric juice is imperative in the correct sequence and concentration [140, 163] . Pepsin and hydrochloric acid are encountered in the stomach. In contrast, bile, bicarbonate, and pancreatic enzymes are found in the small intestine, particularly in the duodenum. Modeling upper GIT enzyme secretions pose another challenge in these systems. In the stomach, acid and enzymes are secreted evenly throughout directly from the stomach lining [164]. Thus, the direct addition of physiological concentrations of enzymes and hydrochloric acid to a model system may not emulate digestion *in vivo*.

In addition to modeling biochemical aspects of the upper GIT, there are many mechanical forces to be considered to achieve a representative simulation. The secretions themselves, whether from the stomach walls or duodenum, exert forces of flow onto the digesta present [163, 164]. These hydrodynamic forces and waves cause shear stress. As food progresses through the GIT, its own viscosity contributes to a decreased rate of diffusion of nutritive food components to their site of absorption in the small intestine[165]. The stomach possesses active churning, and an accurate model must mimic the peristaltic contractions that cause churning [140, 163, 164]. Churning is necessary for the appropriate

mixing and production of chyme. The small intestine experience peristalsis as well, as it pushes chyme along its length, the duodenum, jejunum, and ileum, so nutrient absorption can occur.

At the junction of the stomach and small intestine lies the pyloric sphincter, which selectively allows digested material through, to control the rate of stomach emptying [166]. Liquids pass through the pyloric sphincter with relative ease, while larger particulates will be forced back into the stomach for further breakdown [140, 167]. Without a model sphincter with the proper pressure in place, this critical function cannot be simulated [163]. Indirectly, this affects the modeling of transit time through the GI tract as well [140]. Each of these parameters has been included based the results of on studies done on human subjects and animal *in vivo* studies [140] .

The role of the nervous and endocrine systems in digestion, such as stimulation by the vagus nerve, has yet to be emulated in an *in vitro* GIT model [168]. Pancreatic enzymes and bile can be accurately added to a duodenal approximation, but the hormones that act upon the pancreas and gallbladder are not typically considered. Feedback mechanisms that occur in the stomach and small intestine digestion and absorption have not been factored in either.

With these challenges in mind, a successful gastric and upper intestinal simulator can encompass the dynamic nature of these organs' physiology. One of the earliest dynamic models, and one that is widely used and highly regarded today, is the TNO *in vitro* Gastrointestinal Model (TIM), by Minekus et al [140]. The first model, TIM-1 was created in 1995, followed by TIM-2 in 1999 [86]. This model is significant because it was the first of its kind to be both dynamic and multi-compartmental [140, 168]. At its core,

the system consists of four compartments, representing the stomach, duodenum, jejunum, and ileum. Comprising each region is a glass vessel with an internal compartment, with flexible walls. The space between the glass container and the inner compartment is filled with water controlled by a rotary pump. A separate three part valve pumps connects each discrete region and emulates the forces of peristalsis, contracting 3 times per minute in the stomach compartment, and 9 times per minute in the models of the small intestine. Dialysis was performed after digestion was completed with an added glucose load to simulate absorption by the small intestine, and it was reported that 96% of the glucose was found in the dialysis, demonstrating successful absorption. The pressure exerted on the walls inside also allow the system to simulate churning and mixing of the meal [140].

Although the mechanical forces that are exerted in the stomach and small intestine are accounted for, some of the more sophisticated aspects of contraction and peristalsis may be improved. The regular contractions that TIM-1 exerts through the pumping of water are not entirely representative, as within a single peristaltic contraction, there is gradient in the force felt by the stomach, increasing as the contraction approaches the antrum, the lower, fuller portion of the stomach [167] . Antral grinding is a critical component of the mechanical digestion that occurs in the stomach, as particulate matter is turned into chyme. Sufficient decrease in size of digested food is necessary for entry into the duodenum. If larger pieces of digesta within the stomach are not broken down, the human pylorus is responsible for the phenomenon of retropulsion. Liquids and sufficiently small particles pass through the pyloric sphincter with ease, all the while preventing the entry of large constituents, forcing them back into the stomach for further mechanical breakdown with almost elastic properties [167] .

One model created to meet these needs is the Human Gastric Simulator (HGS) from University of California Davis [167] . In practice, this model is similar to TIM, but contains only a stomach chamber, and addressed the concern specific to gastric simulation that the former system lacked. The stomach itself is modeled with a latex chamber, held up with clamps and supports at a height of 13 inches. Rather than enclosing the "stomach" in a solid vessel and using water to simulate pressure and contraction, this system uses a series of 12 rollers on belts that apply force directly to the latex walls. Three rollers are connected via pulley system on each of the four sides of the vessel such that peristalsis is experience evenly throughout the model. A motor drives each of the four belts to operate simultaneously. This model also uses a rate of 3 contractions per minute to mimic *in vivo* observations [167]. In contrast to the previous models, the roller and pulley system is more sophisticated because they can be adjusted to simulate the pressure differential that occurs in one single peristaltic contraction. The stomach experiences stronger contractions at the antrum, and as such food used in an *in vitro* gastric modeling system should feel the greatest contraction force in the bottom portion of the chamber simulating the stomach. The HGS accomplished this by tapering the latex vessel, indirectly decreasing the area over which the four sets of rollers exert their force, thus increasing the force of the contraction [167]. The latex of the vessel combined with the intricate application of mechanical force make the HGS better for modeling specific parameters of peristalsis, such as frequency, amplitude, and intensity [168].

Gastric secretions are delivered to the chamber via variable flow mini peristaltic pump. The pump flows into a piece of tubing that splits into 5 equivalent tubes, ensuring that the simulated juice is distributed evenly throughout the vessel, as occurs in the human

stomach [167].The pyloric function of selective filtration and retropulsion that is observed *in vivo* is achieved with the addition of a polythene mesh bag inside of the latex vessel, with an average pore size of 1.5 mm. Particles less than 2 mm in diameter are able to continuously pass through the pore for emptying, as is true of liquids and small particles through the pyloric sphincter. However, larges particles are retained in the chamber, exposing them to further digestive action. As such, the "sieving" function of the pyloric sphincter is retained in the HGS [167].

The success of this model was determined based on properties of the experimentally digested food, in this case apples and rice. The criteria they hoped to fill were particle size distribution, pH profile, and desired content remaining in the stomach compared to what was emptied [167] . Experiments performed comparing the HGS to older shaking bath techniques of food disintegration showed that particle size was significantly reduced in the HGS, meaning that it better approximates *in vivo* gastric digestion due to its additional mechanical forces. Smaller particle size confers a greater surface area to the digested food. As a result, it is implied that this *in vitro* system is able to simulate the kinetics of nutrient release for absorption *in vivo,* as surface area plays an outsized role in increasing absorption.

An *in vitro* upper GI tract simulator that has been commonly used in pharmacological studies is the Dynamic Gastric Model (DGM) [164]. While similar in design to other models of its kind, there are differences in how mechanical forces are applied. The DGM consists of inner and outer compartments, like HGS and TIM, but food is exposed to mechanical digestion is found in between the two chambers, as the inner compartment is mobile and acts to crush the food against the walls of the outer chamber

[167]. Contractions, at 3 times per minute, are achieved through water pressure, as in the TIM system [164] . Gastric juice, including enzymes, is also carefully distributed such that it is delivered evenly, but rather than through a system of tubes, the mixture is released from a dispenser floating atop the contents of the vessel. Overall, the DGM was designed to account for many of the considerations mentioned previously, including dynamic pH change, shear stress, churning, and transit time. As this particular study was concerned with the absorption of pharmacological agents in the presence of different meals, the success of the model was determined by the measure of mean breaking time of agar beads, used to represent ingested tablets or capsules [164] .

This model places particular emphasis on simulating antral grinding forces, as discussed with the HGS [164, 167]. A piston is used to achieve shearing in the antrum of the model, and the sieving of the pyloric sphincter is mimicked using an elastic ring [164]. However, it has been claimed that the mechanical forces applied in the DGM do not accurately reflect the forces of peristalsis [167, 168].

All three models – TIM, HGS, and DGM – are dynamic representations of gastric digestion, but each comes with its own strengths and attributes. Only TIM is multi-compartmental, which is useful for whole-system studies, but its approximations of gastric mechanical forces are weakest. Both the HGS and DGM attempt to recreate forces in the stomach, considering both peristalsis and the gradient of force exerted along the stomach. The HGS arguably accomplishes this task with more accuracy, using the system of rollers at different applied pressures, while the DGM uses a water based pressure simulation like TIM. However, TIM is also a better model with which to observe absorption after digestion

is complete. HGS allows for the approximation of nutrient absorption, but this phenomenon cannot be directly measured in this model.

In vitro models of the stomach and small intestine are most representative of *in vivo* conditions when a meal or food matrix is incorporated along with the bacteria of interest. Since some strains have been demonstrated to be resistant to harsh conditions *in vivo* it is important to be able to distinguish between the success of the model and a particular microbe simple exhibiting resilience. For example, sporulating bacteria are known to withstand the conditions of the upper GI tract [166].

In conventional testing of microbes in highly acidic conditions, 100% of strains exposed to hydrochloric acid did not survive. However, food itself has significant buffering capabilities that can protect microbes from pH profiles that would otherwise render them inviable [169]. It is not enough to consider the effects of acid or bile, which is thought to be antibacterial, on their own [170]. Rather, the combination of acid exposure with a buffering meal and subsequent exposure to bile and enzymatic action must be considered as is *in vivo*. Studies using TIM but with these additional considerations, namely a kefir based meal, demonstrated that more bacterial strains survive when in a dynamic model rather than static, and the survival is significantly greater than when on media incorporating acid or bile alone [169] .

Another difference from the conventional TIM set-up is that this study only used the stomach and duodenal compartments. The duodenum is the site of most of the digestion in the small intestine and is considered to be the threshold between the upper and lower gastrointestinal tract. If viability is determined upon emptying into the duodenum, it is likely that the microorganisms will successfully pass through to the colon. Survival rates

of microbes in the duodenum were shown to be more uniform than those of the stomach, likely due to the higher pH [169] . Five strains of lactic acid bacteria were found to have survival rates of over 72%, implying likelihood of a significant number of them remaining viable and reaching the colon [169]. Known genera of beneficial microbes are lactic acid bacteria, including *Lactobacillus* and Bifidobacteria, so this is a promising result.

Though each model discussed is best fit for certain types of studies, at large these models represent a comprehensive arsenal of methods for approximating the human gastrointestinal tract, especially in relation to commensal microbiota. Although the majority of the human gut microbiome resides in the large intestine, it is important to consider the effects of the upper GIT on digested food, and how this affects the nutrients that become available to the microbiome. Future directions for improvement of these studies is to emulate mucosal interactions more accurately, such as gut-on-a-chip strives to do, as well as continue to improve the dynamics of multi-compartmental models. Current studies have also begun to look at the effects of non-nutritive bioactive components in *in vitro* models, which can also have some bearing on the interactions between microorganisms, their human hosts, and the food we digest.

CHAPTER 2

INEFFICIENT METABOLISM OF THE HUMAN MILK OLIGOSACCHARIDES LACTO-*N*-TETRAOSE AND LACTO-*N*-NEOTETRAOSE SHIFTS *BIFIDOBACTERIUM LONGUM* SUBSP. *INFANTIS* PHYSIOLOGY

Ezgi Özcan[1] and David A. Sela[1,2,3]

[1]Department of Food Science, University of Massachusetts, Amherst, MA

[2]Department of Microbiology, University of Massachusetts Amherst, MA

[3]Department of Microbiology & Physiological Systems and Center for Microbiome Research, University of Massachusetts Medical School, Worcester, MA.

2.1 Abstract

Human milk contains a high concentration of indigestible oligosaccharides, which likely mediated the coevolution of the nursing infant with its gut microbiome. Specifically, *Bifidobacterium longum* subsp. *infantis* (*B. infantis*) often colonizes the infant gut and utilizes these human milk oligosaccharides (HMOs) to enrich their abundance. In this study, the physiology and mechanisms underlying *B. infantis* utilization of two HMO isomers lacto-*N*-tetraose (LNT) and lacto-*N*-neotetraose (LNnT) was investigated in addition to their carbohydrate constituents. Both LNT and LNnT utilization induced a significant shift in the ratio of secreted acetate to lactate (1.7–2.0) in contrast to the catabolism of their component carbohydrates (~1.5). Inefficient metabolism of LNnT prompts *B. infantis* to shunt carbon toward formic acid and ethanol secretion. The global

transcriptome presents genomic features differentially expressed to catabolize these two HMO species that vary by a single glycosidic linkage. Furthermore, a measure of strain-level variation exists between *B. infantis* isolates. Regardless of strain, inefficient HMO metabolism induces the metabolic shift toward formic acid and ethanol production. Furthermore, bifidobacterial metabolites reduced LPS-induced inflammation in a cell culture model. Thus, differential metabolism of milk glycans potentially drives the emergent physiology of host-microbial interactions to impact infant health.

2.2 Introduction

Breastfeeding is critical for infant development and health in the absence of formula milk substitutes. Human milk contains a high concentration of indigestible oligosaccharides, as well as other nutritive molecules that promote growth experienced early in life [171–175]. Human milk oligosaccharides (HMOs), are indigestible carbohydrates soluble in human milk, and are composed of five monosaccharides: D-glucose (Glc), D-galactose (Gal), *N*-acetylglucosamine (GlcNAc), L-fucose (Fuc) and *N*-acetylneuraminic acid (Neu5Ac or sialic acid) with a varying degree of polymerization and branching [176–179]. These oligosaccharides are not directly metabolized by the infant; however, commensal bifidobacteria have coevolved within the nursing infant gut to utilize HMO [11, 180].

Bifidobacterium longum subsp. *infantis* (*B. infantis*) colonizes the nursing infant and is typically overrepresented within the infant gut microbiome [10, 181–183]. The *B. infantis* genome encodes an array of glycosyl hydrolases, oligosaccharide transporters, and catabolic enzymes that enable HMO utilization [11, 184–187]. Both glycosyl hydrolases and membrane-spanning transporters feed milk oligosaccharides and their derivatives into

the bifidobacterial fructose-6-phosphate phosphoketolase (F6PPK) central fermentative pathway. The F6PPK is believed to be unique to the genus *Bifidobacterium,* which generates ATP from hexoses via substrate-level phosphorylation resulting in the secretion of endproducts that recycle co-factors [188–191]. Bifidobacteria initially converts one mole of fructose-6-phosphate to one mole of erythrose 4-phosphate and one mole of acetyl-phosphate via F6PPK (EC 4.1.2.22). A transaldolase (EC 2.2.1.2) and transketolase (EC 2.2.1.1) converts erythrose 4-phosphate and one mole of fructose-6-phostphate to two moles of xylulose-5-phosphate, which are converted into two moles of acetyl-phosphate and of glyceraldsehyde 3-phosphate via xylulose-5-phosphate phosphoketolase activity (EC 4.1.2.9). Acetyl-phosphate is dephosphorylated into acetate by an acetate kinase (EC 2.7.2.1), accompanied by a single ATP per acetyl-phosphate [192]. In addition, glyceraldehyde 3-phosphate is oxidized to pyruvate accompanied by the production of a single ATP. Pyruvate is converted to lactate by lactate dehydrogenase (EC 1.1.1.27) along with recycling NAD^+ from NADH [193]. For every 2 moles of hexose entering the F6PPK pathway, 3 moles of acetate and 2 moles of lactate are produced (i.e. ratio of 1.5). Based on transcriptomic evidence, it is likely that *B. infantis* catabolizes HMO derived monosaccharides through the F6PPK pathway to generate ATP [45]. This potentially links bifidobacterial physiology (i.e. flux through the F6PPK pathway) with infant nutritional and health outcomes as *B. infantis* benefits their developing host [194, 195].

In general, all *B. infantis* strains examined to date efficiently utilizes HMOs pooled from several donor mothers with the exception of one [12, 196–200]. The tetrasaccharides lacto-*N*-tetraose (LNT) and lacto-*N*-neotetraose (LNnT) are highly abundant oligosaccharides secreted in breast milk [172, 176]. LNT (Galβ1-3GlcNAcβ1-3Galβ1-

4Glc) is classified as a type I HMO, which incorporates lactosyl coupled to a lacto-*N*-biose (LNB) (Galβ1-3GlcNAc) residue. In contrast, LNnT (Galβ1-4GlcNAcβ1-3Galβ1-4Glc) is an isomer of LNT and classified as a type II oligosaccharide, linking the terminal lactosyl with *N*-acetyllactosamine (LacNAc) (Galβ1-4GlcNAc). These isomers are identical aside from a sole glycosidic linkage (i.e. β1-3 vs. β1-4) thus leading to the hypothesis that this structural variation is responsible for differential phenotypes in bifidobacterial utilization of these major HMOs.

2.3 Materials and Methods

2.3.1 Bacterial strains and propagation

Bacterial strains used in this study are summarized in Table 2.1. Bifidobacterial strains were propagated in De Man Rogosa Sharp (MRS, Oxoid, Hampshire, England) medium supplemented with 0.05 % (wt/v) L-cysteine hydrochloride (Sigma-Aldrich, St. Louis, MO)[201] at 37° C under anaerobic conditions (Coy Laboratory Products, Grass Lake, MI). Bacterial strains were routinely verified using the bifidobacterial-specific phosphoketolase assay [202] and bifidobacterial-specific PCR targeting the 16S rRNA gene sequence using the previously developed Bif164-F (5′-GGGTGGTAATGCCGGATG-3′) and Bif662-R 5′-CCACCGTTACACCGGGAA-3′)[203]. In addition, the PCR-based *Bifidobacterium longum*/*infantis* ratio analysis (BLIR) was performed to verify subspecies as previously described [204].

2.3.2 Microplate growth assay

In order to evaluate growth phenotypes in a 96-well format, overnight cultures were inoculated 1% (v/v) to modified MRS media (mMRS; a defined carbohydrate substrate and no acetate). Carbohydrate substrates used in this study include glucose (Sigma-Aldrich Co.

St. Louis, MO), galactose (Sigma-Aldrich Co. St. Louis, MO), lactose (Sigma-Aldrich Co. St. Louis, MO), L-fucose (Sigma-Aldrich Co. St. Louis, MO), *N*-acetylglucosamine (GlcNAc) (Tokyo Chemical Industry Co, Tokyo Japan), lacto-*N*-tetraose (LNT) (Elicityl-oligotech, Crolles, France) and lacto-*N*-neotetraose (LNnT) (Elicityl-oligotech, Crolles, France) at a final concentration of 2 % (wt/v) as the sole carbon source. Carbohydrate sources were incorporated into culture media in non-limiting concentrations. The growth assay was conducted anaerobically at 37° C for 48 h by assessing optical density at 600 nm (OD_{600nm}) in an automated PowerWave HT microplate spectrophotometer (BioTek Instruments, Inc. Winooski, VT) placed within the anaerobic chamber. Each strain was evaluated in biological triplicates with three technical replicates. Inoculated mMRS media in the absence of carbohydrate substrates served as the negative control. Bacterial growth kinetics were calculated using Wolfram Mathematica 10.3 Student Edition with the equation below as described in Dai et al [205].

$$\Delta OD(t) = \Delta ODasym\{\frac{1}{1+\exp[ktc-t]} - \frac{1}{1+\exp[ktc]}\}$$

ΔOD_{asym} is the growth level at stationary phase with k representing the growth rate and tc is the inflection point indicating the time to reach the highest growth rate.

2.3.3 Characterization of microbial metabolic endproducts

Endproducts from bacterial fermentation were quantitated by HPLC. Bacterial strains were initially propagated as described above. Cell-free supernatants from microplate growths were obtained at early stationary phase and filtered through a 0.22 μm filter (Sartorius Corp, Bohemia, NY) following centrifugation and stored at -20° C until further analysis. Organic acids were quantified using a Schimadzu HPLC system equipped

with a Refractive Index Detector 20A, (Schimadzu Corp., Kyoto, Japan). Separation was carried out using an Aminex HPX-87H column (7.8 mm ID x 300 mm, Bio Rad Laboratories, Hercules, CA) at 30° C in a mobile phase of 5 mM H_2SO_4 at flow rate of 0.6 ml/min with 20 μl of injection volume. Standards including organic acids (i.e. acetic acid, lactic acid, formic acid), ethanol, and carbohydrates (i.e. glucose, galactose, lactose, and GlcNAc) were acquired from Sigma-Aldrich Co. (St. Louis, MO). Metabolite concentrations were calculated from standard curves derived from external standards for six concentrations (0.5, 1, 5, 10, 20 and 50 mM). Metabolite profiling was carried out in triplicate and each measurement was performed in duplicate. The metabolite profiling for each strain subsisting on the panel of carbohydrates were analyzed using MetaboAnalyst 3.0 (http://www.metaboanalyst.ca) [206]. The sugar consumption in percentages was calculated by dividing the amount of mono- and di-saccharide expected after fermentation by the concentration of carbohydrate source prior to fermentation. The carbon recovery in percentages was calculated by dividing the total amount of carbon recovered in the metabolites by the total amount of carbon present in pre-fermentation minus total carbon after fermentation.

2.3.4 Quantitative real-time PCR analysis

B. infantis gene expression was performed by quantitative real-time PCR (qRT-PCR) on a relative basis. One mL samples were harvested at mid-exponential phase (OD600nm ~ 0.4-0.6 varied depending on carbohydrate source), pelleted at 12,000 x g for 2 min, and stored in 1 ml Ambion RNAlater (Life Technologies, Carlsbad, CA). RNA extraction and cDNA conversion was performed as previously described [45]. Briefly, samples were centrifuged at 12,000 x g for 2 min to collect the cell pellet. The pellet was

washed twice with PBS buffer to remove residual RNAlater and centrifuged at 12,000 x g for 2 min. Total RNA was extracted using Ambion RNAqeous-Mini kit (LifeTechnologies, Carlsbad, CA) according to the manufacturer's instructions. Cells suspended in lysis buffer were transferred to the Lysing Matrix E tubes (MP Biomedicals LLC, Solon, Ohio) to disrupt cell walls through beadbeating at 5.5 m/seconds for 30 seconds twice using FastPrep 24 bead beader (MP Biomedicals, Santa Ana, CA). Total RNA was eluted in 50 μl of EB solution and immediately subjected to DNase treatment with the Ambion Turbo DNA-free (Life Technologies, Carlsbad, CA) using 1 μl of DNase I for 30 min. Subsequently, total RNA was converted to cDNA using the High Capacity cDNA Reverse Transcription Kit (Applied Biosystems, Carlsbad, CA) according to the manufacturer's instructions. The resultant cDNA was quantified by a Nanodrop 2000 Spectrophotometer (Thermo Fisher Scientific Inc., Agawam, MA). The qRT-PCR was performed on a 7500 Fast Real-Time PCR System (Applied Biosystems, Singapore) with PowerUP SYBR Green Master Mix (Applied Biosystems, Foster City, CA) using 200ng of input cDNA. The reaction conditions were informed by manufacturer recommendations and optimized for the specific target locus. qRT-PCR primers were designed using the Primer3 software (Table A2.1; http:// frodo.wi.mit.edu). The gene Blon_0393, encoding a cysteinyl-tRNA synthetase was used as an endogenous control as previously [184, 207]. Growth on lactose (2 % wt/v) served as the reference condition for gene expression. Results were expressed as fold change relative to the reference. These experiments were conducted in triplicates and triplicate technical measurements were performed. Following DNase treatment, the absence of genomic DNA was confirmed using total RNA as template by qRT-PCR (i.e. endogenous control reaction).

2.3.5 Statistical analyses

The relationships between asymptotic OD_{600nm}, growth rates and metabolites were characterized with principal components analysis (PCA) and hierarchal clustering with Ward's method and Euclidean distances using R (R.3.4.0). The outliers were determined according to their distance to the average within biological replicates were omitted to maintain at least biological triplicates. When no growth was observed in sugars, the values were assigned as "0" for PCA function(prcomp) analysis and PCA plots were drawn using ggbiplot in R. Growth kinetics, metabolite concentrations, fold change in gene expressions of cell culture for *B. infantis* ATCC 15697 were subjected to one-way analysis of variance (ANOVA) and Tukey's HSD test for multiple comparisons between carbohydrate source. The fold change in gene expression for *B. infantis*, growth kinetics, and metabolites between strains were analyzed with two-way analysis of ANOVA. The simple effects and main factor effects were determined with Tukey's HSD test for multiple comparisons of carbohydrate sources for the same strain and between strains for a defined carbohydrate source.

2.3.6 Bioinformatic analysis of transcriptome data

Transcriptomic data (i.e. raw reads) of B. infantis ATCC 15697 while growing on lactose, LNT, and LNnT was retrieved from a previously performed RNA-seq study [45] publically deposited in the NCBI Gene Expression Omnibus database (http://www.ncbi.nlm.nih.gov/geo/) under the accession number GSE58773 (and personal communication with Danielle Lemay). This data was uploaded to the Massachusetts Green High Performance Computing Cluster (MGHPCC) that was used for all computational/statistical analyses unless specifically noted. The RNA-seq reads were

aligned to the reference *B. longum* subsp. *infantis* ATCC 15697 genome (NC_011593.1). Coding regions of the ATCC 15697 genome were subjected to this analysis. Total and unique gene reads aligning to a specific genomic locus (i.e. locus tag), as well as calculated raw counts was obtained for differential expression analysis.

2.3.7 Differential gene expression

In order to identify and quantify the magnitude of differentially expressed genes, the R package DESeq2 was used to analyze the raw count data [208]. Genes with a mean count < 200 was removed from analysis by pre-filtering. DESeq2 applies the Wald test for statistical analysis. Adjusted p-values ≤ 0.05 were defined as statistically significant.

2.3.8 Anti-inflammation assay performed in a cell culture model

Caco-2 cells (ATCC HTB 37) lines were routinely cultured in High Glucose Dulbecco's Modified Eagle Medium (DMEM) (Corning, Manassas, VA) supplemented with $NaHCO_3$ (Sigma-Aldrich, St. Louis, MO), 1% non-essential amino acids (Gibco), 100 U/ml penicillin-streptomycin (Gibco), 10% (v/v) fetal bovine serum (Seradigm) and 7mM HEPES (Gibco). Caco-2 cells were routinely grown in 20-cm Petri plates and subcultured at 80% confluence and maintained at 37 °C in a humidified atmosphere of 5% (v/v) CO_2 in air.

The cells were differentiated at passages 30–32 and collected by dissociation of a 90% confluent stock culture with 0.25% trypsin/EDTA. For the inflammation assay, Caco-2 cells were seeded in 24-well plate at a concentration of 1-2 x 10^5 cells/cm^2 and were differentiated for 17 days with the medium changed every 2-3 days. Replicate supernatants collected from *B. infantis* ATCC 15697 growing on lactose, LNT, and LNnT were mixed in equal volume and added into the DMEM at the final concentration of 15% (v/v). 100

μM of acetic acid, lactic acid, and formic acid controls were mixed with DMEM. Subsequently, media was added to each well in triplicates and incubated at 37° C in a 5% CO_2 atmosphere for 2 hours. For negative and positive controls, triplicates were seeded with only DMEM. After incubation, 10 μl of 5 mg/ml lipopolysaccharide (LPS) in PBS was added into the wells and incubated for 24 h for treatments. LPS alone was used for negative control. PBS alone served as the carrier solution and a reference control. After incubation, the cells were detached from the plate surface by incubation with trypsin/EDTA, suspended in 500 μl of RNAlater solution and stored at -80°C until RNA extraction.

The relative gene expression of interleukin-8 (IL-8) linked with LPS-induced inflammation expression was quantified using qRT-PCR. Total RNA was extracted using the Ambion RNAqeous-Mini kit (LifeTechnologies, Carlsbad, CA) according to the manufacturer's instructions. Cells suspended in lysis buffer were transferred to Lysing Matrix D tubes specific for eukaryotic cell and tissues culture (MP Biomedicals LLC, Solon, Ohio) and were subject to a speed of 5.5 m/sec for 30 sec twice using the FastPrep 24 bead beader (MP Biomedicals, Santa Ana, CA). The total RNA was eluted in 50 μl of EB solution and immediately subjected to DNase treatment with the Ambion Turbo DNA-free (Life Technologies, Carlsbad, CA) using 1 μl of DNase I for half-hour. Total RNA was converted to cDNA using the High Capacity cDNA Reverse Transcription Kit (Applied Biosystems, Carlsbad, CA) according to manufacturer's instructions. The resultant cDNA was quantified in a Nanodrop 2000 Spectrophotometer (Thermo Fisher Scientific Inc., Agawam, MA). The qRT-PCR analysis was performed using a 7500 Fast Real-Time PCR System (Applied Biosystems, Singapore) with PowerUP SYBR Green

Master Mix (Applied Biosystems, Foster City, CA) using 200ng of cDNA with primers GAPDH-F (5′-GTCGCTGTTGAAGTCAGAGG-3′) and GAPDH-R (5′-GAAACTGTGGCGTGATGG-3′) for endogenous control and primers IL-8-F (5′-GACCACACTGCGCCAACAC-3′) and IL-8-R (5′-CTTCTCCACAACCCTCTGCAC-3′)[209]. The PCR cycling conditions were applied as recommended by the manufacturer and tailored specifically to the target genes. Additional markers of inflammation were tested using primers IL-10-F (5′-GGTTGCCAAGCCTTGTCTGA-3′), IL-10-R (5′-AGGGAGTTCACATGCGCCT-3′)[210] and TNF-α-F (5′-TCAACCTCCTCTCTGCCATC-3′), TNF-α-R (5′-CCAAAGTACACCTGCCCAGA-3′)[211].

2.4 Results

2.4.1 *B. longum* subsp. *infantis* exhibits divergent growth phenotypes during utilization of the milk oligosaccharides lacto-N-tetraose and lacto-N-neotetraose

In order to understand *B. infantis* metabolism of HMOs, the type strain ATCC 15697 was subjected to growth on purified HMO species and constituent mono- and di-saccharides. Accordingly, *B. infantis* ATCC 15697 grew vigorously on lactose ($OD_{600nm, asym}$=1.27±0.12, k=0.56±0.03 h^{-1}) as well as galactose ($OD_{600nm, asym}$ =1.20±0.13, k=0.61±0.02 h^{-1}) (Figure 2.1). The HMO species LNT was utilized as a sole carbohydrate source to a similar extent ($OD_{600nm, asym}$ =1.19±0.24, k=0.51±0.02 h^{-1}) as these two constituent residues (Figure 2.1). Interestingly, the structural isomer LNnT promoted a more moderate growth profile ($OD_{600nm, asym}$ =0.85±0.09, k=0.57±0.04 h^{-1}) ($p<0.05$) (Figure 2.1). The *B. infantis* type strain did not grow on the HMO constituents GlcNAc and fucose as a sole carbohydrate source. It is noteworthy that growth on glucose was inconsistent in

terms of final OD_{600nm}; therefore, a comparison to the other carbohydrates was limited. The significant difference between LNT and LNnT utilization ($p<0.05$) suggests that these HMOs are metabolized via differential mechanisms that vary in efficiency (Figure 2.1A). Differences in growth rates between the HMO species were not observed which indicates an equivalent preference for LNT and LNnT (Figure 2.1B). *B. infantis* ATCC 15697 exhibited similar growth rates for lactose, galactose, and LNnT ($p>0.05$). Although growth efficiencies on galactose and LNT are similar (Figure 2.1A), *B. infantis* ATCC 15697 prefers galactose to LNT as indicated by growth rate ($p<0.05$). In aggregate, the single structural difference between LNT and LNnT is directly linked to the efficiency by which *B. infantis* utilizes these HMO species. Previous studies indicate that ATCC 15697 grows on both LNT and LNnT to achieve a $OD_{600nm} > 0.8$, however these studies did not report the specific asymptotic growth (i.e. efficiency) or growth rate (i.e. preference) when growing on these two HMO species [45, 185, 212, 213]. Thus it is significant that ATCC 15697 exhibits clear differences in utilization between LNT and LNnT when accumulating biomass to OD_{600nm} values greater than 0.8.

2.4.2 Metabolic endproducts are differentially secreted dependent on the milk oligosaccharide substrate lacto-*N*-tetraose or lacto-*N*-neotetraose

Fermentative endproducts were profiled to detail the metabolic consequences of HMO carbohydrate flux through the F6PPK pathway. During hexose fermentation, acetic and lactic acids are typically secreted in a theoretical ratio of 1.5. In contrast, formic acid production is not expected under most conditions tested to date [188, 213]. The absolute concentrations of lactic acid, acetic acid, formic acid, ethanol, and the ratios between these metabolites are depicted in Figure 3.2. *B. infantis* ATCC 15697 produces similar

concentrations of lactic acid while growing on galactose, lactose, and LNT (42.5±5.7, 47.8±5.7 and 46.5±2.5 mM respectively) ($p>0.05$, Figure 2.2A). A much lower lactic acid concentration, however, was secreted while utilizing LNnT (29.5±5.9 mM) compared to the metabolism of other carbohydrates ($p<0.05$). Interestingly, formic acid and ethanol concentrations were significantly higher while growing on LNnT (16.3±4.1 mM and 2.5±1.1 mM respectively). This is contrasted with the relatively smaller concentrations while growing on LNT, lactose, and galactose ($p<0.05$, Figure 2.2C and 2.2D).

LNT metabolism resulted in the highest concentration of secreted acetic acid (84.8±4.4 mM, Figure 2.2B) and significantly differed from LNnT metabolism ($p<0.05$). In general, fermentative endproduct concentrations are expected to be positively correlated with the final biomass [214], as more carbohydrates processed by the F6PPK pathway results in more organic acids secreted. Therefore, it is expected that lactic acid and acetic acid concentrations will be higher when greater biomass is achieved [213]. However, acetic acid concentrations while utilizing galactose, lactose, and LNnT did not significantly differ from each other ($p>0.05$). Although the final biomass achieved during LNnT utilization is slightly lower, absolute acetic acid concentrations remain relatively static. Overall, these data support the hypothesis that *B. infantis* deploys a different mechanism while utilizing LNnT.

2.4.3 The ratio of secreted endproducts indicate an alternative pathway for lacto-*N*-neotetraose metabolism

Bifidobacteria, including *B. infantis*, catabolize 2 moles hexose to secrete 2 moles of lactic acid and 3 moles of acetic acid via the F6PPK pathway (Figure 2.3). This theoretical yield (i.e. acetate:lactate ratio of 1.5) was achieved during growth on galactose

and lactose (1.56±0.01 and 1.58±0.01, respectively, Figure 2.2E). During HMO metabolism, LNT and LNnT utilization shifted the ratio towards greater acetic acid production (1.84±0.01 and 2.08±0.14, respectively, $p<0.05$, Figure 2.2E). Again, this is likely due to the deacetylation of the GlcNAc residue, at least in part. Notably this ratio significantly diverges between LNT and LNnT utilization with the latter experiencing a stronger shift ($p<0.05$). If both HMO isomers increased the relative proportion of acetic acid via GlcNAc deacetylation, the higher ratio during LNnT metabolism is due to either decreased lactic acid production and/or increased acetic acid production from acetyl-CoA conversion.

LNnT metabolism was characterized by a significant increase in formic acid and ethanol production despite lower biomass. Accordingly, the ratio of formic acid to lactic acid was significantly higher during LNnT metabolism ($p<0.05$, Figure 2.2F). Similarly, LNnT metabolism increased the formic acid to acetic acid ratio significantly ($p<0.05$, Figure 2.2G). The theoretical formic acid to acetic acid ratio is 2:5 during more than 50% conversion of acetyl-CoA to acetic acid [193]. This ratio was approached during LNnT metabolism (Figure 2.2G). This means, in part, that pyruvate is shunted towards acetyl-CoA resulting more formic acid and acetic acid production rather than lactic acid. Accordingly, ethanol to lactic acid ratio during LNnT fermentation differed significantly from LNT, as well as the other carbohydrates ($p<0.05$, Figure 3.2H). The theoretical ratio is 1:1 when 50% of acetyl-coA converted to ethanol. The higher ethanol to lactic acid ratio in LNnT indicates that ethanol production occurs for regenerating NAD^+. The theoretical ratio has not been reached (~0.08), thus this explains that acetyl-CoA was mostly converted to acetic acid than ethanol to increase ATP production rather than NAD^+ recycling. This

indicates a clear metabolic shift towards these endproducts occur while subsisting on LNnT.

2.4.4 Oligosaccharide transport gene expression remains similar regardless of lacto-*N*-tetraose and lacto-*N*-neotetraose substrates

As with other bifidobacteria examined to date, the *B. infantis* ATCC 15697 encodes several family 1 solute binding proteins (F1SBPs), ATP-binding domains, and permeases that assemble into ABC transporters with predicted affinity for oligosaccharides [11, 184, 215]. The expression of four F1SBPs and their cognate ABC permeases during LNT and LNnT utilization was evaluated to test the hypothesis that transport contributes to the differential metabolic phenotypes (Figure 2.4A and 2.4B). These F1SBPs were previously identified to bind glycans that incorporate HMO moieties [184]. Three F1SBP (Blon_0883, Blon_2344 and Blon_2347) and four ABC permeases (Blon_2175, Blon_2176, Blon_2345 and Blon_2346) were induced more than 2-fold during the growth of LNT or LNnT as the sole carbon source relative to lactose ($p<0.05$). Only Blon_2347 expression differed significantly between the metabolism of the two HMO species ($p<0.05$, Figure 2.4A). Interestingly, both LNT and LNnT induced the F1SBP Blon_0883, although its adjacent permease proteins Blon_0884 and Blon_0885 were not induced ($p>0.05$). Main effect analysis via two-way ANOVA indicates that Blon_2347 exhibits the strongest induction among the four F1SBP genes regardless of substrate ($p<0.05$, Figure 2.4A). Among the permeases, it is notable that the highest relative expression occurred in transcription of Blon_2346, followed by Blon_2345 ($p<0.05$, Figure 2.4B). These genes are located in a 40-kb catabolic cluster dedicated specifically to HMO metabolism [11]. This indicates that *B. infantis* deploys HMO cluster transporters while utilizing both LNT and LNnT which

differs significantly from its corresponding component, lactose. Although the differential metabolic phenotype between LNT and LNnT is not linked to the expression of these transport genes indicating that it is likely a function of intracellular catabolic operations.

2.4.5 *B. infantis* upregulates *N*-acetylglucosamine metabolic genes while utilizing lacto-*N*-tetraose and lacto-*N*-neotetraose

During HMO hydrolysis, GlcNAc is liberated from the oligosaccharide and likely subjected to deamination and deacetylation before entering the F6PPK pathway (Figure 2.3). This is catalyzed by GlcNAc-6-phosphate deacetylase (*nagA*; Blon_0882, EC 3.5.1.25) and glucosamine-6-phosphate isomerase/deaminase (*nagB*; Blon_0881, EC 3.5.99.6). Both Blon_0881 and Blon_0882 exhibited significant upregulation while growing on LNT and LNnT relative to lactose ($p<0.05$). Specifically, LNT induced fold changes of 19.34±3.21 and 21.84±3.90 of Blon_0881 and Blon_0882 respectively, whereas LNnT prompted a similar induction measured at 18.71±5.43 and 20.61±6.19 (Figure 2.4C). This upregulation is interpreted as consistent with GlcNAc catabolism providing evidence that deacetylation occurs during LNT and LNnT utilization. Significant differences in the expression of these GlcNAc genes were not detected between LNT and LNnT metabolism. This expression profile could reflect the growth rate similarity between LNT and LNnT as depicted in Figure 2.1B.

2.4.6 The *B. infantis* transcriptome diverges during lacto-*N*-tetraose and lacto-*N*-neotetraose metabolism

The *B. infantis* ATCC 15697 transcriptome while utilizing HMOs was previously characterized by RNA-seq [45]. Given the differential metabolism observed in the current study, specific pathways predicted to be relevant to LNT and LNnT utilization were

examined in greater depth according to differential gene expression beyond normalized counts. Accordingly, raw reads were retrieved and subjected to differential expression analysis (i.e. 2-fold change) for HMO utilization cluster genes, galactose catabolic genes (i.e. Leloir pathway), GlcNAc-related genes, glycosyl hydrolases and the F6PPK pathway as listed in Table A2.2.

Genes involved in galactose metabolism (Blon_2171, Blon_2172, and Blon_2174) and adjacent ABC transporters (Blon_2175, Blon_2176, and Blon_2177) are strongly upregulated in both LNT and LNnT compared to lactose ($p<0.05$) (Figure 2.5). Moreover, LNnT prompted stronger induction of these genes relative to LNT ($p<0.05$). Similarly, F1SBPs and permeases localized to the HMO utilization cluster (i.e. Blon_2344-2352) were upregulated by both LNT and LNnT relative to the lactose control ($p<0.05$). In addition, Blon_2344, Blon_2347 and Blon_2352 were significantly upregulated during LNT fermentation when compared to LNnT significantly ($p<0.05$).

The GlcNAc utilization genes Blon_0881 (*nagB*) and Blon_0882 (*nagA*) were significantly upregulated while *B. infantis* utilizes both LNT and LNnT relative to lactose ($p<0.05$, Figure 2.5). However, there is no significant difference between LNT and LNnT metabolism ($p>0.05$). This is consistent with the qRT-PCR gene expression analysis.

The key enzyme fructose-6-phosphate phosphoketolase (*xfp*, Blon_1722, EC 4.1.2.22) has been postulated to be among highly expressed *B. infantis* genes regardless of carbohydrate substrate [45]. Interestingly, F6PPK pathway genes are downregulated by LNT relative to lactose and LNnT ($p<0.05$, Figure 2.5). In addition, LNnT showed strong upregulation of those genes compared to lactose ($p<0.05$), except for Blon_1722, Blon_1096 and Blon_1368 that did not significantly differ ($p>0.05$). This is interesting as

the biomass and growth rate achieved with LNT or lactose did not significantly differ ($p>0.05$, Figure 2.1). Despite the potential for greater flux through the central fermentative pathway as per the transcriptome, LNnT prompted less biomass production ($p<0.05$). Furthermore, lactate dehydrogenase (*ldh;* Blon_0840, EC 1.1.1.37), converts pyruvate to lactate to recycle cofactors and was significantly induced by LNnT relative to lactose and LNT ($p<0.05$). The relationship between *ldh* expression and LNnT prompting lower lactic acid concentrations is unclear. This is potentially indicative of variation between the physiological states of the cells during sample collection (i.e. mid-exponential or stationary phase). Accordingly, high levels of lactic acid was observed at the beginning of fermentation of oligofructose by *B. animalis* and replaced by formic acid at later stages [216].

Interestingly, and potentially underlying differential metabolism, acetate kinase (*ack*; Blon_1731, EC 2.7.2.1) was more strongly upregulated while consuming LNnT relative to lactose and LNT ($p<0.05$). Acetate kinase catalyzes substrate-level phosphorylation in the F6PPK pathway that is both involved in conversion of phosphoketolase to acetyl-P and conversion of acetyl-coA to acetate, and thus reflects relatively higher acetic acid secretion during LNnT fermentation.

As LNnT utilization is characterized by increased formic acid production, putative genes involved in this pathway were interrogated. It is noteworthy that this metabolic process is incompletely characterized in the bifidobacteria. Formate acetyl transferase (Blon_1715, EC 2.3.1.54) and pyruvate formate lyase (Blon_1714, EC 1.97.1.4) potentially converts pyruvate to acetyl-coA and produces of formic acid. Accordingly, Blon_1715 is highly expressed during LNnT utilization relative to lactose and LNT

($p<0.05$). Conversely, LNT metabolism is not characterized by increased formic acid production and prompted a downregulation of both Blon_1714 and Blon_1715 relative to lactose and LNnT ($p<0.05$). Although F6PPK genes were upregulated by LNnT relative to lactose, the strongest change was observed in formate acetyl transferase (2-fold change = 1.20). Again, this is consistent with increased formic acid production during LNnT metabolism to provide evidence that differential phenotypes exhibited between LNnT and LNT is regulated at the gene expression level, at least in part.

25 key glycosyl hydrolases (GHs) were selected for further analysis (Figure 2.5) [11, 185, 217]. A total of 13 loci significantly differ between LNT and LNnT metabolism ($p<0.05$). Among β-galactosidases, Blon_2016 (GH family 42) and Blon_2334 (GH family 2) were downregulated during LNT utilization relative to lactose and LNnT ($p<0.05$). This is interesting because Blon_2016 was shown to have specificity to type I HMO such as LNT [218] and Blon_2334 was shown to be constitutively expressed in the utilization of pooled HMO and other complex oligosaccharides [45, 217]. β-glucosidase Blon_1905 was significantly upregulated by both LNT and LNnT compared to lactose ($p<0.05$) with expression during LNnT growth significantly higher than LNT ($p<0.05$).

Salient to general HMO metabolism, an α-L-fucosidase Blon_0248 (GH family 29) was significantly upregulated by LNnT compared to lactose and LNT ($p<0.05$). Interestingly, another GH 29 α-L-fucosidase (Blon_0426) is strongly upregulated by LNT whereas it is downregulated by LNnT ($p<0.05$). Other fucosidases Blon_2335 and Blon_2336 were strongly upregulated by LNT rather than LNnT ($p<0.05$). Blon_0625 and Blon_2460 were downregulated in both HMO species compared to lactose, with a significantly stronger downregulation observed in LNnT than LNT ($p<0.05$). Blon_2468,

an endo-beta-*N*-acetylglucosaminidase, which generally releases *N*-glycans from human milk glycoproteins was upregulated by LNT while it was downregulated by LNnT ($p<0.05$).

2.4.7 *B. longum* subsp. *infantis* exhibits growth phenotype variance while utilizing lacto-*N*-tetraose and lacto-*N*-neotetraose in a strain-dependent manner

In order to evaluate potential phenotypic variation within *B. infantis*, three strains in addition to ATCC 15697 were subjected to growth on glucose, galactose, lactose, LNT, and LNnT as a sole carbon source (Table A2.3). Both *B. infantis* UMA299 and UMA300 utilized GlcNAc as a sole carbohydrate substrate in contrast to ATCC 15697. None of the *B. infantis* strains tested utilized fucose as a sole fermentative substrate. UMA299 exhibited lower growth on LNT ($OD_{600nm,\ asym}$=0.69±0.09, k=0.57±0.05 h^{-1}) and LNnT ($OD_{600nm,\ asym}$=0.71±0.06, k=0.68±0.06 h^{-1}) compared to constituent carbohydrate residues within HMOs ($p<0.05$, Table A2.3). This is significant, as UMA299 does not utilize pooled HMO efficiently in contrast to other *B. infantis* strains [198]. This is likely due to the absence of two F1SBP transporter genes (Blon_2344 and Blon_2351) in its HMO catabolic cluster [197]. Interestingly, and despite limited growth, UMA299 exhibited a higher preference for LNnT with significantly lower growth rate on LNT ($p<0.05$). In addition, UMA299 exhibited a $OD_{600nm,\ asym}$ of 0.42± 0.09 on soluble GlcNAc with a growth rate of 0.16±0.01 h^{-1} which is significantly lower compared to other carbohydrates tested ($p<0.05$).

B. infantis UMA300 utilized LNnT efficiently ($OD_{600nm,\ asym}$=1.30±0.12, k=0.51±0.05 h^{-1}) which is to the same extent as LNT ($OD_{600nm,\ asym}$= 0.99±0.20, k=0.71±0.05 h^{-1}). The strain utilized galactose to similar cellular concentrations as LNT and LNnT and inefficiently utilizes lactose and GlcNAc (Table A2.3). In terms of growth rate (k),

UMA300 experienced the highest rate on LNT and galactose with a significantly lower growth rate on LNnT ($p<0.05$). This provides additional evidence that the two HMO species are utilized by divergent mechanisms by *B. infantis* strains. Despite achieving highest biomass concentrations on LNnT, UMA300 preference as determined by growth rate did not vary appreciably between LNnT and lactose ($p>0.05$). UMA300 low growth rate on GlcNAc suggests that this aminosugar is not preferred relative to the other carbohydrates tested ($p<0.05$).

In contrast to UMA300, *B. infantis* UMA301 exhibited vigorous growth on lactose ($OD_{600nm, asym}$=1.29±0.05, k=0.56±0.05 h^{-1}), followed by galactose ($OD_{600nm, asym}$=1.22±0.05, k=0.63±0.06 h^{-1}) and LNT ($OD_{600nm, asym}$=1.01±0.17, k=0.44±0.06 h^{-1}) all of which does not differ significantly ($p>0.05$, Table A2.3). UMA301, however, achieved significantly lower biomass concentrations on LNnT ($OD_{600nm, asym}$=0.86±0.04, k=0.40±0.01 h^{-1}) concomitant with a lower growth rate. This suggests a clear preference for LNT rather than LNnT between these two HMO tetrasaccharides. As with ATCC 15697, UMA301 does not utilize GlcNAc as a sole carbohydrate source.

Consistent with the growth, ATCC 15697, UMA299, and UMA301 consumed galactose and lactose greater than 40%, whereas UMA300 consumed lactose at 25% ($p<0.05$, Figure A2.1A). Similarly, UMA299 were consumed GlcNAc to a greater extent than UMA300.

In order to determine phenotypic variation as a function of carbohydrate source and *B. infantis* strain, principal component analysis (PCA) and hierarchal clustering was performed. This analysis incorporated both final asymptotic OD_{600nm} and growth rate data for strains growing on individual substrates (Figure 2.6). The first principal component

(PC1) explains 40.8% variation in $OD_{600nm,\ asym}$ values, whereas PC2 captures 37.7% variation (Figure 6A). The scores of each component grouped as strains clustered closely (within the normal probability). This indicates that the growths are consistent among biological replicates regardless of fermentative substrate. Arrows oriented towards the same direction denote that growth on a particular carbohydrate is correlated with that PC component with the angle between arrows indicating a similar response profile (Figure 2.6A). LNT and galactose utilization vectors emanated towards similar directions that is negatively correlated with both PCs. These two vectors aligned along PC1 where ATCC 15697 and UMA301 growths clustered. UMA300 growth, however, aligned positively with PC1 in the same direction as the LNnT utilization vector. This indicates that UMA300 utilized LNnT well relative to other carbohydrates and strains. This is consistent with strain-dependent utilization, as UMA300 had a higher final $OD_{600nm,\ asym}$ during LNnT utilization compared to other strains (Figure 2.7D). Interestingly, the LNnT and lactose utilization vectors were oriented in opposing directions suggesting utilization differences between them. GlcNAc and glucose utilization had a similar alignment and positively correlated with both components where UMA299 clustered. This indicates that UMA299 growths are mostly correlated with GlcNAc and glucose utilization, which is consistent with its limited ability to utilize HMO efficiently.

Hierarchal clustering was employed to determine quantitative similarities between strains. The height between the lines indicates the distances between the strains and their biological replicates (Figure 2.6B). The PCA and hierarchal clustering were concordant and indicated that ATCC 15697 and UMA301 clustered together with the height of less

than 4 (Figure 2.6B). Interestingly, this reflects the phylogenic relationship of ATCC 15697 with UMA301 [197].

In addition to final biomass achieved, PCA of growth rates observed on multiple substrates resolve onto PC1 to encompass 51.6% variability for each strain and positively correlated with all carbohydrates except lactose (Figure 2.6C). This is interesting as *Bifidobacterium* strains were previously determined to possess a preference for lactose over glucose [207], with lactose often used as a positive control and propagation of bifidobacterial strains. ATCC 15697 and UMA301 co-clustered and negatively correlated with PC1. These two strains exhibited similar utilization rates for all substrates tested. Interestingly, UMA300 growth rates on galactose, LNT, glucose, and GlcNAc were similar and distinctly clustered from other strains (Figure 2.6C) with significantly higher values on these carbohydrate sources compared to other strains ($p<0.05$, Figure 2.7). Hierarchal clustering using the Ward method validated the PCA (Figure 2.6D). Hierarchal clustering of the growth rate is also consistent with the same analysis of the final biomass ($OD_{600nm, asym}$), which yields a similar distance topology. Accounting for the empirical evidence in aggregate, *B. infantis* utilization of LNT and LNnT diverges in a strain-dependent manner.

2.4.8 *B. longum* subsp. *infantis* strains differentially metabolize lacto-*N*-tetraose and lacto-*N*-neotetraose

A comparative analysis of the fermentative endproducts lactic acid, acetic acid, formic acid, and ethanol was conducted on the panel of *B. infantis* strains. These endproducts are secreted as a result of carbon flux through the F6PPK pathway with data reported as a heatmap with hierarchal clustering analysis (Figure 2.8A). As expected, acetic acid and lactic acid production clustered more closely with each other than the ethanol and

formic acid production as these two endproducts are secreted regardless of substrate (Figure 2.8A).

The metabolic profiling of ATCC 15697 and UMA301 while fermenting galactose, lactose and LNT closely clustered together with high acetic and lactic acid and less formic acid and ethanol produced (Figure 2.8A). Interestingly, UMA299 produced higher concentrations of formic acid and ethanol when utilizing GlcNAc, glucose, LNT, and LNnT relative to other carbohydrates (Figure 2.8A). This indicates that UMA299 utilizes LNT via a different metabolic trajectory relative than other strains. This is consistent with its final biomass and general phenotype as an atypical HMO consumer (Figure 2.7C).

ATCC 15697, UMA301, and UMA299 LNnT metabolism was linked to higher formic acid and ethanol concentration. UMA300, in contrast, exhibited a significantly different metabolic profile that is closely linked to LNT with less formic acid and ethanol production than the other strains (Figure 2.8A). This did not differ appreciably from galactose, lactose, and glucose metabolism. This suggests that UMA300, unlike other strains, preferentially converts pyruvate to lactic acid rather than acetyl-CoA regardless of the substrate with the exception of GlcNAc. UMA299 produced higher concentrations of acetic acid relative to other carbohydrates reflecting deacetylation of GlcNAc before entering central metabolism (Figure 2.3).

The carbon recovery in metabolites after utilization of mono- and disaccharides are depicted in Figure S2.1B. UMA299 recovered almost 100% carbon for all sugars except galactose. All strains recovered less than 100% carbon while fermenting galactose. ATCC 15697, UMA299, and UMA301 achieved almost 100% carbon recovery while utilizing lactose. Interestingly, UMA300 exhibited 138% of carbon recovery as determined by

metabolite following growth on lactose. This was significantly higher than ATCC 15697 and UMA301 ($p<0.05$). This might be due to hydrolysis of the remaining lactose into glucose and galactose in the after fermentation medium with UMA300 potentially exhibiting a preference for utilizing monosaccharides over lactose.

The acetic acid:lactic acid ratios secreted after *B. infantis* strains fermented substrates were compared (Figure 2.8B-D). Accordingly, PC1 and PC2 encompass 50.7% and 31.2% of the variation for these ratios (Figure 2.8B). UMA300 and UMA301 displayed a positive correlation with PC1 whereas ATCC 15697 and UMA299 were negatively correlated. This is due to higher ratio values of strains on a particular carbohydrate with each strain clustering distinctly due to PC2. The hierarchical clustering of strains was consistent with the PCA (Figure 2.8C). This is because UMA299 showed a significantly higher ratio in both LNT and LNnT metabolism relative to other strains ($p<0.05$, Figure 2.9A). In addition, the direction of the LNT and LNnT vectors are negatively oriented with both components with a highly similar magnitude and direction in PCA (Figure 2.8B). This explains the close clustering of LNT and LNnT based on Euclidean distance (< 0.95) whereas the HMO carbohydrate constituents segregated away from both HMO species (Figure 2.8D). The agglomerative clustering of strains revealed no differences for LNT and LNnT. This is potentially due to GlcNAc deacetylation increasing acetic acid production during HMO utilization.

Formic acid production underlies divergent mechanisms for LNT and LNnT metabolism. Accordingly, the PCA performed on the acetic acid:lactic acid:formic acid ratios clearly indicates that LNT and LNnT fermentation proceeds via distinctive metabolic routes as these vectors are oriented in opposing directions along PC1 (captures 52.0%

variation) (Figure 2.8E). This suggests that *B. infantis* strains shunt LNnT catabolism towards conversion of pyruvate to acetyl-CoA rather than lactic acid to subsequently secrete formic acid.

UMA300 was positively positioned along PC1 whereas ATCC 15697 and UMA301 were primarily explained by PC2. Interestingly, ATCC 15697 and UMA301 do not cluster together as depicted in Figure 2.8F despite exhibiting phenotypic and phylogenetic similarities. However, if the significance of height in the hierarchical clustering is increased, they cluster together and only UMA300 stands alone. This is due to UMA300 not significantly secreting formic acid except during GlcNAc fermentation. *B. infantis* ATCC 15697 and UMA301 produced significantly more formic acid during LNnT fermentation than LNT that resulted in a decrease of the ratio ($p<0.05$, Figure 2.9B).

The ethanol to lactic acid ratio was dependent on the carbohydrate source and strain (Figure 2.9C). UMA300 did not produce ethanol regardless of the substrate whereas UMA299 exhibited a higher ratio for both LNT and LNnT relative to other strains ($p<0.05$). Interestingly, UMA301 had limited ethanol production during LNT fermentation while the ratio increased in LNnT utilization. This means that all strains except UMA300 utilize LNnT along a similar metabolic route. Thus LNnT utilization in ATCC 15697 and UMA301 might involve NAD^+ regeneration through ethanol production whereas recycling NAD^+ in LNT utilization most likely occur during pyruvate to lactic acid conversion.

2.4.9 Human milk carbohydrate utilization mitigates lipopolysaccharide-induced IL-8 expression in Caco-2 epithelial cells

It is known that metabolism of specific carbohydrates may influence bifidobacterial interactions with intestinal epithelia under certain conditions. Pooled HMO-grown

bifidobacteria reduce inflammatory markers compared to glucose or lactose-grown bifidobacteria [219, 220]. These previous studies examined adhesive properties of bifidobacteria and bacterial translocation in exponential growth instead of cell-free supernatants collected at stationary phase. Differential metabolism of LNT and LNnT inspired the hypothesis that host-microbial interactions may be influenced in a milk oligosaccharide-dependent manner. In order to address this, metabolites present in spent media subsequent to *B. infantis* growth on lactose, LNT, and LNnT were evaluated for their ability to mitigate inflammation. Specifically, it was hypothesized that higher acetic acid and formic acid concentrations secreted from LNnT metabolism will differentially influence inflammation. Gene expression of the cytokine marker of inflammation IL-8 was measured in Caco-2 cells following lipopolysaccharide-induced inflammation (Figure 2.10). Accordingly, spent media from all three fermentations significantly reduced IL-8 expression compared with the negative control ($p<0.05$). However, there was no significant difference between the three milk carbohydrates. In addition, the markers of inflammation IL-10 and TNF-α were assayed to yield inconsistent and thus inconclusive results. Although *B. infantis* metabolism of these human milk carbohydrates protects against inflammation, it is unclear to what extent that *B. infantis* alone is responsible for the anti-inflammatory effect. In addition, purified acetic acid, lactic acid, and formic acid were tested, however, the results were inconclusive due to variation between biological replicates.

2.5 Discussion

Bifidobacterium longum subsp. *infantis* evolved to utilize glycans secreted in human milk to generate ATP as well as provide substrates for anabolic processes.

Accordingly, its genome incorporates a 40-kb locus dedicated to human milk oligosaccharide utilization that is conserved in all *B. infantis* strains isolated to date [11, 197]. The activities encoded by the HMO gene cluster allocate degradation products to be further metabolized prior to entering the F6PPK pathway, the characteristic fermentative pathway unique to the *Bifidobacterium* genus [188]. HMOs evade digestion during gastrointestinal tract transit and thus are available to *B. infantis* to translocate to intracellularly [184, 196]. The F6PPK pathway terminates invariably in the extracellular secretion of acetic acid and lactic acid, with formic acid and ethanol generated to a lesser extent under specific conditions [188–191]. The potential for *B. infantis* to differentially metabolize purified HMO species has not been fully tested. The HMO tetrasaccharides LNT and LNnT differ by a β1-3 and β1-4 linkage between galactose and N-acetylglucosamine at the non-reducing terminus respectively. Accounting for this structural variance, we hypothesized that LNT and LNnT are differentially metabolized after initiating distinct transcriptomic cascades to process these HMOs.

Previous research conducted on *B. infantis* provided the preliminary observations to generate this hypothesis [45, 185]. In this current study, the model HMO-consuming strain *B. infantis* ATCC 15697 exhibits higher growth efficiency (i.e. asymptotic final OD) while metabolizing LNT rather than LNnT. This occurred in the absence of a preference for LNT over LNnT extrapolated from their similar growth rates. Thus ATCC 15697 may experience enhanced fitness when encountering LNT in the infant gut, although this remains to be tested in an *in vivo* system. Moreover, ATCC 15697 diverges in the metabolic fate of carbons during LNT or LNnT utilization. The ratio of secreted acetic acid to lactic acid (AA:LA) is considerably higher for LNT and LNnT than other carbohydrates.

Importantly, LNnT promotes a significantly higher AA:LA ratio relative to LNT. The deacetylation of GlcNAc via deacetylase activity (EC 3.5.1.25, Figure 2.3) likely contributes to the increase in relative concentrations of acetic acid during LNT metabolism.

Of particular importance is that LNnT metabolism significantly increases formic acid production. This is not observed during LNT metabolism and constitutes a major metabolic shift solely attributable to the isomeric composition of LNnT. Thus the AA:LA ratio increases during LNnT fermentation likely due to GlcNAc deacetylation and a simultaneous decrease in lactic acid in shunting pyruvate towards formic acid production. The conversion of pyruvate to acetyl-CoA and subsequently to acetic acid during LNnT utilization results in formic acid and ethanol production. Modulation of acetic acid production harnesses higher levels of ATP during LNnT fermentation. This is consistent with the relative inefficiency LNnT is utilized for biomass as limited ATP restricts cellular growth. Bifidobacteria are known to increase formic acid secretion during inefficient metabolism of unfavorable substrates [193, 216, 221–223]. It is noteworthy that previous studies observed cellular growth considerably lower than the accumulated biomass generated on LNnT in the present study.

In addition, increased ethanol production during LNnT metabolism recycles NAD^+ following reduction of acetyl-coA. Since formic acid is generated at the expense of lactic acid, recovering NAD^+ is critical as lactic acid production recycles cofactors and does not yield ATP [191]. On a molar basis the 2-carbon pathway terminating in ethanol recoups double the amount of NAD^+ than the 3-carbon arm (i.e. pyruvate to lactic acid). Whereas it is clear that LNnT shifts metabolism towards formic acid and ethanol production, the molecular mechanisms underlying these alternative pathways remains incompletely

understood. It is clear, however, that the terminal β1-4 linkage in LNnT prompts this divergent physiological response.

In an effort to determine the contribution of global gene expression to LNT and LNnT metabolism, previously generated RNA-seq data was analyzed in addition to targeting key loci with qRT-PCR. A previous study of *Bifidobacterium breve* UCC2003 concluded that there are overlapping metabolic transcriptional networks with some critical features that are unique between LNT and LNnT metabolism [224]. It is noteworthy that *B. breve* evolved the capacity to hydrolyze HMO extracellularly and imports degradation products. There is limited evidence that *B. infantis* is able to do so, which indicates a fundamental physiological difference between the two species. As *B. infantis* captures HMO from its extracellular environment, the complement and expression transport proteins may catalyze or restrict metabolism of a given HMO species. Among F1SBPs, Blon_2347 expression differed between the two HMO species, whereas Blon_2177 and Blon_2344 was expressed regardless of the specific HMO. Interestingly, the global transcriptome exhibited a different expression profile for these particular genes. Additional studies are required to resolve the conflict between expression of transporters predicted to be active on type I glycans (i.e. LNT)[184] that were observed to be induced by the type II LNnT. Further characterization of the functional interactions between transport systems and HMO substrates may be essential to address these discrepancies.

The aminosugar residue GlcNAc is a constituent of LNT, LNnT, and all HMOs with a degree of polymerization ≥ 4. Prior to entering the F6PPK pathway, GlcNAc is processed by two enzymes putatively encoded within the ATCC 15697 genome. This includes GlcNAc-6-P deacetylase (*nagA*; Blon_0882) that deacetylates GlcNAc prior to

deamination by glucosamine-6-P isomerase (*nagB*; Blon_0881). *B. infantis* expresses both of these proteins when grown on pooled HMO as reported in a previous study [217]. Both LNT and LNnT upregulated these loci supporting the postulate that HMO-bound GlcNAc metabolism contributes to skewing the AA:LA ratio. The elevated AA:LA ratio was observed for pooled HMO and LNT in a previous study that focused primarily on galactooligosaccharides [213]. It is important to note that GlcNAc-bound in HMO may not be fully catabolized through the F6PPK pathway as GlcNAc could serve as a substrate in anabolism including peptidoglycan and other biosynthetic processes [185]. Interestingly, ATCC 15697 does not utilize GlcNAc when supplied as sole carbon source in the media in contrast to other *B. infantis* strains. This may be due to a genetic or regulatory variation inherent to the strain. Moreover, hexosaminadase genes were expressed similarly regardless of the particular HMO isomer. These enzymes liberate GlcNAc from galactose through hydrolyzing the β1-3 linkage that is present in both LNT and LNnT.

The terminal galactose, contrastingly, is connected to GlcNAc via a β1-3 linkage in LNT and a β1-4 linkage in LNnT. Thus it was unexpected that a type I glycan-active (e.g. LNT) β-galactosidase (Blon_2016) is downregulated by LNT and not LNnT ($p<0.05$) [218]. This may be due to constitutive expression of other β-galactosidase that cleaves the terminal galactose *in vivo*. It is significant that both HMO isomers upregulate two genes that are predicted to feed galactose into the F6PPK pathway. This includes gal-1-P uridylyltransferase (*galT*; Blon_2172) and UDP-glc epimerase (*gale*; Blon_2171) that are localized adjacent to HMO transporters on the ATCC 15697 chromosome. Furthermore, LNnT induces these genes to a greater extent than LNT. This provides mechanistic detail for the physiological differences between LNnT and LNT fermentation.

Interestingly, LNT and LNnT upregulates α-L-fucosidase gene expression despite lacking fucosyl moieties within their respective oligosaccharide structure. Accordingly, LNT strongly upregulates two fucosidases localized to the HMO catabolic cluster. This suggests that there is overlapping regulatory systems or *B. infantis* recognizes LNT and LNnT as signaling molecules to prepare for metabolizing fucosylated HMO. HMO tetrasaccharides is utilized early in fermenting pooled HMOs prior to fucosylated glycans[187].

Constituent monosaccharides bound in HMO are transformed into substrates catabolized through the F6PPK pathway. Accordingly, LNnT upregulates several genes in this central metabolic pathway likely to satisfy energy demands from a more inefficiently metabolized oligosaccharide. It is interesting that both acetate kinase and lactate dehydrogenase are upregulated by LNnT relative to LNT or lactose. The former is expected given the physiological evidence for increased acetic acid secretion. Lactate dehydrogenase upregulation may be a consequence of fully activating a central metabolic regulon to maintain the NAD^+/NADH homeostasis. There is a significant link between formic acid production and transcriptional processes. LNnT strongly induces formate acetyl transferase (*pfl*; EC 2.3.1.54), which catalyzes formic acid and acetyl-CoA production from pyruvate. In contrast, LNT downregulates this gene as well as pyruvate formate lyase, the latter of which appears to be constitutively expressed during LNnT fermentation. This represents a strong mechanistic association between the LNnT structure and *B. infantis* genomic features to drive the metabolic phenotype.

As bacterial strains of a given taxon may exhibit profoundly dissimilar phenotypes, three additional *B. infantis* strains were examined. *B. infantis* UMA301 exhibits a very

similar metabolic response to the LNT and LNnT relative to ATCC 15697. Interestingly, these two strains are closely related phylogenetically [197] which suggests that metabolic signature may be a function of phylogenetic divergence for *B. infantis* HMO utilization. Similarly to ATCC15697, LNnT shifts UMA301 metabolism towards formic acid and increases the ratio of acetic acid to lactic acid secretion.

In contrast, UMA300 efficiently utilizes both LNnT and LNT and does not produce formic acid and ethanol on either substrate to the same extent as ATCC 15697 and UMA301. This is likely a function of UMA300 processing LNnT in a similar manner as LNT, which obviates the need for a metabolic shift. The inefficient HMO-consumer UMA299 exhibits a metabolic response congruent with this unique phenotype among *B. infantis* examined to date [197]. The limited capacity to utilize HMO has been attributed to genetic defects within its HMO genomic cluster and provides a control strain linking genotype with metabolic phenotypes. As a result of inefficient growth on LNT and LNnT, UMA299 increases the AA:LA ratio and formic acid/ethanol production. This is consistent with the hypothesis that diminished capacity for utilizing HMO promotes higher acetic acid concentrations compared to other carbohydrates despite achieving low optical density.

A cell culture approach was used to further develop a model of host-microbial interactions that incorporates inefficient metabolism of specific HMOs. Cell-free supernatants from *B. infantis* HMO fermentations were evaluated for their anti-inflammatory properties on Caco-2 cells. Given the parameters tested, it appears that *B. infantis* reduces inflammation regardless of milk carbohydrate source. Specific anti-inflammatory molecules presented or secreted by *B. infantis* remains hypothetical.

Moreover, the extent to which other HMO structures diminish inflammatory outcomes is not understood.

In conclusion, LNT and LNnT utilization increased the AA:LA ratio in all strains. In instances where LNT or LNnT was inefficiently utilized, carbon was shunted towards formic acid and ethanol secretion. A fully integrated mechanistic model underlying this phenotype remains incompletely developed. Thus, there is a scientific need to investigate all purified HMO species, additional *B. infantis* strains, as well as other bifidobacterial species to ascertain linkages between HMO structure and physiological responses. This will further refine the metabolic model by which bifidobacteria utilize HMO to colonize the nursing infant colon. In addition to fundamental biological research, there are broad implications to infant nutrition and health. There is accumulating evidence that rationally designing interventions to enhance infant nutrition will require judicious selection of HMOs. This could involve incorporating a single HMO species or a mixture. Clearly a specific HMO tetrasaccharide has different metabolic consequences depending on the *B. infantis* population. There is the potential for strain-level effects to influence the emergent properties of the infant gut microbiome community. Accounting for variation between bifidobacteria, HMO structures, the biology of the infant, and their hosted microbiome communities may enable delivery of precision nutrition and increase impact of the intervention.

Table 2.1 List of strains used in this study [a]

Strain	Species	Origin
ATCC 15697	*B. longum* subsp. *infantis*	Human infant feces
UMA299	*B. longum* subsp. *infantis*	Human infant feces
UMA300	*B. longum* subsp. *infantis*	Human infant feces
UMA301	*B. longum* subsp. *infantis*	Human infant feces

[a] UMA: University of Massachusetts Amherst Culture Collection, ATCC: American Type Culture Collection.

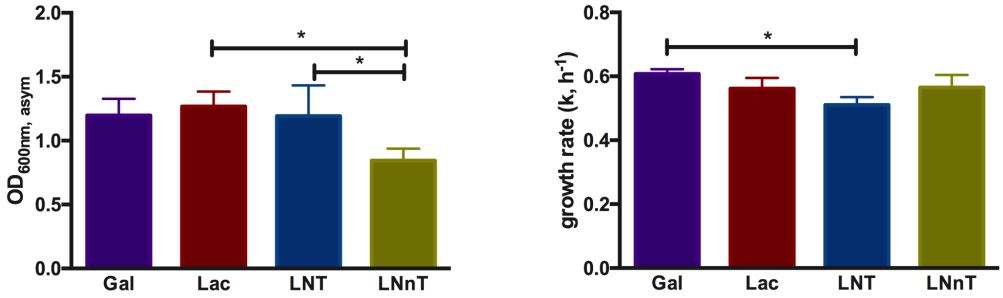

Figure 2.1 *B. longum* subsp. *infantis* ATCC 15697 growth kinetics while utilizing milk carbohydrates. The final asymptotic OD600nm (A) and growth rate (k, h^{-1}) (B) of *B. infantis* ATCC15697 subsisting on mMRS medium containing 2% (wt/v) galactose (Gal), lactose (Lac), lacto-N-tetraose (LNT) or lacto-N-neotetraose (LNnT). The growth kinetics was calculated with Wolfram Mathematica 10.3. The data depicts mean ±SD of three independent experiments. The single asterisk (*) indicates the significant differences between carbohydrate utilizations evaluated by one-way ANOVA and Tukey's multiple comparison ($p<0.05$).

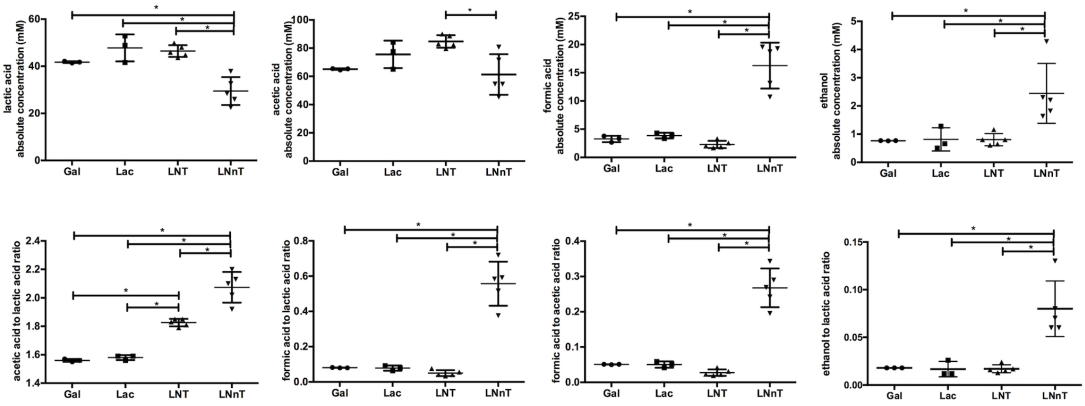

Figure 2.2 *B. longum* subsp. *infantis* ATCC 15697 fermentative endproducts while utilizing milk carbohydrates through the F6PPK pathway. Absolute concentrations of lactic acid (A), acetic acid (B), formic acid (C), and ethanol (D). In addition, acetic acid to lactic acid ratio (E), formic acid to lactic acid ratio (F), formic acid to acetic acid ratio (G), and ethanol to lactic acid ratio (H). All panels represent *B. infantis* ATCC15697 growing on mMRS medium containing 2% (wt/v) galactose (Gal), lactose (Lac), lacto-*N*-tetraose (LNT), or lacto-*N*-neotetraose (LNnT). Averages from independent biological replicates (triplicate or more) are shown with bars representing standard deviations of the means. The values for organic acid production are expressed in millimolar (mM) absolute concentration. A single asterisk (*) denotes significant differences between metabolite production evaluated by one-way ANOVA and Tukey's multiple comparison test ($p<0.05$).

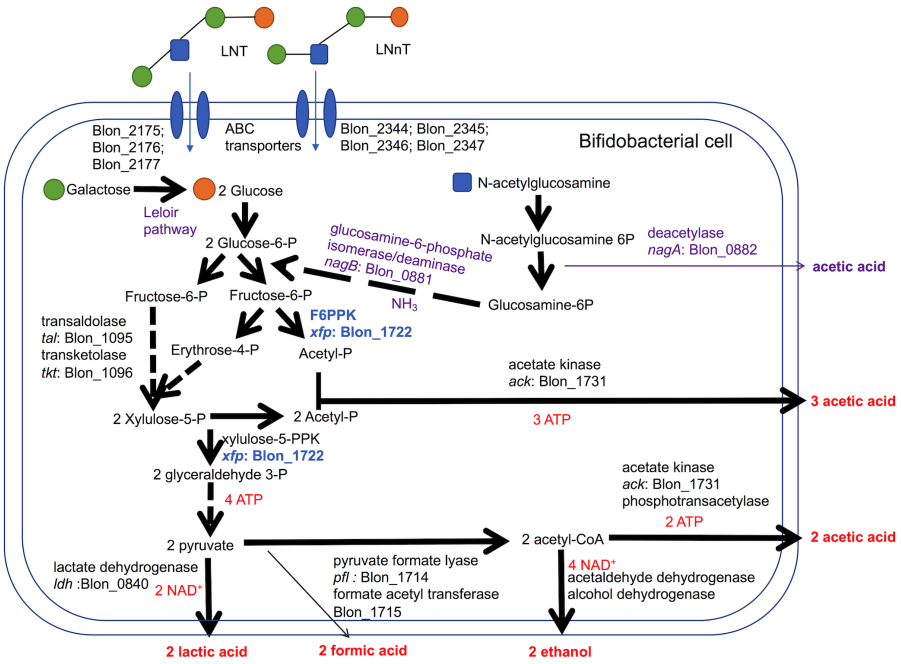

Figure 2.3 *Bifidobacterium longum* subsp. *infantis* metabolic pathways for utilization of lacto-*N*-tetraose (LNT) and lacto-*N*-neotetraose (LNnT) and their constituent monosaccharides. LNT and LNnT translocate through the cell membrane facilitated by ABC transporters. Intracellular glycosyl hydrolases process HMO into constituent monosaccharides to enter the central fermentative pathway. This pathway involves the characteristic fructose-6-phosphate phosphoketolase (F6PPK) activity denoted in blue. Genes encoding intracellular metabolic enzymes are depicted next to arrows according to their locus tag in the ATCC 15697 genome. Solid arrows are direct conversions with dashed arrows depicting the sequential actions of multiple enzymes. Predicted catabolic operations that feed into the F6PPK pathway and their corresponding products are denoted as purple. Stoichiometric coefficients of secreted metabolites, ATP, and NAD^+ produced during metabolism are labeled in red. Experimental observations depicted in Figure 2.1 and 2.2 including stoichiometry are incorporated.

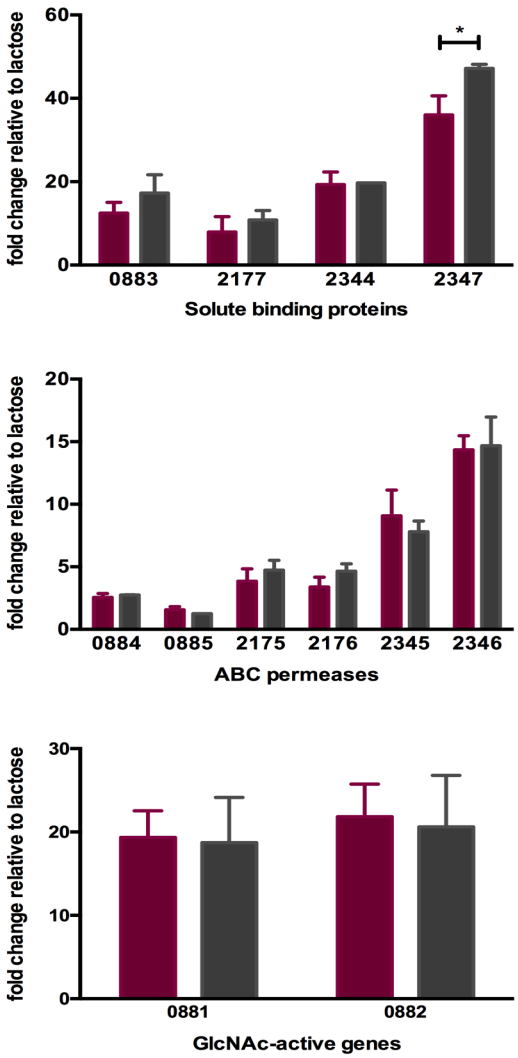

Figure 2.4 ATCC 15697 gene expression while subsisting on milk oligosaccharides as a sole carbon source. The x-axis represents gene locus tags of Family 1 solute binding proteins (A), ABC permeases (B), and GlcNAc-active genes (C). The y-axis depicts the fold changes in gene expression relative to the control lactose as measured by qRT-PCR. LNT and LNnT are denoted in purple and gray. The error bars show standard deviations of three biological replicates except for LNnT. Single asterisk (*) indicate $p<0.05$ evaluated by one-way ANOVA and Tukey's multiple comparison.

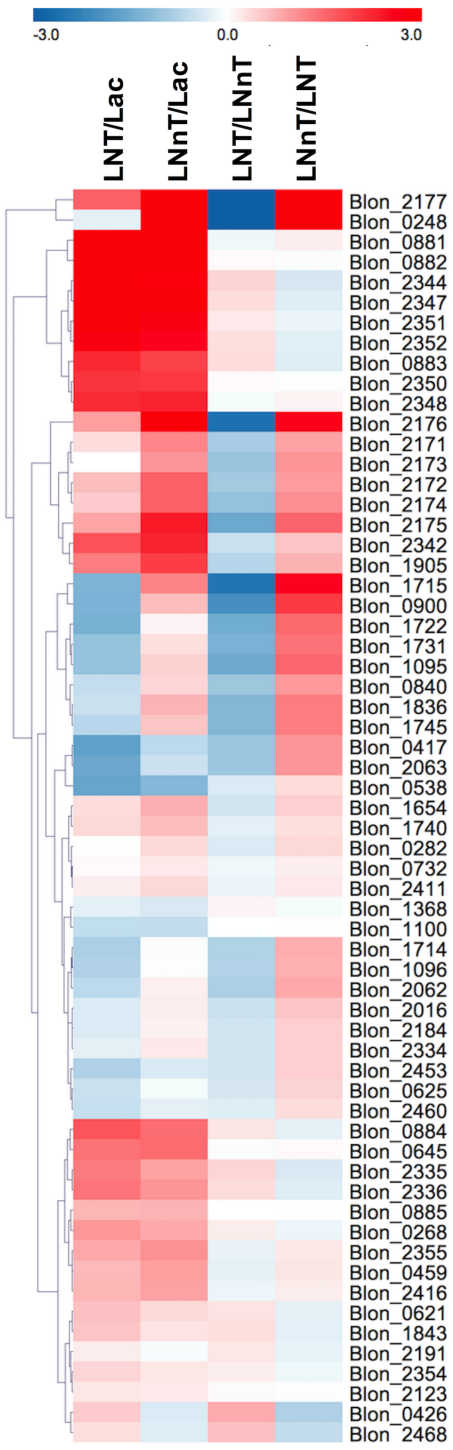

Figure 2.5 Relative gene expression within the global transcriptome depicted as log2-fold change. The log2-fold change gene expression from independent biological duplicates was performed from raw reads using the R package DESeq2. The 2-fold change expressions were subjected to hierarchal clustering using Euclidean distance and depicted as z-scores. Gene annotations and predicted functions are reported in Table A2.2.

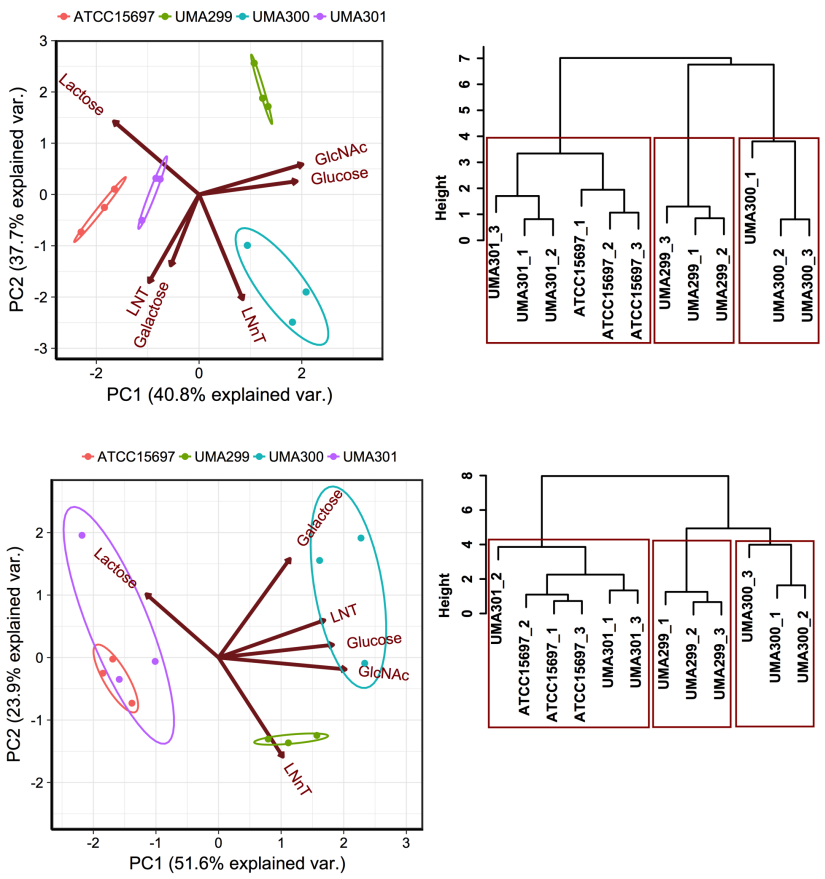

Figure 2.6 Strain dependent variation of human milk oligosaccharide utilization. (A) and (C) depict the 2D-principal component analysis (PCA) performed on the final asymptotic OD_{600} and the growth rate (k, h^{-1}) respectively. The arrows in PCA plot represent the correlation of variables with the principal components (PC1 and PC2). Points represent the scores of each component grouped as biological replicates. The ellipses encompassing each strain capture 68% of the normal probability of the scores within corresponding strains. Panels (B) and (D) show the hierarchal clustering dendrogram of strains on the final asymptotic OD_{600nm} and the growth rate (k, h^{-1}) using ward method and Euclidean distance. The y-axis measures closeness of either individual strains or clusters. The boxes show the 95 % of clustering and closeness of the strains.

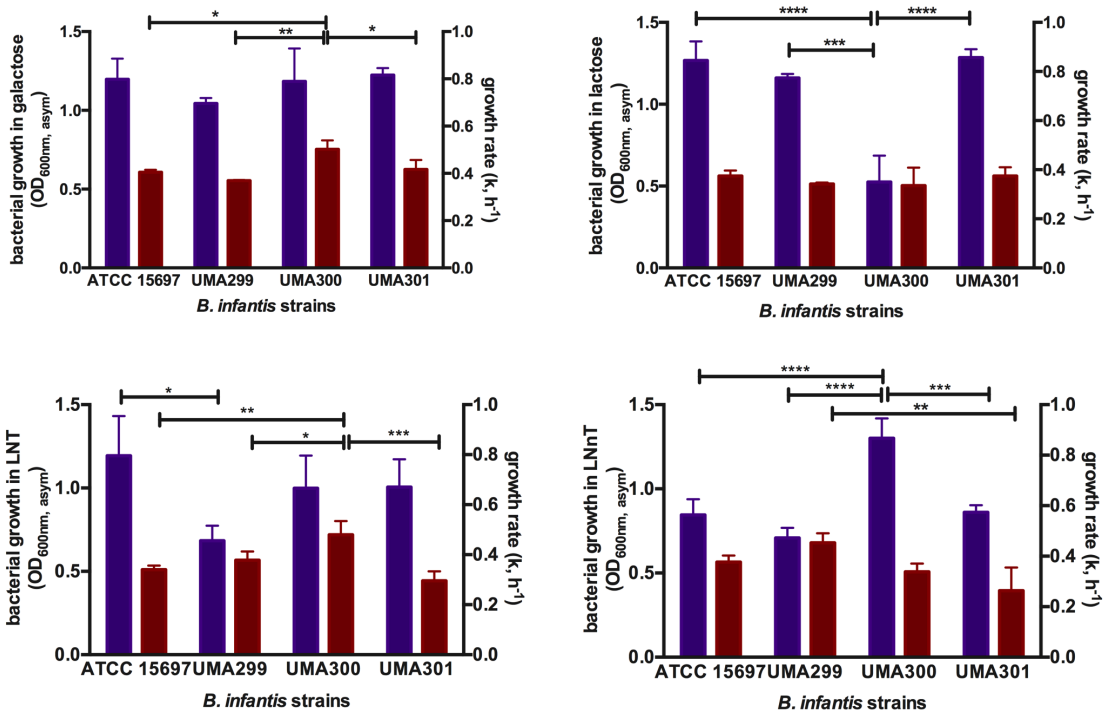

Figure 2.7 Growth kinetics of *B. longum* subsp. *infantis* strains subsisting on milk carbohydrates. The final asymptotic OD_{600nm} and growth rate (k, h^{-1}) of *B. infantis* strains while growing on mMRS medium containing 2% (wt/v) galactose (A), lactose (B), lacto-*N*-tetraose (LNT) (C), and lacto-*N*-neotetraose (LNnT) (D). The growth kinetics was calculated with Wolfram Mathematica 10.3 and represents the mean ±SD of three independent experiments. Purple and red bars indicate bacterial growth and growth rate respectively. The asterisks indicate the significant differences between strains evaluated by one-way ANOVA and Tukey's multiple comparison. Single asterisk (*) indicates $p<0.05$, double asterisks (**) $p<0.005$, triple asterisks (***) $p<0.0005$, and quadruple asterisks (****) $p<0.0001$. The growth kinetics for glucose and GlcNAc were not included as not all strains consume these monosaccharides.

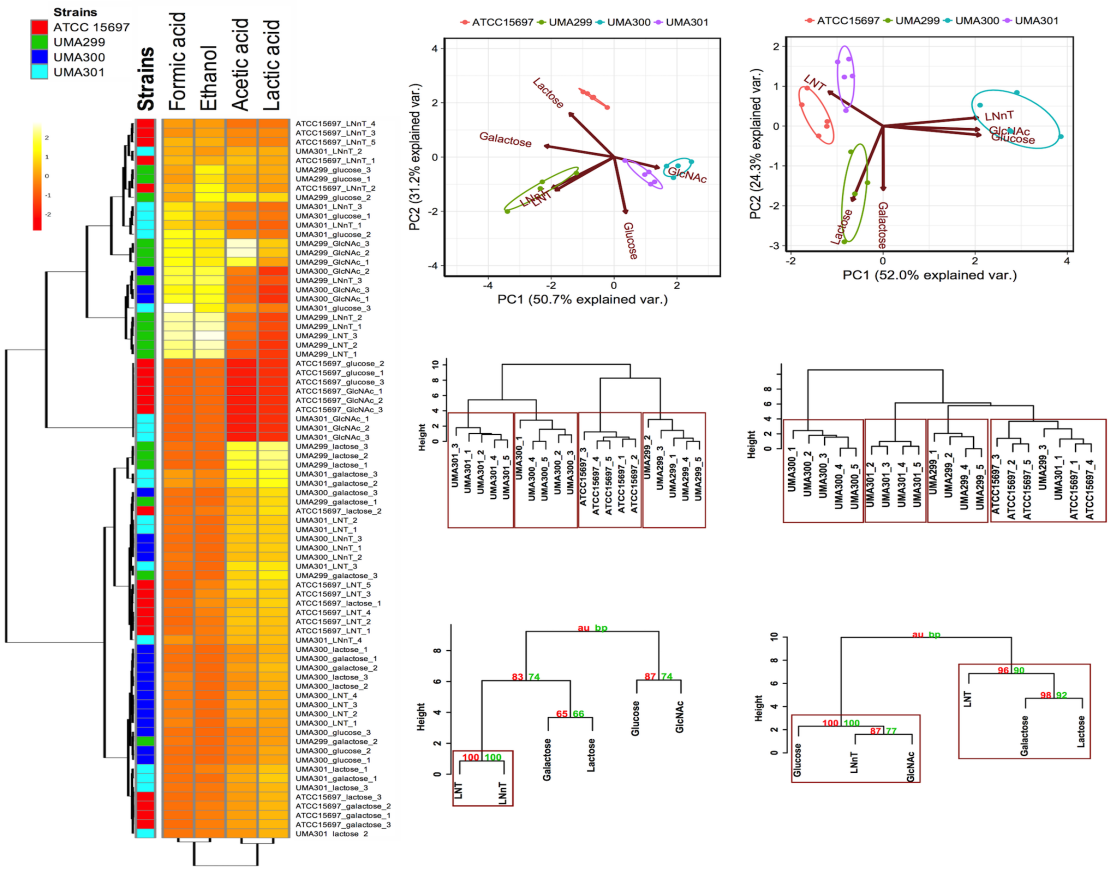

Figure 2.8 Analysis of *B. longum* subsp *infantis* strains secreted fermentative endproducts while utilizing milk carbohydrates.(A) metabolites secreted by *B. infantis* strains for each carbohydrate clustered by Euclidean distance calculated with MetaboAnalyst 3.0. The scaling was performed by mean-centering and dividing by the standard deviation of each metabolite. The red denotes lower concentrations of the metabolite with yellow approaching higher concentrations. Panels (B) and (E) display the 2D-principal component analysis (PCA) plot depicting acetic acid to lactic acid ratios and acetic acid to lactic acid to formic acid ratios respectively. The arrows in PCA plot represent the correlation of the variables with the principal components (PC1 and PC2). Points represent the scores of each component grouped as biological replicates. The ellipses for each strain incorporate 68% of the normal probability of the scores for corresponding strains. Panels (C) and (F) are hierarchal clustering dendrogram of strains according to acetic acid to lactic acid ratios and acetic acid to lactic acid to formic acid ratios using the Ward method and Euclidean distance. The y-axis measures the closeness of either individual strains or their calculated clusters. Panels D) and (G) represent hierarchal clustering based on p-values calculated with multiscale bootstrapping between acetic acid to lactic acid ratio and acetic acid to lactic acid to formic acid ratio. The y-axis measures the closeness of either individual substrates or clusters according to two metrics: Approximately Unbiased p-value (AU in red) and Bootstrap Probability value (BP in blue). Clusters exhibiting AU values greater than 95% are highlighted by rectangles.

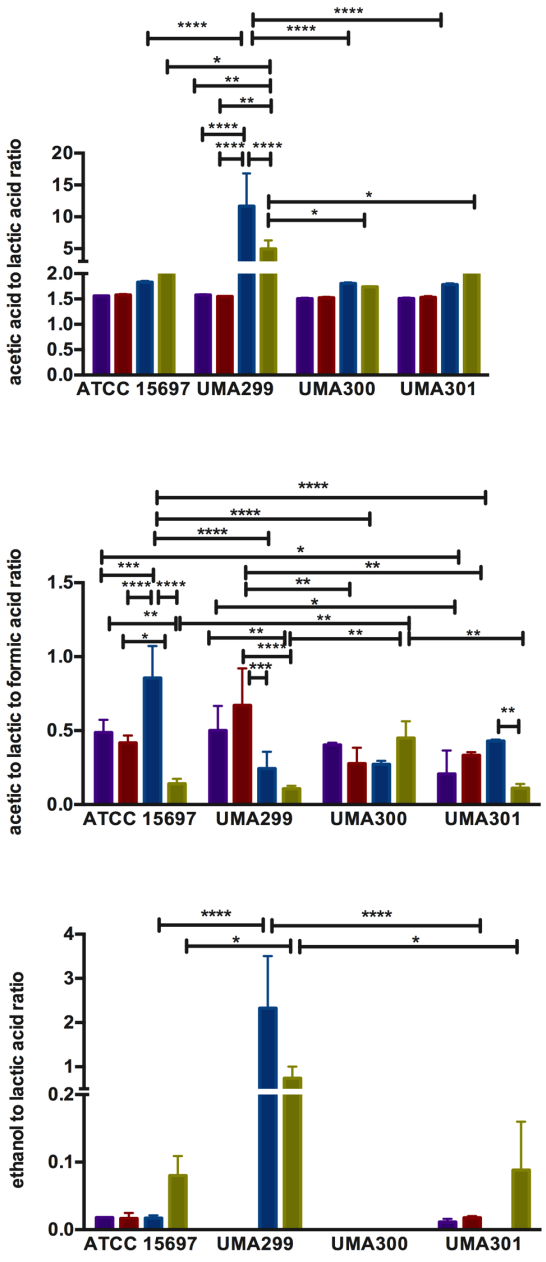

Figure 2.9 Endproduct ratios of *B. longum* subsp. *infantis* strain fermentative endproducts while utilizing the milk carbohydrates. Acetic acid to lactic acid ratio (A), acetic acid to lactic acid to formic acid ratio (B), and ethanol to lactic acid ratio (C). Colors indicate the following carbohydrate substrates: Purple, galactose; red, lactose; dark blue, lacto-*N*-tetraose; green, lacto-*N*-neotetraose. Averages from independent biological replicates (at least triplicate) are shown with bars representing standard deviation from the mean. The asterisks indicate the significant differences evaluated by two-way ANOVA and Tukey's multiple comparison. Single asterisk (*) indicates $p<0.05$, double asterisks (**) $p<0.005$, triple asterisks (***) $p<0.0005$ and quadruple asterisks (****) $p<0.0001$.

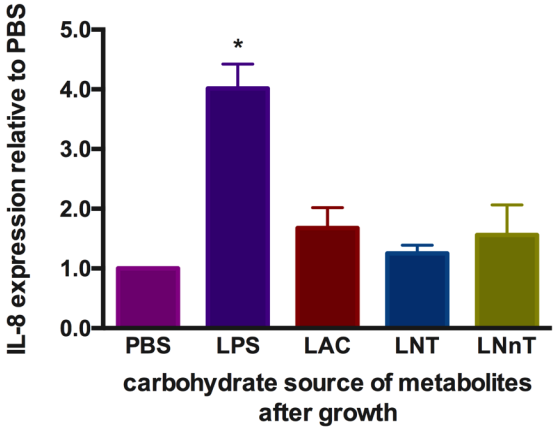

Figure 2.10 Gene expression of inflammatory marker Interleukin-8 in Caco-2 epithelial cells exposed to spent media following milk oligosaccharide fermentation. The y-axis represents the fold change in IL-8 expression relative to phosphate buffer solution (PBS). The x-axis depicts the sources of *B. infantis* metabolites which are used to treat Caco-2 cells after lipopolysaccharides (LPS) induction. The error bars show standard deviations of biological duplicates, each measured with three technical replicates. The single asterisks (*) indicate the significant differences evaluated by one-way ANOVA and Tukey's multiple comparison ($p<0.05$).

CHAPTER 3

BIFIDOBACTERIUM INFANTIS UTILIZATION OF POOLED HUMAN MILK OLIGOSACCHARIDES IS STRUCTURE AND STRAIN SPECIFIC

Ezgi Özcan[1], Apichaya Bunyatratchata[2], Daniela Barile[2], and David A. Sela[1,3,4]

[1]Department of Food Science, University of Massachusetts, Amherst, MA

[2]Department of Food Science and Technology, University of California, Davis, CA

[3]Department of Microbiology, University of Massachusetts Amherst, MA

[4]Department of Microbiology & Physiological Systems and Center for Microbiome Research, University of Massachusetts Medical School, Worcester, MA.

3.1 Introduction

Human milk contains host-indigestible oligosaccharides at high concentrations (5–20 g/l) [175] which are often utilized for energy and metabolite production by the infant gut microbiome, specifically bifidobacteria [9, 225, 226]. These oligosaccharides enhance bifidobacterial fitness to establish representation relative to competing genera [183]. *Bifidobacterium longum* subsp. *infantis* (*B. infantis*) is a special member of infant gut microbiome with a 43-kb gene cluster that lead the utilization of human milk oligosaccharides (HMOs)[11]. The *B. longum* subsp. *infantis* ATCC 15697 genome features five distinct gene clusters with the predicted capacity to bind, cleave, and import milk oligosaccharides. These contain solute binding proteins, ABC permeases, and glycosyl hydrolases such as fucosidases and sialysidases which are active for respective

HMOs utilization [45, 186, 187, 197, 199, 227, 228]. Importantly, solute binding proteins and ABC permeases, a transport mechanism for *B. infantis* to recognize oligosaccharides and transport them inside the cells in their intact form [45, 229]. Previous comparative genomic hybridizations (CGHs) were used to associate genotypic biomarkers among *B. longum* strains exhibiting various HMO utilization phenotypes and host associations [197]. Interestingly, *B. infantis* UMA299 (JCM 1260) misses two F1SBP transporter genes (Blon_2344 and Blon_2351) in its HMO catabolic cluster [197]. The missing transporters might contribute to the inefficient metabolism of HMOs, especially LNT and LNnT [229, 230]. Additionally, not all the types of HMOs are utilized at the same rate by *B. infantis*.

Previously, we interrogated four *B. infantis* strains for their ability to utilize LNT and LNnT [229]. Multilocus sequence typing provided taxonomic subspecies designations and grouped the strains between *B. infantis* [197]. Therefore, we chose the strains according to their distance to ATCC 15697. We observed that *B. infantis* strains deployed differential mechanisms on the human milk tetrasaccharides determined by growth and metabolite production. In this study, we interrogate same strains for their strain-dependent utilization of pooled HMO followed by growth, glycoprofiling, and metabolite production. Metabolite production shows us the efficiency of the energy metabolism during utilization of HMOs whereas glycoprofiling allows us to display which type of HMOs from pooled donors are utilized or preferred by each *B. infantis* strains.

3.2 Materials and Methods

3.2.1 Bacterial strains and propagation

Bifidobacterium longum subsp. *infantis* strains ATCC 15697, UMA299, UMA300 and UMA301 were propagated in De Man Rogosa Sharp (MRS, BD Difco, Sparks, MD)

medium supplemented with 0.05 % (wt/v) L-cysteine hydrochloride (Acros Organics, New Jersey, USA) [201] at 37° C under anaerobic conditions (Coy Laboratory Products, Grass Lake, MI). Bacterial strains were routinely verified as described previously [229].

3.2.2 Microplate growth assay

Growth phenotypes were evaluated in a 96-well plate using microplate reader. Overnight cultures were inoculated 1% (v/v) to modified MRS media (mMRS; a defined carbohydrate substrate and no acetate). Pooled HMO, LNT and LNnT (Glycom, Denmark) and 2´FL (donated from Mills Lab at UC Davis) were used at a final concentration of 2 % (wt/v) as the sole carbon source. Carbohydrate sources were incorporated into culture media in non-limiting concentrations. The growth assay was conducted anaerobically at 37 °C for 48 h by assessing optical density at 600 nm (OD_{600nm}) in an automated PowerWave HT microplate spectrophotometer (BioTek Instruments, Inc. Winooski, VT) placed within the anaerobic chamber. Each strain was evaluated in biological triplicates with three technical replicates. Inoculated mMRS media in the absence of carbohydrate substrates and in the presence of lactose were served as the negative and positive control, respectively. Growth kinetics were calculated using growthcurver package in R [231].

3.2.3 Analysis of human milk oligosaccharides (HMO) by Nano-LC Chip Q-TOF MS

The diluted and purified HMO were analyzed by an Agilent 6520 accurate-mass Quadrupole-Time-of-Flight (Q-TOF)-LC/MS with a microfluidic nano-electrospray chip (Agilent Technologies, Santa Clara, CA, USA). Oligosaccharides were separated by a HPLC-chip with a 40-nL enrichment column and a 43-mm x 75μm analytical column, both packed with 5μm graphitized carbon. The system composed of a capillary pump with a flow rate of 4.0μL/min and a nanopump with a flow rate of 0.3μl/min. Both systems use

binary solvent: 3% ACN, 0.1% formic acid in water (A) and 90% ACN, 0.1% formic acid in water (B). Two microliters of samples were carried by capillary pump with isocratic 100% solvent A (0%B). HMO separation and elution was performed by nanopump with 65 mins binary gradient followed the program: 0–2.5 min (0% B), 2.5–20 min (0–16% B), 20–30 min,(16–44% B), 30–35 min (44–100% B), 35–45 min (100% B), 45–45.01 min (100-0% B), 45.01-65 min (0% B). Data were acquired within the mass range of 450-2500 m/z in positive ionization mode with an acquisition rate of 1 spectra/s. An internal calibration ion was performed using 922.009798 and 1221.990637 m/z for continual mass calibration (ESI-TOF Tuning Mix G1969-85000, Agilent Technologies, Santa Clara, CA, USA). For Tandem MS (MS/MS), the spectra were acquired with MS/MS scan 100-2500 m/z with acquisition rate of 1 spectra/s. The collision energy was set at 1.3V/100Da with an offset of -3.5V.

3.2.4 Human milk oligosaccharides (HMO) identification

HMO were identified using the Find Compounds by Formula function of Mass Hunter Qualitative Analysis Version B.07.00 (Agilent Technologies, Santa Clara, CA). The function matched oligosaccharide masses in the positive control sample with the human milk library [177, 232] using a mass error tolerance of 20 ppm. The oligosaccharides were extracted with minimum peak height of 1000 counts and allowing charge state of +1-2. The compositions of each identified oligosaccharides were confirmed by Tandem MS and only confirmed HMO structures were selected to created HMO sample library with specific mass and retention time. Any HMO in the positive control sample that were not previously identified by Find Compounds by Formula function but were structurally confirmed by Tandem MS were also included in the HMO sample library. This

library was used in MassHunter Profinder Version B.08.00 (Agilent Technologies, Santa Clara, CA, USA) as an input library for peak integration.

The individual peaks of HMO in each sample were automatically integrated using the Batch Targeted Feature Extractor from MassHunter Profinder Version B.08.00 (Agilent Technologies, Santa Clara, CA, USA). The software matched the confirmed HMO mass and their retention time from the HMO sample library with the MS data automated integration the peak with mass tolerance of 20ppm and allowed charge stage of +1-2. All integrated peaks were manually checked and reintegrated for any incorrect integration.

3.2.5 Characterization of microbial fermentative end products

End products from bacterial fermentation were quantitated by HPLC. Bacterial strains were initially propagated as described above. Cell-free supernatants from microplate growths were obtained at stationary phase and filtered through a 0.22 μm filter (Sartorius Corp, Bohemia, NY) following centrifugation and stored at -20° C until further analysis. Organic acids were quantified using an Agilent 1260 Infinity HPLC system (Agilent Technologies, Santa Clara, CA) equipped with a Wyatt Optilab T-rEX refractive-index detector (Wyatt Technology Corp., Santa Barbara, CA). Separation was carried out using an Aminex HPX-87H column (7.8 mm ID x 300 mm, Bio Rad Laboratories, Hercules, CA) at 30° C in a mobile phase of 5 mM H_2SO_4 at flow rate of 0.6 ml/min with 20 μl of injection volume. Standards including organic acids (i.e. acetic acid, lactic acid, formic acid), ethanol, 1,2-propanediol and carbohydrates (i.e. glucose, galactose, lactose, GlcNAc, fucose) were acquired from Sigma-Aldrich Co. (St. Louis, MO). Metabolite concentrations were calculated from standard curves derived from external standards for seven concentrations (0.1, 0.5, 1, 5, 10, 20 and 50 mM). Metabolite profiling was carried

out in triplicate and each measurement was performed in duplicate. The metabolite profiling for each strain were analyzed using MetaboAnalyst 3.0 (http://www.metaboanalyst.ca)[206].

3.2.6 Enzyme Assay

The enzymatic assay was performed to determine the localization of the enzymes β-galactosidase, β-N-acetylhexosaminidase, and α-L-fucosidase. Bifidobacterial cells were grown in MRS overnight and harvested by centrifugation at 16, 000 x g for 2 min. The pelleted cells were resuspended in 50mM sodium phosphate buffer (pH 7.0). Extracts were separated in two and cell free extracts were obtained through beadbeating at 5.5 m/sec for 30 seconds twice using FastPrep 24 (MP Biomedicals, Santa Ana, CA). This was done to separate cytoplasmic fraction from the cell walls. Each fraction (50 µl) was incubated with 1mM substrate (250 µl) in 50 mM sodium phosphate buffer at 37° C for 30 min in 1.5 ml centrifuge tubes. The substrates used were 4-nitrophenyl-N-acetyl- β-D-glucosaminide, 2-nitrophenyl-N-β-D-galactopyranoside, 2-chloro-4-nitrophenyl-α-L-fucopyranoside. The reaction was stopped by adding 300 µl of 1 M Na_2CO_3. The amount of released 4-nitrophenol were determined by measuring the absorbance at 405 nm in a microplate reader (BioTek Instruments, Inc. Winooski, VT). When lactose, LNT, LNnT, HMO and 2´-fucosyllactose were used as the substrates, the reaction terminated by heating 95° C for 5 min. The released monosaccharides were visualized by HPLC as described above.

3.3 Results

3.3.1 *B. infantis* strains differentially grow on pooled HMO

The most vigorous growth was observed in UMA301 with 0.62±0.08 of $OD_{600nm,\ asym}$ followed by ATCC 15697 with 0.55±0.06 and UMA299 with 0.49±0.04 (Figure 3.1A,

p>0.05). A significantly lesser growth observed in UMA300 with 0.34±0.05 of $OD_{600nm, asym}$. Similarly, concordance with the final biomass, growth rate was significantly lower in UMA300 (k=0.23±0.02 h^{-1}, Table A3.1, p<0.05). As expected significantly higher growth rate occur in type strain ATCC 15697 (k=0.78±0.05 h^{-1}) followed by UMA301(0.63±0.01 h^{-1}) (Table A3.1, p<0.05). This indicates a clear adaptation to HMO utilization in ATCC 15697 than other strains.

3.3.2 *B. infantis* strains differentially consume human milk oligosaccharides

In total, 36 HMOs including isomers/anomers were monitored and structures were confirmed by Tandem MS. Total and individual HMO consumptions by four *B. infantis* strain were visualized in Figure 3.2 and 3.3. The total consumptions of HMO by ATCC15697 with 84.0±1.3 % and UMA301 with 79.8±2.0 % were significantly higher compared to UMA299 and UMA300 (p<0.05, Figure 3.2). ATCC 15697 and UMA301 consumed all lacto-N-(neo)tetraose isomers effectively (Figure 3.3A), while smaller carbohydrates contained 2_1_0_0 structures consumed partially. ATCC15697 and UMA301 consumed all LNFP, LNDFH, FLNH, DFLNH isomers completely (Figure 3.3B). On the other hand, they partially consumed FL (2_0_1_0) and LDFT (3_1_2_0). The compounds contain only hexose and fucose did not seem to be consumed effectively by ATCC 15697 and UMA301 strains. It was observed that larger fucosylated HMOs were preferred over smaller ones. Sialylated HMOs were partially consumed by ATCC15697 and UMA301 (Figure 4.2B).

UMA299 and UMA300 showed very low consumption overall (Figure 3.2). This is expected due to their lower biomass and growth rate experienced in microplate. However, the identification of individual HMOs reveals that there seems to be an

accumulation of some compounds that lead to the low consumptionn. The accumulation was observed in some of neutral HMOs, some of fucosylated compounds, and all sialylated HMOs (Negative consumption means that the area of that respective compound in bacterial fermentation samples is higher than that in pre-fermentation samples, data not shown). UMA299 and UMA300 did not consume all lacto-N-(neo)tetraose isomers as effective as other two strains (Figure 3.3A, $p<0.05$). This is consistent with previous results for UMA299 as it utilizes LNT and LNnT inefficiently. Interestingly, UMA300 was previously shown to utilize both LNT and LNnT effectively whereas it did not consume them effectively in pooled HMOs. This might be due to its higher preference towards other compounds. Nevertheless, main effect analysis showed that UMA299 and UMA300 consumes neutral HMO different than each other ($p<0.05$). UMA300 showed an accumulation in 3 of trisaccharide neutral HMOs and a $Hexose_2HexNAc_2$, whereas UMA299 was effectively utilizing $Hexose_2HexNAc_2$.

UMA299 consumed all fucosyllactose isomers (2_0_1_0) and LDFT (3_1_2_0) and only 2 of 5 lacto-N-fucopentaose (LNFP) isomers (3_1_1_0). UMA299 did not consume lacto-N-difucohexaose (LNDFH) isomers which were accumulated in the supernatants. On the other hand, UMA300 only consumed one isomer of fucosyllactose, 3 of 5 lacto-N-fucopentaose (LNFP) isomers (3_1_1_0), all isomers of FLNH and DFLNH. The linkage difference between the isomers might prevent them from consuming one or the others. The consumption of sialylated HMOs showed that UMA299 and UMA300 displayed an accumulation of all identified compounds (Figure 3.3C).

3.3.3 Secretion of carbon metabolites alter among four *B. infantis* strains during pooled HMO consumption

The secreted metabolites through fructose-6-phosphate phosphoketolase (F6PPK) pathway were shown in Figure 3.4. Lactic acid, acetic acid and formic acid were secreted constitutively but variably among strains. Ethanol concentration were incomparable due to ethanol existences in pre-fermentation HMO samples. ATCC15697 and UMA301 highly secreted lactic acid (23.19±0.15 mM and 26.49±1.26) and acetic acid (40.10±0.78mM and 43.99±1.59 mM) (Figure A3.1 and Figure 3.4A). Lactic acid concentrations for both strains were significantly higher than UMA299 ($p<0.05$). UMA301 also showed significantly higher acetic acid concentrations than UMA299 and UMA300 ($p<0.05$). On the other hand, UMA299 showed significantly higher concentrations of formic acid (6.80±0.91 mM) than ATCC15697 (4.16±1.17 mM) and UMA300 (3.42±0.94 mM) (Figure A3.1, $p<0.05$). In addition, the metabolite secretion in UMA299 while utilizing pooled HMOs was clustered differently than other strains while the others showed similar phenotypes (Figure 3.4A).

The theoretical ratio of acetic acid to lactic acid in hexose fermentation through F6PPK pathway is 1.5. The Figure 3.4B shows the acetic acid to lactic acid ratio after pooled HMO consumption. The theoretical ratio was reached in UMA300 with the ratio of 1.56±0.02 and it was significantly lower than other strains ($p<0.05$). This is interesting that UMA300 also produced lower concentrations of formic acid. The highest ratio was observed in UMA299 with 1.95±0.03. UMA301 and ATCC15697 showed similarity to each other but higher ratio than their corresponding lactose control (data not shown). Pooled HMO fermentation revealed shift in central metabolism and resulted in increase in the ratio of acetic acid to lactic acid.

Additionally, secretion of 1,2-propanediol (1,2PD) was observed in all strains. This metabolite is expected in fucose degradation which is not utilized by F6PPK. Interestingly, B. infantis does not possess genes required for production of 1,2PD, instead the genes possessed leads to the production of lactate and pyruvate. In our study, we observed smaller amounts of 1,2-propanediol after fermentation of pooled HMOs, indicating a more complex utilization of fucosylated compounds. UMA299 showed significantly higher concentrations of 1,2PD than other strains (7.76±0.48 mM, $p<0.05$, Figure A3.1). In order to see the significance of 1,2PD to fucosylated HMOs utilization, we checked lactose samples and no 1,2PD was observed.

3.3.4 Utilization of 2´-fucosyllactose among four *B. infantis* strains leads 1,2-propanediol production

We observed a differential utilization of 2´FL in pooled HMOs and its differential utilization within the HMO species; therefore, we analyzed its utilization using pure compound by *B. infantis* strains. UMA299 showed higher growth in 2´-fucosyllactose (2´FL) with asymptotic OD_{600nm} of 0.79±0.08 which was significantly higher than ATCC 15697 with asymptotic OD_{600nm} of 0.41±0.11 (Figure 3.5A). UMA300 and UMA301 showed moderate growths. The growth rate of all strains did not significantly differ ($p>0.05$, Table A3.1).

The metabolite production for 2´FL was shown in Figure A3.2 and Figure 3.5B. All strains produced 1,2PD, acetic acid, lactic acid, formic acid and ethanol during consumption of 2´FL. UMA299 showed significantly higher concentrations of acetic acid (59.64±3,62 mM), lactic acid (29.14±1.86 mM), and 1,2PD (14.37±1.20 mM) compared to other strains ($p<0.05$) accompanied by low formic acid (11.67±0.91 mM) and ethanol

(4.24±0.24 mM) concentrations during the growth of 2´FL. This was consistent with its higher growth. This also led UMA299 cluster differently than other strains (Figure 3.5B). Consistent with the growth, inefficient utilization of 2´FL by ATCC 15697 revealed higher formic acid (19.94±0.82 mM) than both UMA299 and UMA301 ($p<0.05$), but lower lactic acid (8.89±2.43 mM), acetic acid (39.32±1.49 mM) concentrations ($p<0.05$). 1,2PD concentrations was similar with other strains except UM299. Similarly, UMA300 utilization of 2´FL yielded higher formic acid (19.99±0.91 mM) and ethanol (5.46±0.26 mM) production compared to UMA299 and UMA301 ($p <0.05$), but moderate acetic (47.11 ±1.29 mM) and lactic acid (13.27±1.32 mM) concentrations (Figure A3.2). This also led this strain to be clustered far from UMA301 and ATCC 15697 (Figure 3.5B). UMA301 showed significantly lower ethanol concentration (1.91±0.26 mM) than other strains ($p<0.05$).

Acetic acid to lactic acid ratio was shown in Figure A3.2F. 2´FL utilization showed higher ratio than their lactose control ($p<0.05$). UMA299 showed lower ratio of acetic acid and lactic acid with 2.05±0.02 consistent with high consumption. This was significantly lower than ATCC 15697 and UMA300. Highest ratio was observed in ATCC 15697 with 4.60±0.94 followed by UMA300 with 3.60±0.28. UMA 301 showed a ratio of 2.92±0.05.

3.3.5 Not the locations and but the activities of β-galactosidase, β-N-acetylhexosaminidase and α-fucosidase differ among *B. infantis* strains

Through glycoprofiling, we observed that there could be an accumulation on some individual HMOs. This led us to consider if this accumulation occurs extracellular activities of larger HMO compounds. We determined the localization of enzymes (intracellular vs extracellular) by incubating several substrates with whole cells and cell lysates. All *B.*

infantis strains possess both extracellular and intracellular β-galactosidase as we observed release of p-nitrophenol (pNp) (Figure 3.6). UMA300 showed the lowest enzymatic activity on all comparisons, although the cell densities were adjusted before the enzymatic assay. Although there were some nitrophenol amount released in the whole cell incubation with pNp-N-acetylglucosaminide, we count that as a background where all strains possess only intracellular β-N-acetylhexosaminidase. This indicated that the localization of enzymes did not differ among strains but the enzyme activity (the amount of nitrophenol released) differed. UMA299 released significantly higher amounts of nitrophenol ($p<0.05$) compared to other strains. We also confirmed these activities of the sugar release after fermentations of *B. infantis* strains cell-free lysates or whole cell with LNT, LNnT, 2´FL. ATCC 15697 lysates showed release of glucose, galactose and GlcNAc after incubation with 1mM LNT and LNnT (Figure A3.3). The chromatograms of whole cell ATCC 15697 incubation with LNT and LNnT showed very little amounts of glucose and galactose (Figure A3.3) but not GlcNAc. ATCC 15697 is known to utilize HMOs in their intact form due to intracellular β-galactosidase, β-N-acetylhexosaminidases. This might be due to the release of sugars after chopped intracellular but not extracellular degradation due to the osmosis balance in the cells. The lysates of UMA300 incubation with LNT and LNnT showed a release of galactose and GlcNAc but not glucose. The whole cell incubation of UMA300 with LNT and LNnT did not show any released sugar.

3.4 Discussion

Following birth, microbes resides in the human gut where they create a commensal ecosystem. Combination of the dietary pattern and the genetic evolution of a microbe allow them to adapt the environment which they are living in. Microbial metabolic networks such

as carbon acquisition and assimilation establish the activities in the gut and determine the infant's wellness being as well. Bifidobacteria were known to be a representative member of the infant gut [233] and *B. infantis* was found to have an adaptive mechanism for human milk oligosaccharides which provides them advantage over residence in the gut [11, 234]. Human milk contains various prebiotics components that promote the growth of bifidobacteria [183]. The composition of oligosaccharides in human milk varies among individuals [235, 236] and this variety determines the composition of the microbes in the infant gut [237]. In addition, the genetic traits of species also determines the type of the strains to reside [197, 238].

B. infantis strains represent two different group in their ability to utilize human milk oligosaccharides (Albert et al, In preparation). For example, *B. infantis* UMA299 (JCM 1260) misses two F1SBP transporter genes (Blon_2344 and Blon_2351) in its HMO catabolic cluster [197]. In this study, we determine whether these genetic characteristics affect the utilization phenotype.

UMA299 grew moderately on the pooled HMOs. Although its total consumption of HMOs lower than 20 %, most of these were fucosylated compounds with DP=3 and 4. Its capacity with missing two transporters explains its inefficient utilization of pooled HMOs and LNT and LNnT [229]. The two solute binding proteins Blon_2344 and Blon_2351 resides next to sialidases and hexosaminidases. This coincides that this strain showed no utilization of sialylated HMOs and limited utilization of neutral HMOs. However, fucosylated HMOs might require different set of transport mechanism that UMA299 likely to deploy and able to grow on these compounds. The ability of UMA299 grown on fucosylated compounds was also confirmed by its efficient growth on pure 2´FL.

In both pooled HMO metabolism and 2´FL metabolism, this strain produced significantly higher amounts of 1,2PD, which was suggested to be a metabolite for fucose metabolism [239]. Although *B. infantis* did not have the genes necessary for this metabolite to be produced [239], we observed the presence of 1,2PD, which might need for further investigation for the mechanisms deployed and the preference of this strain on the fucosylated compounds in pooled HMOs.

Interestingly, UMA300 does not utilize pooled HMO efficiently, however, our previous results showed that this strain used both LNT and LNnT to high concentrations [229]. This might be due to the preference of other HMO types for carbohydrate and energy assimilation for this strain. UMA300 showed up to 100 % utilization of fucosylated HMOs with DPs over 5. It consumes moderately fucosylated lactose in both pooled HMOs and pure 2´FL.

Generally, we observed that inefficient utilization of carbohydrates leads formic acid formation and lower acetic acid to lactic acid ratio in *B. infantis* metabolism. However, although UMA300 did not utilize pooled HMOs efficiently, its metabolism contradicts with our previous observations. In contrast to its other phylogenetically relative neighbors, this strain does not follow that hypothesis. This is of importance to further investigate whether this strain possesses genes to produce formic acid. Interestingly, 2´FL metabolism leads to higher formic acid production and acetic acid to lactic acid ratio in UMA300. This means that phenotype related to formic acid production is not related to the genetic predisposition, it might be related to the phenotypic response. It is still unclear what regulates for strains to deploy higher formic acid production.

ATCC 15697 and UMA301 (JCM7007) are phylogenetically close to each other [197]. Our previous results on pure LNT and LNnT growths and corresponding metabolic activity showed that these strains deploys similar growth and metabolic phenotype [229]. This was consistent with our observations in growth on pooled HMOs and metabolic end production in this study. They also deployed similar utilization profiles with neutral and fucosylated HMOs glycoprofiling in this study. However, they were different on utilizing sialylated HMOs with DP=3. Although they showed similar growth pattern in pure 2´FL, the metabolite production differed between these strains. Ethanol, lactic acid, formic acid production showed significantly different concentrations between these two strains as well as the acetic acid to lactic acid ratio. In addition, the amount of nitrophenyl produced during enzymatic assay was also different on both N-acetyl-glucosaminide and galactopyronoside.

In conclusion, the strain-dependent utilization of pooled HMO is deployed to be determined by growth, glycoprofiling, and metabolite production. However, the specific genes and mechanism involved in the metabolism of HMOs needs to be investigated; on the other hand, we can identify the strain-dependent variances in HMO utilization in genomic and functional level.

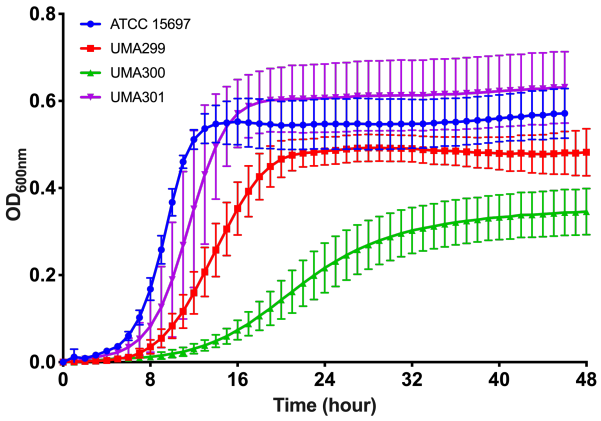

Figure 3.1 *Bifidobacterium infantis* growth while utilizing pooled human milk oligosaccharides. Growth curves of *Bifidobacterium infantis* ATCC 15697, UMA299, UMA300 and UMA301 on modified MRS containing 2 % (w/v) pooled human milk oligosaccharides. The curves are drawn from average of three independent experiments.

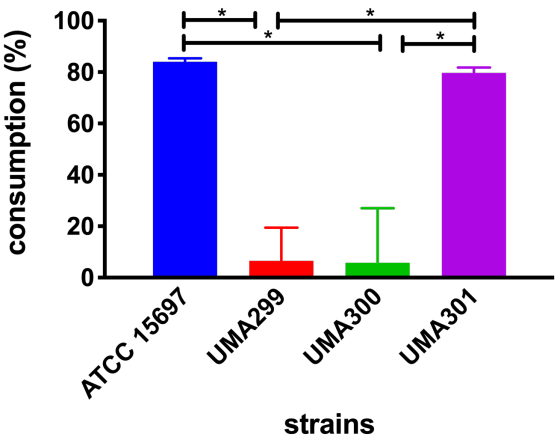

Figure 3.2 Total HMO consumption glycoprofiling for *B. longum* subsp. *infantis* strains. Total HMO abundance was represented as the normalized percent consumption of total HMO. The total HMO area are normalized by area of internal standard. The percent consumption was calculated by the difference between the normalized area of post-fermentation samples and pre-fermentation samples divided by area of the pre-fermentation samples. Averages from independent biological triplicates are shown with bars representing standard deviations of the means. A single asterisk (*) denotes significant differences between strains evaluated by one-way ANOVA and Tukey's multiple comparison test ($p<0.05$).

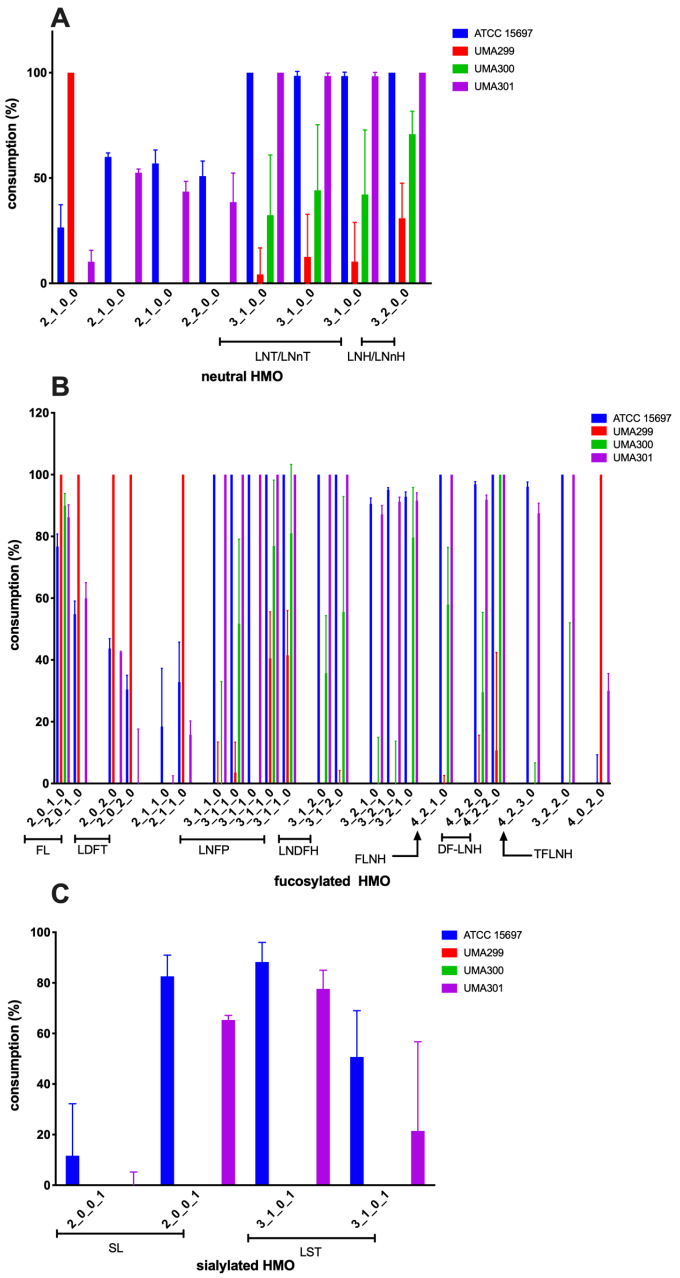

Figure 3.3 Total HMO consumption glycoprofiling for *B. longum* subsp. *infantis* strains. Individual HMO (A) neutral HMOs (B) fucosylated HMOs and (C) sialylated HMOs abundance was represented as the normalized percent consumption. The individual HMO area are normalized by area of internal standard. The percent consumption was calculated by the difference between the normalized area of post-fermentation samples and pre-fermentation samples divided by area of the pre-fermentation samples. Negative consumption values are cut from the y-axis. Averages from independent biological triplicates are shown with bars representing standard deviations of the means.

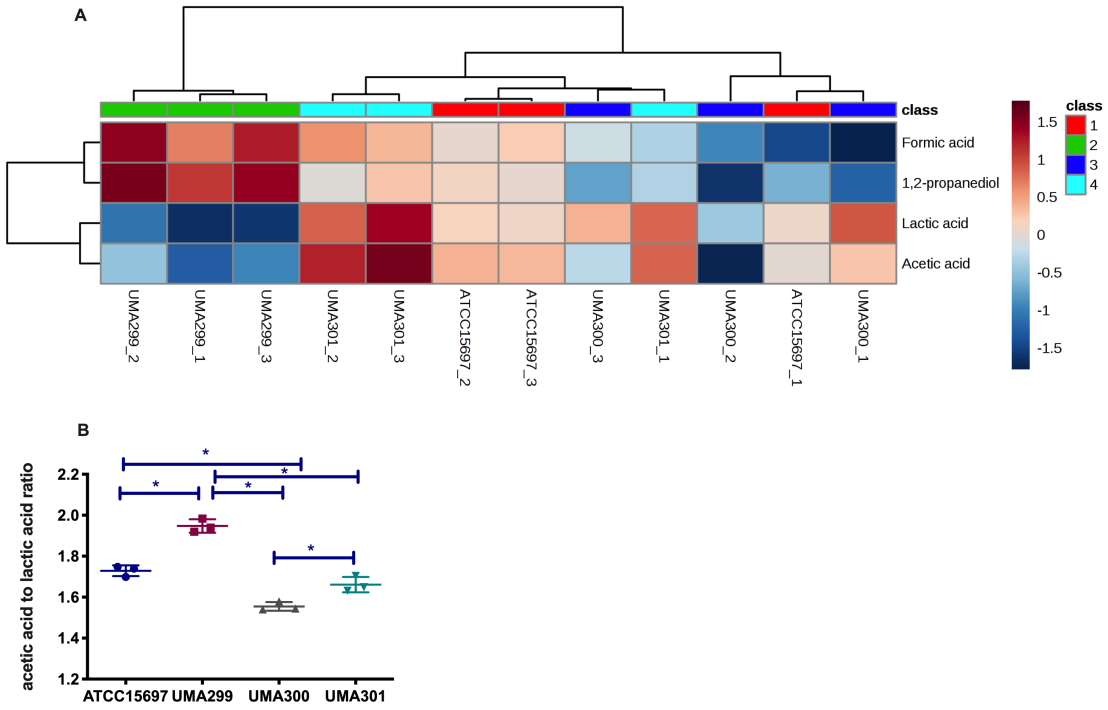

Figure 3.4 Analysis of *B. longum* subsp *infantis* strains secreted fermentative endproducts while utilizing pooled human milk oligosaccharides. Panel (A) denote metabolites secreted by *B. infantis* strains clustered by Euclidean distance calculated with MetaboAnalyst 3.0. The scaling was performed by mean-centering and dividing by the standard deviation of each metabolite. The red denotes higher concentrations of the metabolite with blue approaching lower concentrations. Panel (B) represents acetic acid to lactic acid ratio of *B. infantis* ATCC15697 growing on mMRS medium containing 2% (wt/v) human milk oligosaccharides. Averages from independent biological triplicates are shown with bars representing standard deviations of the means. A single asterisk (*) denotes significant differences between strains evaluated by one-way ANOVA and Tukey's multiple comparison test ($p<0.05$).

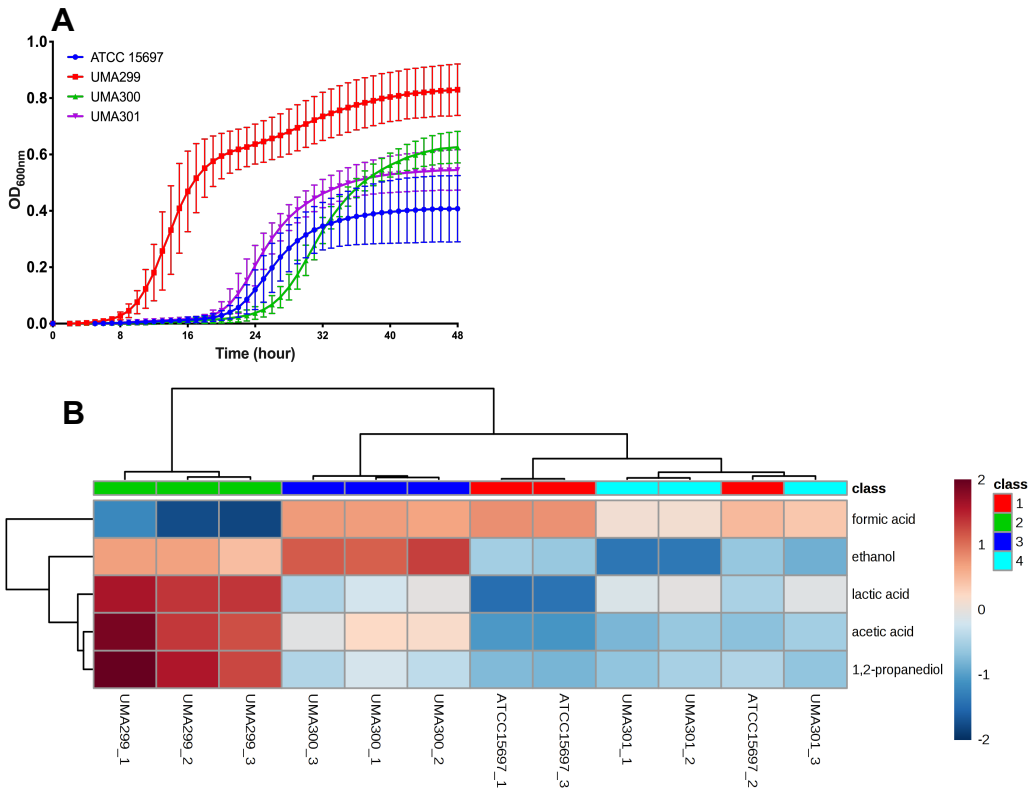

Figure 3.5 Analysis of *B. longum* subsp *infantis* strains while utilizing pooled 2´-fucosyllactose. (A) Growth curves of *Bifidobacterium infantis* ATCC 15697, UMA299, UMA300 and UMA301 on modified MRS containing 2 % (w/v) 2´-fucosyllactose. The curves are drawn from average of three independent experiments. (B) metabolites secreted by *B. infantis* strains clustered by Euclidean distance calculated with MetaboAnalyst 3.0. The scaling was performed by mean-centering and dividing by the standard deviation of each metabolite. The red denotes higher concentrations of the metabolite with blue approaching lower concentrations.

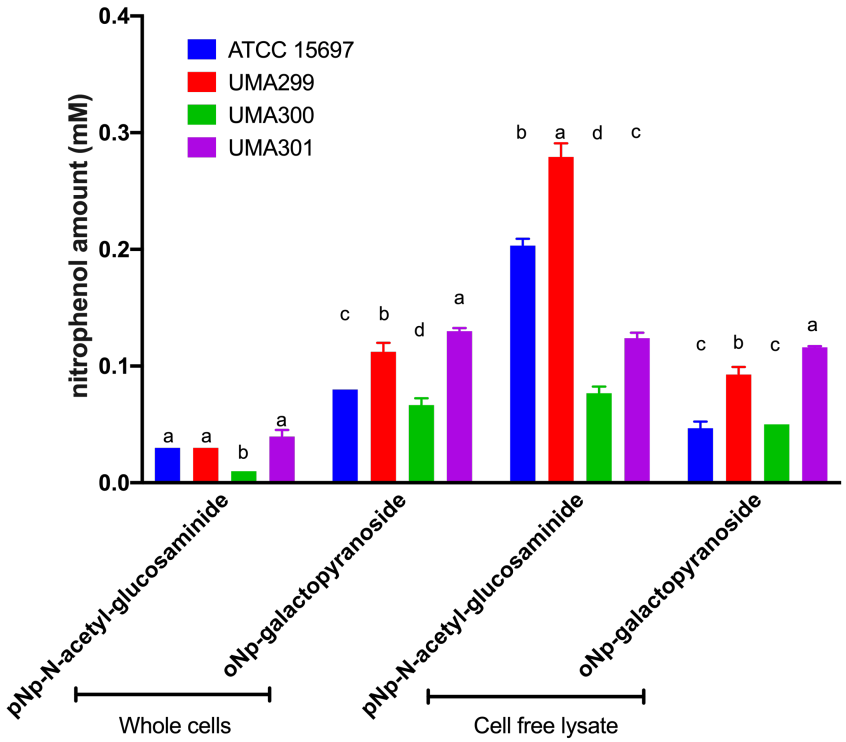

Figure 3.6 Enzyme assay of *B. longum* subsp. *infantis* strains. The nitrophenol amounts represented as millimolar were produced after *p*-nitrophenol-N-acetyl-glucosaminide and *o*-nitrophenol-galactopyronoside fermentation of whole cells and cell-free lysates of *Bifidobacterium infantis* ATCC 15697, UMA299, UMA300 and UMA301. Averages from independent biological triplicates are shown with bars representing standard deviations of the means. Letters denote the significant differences between strains evaluated by one-way ANOVA and Tukey's multiple comparison test ($p<0.05$).

CHAPTER 4

MICROBE-MICROBE INTERACTIONS DURING HUMAN MILK OLIGOSACCHARIDES UTILIZATION DIFFER WITHIN MODELED INFANT GUT MICROBIOMES

Ezgi Özcan[1], Margaret Hilliard[1,2], Shuqi Li[1], Michelle Rozycki[1] and David A. Sela[1,3,4]

[1]Department of Food Science, University of Massachusetts, Amherst, MA

[2]Organismic and Evolutionary Biology Graduate Program, University of Massachusetts, Amherst, MA

[3]Department of Microbiology, University of Massachusetts Amherst, MA

[4]Department of Microbiology & Physiological Systems and Center for Microbiome Research, University of Massachusetts Medical School, Worcester, MA.

4.1 Introduction

Human milk contains high concentrations of indigestible oligosaccharides, as well as other nutritive molecules that promote growth early in life [171, 175]. These oligosaccharides are not digested by the infant; however, they are utilized by commensal gut microbiota such as bifidobacteria. Tetrasaccharides lacto-N-tetraose (LNT) and lacto-N-neotetraose (LNnT) are highly abundant oligosaccharides in human milk. These isomers are identical aside from a glycosidic linkage (i.e., β1-3 vs. β1-4), which leads to the hypothesis that this dissimilarity might reveal differences in microbial physiology. We previously investigated this phenomenon for *Bifidobacterium longum* subsp. *infantis* type

strain ATCC 15697 supported by growth phenotype, microbial fermentative metabolite production and comparative transcriptome analysis [229].

The utilization of pooled and individual oligosaccharides by pure cultures of gut microbiome members was previously investigated [186, 200, 212, 220, 240–242]. However, the metabolic activity driven by this utilization was not clearly underlined. Gut microbes produce metabolites sequestered by the host, including short chain fatty acids (SCFAs) [49, 75, 77, 243]. They compete for food, with metabolites secreted by one member often utilized by a secondary microbial population [74]. Adaptation of *B. infantis* to grow on human milk oligosaccharides (HMOs) might reveal interactions with microbes in the infant gut which do not possess capacity to utilize HMOs. For instance, some bacteria require formate for acetogenesis and butyrate and acetate as the fermentative end products [244]. Bacteria that utilize lactic acid may also convert lactate to butyrate [245]. The gut microbiome also harbors acetate converting bacteria that produces butyrate [246]. These activities simultaneously occur during digestion of dietary oligosaccharides. These cross-feeding activities between the two members of the gut microbial community have also been investigated in their response to dietary oligosaccharides [240, 247–250]. However, these are limited to few species. The interactions of the complex communities are still of interest. Previously, dietary oligosaccharides were tested for their capacity to manipulate microbial interactions in the *in vitro* batch culture models [52, 251] as well as the human milk oligosaccharides [51, 252–254].

B. infantis utilizes HMOs in their intact form and produce metabolites. Therefore, during microbe-microbe interactions, if their adaptation for HMO utilization provides domination over other microbes, those microbes will not consume degradant products but

rather the metabolites to survive. The difference between the metabolite profile will manipulate the community structure. *B. infantis* mainly produces acetate and lactate; however, we showed that inefficient utilization of HMOs results in production of formate by *B. infantis* strains [229].

Not much is known about formate production and its role in the intestine. It has been previously shown that formate concentrations in the gut were elevated during inflammation-associated dysbiosis and this led a fitness of formate utilizing *E.coli* in the gut, which requires oxygen respiration [255]. *In vitro* models simulating microbe-microbe interactions allow us to identify networks of metabolic pathways in the intestine with their simultaneous interaction with dietary oligosaccharides. The microbe-microbe interactions give signatures for metabolic dysbiosis in the gut during the administration of dietary oligosaccharides.

In this chapter, we investigate the microbe-microbe interaction during simultaneous digestion of human milk tetrasaccharides (LNT and LNnT) within a modeled microbial community derived from fecal samples from nursing infants. This chapter follows the findings and questions regarding differential utilization of tetrasaccharides by *B. infantis* and its effects in the gut microbial interactions. We chose a model that would best accommodate our needs for investigation of microbe-microbe interactions in given conditions.

4.2 Materials and Methods

4.2.1 Preparation of fecal derived communities

The diapers from two infant donors were collected from week one to five and saved in biohazard bags containing oxygen absorber packs (FreshUS, Brea CA) and stored at -

20°C by mothers until transportation. The fecal samples were transported to the laboratory with ice packs. A piece from the diapers was cut and suspended in 1:1 (v/v) 10X phosphate buffered saline (0.1M, containing 0.05 % L-cysteine.HCl (Across Organics, UK) : 20 % glycerol solution to make a final glycerol concentration of 10% (a standard glycerol concentration used for fecal transplants (Hamilton et al., 2012)). The piece was then squeezed into the solution using a tongue depressor, and then discarded after a slurry formed. The fecal slurries were then aliquoted into cryo vials and stored at −80ºC until the experiments were conducted. The day before inoculation into bioreactors, fecal glycerol stocks were thawed, and samples were pooled (30 ul) and inoculated into colon media with lactose (1 % w/v). The fecal derived microbial communities were then incubated at 37ºC under anaerobic conditions (Coy Laboratory Products, Grass Lake, MI). This step was performed to satisfy enough bacterial density before inoculation into bioreactors.

In addition to fecal derived microbial communities, *Bifidobacterium longum* subsp. *infantis* ATCC 15697 (*B. infantis*) was incubated in De Man Rogosa Sharp (MRS, Oxoid, Hampshire, England) medium supplemented with 0.05% (wt/v) L-cysteine (Sigma-Aldrich, St. Louis, MO) at 37 ºC under anaerobic conditions (Coy Laboratory Products, Grass Lake, MI). The day before the inoculation into bioreactors, overnight grown cultures in MRS broth were conditioned to the colon media with lactose (1 % w/v) and incubated under same conditions overnight.

The fecal slurries were formed from the two infant diapers and were used in fermentations. In addition, the fecal communities were mixed with equal volumes of *B. infantis* and used for fermentations. In total, 4 different communities were tested in their ability to ferment lactose, LNT and LNnT.

4.2.2 Colon media composition

The colon media was prepared as described previously [252] and modified accordingly. The media consist of 0.5 g/l bile salts (Oxoid), 2 g/l peptone water (Fluka), 2 g/l yeast extract (Sigma-Aldrich), 0.1 g/l NaCl (Fisher Chemicals), 0.04 g/l K_2HPO_4 (Fisher Chemicals), 0.01 g/l $MgSO_4 \times 7H_2O$ (Sigma), 0.01 g/l $CaCl_2 \times 6H_2O$(sigma), 2 g/l $NaHCO_3$ (Sigma-Aldrich), 0.5 g/l L-Cysteine.HCl (Acros Organics) and Tween-80 2 ml (Sigma-Aldrich). Hemin (Sigma-Aldrich) was autoclaved separately by dissolving 2 mg/ml in 0.5 M NaOH and mixed with colon media at the final concentration of 0.002 g/l. Similarly, Vitamin K_1 (Sigma-Aldrich) was added to colon media after autoclaving at the final concentration 10 μl/l.

For the bioreactors, 400 ml freshly prepared media was supplemented with 4 g of lactose, lacto-*N*-tetraose (LNT) and lacto-*N*-neotetraose (LNnT) to make 1 % (w/v) of carbohydrate source necessary for fermentations. Then, the prepared media was filtered by using sterile bottle top filters (PES membrane, 0.22 μm, CellTreat) and aseptically fed into already autoclaved bioreactor vessels.

4.2.3 In vitro fermentations

An Eppendorf DASGIP MP-8 4 vessel bioreactor system for *in vitro* microbial community fermentations was used. The three bioreactors containing in-place pH (Hamilton Company, Reno, NV), Redox (Hamilton Company, Reno, NV) and Optical Density (Exner Process Equipment GmbH, Etllingen, Germany) probes were autoclaved at 121 ºC for 15 min. After they were filled with media, the vessels were mounted onto the DASGIP reactor base. Then, the vessels were flushed with gas mix (85% N_2, 10 % CO_2, 5 %H_2) at a constant rate of 25 l/h overnight and the temperature was set to 37 °C and pH

was maintained at 6.8 by addition of 4M NaOH. The pumps were designed to feed the vessels at a rate according to value of pH. The overnight grown microbiome culture obtained from baby fecal samples (4 ml) with or without addition of *B. infantis* ATCC 15697 (4 ml) were inoculated into the parallel reactor vessels containing lactose, LNT, or LNnT. 3 ml of sample was taken at hour 0, 4, 6 (only lactose), 8, 12, 14 (only LNT and LNnT), 16, 18 (only LNT and LNnT), 20, 24, 30, 36, and 48. Samples from each reactor were aliquoted equally and centrifuged at 16,000 x g for 2 min. The supernatants were separated from the pellet and stored in -20 ºC until HPLC analysis. The pellets were dissolved in 1 ml Ambion RNAlater (Life Technologies, Carlsbad, CA) and stored in 4 ºC overnight, transferred into -80 ºC until DNA extraction.

4.2.4 Targeted fermentative end product profiling using HPLC

Cell-free supernatants stored in -20 ºC were filtered through a 0.22μm filter (Sartorius Corp, Bohemia, NY). Short chain fatty acids and lactic acid were quantified using an Agilent 1260 Infinity HPLC (Agilent Technologies, Santa Clara, CA) system equipped with a Wyatt Optilab T-rEX detector (Refractive Index detector, Wyatt Technology Corp, Santa Barbara, CA). Separation was carried out using an Aminex HPX-87H column (7.8mm ID × 300mm, Bio Rad Laboratories, Hercules, CA) at 30 ºC in a mobile phase of 5mM H_2SO_4 at flow rate of 0.6 ml/min with 20 μl of injection volume. Standards including organic acids (i.e., acetic acid, lactic acid, formic acid, propionic acid and butyric acid), ethanol, and carbohydrates (i.e., glucose, galactose, lactose, and N-acetylglucosamine) were acquired from Sigma-Aldrich Co. (St. Louis, MO). Metabolite concentrations were calculated from standard curves derived from external standards for six concentrations (0.1, 0.5, 1, 5, 10, 20, 50, and 100mM).

4.2.5 DNA extraction

The cell pellets in RNAlater were first washed twice with 1X PBS buffer to remove residual RNAlater and centrifuged at 12,000 × g for 2min. Then the samples were subjected to DNA extraction using DNeasy Powerlyzer PowerSoil (Qiagen, Germany) kit. Briefly, the samples were transferred into PowerBead tubes containing PowerBead solution and bead beaded at 4.5 m/sec for 45 sec twice with 5 min ice incubation in between cycles. The rest was followed according to the manufacturer's instructions. The DNA was eluted in 50 µl Tris buffer provided by the kit. DNA was stored -20 ºC until qPCR and library preparation.

4.2.6 Quantitative real time-PCR

The qRT-PCR was performed on a 7500 Fast Real-Time PCR System (Applied Biosystems, Singapore) with PowerUP SYBR Green Master Mix (Applied Biosystems, Foster City, CA) using 5 ng of input DNA. *Bifidobacterium infantis/longum* (BLIR) [204] specific primers were optimized for qPCR conditions by using FWD_BL_BI (5-[HEX]-AAAACGTCCATCCATCACA) and REV_BI (5-CGCCTCAGTTCTTTAATGT). The qPCR reaction run in fast cycling mode with 10 µl reaction volume with conditions as follows: 95 ºC for 2 min, 40 cycles of 95 ºC for 1 min, 54 ºC for 1 min, 72 ºC 30sec, followed by melting curve 95 ºC for 15 sec, 60 ºC for 1 min and 95 ºC for 15 sec.

4.2.7 16S profiling library preparation and data analysis

Purified DNA samples (1 to 50 ng total in up to 36 µl water) were used to PCR amplify the V4 region of the 16S rRNA provided by BiooScientific NEXTFlex™ 16S V4 Amplicon-Seq Kit 2.0 (PerkinElmer Company, BiooScientific Corporation, Austin, TX). The primers were developed by BiooScientific as 16S V4 Forward (5'-

GACGCTCTTCCGATCTTATGGTAATTGTGTGCCAGCMGCCGCGGTAA-3') and 16S V4 Reverse (5'-TGTGCTCTTCCGATCTAGTCAGTCAGCCGGACTACHVGGGTWTCTAAT-3'). PCR amplification was performed under following conditions: 95 °C for 4 min, 8 cycles of 95 °C for 30 s, 56 °C for 30 s, and 72 °C for 90 s, and 72 °C for 4 min. AMPure XP beads (Beckman Coulter, Danvers, MA, USA) were used to purify the PCR products free from primers and other contaminants. A second PCR was performed for barcoded indices and adaptors using the NEXTflex kit, followed by bead cleanup. Purified PCR products were quantified using the Qubit double-stranded DNA (dsDNA) High Sensitivity assay (Life Technologies, Carlsbad, CA, USA). The quality of PCR products was measured by High Sensitivity DNA ScreenTape assay on the TapeStation 2200 system (Agilent Technologies, Santa Clara, CA, USA). PCR products were pooled in equimolar concentration (0.5 nM). Sequencing was performed on an Illumina MiSeq platform (paired-end, MiSeq reagent kit v2, 30% Phi-X) at the Genomics Resource Laboratory, University of Massachusetts Amherst, MA.

Sequences of 16S rRNA gene amplicons of all 72 bioreactor samples were analyzed in QIIME2 (version 2018.8) [256]. Demultiplexed forward and reverse reads were input to dada2 method to denoise and dereplicate paired-end sequences as well as filter potential chimeras. Forward and reverse reads were truncated at base position 230 and 190 respectively due to the decrease in quality and reads with number of expected errors higher than 1.0 were discarded as a natural choice [257], the method used to remove chimeras was set to "pooled" and other parameters followed default [258]. Taxonomic annotations were assigned to denoised sequences by using a pre-trained Naïve Bayes classifier [259] based

on Greengenes database 13_8 release (99% OTUs, V4)[260] and the q2-feature-classifier plugin [261]. Reads were further filtered to remove mitochondria, chloroplast and the genus Shigella regarded as contamination. The amplicon sequence variant (ASV) table [262] was finally narrowed down to 48 features with total frequency of 537,276. Taxa bar plots of phylogenetic level 2 and level 6 were visualized online [263] and further edited and colored by GraphPad. In order to proceed to downstream phylogenetic diversity metrics, a rooted phylogenetic tree was generated through align-to-tree-mafft-fasttree pipeline from the q2-phylogeny plugin [264, 265]. The ASV table was rarefied [266]alpha and beta diversity analysis were conducted, with sampling depth 350, through the q2-diversity and q2-longitudinal (Bokulich N. a., 2017) plugins. Principal Coordinates Analysis (PCoA) plots were further downloaded and edited in Inkscape (version 0.92).

4.3 Results

4.3.1 Fermentation profile and conditions

The fermentations of lactose, LNT and LNnT in the bioreactor were monitored using optical density, pH and redox probes. The communities followed sigmoid growth curve in all fermentations (Figure A4.1). The decreased in pH during growth was maintained by addition of 4 M NaOH at most 3ml/min depending on pH. After growth reaches a plateau phase, NaOH feeding stopped and pH started to increase for all fermentations (Figure A4.1). Redox was stabilized around -300 and -400 before inoculation and after inoculation during growth, redox potential decreased over time (Figure A4.1); however, the flow rate kept constant for all fermentations.

4.3.2 Fecal derived microbiomes exhibit differential metabolite production

Regardless of *B. infantis* addition, the SCFA profiling between fecal derived microbiomes from 1st and 2nd baby differed from each other (Figure 4.1). In the 1st fecal microbiomes, lactate concentrations increased, then decreased after 24th h of fermentation and reached undetectable levels after 36th h (Figure 4.1A). *B. infantis* addition to the 1st microbiomes increased lactate production until 24th h of fermentation in LNT whereas it decreased in LNnT (Figure 4.1A). This shows that addition of *B. infantis* facilitated LNT fermentation by increasing the lactate production whereas it adversely affected LNnT fermentation. This is consistent with the hypothesis that *B. infantis* does not utilize LNnT efficiently and results in lower lactate concentrations as observed in pure cultures.

In the 2nd fecal microbiomes, lactate concentrations increased in the early hours of fermentation, then reached a plateau after the 12 hours of fermentation for lactose, 14 hour of fermentation for LNT, 18 hour of fermentation for LNnT (Figure 4.1B). Interestingly, LNnT fermentation by microbiomes 2 without *B. infantis* reached higher lactate concentrations compared to other substrates and addition of *B. infantis*. This coincides with microbiomes 1 considering the fact that *B. infantis* does not utilize LNnT efficiently that could have an adverse effect on fermentation profile. In LNT fermentation, addition of *B. infantis* slightly increased the lactate concentrations.

Acetate concentrations in the 1st microbiomes without *B. infantis* did not differ much between LNT and LNnT concentrations (Figure 4.1C). The concentrations increased over time and continued to increase at a slower rate after 24 h. This increase might indicate that there are other members of the fecal communities that might use other sources to

produce more acetic acid or they use acetate as an energy source therefore we did not observe a sharp increase.

In in the 2nd microbiomes, regardless of carbohydrate source and *B. infantis* addition, acetate concentrations reached to a plateau after 20 hours of fermentation (Figure 4.1D). This phenomenon might be explained if either there are no other sources leading production of acetate or utilization of acetate as a substrate is more prominent in fecal communities.

Formate is a metabolite occurring during *B. infantis* utilization of LNnT over LNT. It was previously indicated that formate was being produced during bifidobacterial fermentation with lower optical density [229]. The difference in formate production between human milk tetrasaccharides led us to that hypothesis which we argue that inefficient LNnT utilization of *B. infantis* with production of formate might change the microbiome structure with divergent metabolite profiling. In this bioreactor set up, we also saw that formate production in LNnT fermentation by 1st microbiomes with *B. infantis* addition reached to higher levels compared to that of LNT and LNnT fermentation by 1st microbiomes without *B. infantis* (Figure 4.1E). Then, there was a sudden decrease in their concentration after 16th hour. This means that formate was also utilized by other members of the microbiome.

Similarly, the addition of *B. infantis* into 2nd fecal derived microbiomes increased the formate production for LNnT fermentation (Figure 4.1F). *B. infantis* addition did not change the production of formate for LNT fermentation.

Regardless of fermentation, there was a decrease in formate concentrations for all fermentations. This means that formate was being utilized by the other members of the

fecal communities leading the production of other metabolites. Formate utilization might lead butyrate and acetate production by the acetogens [267]. However, in microbiomes 2, we did not observe butyrate production. This means that there are also other members involved in formate utilization that does not lead butyrate production.

The decrease after the 24th h in the lactate concentrations for all fermentation in 1st microbiomes indicates that there are other members of the community which are able to use lactic acid as an energy and carbon source and produce other metabolites i.e. butyric acid. During LNT and LNnT fermentations in fecal communities 1 without *B. infantis*, butyric acid production was observed after the 24 h of fermentation (Figure 4.1G). This coincides with the sudden drop at 24th in lactate concentrations. It was previously shown that lactate utilizing bacteria produce butyric acid as a major fermentative end product [245]. For 1st fecal microbiomes with *B. infantis* addition, we saw early increase in the butyrate concentrations, especially in LNnT fermentation (Figure 4.1G).

In the fecal microbiomes 2, there was no production of butyrate in any of the fermentations. This could be explained by the differences in the composition of the two fecal derived microbiomes used at the beginning, regardless of addition of *B. infantis*.

Another metabolite produced during fecal fermentations (that bifidobacteria cannot produce) is propionate. In the first baby microbiomes supplemented with *B. infantis* we observed propionate production at the 36th hour in LNT fermentation and 48th hour in LNnT fermentation (Figure 4.1H), whereas both HMO fermentation showed propionate at the 48th h of fermentation in fecal microbiomes 1 without *B. infantis*. In contrast to butyrate absence in fecal microbiomes 2, we observed propionate production in both HMO fermentation

regardless of *B. infantis* addition. However, the concentrations were lower compared to that of microbiomes 1 (data not shown).

Lactose was used as a control fermentation. The microbiome metabolite structure differed between the two inoculums (Figure A4.2). For microbiome 1, lactate concentration increased over time until 8-12 hour then reached a plateau and after 20th hour it decreased and reached non-detectable levels at the 30th hour (Figure A4.2A). This means it has been involved in other catabolic activities and this did not change whether *B. infantis* was added or not. In 2nd microbiomes, lactate levels reached at highest around 12 hour and then reached a plateau until the end of incubation (Figure A4.2B). The addition of *B. infantis* did not change the behavior of the microbiome community in presence of lactose.

In lactose fermentation, acetate levels increased until 12 h for all fermentations and reached a plateau, while 1st microbiome acetate levels increased, for 2nd microbiome, they stayed steady regardless of *B. infantis* addition (Figure A4.2B). Production of formate increased until 8h then decreased for both microbiome communities and regardless of carbohydrate source (Figure A4.2C). Butyrate was not observed in the second microbiome communities whereas it reached between 10-15mM at the 30th hour regardless of *B. infantis* addition (Figure A4.2D). 1st microbiome propionate levels increased after 30th hour whereas it did not change for microbiome 2 fermentations (Figure A4.2E).

4.3.3. *B. infantis* counts mostly increase during *in vitro* fecal fermentation of LNT, LNnT and lactose

To determine how *B. infantis* abundance changes during HMO metabolism, *B. infantis* concentrations were identified by RT-qPCR. Figure 4.2 shows the *B. infantis* for microbiomes 1 and 2 counts over time. *B. infantis* inoculated at 10^4 cfu/ml for both

microbiomes as determined by qPCR. In the 1st fecal communities, LNT utilization increased *B. infantis* levels from 12 h to 16 h of fermentation and then stayed steady whereas LNnT showed increase from 24 h to 48 h (Figure 4.2A). In 2nd fecal communities, only LNnT increased *B. infantis* concentrations (Figure 4.2B). *B. infantis* levels in lactose fermentations changed over time (Figure A4.3).

4.3.4 Microbial community structure shifts based on carbon source and *B. infantis* addition

The fermentative abilities of microbial communities to utilize HMOs displayed a donor effect, meaning that the composition of the initial microbiome structure differs. Principal Coordinates Analysis (PCoA) on beta diversities revealed a clear separation between 1st and 2nd fecal microbiomes (Figure 4.3). The mean phyla composition of initial communities was dominated by Firmicutes and Actinobacteria. Actinobacteria relative abundance was as follows in initial communities: microbiomes 1 without *B. infantis* addition, 70.2 %; microbiomes 1 with *B. infantis* (before adding *B. infantis*), 84 %; microbiomes 2 without *B. infantis* 74 %; microbiomes 2 with *B. infantis* (before adding *B. infantis*) 74 % (Figure A4.4A) In the 1st fecal microbiomes, without addition of *B. infantis*, the Actinobacteria abundance comprise the 45 % of the total bacteria at the 12th hour for both LNT and LNnT, they increased to 61% for LNT and 87 % for LNnT at 20th hour, then it decreased to 41 % for LNT and 60 % for LNnT (Figure 4.4A). At the 48th hour, we observed a presence of Bacteriodetes (1 % of the total) in LNT, and did not observe the same in LNnT. In lactose fermentation, Actinobacteria abundance decreased over time from 41 % to 4% with Bacteriodetes presence after 24th hour (1.6 %) until the end of fermentation (9.9 %) (Figure A4.5). Supplementation of *B. infantis* caused clear shifts in

the microbial structure. Although the bioreactors did not reach significant biomasses at the hour of 12th, presence of *B. infantis* inversely affected the total Actinobacteria abundance in the microbial communities for both LNT (13 %) and LNnT (2 %) (Figure 4.4A). For LNnT, Actinobacteria abundance stayed the same until the 30th hour (around 2.5 %) and then increased (6.8 %) with increased appearance of Bacteriodetes (12.8 %) and decreased Firmicutes abundance (from 97 % to 80 %) till the end of fermentation. This was not observed in the communities without *B. infantis*. For LNT, Actinobacteria abundance increased steadily until 30th hour (from 13 % to 40 %). When it started decreasing, Bacteriodetes reached to 4 % (Figure 4.4A). In the meantime, lactose as a control also started with lower Actinobacteria abundance (4.8 %) than the microbiomes without *B. infantis* (Figure S4.5)

The 2nd fecal microbial community in LNnT fermentation (without the addition of *B. infantis*) showed a sharp increase in Actinobacteria from 50 % to 71 % of the total bacteria at 16th hour and then it stayed relatively steady (Figure 4.4B). On the other hand, Actinobacteria only increased from 50 % to 66 % at the 24th hour in the communities with addition of *B. infantis*. As observed in the 1st community samples, Bacteriodetes was also not observed in LNnT fermentation without *B. infantis* whereas it appeared at 48th hour in fermentations with *B. infantis* (Figure 4.4B). This indicates that *B. infantis* addition changes the microbial structure during LNnT fermentation. In LNT fermentation, the addition of *B. infantis* did not affect the fermentation structure in the 2nd microbiomes. The Actinobacteria increased from 15 % to 23 % for communities without *B. infantis* and from 18 % to 39 % in the microbiomes with *B. infantis* (Figure 4.4B). It relative stayed relatively steady despite the appearance of Bacteriodetes (21.8 % without *B. infantis* and 18.9 % with

B. infantis) while Firmicutes decreased. This might be explained by the replacement of Firmicutes with Bacteriodetes over time. In lactose, as opposed to both HMOs, Actinobacteria concentrations sharply decreased regardless of *B. infantis* addition (Figure A4.5A). This is because lactose is available to other species whereas Actinobacteria, especially *Bifidobacterium* spp. are more likely to ferment HMOs than other microbial species.

Since the diversity between the communities and different carbon sources is limited to 3 different phyla in all fermentations, we determined the microbial structural shifts at the genus level. In general, we observed distinctive differences in the communities with or without the addition of *B. infantis*. Actinobacteria levels all belong to *Bifidobacterium* spp. In LNT fermentations, in 1st microbial communities without the addition of *B. infantis*, the second abundant species were *Lactobacillales* spp. (51 %) at the beginning whereas with *B. infantis* addition we observed clear abundance of *Clostridium* spp. (75 %) (Figure 4.5A). The changes in the abundance of *Clostridium* spp. over time showed significant correlation with acetate (R^2=0.8784, p=0.0018), formate (R^2=0.7804, p=0.0084) and butyrate (R^2=0.8779, p=0.0019) productions (Table 4.1) in LNT fermentations with *B. infantis*. In 1st community structures regardless of *B. infantis* presence in LNT fermentations, we observed increased abundance of *Eubacterium* spp. after 24 hours till the end of fermentation (14-15 %) (Figure 4.5A). Some *Eubacterium* spp. were characterized as lactate utilizing and butyrate producing [74, 245]. Our linear regression analysis showed that the butyrate production in LNT fermentations were strongly correlated with *Eubacterium* spp. (R^2=0.9579, p=0.0001 without *B. infantis* and R^2=0.9679, p<0.0001 with *B. infantis*). We also observed decreasing lactate concentrations after 24th hour regardless

of *B. infantis* addition. This coincides with the appearance of *Eubacterium* spp. which could be explained the species belonging to this genus are lactate utilizers and butyrate producers. *Eubacterium* spp. showed significant correlation with decreasing lactate concentrations in LNT fermentations without *B. infantis* (R^2=0.5979, p=0.0414) and with *B. infantis* (R^2=0.6045, p=0.0396) (Table 4.1). Samples with *B. infantis* addition showed increased abundance of *Bacteriodes* spp. after 36th hour (4 %). Some strains of *Bacteriodes* spp. can produce propionate, which coincides with propionate production at 30th hour LNT fermentations with *B. infantis*. Propionate production in LNT fermentations showed significant correlation with *Bacteriodes* spp. (R^2=0.8596, p=0.0026 without *B. infantis*, R^2=0.8383, p=0.0038 with *B. infantis*, Table 4.1). In addition, *Phascolarctobacterium* spp. displayed after 36th hour in communities with *B. infantis* (3 %) and 48th hour communities without *B. infantis* (11 %). This genus can produce propionate and utilizes succinate [268]. Our linear regression analysis showed a strong correlation between *Phascolarctobacterium* spp. with propionate production in both 1st fecal communities with and without *B. infantis* (R^2=0.9859, p<0.0001 and R^2=0.9322, p=0.0004, Table 4.1).

In LNnT fermentation without the addition of *B. infantis* in the 1st microbial communities, *Bifidobacterium* spp. dominated the microbial community and increased up to 87 % at 20th hour and then decreased to 60 % at the end of fermentation. In contrast, we observed high abundance of *Clostridium* spp. in the fermentation with *B. infantis* up to 92-93 %. This coincides with observations in pure cultures [229] because *B. infantis* does not utilize LNnT efficiently, therefore in the presence of *B. infantis,* other species thrives or *B. infantis* competes with other bifidobacterial species for resources which suppresses them. Interestingly, *Lactobacillales* spp. was in high abundance in the beginning of fermentation

(53 %) then it decreased to 14 % over time in the communities without *B. infantis*. Similar to LNT fermentations, abundance of *Eubacterium* spp. increased starting 30th hour regardless of *B. infantis* addition and reached to 17-19 % of the total population. *Eubacterium* spp. are responsible of butyrate production, and some *Eubacterium* spp. are also propionate producers [269]. Propionate concentrations increased after 30th in LNnT fermentations with *B. infantis* and 36th h in fermentations without *B. infantis*. Our linear regression analysis showed that *Eubacterium* spp. presence in LNnT fermentations without *B. infantis* strongly correlated with butyrate concentrations (R^2=0.9998, p<0.0001) but propionate production in samples with *B. infantis* (R^2=0.9769, p<0.0001). Similar to LNT, *Phascolarctobacterium* spp. was observed in both communities regardless of *B. infantis* addition and they found to be correlated with propionate production (R^2=0.9859, p<0.0001 without *B. infantis* and R^2=0.9427, p=0.0003 with *B. infantis*) (Table 4.1).

In 2nd fecal microbial communities, the diversity of species was distinctive from the 1st one. In all fermentations, *Lactobacillales* and *Bifidobacterium* spp. were the predominant groups (Figure 4.5B). In LNT fermentation, *Bifidobacterium* spp. levels first increased and then decreased in communities without *B. infantis*, whereas it increased until the end of fermentation point in the communities with *B. infantis*. LNT fermentations without *B. infantis* showed a positive correlation with the production of lactate (R^2=0.9181, p=0.0102) and acetate (R^2=0.8956, p=0.0125) whereas we did not observe significant correlation with metabolite production in LNT fermentations with *B. infantis*. Although we observed *Clostridium* spp. in communities with *B. infantis* at 48th hour in LNT fermentations we did not observe this without addition of *B. infantis*. There is no butyrate production in 2nd fecal communities regardless of HMO type and addition of *B. infantis*.

On the other hand, propionate production might be linked to the presence of *Bacteriodes* spp. and *Clostridium* spp. in the 2nd microbial communities. Previously, *Bacteroides eggerthii*, *Bacteroides fragilis*, and *Eubacterium dolichum* were reported to associate with propionate production in human intestine [269]. However, we did not observe positive correlation in propionate production with the *Bacteriodes* spp. and *Clostridium* spp. in LNT fermentations with *B. infantis*.

In LNnT fermentation, *Bifidobacterium* spp. and Lactobacillales (specific genus could not be identified) were dominant members regardless of *B. infantis* addition. *Bifidobacterium* spp. increased over time in both fermentations (from 50 % to 74 % in microbiomes without *B. infantis*, from 52 % to 62 % with *B. infantis*) (Figure 4.5B). Interestingly, Lactobacillales showed a decreased pattern for both fermentations (from 47 % to 26 % in microbiomes without *B. infantis* and from 47 % to 27 % with *B. infantis*). *Clostridium* spp. appeared at 20th hour and disappeared in the communities without *B. infantis* addition. Similarly, it disappeared after 12th hour in communities with *B. infantis*. We did not observe *Bacteriodes* spp. in the fermentations without *B. infantis* whereas it appeared at the 48th h of fermentation in LNnT fermentations with *B. infantis* (10 %). We did not observe any positive correlation with any metabolite production in LNnT fermentations with *B. infantis*.

In lactose fermentations, the dynamics of species was distinct between the two microbiomes (Figure A4.5). In the 1st microbiomes, we observed decreased abundance of *Bifidobacterium* sp., and species such as Streptococcus that we did not observe either of the HMO fermentation (Figure A4.5A). That is not surprising that lactose is more available for most of the bacteria. In the 2nd microbiomes, Lactobacillales dominated the

fermentations regardless of *B. infantis* presence which is different than the LNnT fermentations (Figure A4.5B).

4.4 Discussion

In this study, we demonstrate the HMO utilization in modeled microbiomes using an *in vitro* bioreactor system. This system allowed us to simultaneously control pH, anaerobiosis and optical density as well as sample from numerous timepoints in order to monitor SCFA concentrations and microbial abundance. Within the infant gut microbiome, the *B. infantis* genome contains 40-kb gene cluster dedicated to the use of oligosaccharides in the milk [11]. This provides an advantage to survival in the infant gut microbiome during nursing. *B. infantis* utilizes oligosaccharides in their intact form; therefore, does not degrade tetrasaccharides to mono- or di-saccharides which are available for other members of the microbiome. Instead, *B. infantis* secrete metabolites, mainly acetate and lactate in the infant gut. These metabolites might be directly used by the infant gut epithelial cells or used by the other members of the gut microbiome [75]. Our previous results indicated that human milk tetrasaccharides LNT and LNnT are differentially utilized by *B. infantis* strains [229]. In addition, the inefficient utilization of LNnT by *B. infantis* ATCC 15697 shifts towards microbial metabolism towards formate production [229]. To this point, our knowledge about the influence of increased formate production is limited. Elevated formate concentrations in the gut were found to be related with inflammation-associated dysbiosis and increased abundance of formate utilizing *E.coli* [255]. On the other hand, formate cross-feeding are of interest for cooperative interactions within the gut bacterial metabolism. Methanogenic microbes were reported to utilize formate and facilitate the syntrophic interactions in anaerobic environmental conditions [270]. Acetogen *Blautia*

hydrogenotrophica was identified to utilize formate and produce acetate in return [267, 271]. Due to differential utilization of HMOs and our interest on syntrophic interactions and role of formate production, we conducted an infant fecal derived modeled microbiome in bioreactor systems, in order to identify the microbial interactions during HMO utilization in regard to the absence and presence of *B. infantis*.

In this study, we used two baby fecal samples for microbiome modelling. The fecal samples from different weeks on same baby were pooled and grew before inoculation into bioreactors containing lactose, LNT and LNnT. These inoculums either supplemented with *B. infantis* or not at the time of inoculation. According to *B. infantis* specific qPCR results on fecal samples, *B. infantis* was not present; therefore, this allowed us to identify the manipulations that occur during the microbial interactions due to *B. infantis*.

The two fecal sources structure initially regardless of the *B. infantis* addition were not distinct from each other at phyla level. At genus level, similar genera occur in the fecal microbiomes, but the abundances were different. However, during fermentation they responded HMOs differentially. In the 1st microbiome communities, elevated butyrate production and propionate production were observed regardless of carbohydrate source whereas there were no butyrate production and propionate concentrations remained steady during the fermentations of 2nd microbiomes.

It was previously found that LNT abundance in infant fecal samples were positively correlated with Bacillales and negatively correlated with Bifidobacteriales [272]. It is also noted Bifidobacteria levels increased over time when the most fecal HMO compositions have dropped dramatically. We observed that *Bifidobacterium* sp. levels increased over

time and *Bacillus* sp. levels dropped during the fermentations with LNnT in 1st microbiomes with *B. infantis* and *B. infantis* counts increased accordingly.

The clear distinction was abundant occurrence of *Clostridium* spp. in the both HMOs with *B. infantis*, increased abundance of *Eubacterium* spp. over time in all 1st microbiome fermentations. These two genera are associated with butyrate production. In fact, our correlation analysis showed that *Eubacterium* spp. was strongly correlated with butyrate production in both HMOs regardless of addition of *B. infantis*. Accordingly, *Eubacterium* spp. showed correlation with lactate concentrations in LNT fermentations. Lactate concentrations decreased in all fermentations of 1st microbiomes later hours of fermentation. This indicates that lactate is utilized by the other members of microbiome. In a previous study, *Eubacterium hallii* was reported to produce butyrate in mono-cultures and use lactate in co-cultures with *B. infantis* during fucose fermentation [273]. *Eubacterium* spp. has been reported to utilize lactate and produce butyrate in co-cultures with other bifidobacteria [245, 249]. In the 2nd microbiome fermentations, lactate concentrations remained similar after 24th hour and no *Eubacterium* spp. and butyrate production were observed regardless of carbohydrate source and *B. infantis* addition. This might mean that presence of *Eubacterium* spp. facilitates the lactate utilization as well as the butyrate production. Increased abundance of lactate utilizing bacteria was associated with colic in infants [274], however, butyrate is an energy source for the colon epithelial cells, contributes to the maintenance of the gut barrier functions, and has immunomodulatory and anti-inflammatory properties [192].

Propionate production in the gut was previously suggested to associate with interleukin (IL)10-producing regulatory T (Treg) cell differentiation [275]. We observed

increased production of propionate in 1st microbiome fermentations and it has been linked to *Phascolarctobacterium* spp. Similarly, we did not observe this genus in the 2nd microbiomes; but observed unchanged propionate productions. This genus has been identified to utilize succinate and produce propionate [268]; however, we did not identify succinate presence in our study.

As observed in pure cultures [229], LNnT fermentations in both fecal microbiomes revealed elevated amounts of formate production when *B. infantis* added. This might indicate that *B. infantis* preference between these tetrasaccharides manipulated the microbial interactions in the complex infant gut derived communities. In both microbiomes, formate showed at first increase and then decrease. This indicates that formate becomes an energy source for the other members of the community. We see an increase in the acetate concentrations that might be related with formate decrease. However, we did not observe any known acetogens that are formate utilizers in the both microbiomes. In LNT fermentations, formate production was correlated with *Bifidobacterium* spp. *Clostridium* spp., and *Eubacterium* spp. abundance; however, these correlations were not found in the LNnT fermentations with *B. infantis*. Previously, *E. limosum* and *E. acidaminophilum* were identified to require formate under certain conditions [276, 277]. On the other hand, the bacteria that elevate formate production in LNnT fermentations and result in its utilization were not clear. Since inefficient utilization of LNnT by *B. infantis* elevates formate production, there might be inverse relationship between *B. infantis* and formate.

4.5 Conclusions

This study constitutes a tool for the investigation of various microbe-microbe and microbe-human milk oligosaccharides interactions in vitro. In this study we demonstrated a hallmark of a syntrophic interaction with heterologous members of the modeled community. This indicates that the specific microbiome architecture may decrease the competitive advantage experienced by *B. infantis* through HMO utilization. This study provides characterization of the structure-function relationships between specific HMO isomers and their activity on the composition of the infant microbiome, therefore, ascribing a microbiologically-active function to human milk that potentially impacts infant health through its microbiome.

Table 4.1 Pearson correlation between genus-level taxa and metabolite production in 1st microbiomes

			Lactate	Acetate	Formate	Butyrate	Propionate
Bifidobacteriaceae;Bifidobacterium	LNT	without BI	0.4443	0.01687	0.2065	0.2413	0.5364*
		with BI	0.01341	**0.8168***	0.6544*	0.5818*	0.1701
	LNnT	without BI	0.4804	0.08768	0.3199	0.1343	0.04192
		with BI	0.6346*	0.3967	0.4535	0.2555	**0.9086***
Bacteroidaceae;Bacteroides	LNT	without BI	0.4577	0.3485	0.3884	0.6107*	**0.8596***
		with BI	0.399	0.2953	0.294	0.507	**0.8383***
	LNnT	without BI	NA	NA	NA	NA	NA
		with BI	0.4191	0.3807	0.2968	0.2156	**0.9753***
Bacillaceae;Bacillus	LNT	without BI	NA	NA	NA	NA	NA
		with BI	0.0113	**0.9931***	0.439	0.6391*	0.4421
	LNnT	without BI	NA	NA	NA	NA	NA
		with BI	0.03463	**0.8402***	0.01415	**0.9132***	0.1577
Lactobacillales	LNT	without BI	0.1408	0.6633*	0.3659	0.5819*	0.3575
		with BI	0.04726	**0.7602***	0.228	0.2896	0.1279
	LNnT	without BI	0.1395	0.5484	0.0033	0.06404	0.0808
		with BI	0.372	0.5107	0.3394	0.3329	**0.9724***
Clostridiaceae;Clostridium	LNT	without BI	NA	NA	NA	NA	NA

		with BI	0.156	**0.8784***	**0.7804***	**0.8779***	0.504
	LNnT	without BI	0.281	0.0003	0.386	0.1039	0.0688
		with BI	0.4473	0.3529	0.3139	0.1935	**0.9652***
Eubacteriaceae;Pseudoramibacter_Eubacterium	LNT	without BI	0.5979*	0.5487	**0.7584***	**0.9579***	0.5583
		with BI	0.6045*	0.5121	**0.7624***	**0.9679***	**0.7705***
	LNnT	without BI	0.2998	0.4847	**0.7641***	**0.9998***	0.4765
		with BI	0.4977	0.4332	0.3687	0.2698	**0.9769***
Veillonellaceae;Phascolarctobacterium	LNT	without BI	0.265	0.226	0.2096	0.3518	**0.9985***
		with BI	0.6151*	0.3733	0.4811	**0.8068***	**0.9322***
	LNnT	without BI	0.1447	0.2438	0.2798	0.5044	**0.9859***
		with BI	0.3323	0.3103	0.207	0.1547	**0.9427***

The asterisk means (*) that the correlation is significant ($p<0.05$). the bold color means that the R^2 is above 0.7.

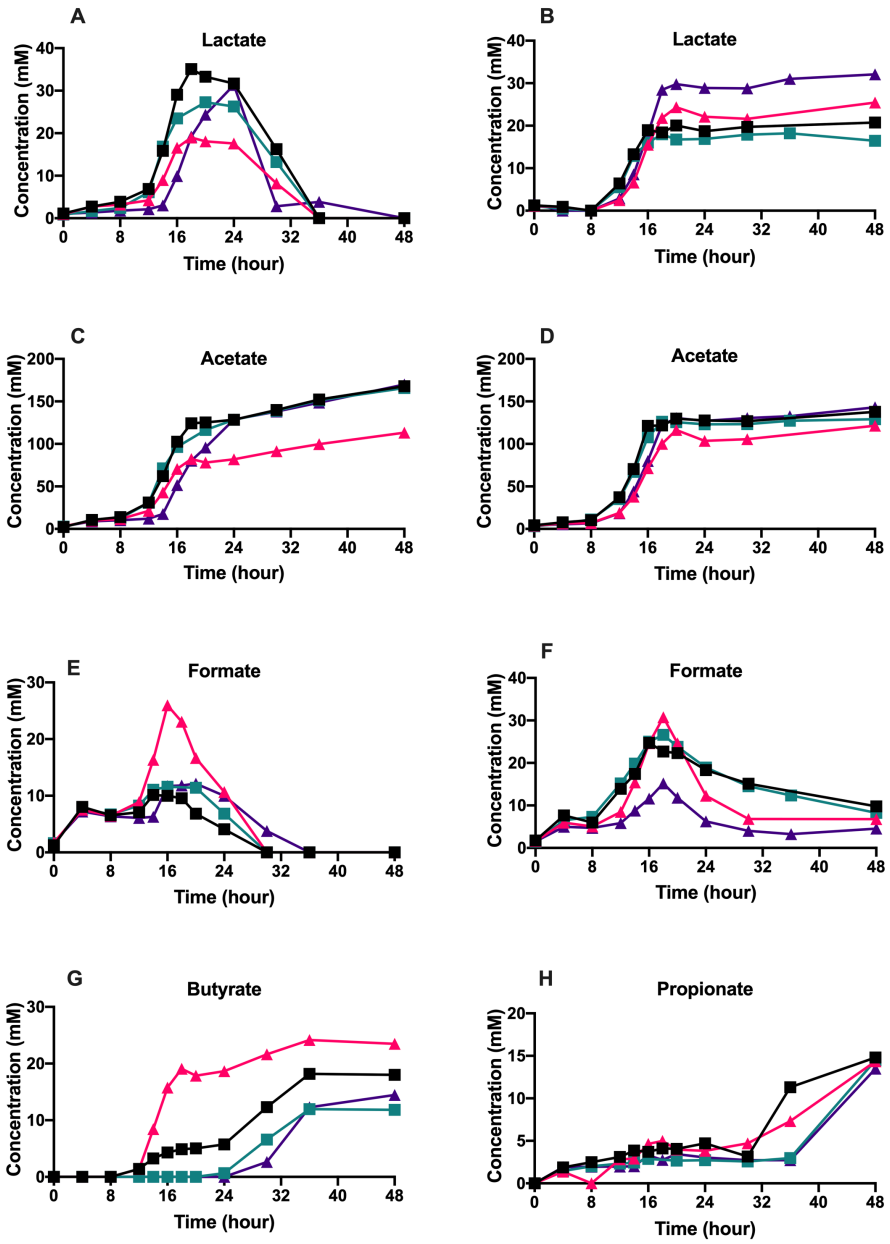

Figure 4.1 Microbial metabolites produced during the growth of infant fecal inoculated microbiomes with and without *B. infantis* addition on LNT and LNnT within a modeled system. Absolute concentrations of lactate (A), acetate (C), formate (E), butyrate (G), and propionate (H) of 1st microbiomes and lactate (B), acetate (D), formate (F) of 2nd microbiomes All panels represent fecal bacterial communities with or without supplementation of *B. infantis* ATCC15697 growing on colon medium containing 1% (wt/v) lacto-*N*-tetraose (LNT) and lacto-*N*-neotetraose (LNnT). The values for organic acid production are expressed in millimolar (mM).

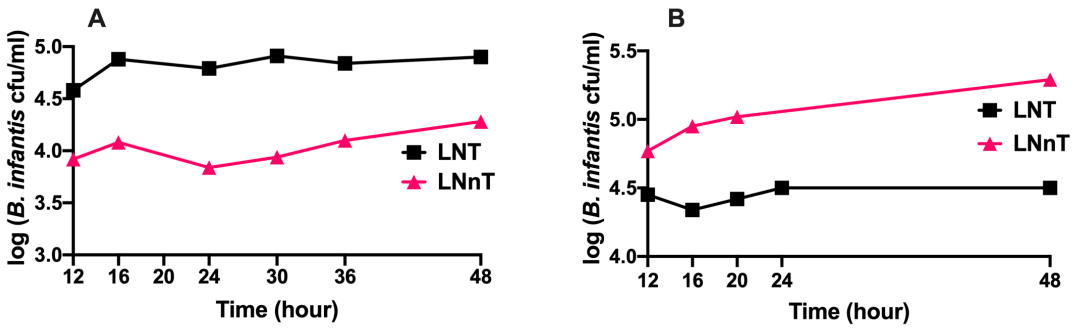

Figure 4.2 *B. infantis* levels as determined by qPCR represented as log (cfu/ml). (A) microbiomes derived from 1st baby fecal and (B) microbiomes derived from 2nd baby fecal. B. infantis initially inoculated at 104 cfu/ml at time 0.

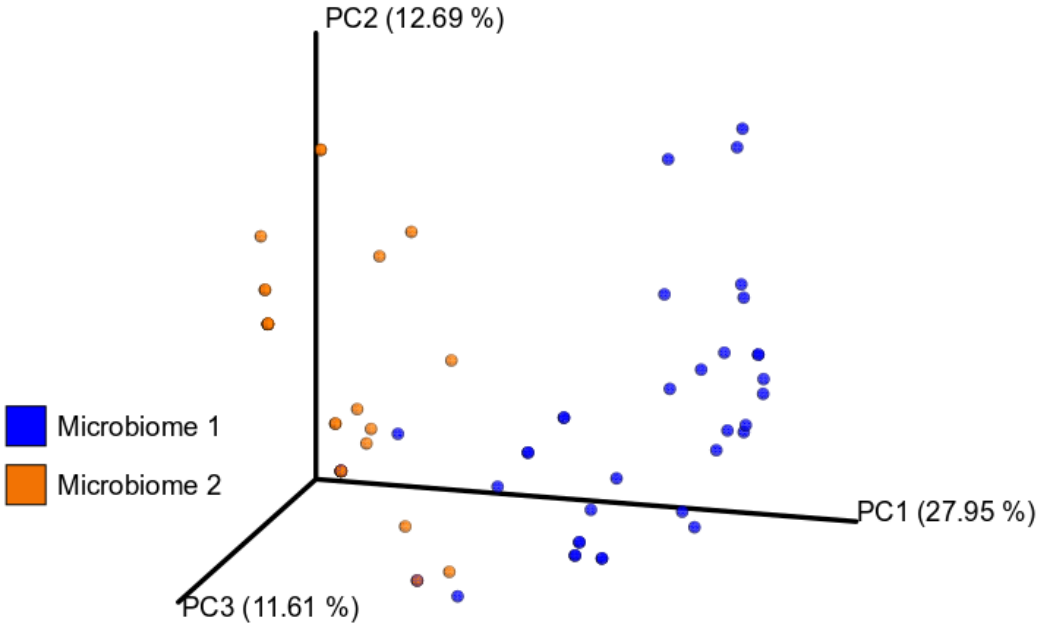

Figure 4.3 Principal-coordinate score plot of 16S rRNA gene amplicon sequence reads using Jaccard distance metrics on beta diversities. The dots represent each time point in three fermentations (LNT, LNnT, lactose) of 1st (blue) and 2nd (orange) fecal derived microbiomes regardless of addition of *B. infantis*.

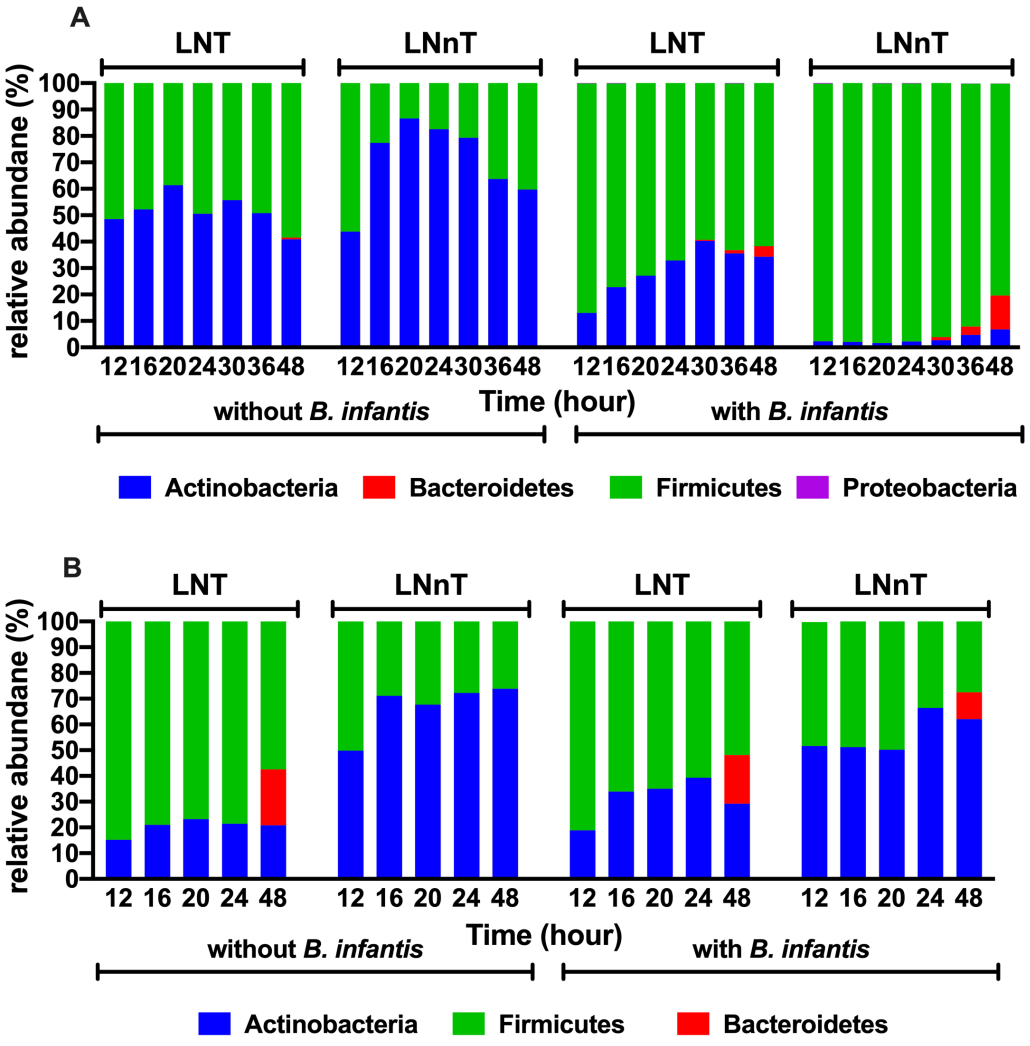

Figure 4.4 Phyla composition (as determined by 16S rRNA gene amplicon sequencing) of *in vitro* modeled microbiomes with or without addition of *B. infantis* during LNT and LNnT fermentation. (A) microbiomes derived from 1st baby fecal and (B) microbiomes derived from 2nd baby fecal.

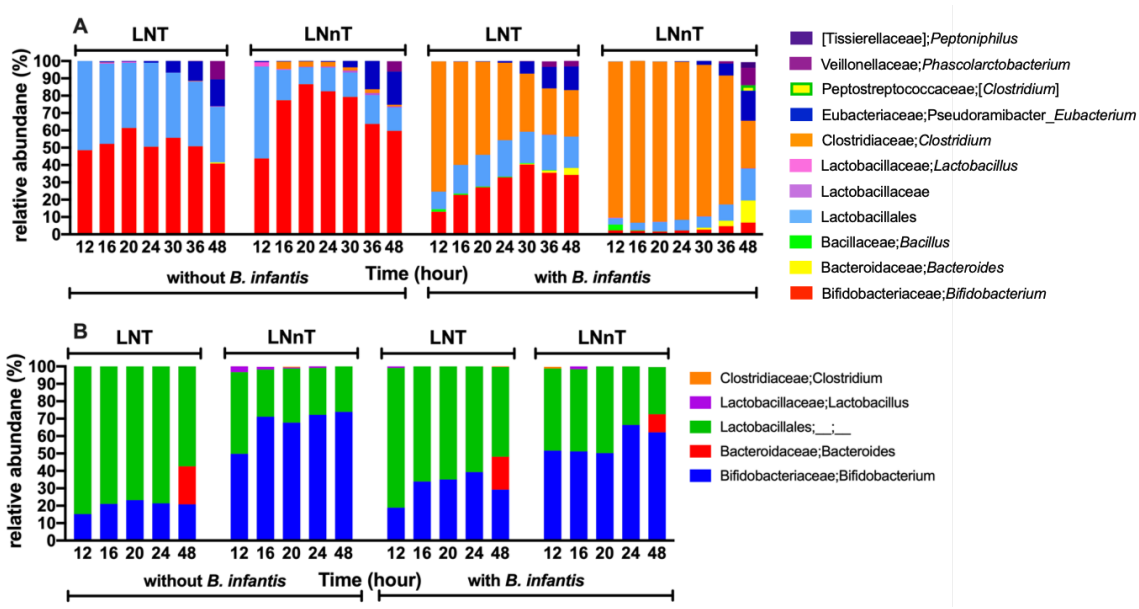

Figure 4.5 Relative abundances of bacterial genera during LNT and LNnT fermentations of in vitro modeled microbiomes with and without addition of *B. infantis*. (A) microbiomes derived from 1st baby fecal and (B) microbiomes derived from 2nd baby fecal.

CHAPTER 5

A HUMAN GUT COMMENSAL FERMENTS CRANBERRY CARBOHYDRATES TO PRODUCE FORMATE

Ezgi Özcan[1], Jiadong Sun[2], David C. Rowley[2], and David A. Sela[1, 3]

[1]Department of Food Science, University of Massachusetts, Amherst, Massachusetts 01003, United States

[2]College of Pharmacy, University of Rhode Island, Kingston, RI 02881, United States

[3]Department of Microbiology & Physiological Systems, University of Massachusetts Medical School, Worcester, MA

5.1 Abstract

Commensal bifidobacteria colonize the human gastrointestinal tract and catabolize glycans that are impervious to host digestion. Accordingly, *Bifidobacterium longum* typically secretes acetate and lactate as fermentative end products. This study tested the hypothesis that *B. longum* utilizes cranberry-derived xyloglucans in a strain-dependent manner. Interestingly, the *B. longum* strain that efficiently utilizes cranberry xyloglucans secretes 2.0 to 2.5 mol of acetate-lactate. The 1.5 acetate:lactate ratio theoretical yield obtained in hexose fermentations shifts during xyloglucan metabolism. Accordingly, this metabolic shift is characterized by increased acetate and formate production at the expense of lactate. α-L-Arabinofuranosidase, an arabinan endo-1,5-α-L-arabinosidase, and a β-xylosidase with a carbohydrate substrate binding protein and carbohydrate ABC

transporter membrane proteins are upregulated (2-fold change), which suggests carbon flux through this catabolic pathway. Finally, syntrophic interactions occurred with strains that utilize carbohydrate products derived from initial degradation from heterologous bacteria.

5.2 Introduction

Microbial commensals colonize the mammalian gut and interact with their host through various interwoven metabolic networks. A well-characterized operation performed by microbiota is energy liberation from dietary polysaccharides. These complex carbohydrates are impervious to host digestion and thus available for microbial populations to utilize. In turn, gut microorganisms produce metabolites sequestered by the host, including short chain fatty acids (SCFAs) [49, 75, 77, 243]. Briefly, gut microorganisms compete for food, with metabolites secreted by one member often utilized by a secondary microbial population [74]. This syntrophic metabolism is extended towards interactions with their host. For instance, microbial SCFAs (i.e. acetate, propionate, butyrate, and valerate) are substrates for specific host tissues. This includes butyrate that provides a primary energy source for enterocytes [75–77].

Bifidobacterium longum as taxon is often dominant in the infant gut and colonizes adults at lower concentrations [10]. Whereas *B. longum* subsp. *infantis* colonizes the infant gut, *B. longum* subsp. *longum* tends to populate adult microbiomes. As with all bifidobacteria, *B. longum* catabolizes carbohydrates via their fructose-6-phosphate phosphoketolase pathway, which is characteristic of the genus and termed the bifid shunt. This ATP generating pathway results in acetate and lactate secretion to recycle cofactors required in substrate-level phosphorylation [189, 190]. The theoretical yield is 3:2 moles of acetate to lactate produced for every 2 moles hexose that enters the bifid shunt.

Bifidobacteria encode an assortment of glycosyl hydrolases (GH) in order to utilize dietary glycans as fermentative substrates [215, 278, 279]. Oligosaccharide utilization phenotypes are often consistent with the ecological niche that the bifidobacterial strain occupies (e.g. adult vs. infant gut)[183]. The *B. longum* subsp. *longum* genome, for example, encodes a large number of GHs dedicated to arabinose and xylose utilization [280]. In contrast, the phylogenetic near-neighbor and infant-colonizing *Bifidobacterium longum* subsp. *infantis* chromosome encodes genes to enable human milk oligosaccharide utilization within the nursing infant gut [11, 186, 187, 197]. In general, *B. longum* subsp. *infantis* varies in its ability to utilize plant-derived carbohydrates [183].

Xyloglucans are a cross-linking oligosaccharide found in type 1 plant cell walls [281] and exhibit a β(1→4)-glucan primary backbone with α(1→6)-linked xylosyl residues as substituents. Depending on the plant species and tissue of origin, xyloglucan branches may be extended by galactose, fucose, or arabinose residues [282, 283]. The predominant cranberry xyloglucan structure was previously characterized as SSGG (S, β-D-glucose with α-L-Ara-(1–2)-α-D-Xyl at the O-6 position; G, β(1→4)-glucan main chain) [284].

Oligosaccharides isolated from the cranberry cell wall (*Vaccinium macrocarpon*) prevent adhesion of uropathogenic *Escherichia coli* and may limit biofilm production [285, 286]. With regards to xyloglucan metabolism, certain gut microorganisms produce enzymes to degrade tamarind seed xyloglucans in their extracellular environment [287]. However, the structure-function relationship between the xyloglucan and specific populations of commensal bacteria remains unresolved. Thus, we evaluated *B. longum* strains in their capacity to utilize cranberry-derived xyloglucans as a sole carbon source. In

order to further understand *in vitro* metabolism, organic acids produced during fermentation were profiled. In addition, few lactobacilli strains that are recognized as probiotics [288], and potentially used as synbiotics, were subjected to growth on xyloglucans as the sole carbohydrate source.

5.3 Materials and Methods

5.3.1 Isolation of xyloglucans from the cranberry cell wall

Cranberry hulls were degraded with pectinase (Klerzyme 150, DSM Food Specialties, South Bend, IN, USA) and fractionated as previously described [286] with modifications. Briefly, 2 g of the cranberry pectinase treated powder was dissolved in 20 ml distilled water and loaded onto a RediSep GOLD C18 Reverse-phase column (Teledyne ISCO, Inc., Lincoln, NE, USA) and connected to a CombiFlash Rf purification system (Teledyne ISCO, Inc.) The column was eluted sequentially with 500 ml deionized water, 500 ml 15% methanol/water and 500 ml methanol. Fractions from each gradient were individually pooled and lyophilized to obtain three major fractions, Cranf1W (761 mg, 38.1%) eluted with 100% deionized water, Cranf1b (476 mg, 23.8%) eluted with 15% methanol/water, and Cranf1M (562 mg, 28.1%) eluted with 100% methanol. 100 mg of Cranf1b was then dissolved in 2 ml distilled water and further purified by a size-exclusion column Hiprep Sephacryl S-100 HR 16/60 (GE healthcare Life Sciences, Pittsburgh, PA, USA). The column was isocratically eluted with deionized water at 0.5 ml/min. Eluates were collected every 5 ml and evaluated for their total carbohydrate content by phenol sulfuric acid assay [289]. The total carbohydrate content was assessed in a 96-well microtiter plate as previously reported [289]. Briefly, in each well of a 96-well microtiter plate, 30 μl of each fraction was mixed with 100 μl concentrated sulfuric acid and 20 μl

5% phenol solution. The microtiter plates were than incubated at 90 °C for 5 min and recorded for absorbance at 490 nm using a Spectramax M2 microplate reader (Molecular Devices, Sunnyville, CA, USA).

5.3.2 Xyloglucan structural analysis

Oligosaccharide fractions were pooled and freeze-dried to obtain 59.5 mg of cranberry xyloglucans, which were then chemically verified by a combination of Matrix-assisted Laser Desorption/Ionization-Time of Flight-Mass Spectrometry (MALDI-TOF-MS) and ^{1}H Nuclear Magnetic Resonance (^{1}H-NMR) spectroscopy. Briefly, 1 μl of xyloglucan (1 mg/ml in H_2O) was mixed with 1 μl of 2, 3-dihydrobenzoic acid (DHB) matrix solution. 2 μl of this mixture was analyzed by MALDI-TOF-MS (Axima Performance, Shimadzu, Kyoto, Japan) in positive reflectron mode. 500 profiles were collected for each experiment. Furthermore, the cranberry xyloglucans were dissolved in D_2O (99.96%, Cambridge Isotope Laboratories Inc., Tewksbury, MA, USA). The ^{1}H spectrum was obtained on a 500 MHz NMR spectrometer (Varian VNMR, Agilent Technologies, Santa Clara, CA, USA) at 25 °C.

5.3.3 Bacterial strains and propagation

Bacterial strains used in this study are summarized in Table 5.1. Bifidobacterial strains were propagated in Bifidobacterial Selective Media (BSM) or De Man Rogosa Sharp (MRS, Oxoid, Hampshire, England) medium supplemented with 0.05% (wt/v) L-cysteine (Sigma-Aldrich, St. Louis, MO) [201] at 37 °C under anaerobic conditions (Coy Laboratory Products, Grass Lake, MI). *Lactobacillus* cultures were propagated in MRS supplemented with 0.05% (wt/v) L-cysteine as a reducing agent at 37 °C under anaerobic conditions. Bacterial strains were routinely verified using the bifidobacterial-specific

phosphoketolase assay [202], and through microscopy. The strains used in this study have previously confirmed by multilocus sequence typing (MLST), and urease assay to distinguish *infantis*/*longum* (urease+/urease-) [197]. In addition, a PCR-based *Bifidobacterium longum*/*infantis* ratio analysis (BLIR) were performed to differentiate *B. longum* subspecies as previously described [204].

5.3.4 Microplate growth assay

In order to evaluate growth phenotypes in a 96 well format, overnight cultures were centrifuged and washed with phosphate buffer solution that was inoculated (1% (v/v)) into modified MRS (mMRS, without acetate and carbohydrate substrate). The sole carbon source was defined as purified xyloglucans at a final concentration of 2% (wt/v). The growth assay was conducted anaerobically at 37 °C for 72 h by assessing optical density at 600 nm (OD_{600nm}) in an automated PowerWave HT microplate spectrophotometer (BioTek Instruments, Inc. Winooski, VT). Each strain was evaluated in biological triplicates with three technical replicates. Negative and positive controls consisted of inoculated medium in the absence of substrate and presence of glucose (2% wt/v), respectively. Bacterial growth kinetics were calculated using Wolfram Mathematica 10.3 Student Edition with the equation below as described in Dai et al [205].

$$\Delta OD(t) = \Delta ODasym\{\frac{1}{1+\exp[ktc-t]} - \frac{1}{1+\exp[ktc]}\}$$

ΔOD_{asym} is the growth level at stationary phase with k representing the growth rate and tc is the inflection point indicating the time to reach the highest growth rate.

5.3.5 Modeled syntrophic interactions

In order to determine if degradative or secreted metabolites are utilized by a heterologous strain, supernatants from the microplate growths were analyzed. Accordingly,

800 μl of the conditioned supernatant was dissolved in 1200 μl of mMRS medium. Bacterial strains were washed with PBS once in order to remove the residual carbohydrates from initial propagation and were inoculated 1% (v/v) and evaluated for growth in a 96 well format as described. Bacterial growth kinetics were calculated, and the supernatant obtained after the secondary growth was analyzed by HPLC.

5.3.6 Xyloglucan profiling following bacterial fermentation

Following *in vitro* fermentation, filtered bacterial culture supernatants were derivatized with 2-aminobenzamide (2-AB) for oligosaccharide purification. Briefly, 50 µl of cell-free supernatants were diluted with 2 ml deionized water and loaded onto Porous Graphitized Carbon (PGC) cartridge (1 g, Thermo Scientific, Waltham, MA, USA). The cartridge was pre-washed with 5 ml 50% (v/v) acetonitrile/H_2O and equilibrated with three times of 5 ml deionized water. First, the cartridges were eluted with 5 ml deionized water three times with oligosaccharide fractions eluted with 30% (v/v) acetonitrile/H_2O with 0.1% trifluoroacetic acid (TFA) three times. The resulting fractions were spiked with 0.036 mg glucose as an internal standard and freeze-dried. 7 mg/ml of 2-AB and 3.2 mg/ml of 2-picoline borane were prepared in 10% (v/v) acetic acid/H_2O and 200 µl was added into each mixture. The solutions were held at 40 °C for 4 h, centrifuged and dried *in vacuo*. The derivatized oligosaccharide mixtures were re-dissolved in 400 µl deionized water for FL-HPLC and LC-MS analyses.

5.3.7 FL-HPLC and LC-MS analyses

The 2-AB labeled xyloglucans were analyzed by FL-HPLC and LC-MS. FL-HPLC analysis performed on a Hitachi Elite LaChrom HPLC system (Hitachi, Tokyo, Japan) connected to a fluorescence detector (L-2485, Hitachi). The samples were analyzed on a

Kinetex RP-C18 column (150 mm × 3 mm, 2.6 μm, Phenomenex, Torrance, CA, USA) at 40 °C. The column was first eluted with isocratic 10% (v/v) methanol in H_2O (with 0.1% TFA) for 10 min at 0.2 ml/min, followed with a linear gradient of 10%-20% methanol in H_2O for 90 min, and then a linear gradient of 20% to 100% methanol in H_2O for 15 min and stayed at 100% for 30 min. The elution was monitored by fluorescence detector with an excitation wavelength of 330 nm and emission wavelength at 420 nm. The LC-MS analysis was performed on a Shimadzu Prominence UFLC system (Shimadzu, Kyoto, Japan) coupled to an AB sciex Qtrap 4500 mass spectrometer (AB sciex, Framingham, MA, USA) with electrospray ionization source. The LC-MS analysis was performed with the same column and same HPLC program as aforementioned for FL-HPLC. The mass spectrometer was operated in positive mode and ions at m/z 200 to m/z 2000 were scanned. Quantification of extracted ions was normalized by 2-AB derivatized glucose.

5.3.8 Characterization of bacterial organic acid production

Endproducts from bacterial fermentation were quantitated by HPLC. Bacterial strains were initially propagated as described above. Cell-free supernatants from microcentrifuge tubes were obtained at early stationary phase and filtered through a 0.22 μm filter following centrifugation and stored at -80 °C until analysis. Organic acids were quantified using an Agilent 1260 Infinity HPLC (Agilent Technologies, Santa Clara, CA) system equipped with a Wyatt Optilab T-rEX detector (Refractive Index detector, Wyatt Technology Corp, Santa Barbara, CA). Separation was carried out using an Aminex HPX-87H column (7.8 mm ID x 300 mm, Bio Rad Laboratories, Hercules, CA) at 50 °C in a mobile phase of 5 mM H_2SO_4 at flow rate of 0.6 ml/min with 50 μl of injection volume. Organic acids (i.e. acetic acid, lactic acid, formic acid) were acquired from Sigma-Aldrich

Co. (St. Louis, MO). Metabolite concentrations were calculated from standard curves derived from external standards for six different concentrations (0.05, 0.1, 0.5, 1, 5, and 10 mg/ml) and converted to millimolar (mM). Metabolite profiling was carried out in triplicate and each measurement was performed in duplicate.

5.3.9 Gene expression by quantitative real-time PCR

Relative gene expression was performed by qRT-PCR. Four ml samples were collected at mid-exponential phase and pelleted at 12,000 x g for 2 min and stored in 1 ml Ambion RNAlater (Life Technologies, Carlsbad, CA). Total RNA was extracted using Ambion RNAqeous-Mini kit (Life Technologies, Carlsbad, CA) according to the manufacturer's instructions. The cells were placed in lysis buffer to be transferred to MP Bio Matrix E tubes and were subjected to bead-beating using FastPrep 24 instrument (MP Biomedicals, Santa Ana, CA) (2 X 5.5 m/sec for 30 sec). Total RNA was eluted in 50 μL of EB solution and immediately subjected to DNase treatment with the Ambion Turbo DNase-free (Life Technologies, Carlsbad, CA) using 1 μL of DNase I for half-hour. Total RNA was converted to cDNA using the High Capacity cDNA Reverse Transcription Kit (Applied Biosystems, Carlsbad, CA) according to manufacturer's instructions. cDNA concentrations were measured by a Nanodrop 2000 Spectrophotometer (Thermo Fisher Scientific Inc., Agawam, MA). qRT-PCR analysis was performed using a 7500 Fast Real-Time PCR System (Applied Biosystems, Singapore) with PowerUP SYBR Green Master Mix (Applied Biosystems, Foster City, CA) using parameters suggested by the manufacturer. Primers were designed using Primer3 (Table 5.2; http:// frodo.wi.mit.edu). The gene Blon_0393 was used as an endogenous control as previously validated [184]. Gene expression levels while growing on glucose (2 % w/v) was used as a reference.

Results were expressed as fold change relative to control. Bacterial growths were performed in triplicates with triplicate measurements by qRT-PCR.

5.3.10 Statistical Analysis

Bacterial growth kinetics were subjected to two-way ANOVA and Tukey's HSD test for multiple comparisons of strains within treatment compared with the positive control. Metabolite concentrations were subjected to two-way ANOVA and the Sidak's correction was used to account for multiple comparisons. Significant differences in modeled syntrophic interactions were determined by paired-t test for bacterial growth kinetics. The fold change gene expression was analyzed by paired t-test compared to control.

5.4 Results

5.4.1 The cranberry cell wall contains xyloglucans

Oligosaccharides were purified from a cranberry derivative through reverse-phase C18 and size exclusion chromatography (see Figure A5.1 in the supplemental material). The chemical properties of the purified oligosaccharides were subsequently assessed by matrix-assisted laser desorption ionization (MALDI-TOF) mass spectrometry (MS) (Figure 5.1) and 1H nuclear magnetic resonance (NMR) spectroscopy (Figure A5.2). Consistent with previous studies [284, 286], the purified oligosaccharides were identified as xyloglucans with degrees of polymerization (DPs) ranging from 6 to 9. MALDI-TOF MS analysis identified sodium adduct ions at 923, 953, 1,055, 1,085, 1,217, 1,247, and 1,379, which were interpreted as xyloglucan compositions of hexose3-pentose3 (H3P3), H4P2, H3P4, H4P3, H4P4, H5P3, and H5P4, respectively. Putative cranberry xyloglucan oligosaccharide structures were provisionally assigned as reported in Table A5.1.

5.4.2 *B. longum* xyloglucan utilization is strain dependent

Among the bifidobacterial strains tested (Table 5.1), *B. longum* subsp. *longum* UCD401 exhibits the most growth on the purified xyloglucans, achieving a final optical density at 600 nm (OD600) of 0.15±0.02 (Figure 5.3). The growth rate of *B. longum* subsp. *longum* UCD401 while utilizing xyloglucans does not significantly differ from that during glucose utilization ($p>0.05$) (Table 5.3). This indicates that *B. longum* subsp. *longum* UCD401 does not have a metabolic preference for glucose relative to xyloglucans. As expected, while fermenting xyloglucans, *B. longum* subsp. *longum* UCD401 achieves a modest biomass relative to that achieved on glucose ($p<0.05$) and no growth was observed on the negative control. This indicates that UCD401 does not utilize these carbohydrates with similar efficiency. Bifidobacteria that utilize both plant and milk oligosaccharides have exhibited similar growth profiles [242, 290]. Despite similar growth rates on glucose and xyloglucans, *B. longum* subsp. *longum* UCD401 ferments xyloglucans more slowly than glucose to achieve maximal growth (tc) ($p<0.05$) (Table 5.3). In contrast to UCD401, *B. longum* subsp. *infantis* ATCC 15697 and JCM1260 did not metabolize cranberry xyloglucans.

Lactobacillus strains were evaluated to test if other fermentative bacteria could harness cranberry xyloglucan carbon. *Lactobacillus plantarum* ATCC BAA-793 and *Lactobacillus johnsonii* ATCC 33200 were subjected to growth on xyloglucans as a sole carbohydrate source as depicted in Figure 5.2 with growth kinetics displayed in Table 5.3. *L. johnsonii* ATCC 33200 did not utilize cranberry-derived oligosaccharides. In contrast, *L. plantarum* ATCC BAA-793 achieved a final OD600 of 0.29±0.03, which is higher than that of all of the *B. longum* strains tested ($p<0.05$) (Figure 5.2). This *Lactobacillus* strain

does prefer glucose, as it has a significantly lower growth rate while consuming xyloglucans ($p<0.05$, Table 5.3). Its maximal growth (tc) did not vary between xyloglucan and glucose utilization ($p>0.05$), despite the lower growth rate during xyloglucan utilization. Interestingly, *L. plantarum* has a lower growth rate than *B. longum* subsp. *longum* UCD401 while fermenting purified xyloglucans despite achieving a higher biomass ($p<0.05$). The time required to achieve maximum growth (tc) while utilizing xyloglucan is significantly shorter for *L. plantarum* than for *B. longum* subsp. *longum* UCD401 ($p<0.05$). This suggests that *L. plantarum* does not prefer these complex carbohydrates, despite having a higher utilization efficiency than the *B. longum* strain.

5.4.3 *B. longum* consumes xyloglucans from the growth medium.

The extent to which UCD401 utilizes xyloglucans was determined by profiling spent fermentation medium from growth conducted in microcentrifuge tubes. Interestingly, degraded glycans were not detected in spent medium compared with the control (i.e., preinoculated medium) (Figure A5.3 and A5.4). The extracted ion counts for each xyloglucan were quantitated as percentages of the baseline control (t=0) (Figure A5.5 and A5.6). Of interest, detectable xyloglucans with DPs of 6 to 9 exhibited 120% of the extracted ion counts of the baseline (t=0). Thus, there was an extensive accumulation of xyloglucans with all DPs following fermentation by *B. longum* subsp. *longum* UCD401. Significantly, xyloglucans with DPs of <7 did not accumulate to the same extent. This is indicative of an ability to utilize the short-chain oligosaccharides. Accordingly, we did not detect monosaccharide accumulation in the spent fermentation medium. A similar observation has been reported previously with bifidobacterial metabolism of human milk oligosaccharides [198, 199]. As previously postulated, *B. longum* is able to transport only

lower molecular-weight oligosaccharides across its envelope. This suggests that a dynamic equilibrium has been achieved between the import of lower-DP molecules and the extracellular hydrolysis of higher-DP molecules. This is consistent with higher-DP oligosaccharide accumulation in the growth medium. A similar glycan distribution was observed in *L. plantarum* qualitatively, along with corresponding degradation phenotypes (Figure A5.3). It is important to note that glycoprofiling was performed with bacteria grown in microcentrifuge tubes.

5.4.4 Bifidobacteria metabolize xyloglucans via the bifid shunt

Metabolite end products secreted while utilizing xyloglucans were quantified by high-performance liquid chromatography (HPLC) of cell-free supernatants. The absolute concentrations of acetate, lactate, and formate secreted by *B. longum* subsp. *longum* UCD401 in the early stationary phase of xyloglucan or glucose utilization are depicted in Figure 5.3. *B. longum* subsp. *longum* UCD401 secretes significantly lower lactate and acetate concentrations while utilizing xyloglucans (4.08±0.16 and 8.78±0.10 mM, respectively) than when subsisting on glucose (37.60±9.41 and 54.11±13.40 mM, respectively). This is expected and consistent with the lower biomass achieved ($p<0.05$). In addition, less metabolic investment is required to catabolize glucose in the bifid shunt. The absolute concentrations were normalized with respect to the OD600 reached in microcentrifuge tubes. UCD401 exhibited higher acetate concentrations in xyloglucan metabolism (172.54±10.52 mM) than in glucose metabolism (124.56±22.70 mM), whereas the lactate concentrations were similar (80.31±6.76 and 86.50±15.98 mM). Interestingly, and despite a lower biomass, *B. longum* subsp. *longum* UCD401 secretes high concentrations of formate while metabolizing cranberry xyloglucans (10.01±0.86 mM).

This is significantly higher than during glucose utilization (1.62±1.30 mM) ($p<0.05$), indicating a shift in metabolism to harvest energy more efficiently from this substrate.

The bifid shunt catabolizes hexose sugars to yield a theoretical acetate:lactate ratio of 1.5. As expected, UCD401 achieved this while utilizing glucose (1.44±0.01); however, xyloglucan fermentation shifted the ratio significantly toward acetate at the expense of lactate (2.15±0.08) ($p<0.05$) (Figure 5.3d). When normalizing the absolute concentrations with respect to biomass, more acetate production from xyloglucan metabolism than from glucose metabolism occurred. This has been observed in a previous study, as more ATP is produced by flux through acetate-producing pathways [193]. Accordingly, formate secretion was significantly increased with a formate:lactate ratio of 2.50±0.28 while fermenting xyloglucans, in contrast to 0.05±0.01 during glucose metabolism (Figure 5.3e). Organic acids produced while lactobacilli ferment xyloglucans were subsequently profiled (Figure 5.3). In addition to comparative physiology, this approach may inform future mixed-culture probiotics (i.e., lactobacilli and bifidobacteria), as well as synbiotic strategies that incorporate xyloglucans with one or more probiotic strain. Lactate was produced at significantly lower concentrations (5.27±0.19 mM, $p<0.05$) by *L. plantarum* ATCC BAA-793 than during glucose consumption. In addition, acetate secretion was observed with an acetate:lactate ratio of 1:1 when L. plantarum ATCC BAA-793 utilized cranberry xyloglucans (Figure 5.3d). While fermenting glucose, *L. plantarum* exhibited an acetate:lactate ratio of 0.05±0.01 ($p<0.05$) (Figure 5.3d). We expected *L. plantarum*, as a heterofermentative species, to secrete acetate. Interestingly, formate production was detected during xyloglucan consumption, although it was not detected following glucose

fermentation. The secretion of acetate and formate has been previously observed when inefficient substrate utilization yielded less biomass [291, 292].

5.4.5 Bacterial commensals exhibit differential growth phenotypes while consuming oligosaccharide extracts containing secondary plant material

In addition to purified xyloglucans, crude cranberry cell wall extracts were evaluated as a growth substrate. These fractions are more crudely enriched for oligosaccharides and thus more closely mimic what would be encountered by the microbiota following the ingestion of cranberries. Moreover, prebiotic formulations would likely use a crude cranberry extract for functional or processing reasons. We tested two crude fractions, termed A2, which retains a pink color and is extracted from whole cranberries, and A6, which is derived from the primary A2 fraction. Both of these preparations have been previously reported [284]. However, the precise distribution of glycans and noncarbohydrate molecules in A2 is not fully characterized.

Accordingly, *B. longum* strains achieved more pronounced growth phenotypes while consuming A2 and A6. Cellular growth (Figure 5.4) and kinetics varied by the particular strain tested (Table 5.4). A2 was most vigorously utilized by *B. longum* subsp. *infantis* JCM7007 (OD600 of 0.58±0.34), *B. longum* subsp. *infantis* JCM1272 (OD600 of 0.38±0.10), and *B. longum* subsp. *longum* UCD401 (0.37±0.07) (Figure 5.4a; Table 5.4). With the exception of UCD401, these strains did not grow on purified xyloglucans. Interestingly, there are two *B. longum* subsp. *infantis* strains that utilize A2 as a substrate. This is significant, as *B. longum* subsp. *infantis* is predicted not to utilize xyloglucans; thus, other components of the A2 fraction were fermented or cofermented. In addition, *B. longum* subsp. *infantis* JCM1272 achieved moderate growth on A2 (OD600 of 0.17±0.08),

whereas growth on purified xyloglucans was not observed. In contrast, the more purified A6 fraction was utilized only by *B. longum* subsp. *longum* UCD401 and *B. longum* subsp. *infantis* JCM 1260, with final OD600s of 0.27±0.03 and 0.08±0.02, respectively (Figure 5.4b). Clearly, the A6 fraction is not as efficiently utilized as the cruder and likely polyphenol-containing A2 fraction (Table 5.4; Figure A5.7). UCD401 exhibited a gradual decline in growth efficiency while utilizing the crudest extract to the most purified form (Figure A5.7b) ($P<0.05$). This mirrors the general trend that the majority of bifidobacterial strains tested do not metabolize highly purified xyloglucans. This includes all *B. longum* subsp. *infantis* strains (Figure A5.7c). *B. longum* subsp. *longum* UCD401 utilizes A6, leading to an increase in the acetate: lactate ratio (1.90±0.16) and absolute formate production (8.87±2.63 mM) relative to those achieved with glucose, despite the lower biomass ($p<0.05$) (Figure 5.5). Formate production by UCD401 is greater than that by *B. longum* subsp. *infantis* JCM1260 when catabolizing A6 ($p<0.05$). This is consistent with formate secretion while utilizing highly purified xyloglucans and suggests that UCD401 is specifically consuming this substrate in the mixed-purity preparation. Interestingly, *B. longum* subsp. *infantis* JCM1260 exhibits an acetate:lactate ratio of 2.44±0.32 and 6.39±0.57 mM formate secreted (Figure 5.5c). Glucose flux through the bifid shunt was metabolized, as expected, to approximate the theoretical yield of 1.5 (1.82±0.15 and 1.43±0.01) ($p<0.05$) (Figure 5.5d). Again, this is consistent with utilization of the carbohydrate constituents of the A6 fraction.

5.4.6 Expression of arabinose utilization genes while utilizing the A6 cranberry xyloglucan fraction

The expression of four GH family genes in the UCD401 chromosome while metabolizing A6 was evaluated. This includes an α-L-arabinofuranosidase gene (BL_0405), two arabinan endo-1,5-α-L-arabinosidase genes (BL_0404, BL_0403), and a β-xylosidase gene (BL_0402). We observed that BL_0405, BL_0404, and BL_0402 were significantly upregulated, with a minimum of a 2-fold increase during exponential phase (Figure 5.6a, $p<0.05$). This indicates that the expression of these genes and their products is modulated during the utilization of the A6 xyloglucan fraction. Interestingly, BL_0403 expression did not significantly change relative to that of the glucose control ($p>0.05$). This indicates that the adjacent BL_0404 gene is responsible for xyloglucan hydrolysis. Moreover, differential regulation of these paralogs potentially reflects divergent enzymatic functions. Fermentation of the A6 fraction induces UCD401 to express transport-related proteins that may be involved in xyloglucan transport across the membrane. Upregulated transport genes, including those for a carbohydrate ABC transporter substrate-binding protein (BL_0398) and carbohydrate ABC transporter membrane proteins (BL_0397, BL_0396) exhibit >2-fold induction relative to the control (Figure 5.6b, $p<0.05$). This suggests recognition and a potential uptake of arabinose and xylose backbone motifs across the cell envelope.

5.4.7 Modeled bidirectional syntrophic interactions

Conditioned spent medium from xyloglucan fermentations was used to assess *in vitro* bidirectional syntrophic interactions in microplate growth. This occurs when fermentation by a primary strain provides hydrolysis products to be used by a heterologous

secondary strain that is incapable of utilizing the initial substrate. Since *L. johnsonii* does not grow on xyloglucans on a microplate, we included this strain as a negative control. Interestingly, *B. longum* subsp. *infantis* ATCC 15697 does not utilize purified xyloglucans as a sole carbon source; however, conditioned supernatants from *L. plantarum* and *L. johnsonii* enabled growth to final OD600s of 0.066±0.008 and 0.093±0.008 with growth rates of 0.940±0.106 h^{-1} and 0.801±0.077 h^{-1}, respectively (Table 5.5). We interpret this as moderate growth because of the characteristic sigmoidal response curve produced during fermentation. In contrast, supernatant harvested from *B. longum* subsp. *longum* UCD401 did not enable *B. longum* subsp. *infantis* ATCC 15697 to grow (Figure 5.7). This is likely due to the inability of *B. long*um subsp. *infantis* ATCC 15697 to utilize arabinosyl-reducing ends, as predicted by comparative genomics (15). UCD401 may potentially sequester and metabolize molecules that would otherwise be utilized by other bifidobacterial strains. Furthermore, it is possible that the lactobacilli secreted other products to enhance *B. longum* subsp. *infantis* growth (e.g., exopolysaccharides) (34). *B. longum* subsp. *infantis* ATCC 15697 utilization of carbohydrates liberated from lactobacilli and UCD401 primary fermentations were analyzed by liquid chromatography (LC)-MS (Figure A5.8). Of interest, ATCC 15697 grew on the spent medium from lactobacillus primary fermentations, albeit with a stronger peak intensity observed by LC-MS. This may be due to hydrolysis of higher-molecular-weight xyloglucans or the production of exopolysaccharides, as hypothesized with primary fermentations. In addition, we determined that ATCC 15697 is incapable of utilizing the spent medium from UCD401 in a secondary fermentation.

When *B. longum* subsp. *longum* UCD401 was grown on the *L. plantarum* supernatant, it achieved a lower final OD600 (0.096±0.005) than when it was grown on

purified xyloglucans in a primary fermentation ($p<0.05$), although the growth rates are similar regardless of whether UCD401 is conducting a primary or a secondary fermentation (Table 5.5). Conversely, the growth rate of *L. plantarum* on conditioned medium from *B. longum* subsp. *longum* UCD401 was significantly higher whereas its biomass production (final OD600 of 0.115±0.009) was significantly lower than that of purified xyloglucans (final OD600 of 0.29±0.03) ($p<0.05$) (Table 5.5). This may indicate the production of inhibitory compounds or a preference for intact oligosaccharides.

5.5 Discussion

It has been established that genotypic and phenotypic variations contribute to bifidobacterial preferences for carbon sources [215]. For the former, the *B. longum* subsp. *infantis* genome has evolved to enable milk oligosaccharide utilization at the expense of plant carbohydrates. Bifidobacteria deploy transporters to capture intact oligosaccharides or their derivatives from the extracellular milieu [183, 293]. Thus, the inability of *B. longum* subsp. *infantis* strains to utilize xyloglucans may be due to absence of specific transporters. This is consistent with *B. longum* subsp. *infantis* ATCC15697 utilization of lactobacilli hydrolysis products. These lactobacilli perform extracellular digestion to provide ATCC15967 with fermentable substrates. In contrast, UCD401 internalizes intact oligosaccharides to withhold potential growth substrates from ATCC15697.

It is likely that *B. longum* subsp. *longum* UCD401 utilize xyloglucans from the terminal arabinose positioned at the reducing end. This is consistent with expression of arabinose utilization genes within the UCD401 genome (Figure A5.9). This arabinose utilization cluster is conserved in *B. longum* subsp. *longum* strains with an *araC* transcriptional family operon upstream of α-L-arabinofuranosidase and β-xylosidase genes

adjacent to an ABC transporter cassette. Importantly, *B. longum* subsp. *longum* ATCC15707 does not grow on xylose but metabolizes arabinose as a sole carbohydrate source [294]. Accordingly, *B. longum* subsp. *longum* UCD401 utilizes arabinose more efficiently in comparison to other *B. longum* subsp. *longum* strains tested (Figure A5.10). It is noteworthy that this *B. longum* strain was isolated from an infant stool sample and the stronger utilization phenotype may reflect recent isolation and limited passages.

Bifidobacterial xyloglucan utilization requires transport of arabinose following extracellular hydrolysis of higher DP oligosaccharides. β-D-glucopyranosyl and α-D-xylopyranosyl residues are not metabolized extracellularly. This likely causes the accumulation of lower DP xyloglucans. Arabinose metabolism has been linked to genes encoding extracellularly secreted α-arabinofuranosidases, which is encoded within the UCD401 genome (Figure A5.4) [295]. As we predicted, *B. longum* subsp. longum UCD401 utilizes xyloglucan within the crude A6 fraction likely using an extracellular arabinofuranosidase (BL_0405). Arabinose liberated from xyloglucans was completely sequestered, as it was not detected in spent medium. It has been posited that bifidobacterial strains cannot use xylose backbones longer than xylotetraose (DP=4) [295]. The *B. longum* subsp. *longum* arabinose cluster encodes predicted intracellular xylosidases, which supports the hypothesis that transport is essential for catabolism of higher (DP>4) xylooligosaccharides (Figure A5.4). The up-regulation of solute binding transport proteins (BL_0398) and permeases (BL_0397 and BL_0396) suggest that uptake of arabinose and lower DP xyloglucans including xylose and glycosyl residues occur after releasing arabinose moieties.

In bifidobacterial carbohydrate metabolism, pyruvate is converted to lactate via lactate dehydrogenase which does not produce additional ATP but recycles NAD^+ [191]. Pyruvate-formate lyase (*pfl*; EC: 2.3.1.54) catalyzes formate and acetyl-coA production from pyruvate. Acetyl-coA is subsequently metabolized to acetate or ethanol secretion [191]. This results in increasing the acetate to lactate ratio and correspondingly higher ATP production [191, 193]. We predicted increased acetate secretion during UCD401 xyloglucan fermentation, although the lower biomass on this substrate hinders comparisons in absolute concentrations. However, formate and ethanol secretion was previously determined to impact the acetate:lactate ratio in bifidobacteria [191]. Thus, the shift towards formate production coincides with an increased need for ATP while metabolizing xyloglucans. Bifidobacterial secretion of formate while utilizing certain oligosaccharides has been previously observed [188, 222, 296]. Under certain conditions bifidobacterial oligosaccharide metabolism is characterized by high levels of lactate produced initially, with a shift occurring towards formate production later in the fermentation [214, 216, 222]. This suggests that formate production benefits the cell by generating additional ATP when oligosaccharides are catabolized slowly. In general, bifidobacteria secrete secondary products such as formate, succinate, and ethanol when achieving lower biomass concentrations (OD_{600nm}<0.5) and when the carbohydrate consumption rate is diminished [188, 193, 216, 222]. Our results are consistent in that formate production increases while utilizing xyloglucans slowly, ostensibly to bolster ATP production under these conditions.

Crude oligosaccharide extracts were tested as this is of interest for preparation of cranberry xyloglucans for prebiotic applications. The cranberry cell wall does not contain appreciable quantities of monosaccharides [297] and is not expected to influence growth

[284]. As the A2 fraction retains a pink color there is likely small quantities of phenolic compounds that may contribute to differential growth observed between A2 and the highly purified xyloglucans. Furthermore, the most abundant oligosaccharides within the A6 fraction are identical to the xyloglucans purified in this study [284]. However, XSGGG-Ac and XSGGG-Ac2 structures (i.e. acetylated xyloglucan oligosaccharides) have been identified in the A6 fractions and did not remain in the highly purified xyloglucans. Thus, these oligosaccharides may be responsible for promoting *L. johnsonii* and *B. longum* subsp. *infantis* JCM1260 growth. *B. longum* typically consumes short-chain oligosaccharides, likely subsequent to intracellular transport [183, 298]. Thus, it is possible that differential phenotypes may be due to variation in xyloglucan DP.

Lactobacilli are natural inhabitants of the human gastrointestinal tract and may be used as probiotics and in concert with prebiotics in synbiotic applications [288, 299]. Lactobacilli strains may utilize carbohydrates as well as bifidobacteria [300]. It is likely that *L. plantarum* uses the phosphoketolase pathway while consuming xyloglucans to secrete formate and acetate with lactate being reduced. This was previously observed in *L. plantarum* VTT E 79098 fermentation of arabino-xylooligosaccharide [292, 301, 302].

Our experiments suggest that syntrophic interactions following xyloglucan degradation may occur between other members of the gut consortium. The interactions between lactobacilli, bifidobacteria, and oligosaccharides are of interest in engineering synbiotic interventions. Moreover, lactobacilli-mediated cleavage of xyloglucans within the small intestine would impact substrates available to bifidobacterial commensals of the lower gastrointestinal tract. Syntrophic interactions during bifidobacterial *in vitro* co-fermentations on various carbohydrate sources has been previously described which

includes members of the genus *Bifidobacterium* [215, 247, 298]. Cooperative or cross-feeding between strains that colonize the gastrointestinal tract may contribute to competitive exclusion of sensitive taxa and maintain diversity through specialist adaptation to colonize unique niches [303]. Such syntrophic interactions under *in vivo* conditions might prompt a shift in the gut microbiome towards metabolism of plant-derived carbohydrates with a metabolome characteristic of saccharolytic activities [304]. We did not detect monosaccharides in spent media by HPLC leading to the hypothesis that liberated monosaccharides would be sequestered thus rendering them undetectable. Furthermore, it is possible that the transfer of conditioned media from the primary fermentation introduced endproducts to the secondary fermentation although at very low concentrations with minimal impacts to growth.

5.6 Conclusions

Among the bifidobacterial strains tested, *B. longum* subsp. *longum* UCD401 utilizes cranberry xyloglucans as a sole energy and carbon source. This is potentially significant as it was recently isolated from an infant and subjected to limited passages. This may be due to conserving phenotypic function, as genomic or regulatory features likely remained intact in the limited generations since isolation [305]. Furthermore, it hints at the potential for strain variation within infants and adults in their capacity to utilize cranberry xyloglucans. *B. longum* subsp. *longum* colonizes both infants and post-weaning individuals. The phenotypic versatility underlying the broad host range to subsist on a substrate encountered in the adult diet suggests a post-weaning strategy. It is notable that xyloglucan catabolism prompts a shift in the central fermentative pathway to obtain more

ATP. The significance of the altered metabolic profile to microbiome function or host health remains an outstanding question.

Table 5.1 List of strains used in this study [a]

Strain	Species	Origin
ATCC 15697	*B. longum* subsp. *infantis*	Feces of human infant
JCM 1260	*B. longum* subsp. *infantis*	Feces of human infant
JCM 1272	*B. longum* subsp. *infantis*	Feces of human infant
JCM 7007	*B. longum* subsp. *infantis*	Feces of human infant
JCM 11347	*B. longum* subsp. *longum*	Feces of human
ATCC 15708	*B. longum* subsp. *longum*	Feces of human
UCD 401	*B. longum* subsp. *longum*	Feces of human
ATCC BAA-793	*Lactobacillus plantarum*	Saliva- human oral cavity
ATCC 33200	*Lactobacillus johnsonii*	Human blood

[a] UCD: University of California Davis Culture Collection, ATCC: American Type Culture Collection, JCM: the Japanese Collection of Microorganism

Table 5.2 Primers used in this study.

Primer	**Sequence (5' – 3')**
Blon_0393F	CCATGTCCCACCGTTACCT
Blon_0393R	CCAGCGACTTCGACATCTTC
BL_0405F	AACCGCTTCCAGCAGATTTT
BL_0405R	TGGTAGGAATGCTCGTCCAC
BL_0404F	CAACGGCTGGTGGTATCTGT
BL_0404R	GGTCTGATTGTCGGGGATTT
BL_0403F	ACGATCCATCCATCGTCAAG
BL_0403R	CGACCAGTTGGTCCAGATGT
BL_0402F	ATCTACTCCGGATCGCTCGT
BL_0402R	TATCGCCCGTTGTCGTACTC
BL_0398F	GACGGCACCTACAAGTACGC
BL_0398R	AGGGACCACTTCACCTGGTT
BL_0397F	GCTCCTTCCAGGTCTTCGAT
BL_0397R	TGATGAGCAGCACGTACGAC
BL_0396F	GGTCACGATCATCTCCGTGT
BL_0396R	CCGAGGTAGCTGTTGACGAG

Table 5.3 Analysis of bacterial growth kinetics calculated with Wolfram Mathematica 10.3

Strain	2 % xyloglucans			2 % Glucose		
	k (h^{-1})	**ΔOD_{asym}**	**tc(h)**	**k (h^{-1})**	**ΔOD_{asym}**	**tc(h)**
B infantis JCM 1260	ND[a]	ND	ND	ND	ND	ND
B. infantis ATCC 15697	ND	ND	ND	ND	ND	ND
B. longum UCD 401	0.555±0.055	0.15±0.02[b]	19.7±2.5[c]	0.614±0.048	1.25±0.09[b]	13.7±0.6[c]
L. plantarum ATCC BAA-793	0.386±0.049[d]	0.29±0.03[b]	2.3±0.60[c]	0.569±0.005	1.48±0.02[b]	5.3±0.60[c]
L. johnsonii ATCC 33200	ND	ND	ND	ND	ND	ND

[a]ND, not determined.
[b]Significant difference in the asymptotic OD value of each strain compared to each other and to the positive control, glucose ($p < 0.05$).
[c]Significant difference in the inflection point (tc) of each strain compared to each other and to the positive control, glucose ($p < 0.05$).
[d]Significant difference between the growth rate (k) of *L. plantarum* on xyloglucans and that of other strains on xyloglucans and glucose ($p < 0.05$).

Table 5.4 Kinetic analysis of bacterial growth on A2 and A6 fractions xyloglucans calculated using Wolfram Mathematica 10.3.

Strain	A2 fraction xyloglucans			A6 fraction xyloglucans		
	k (h^{-1})	**ΔOD_{asym}**	**tc(h)**	**k (h^{-1})**	**ΔOD_{asym}**	**tc(h)**
B infantis JCM 1260	0.464±0.280	0.17±0.08	6.4±3.3	1.188±0.79	0.08±0.02[b]	3.3±1.8
B infantis JCM 1272	0.427±0.039	0.38±0.10	12.4±0.6	ND	ND	ND
B infantis JCM 7007	0.215±0.137	0.58±0.34	17.6±6.1	ND	ND	ND
B. infantis ATCC 15697	NA	NA	NA	ND	ND	ND
B. longum JCM 11347	ND	ND	ND	ND	ND	ND
B. longum ATCC 15708	ND	ND	ND	ND	ND	ND
B. longum UCD 401	0.438±0.152	0.37±0.08	11.3±3.0	0.270±0.084	0.27±0.03[a]	16.3±0.6
L. plantarum ATCC BAA-793	NA	NA	NA	0.513±0.061	0.25±0.02[a]	2.9±0.5
L. johnsonii ATCC 33200	NA	NA	NA	0.944±0.166	0.12±0.01[b]	1.4±0.3

[a]Significant difference between asymptotic OD values of strains in A6 fraction treatment ($p < 0.05$).
[b]ND, not determined.
[c]NA, not available.

Table 5.5 Growth kinetics of strains during syntrophic interaction

Strain	Supernatant from *B. longum* UCD 401			Supernatant from *L. plantarum* ATCC BAA-793			Supernatant from *L. johnsonii* ATCC 33200		
	k (h^{-1})	**ΔOD_{asym}**	**tc(h)**	**k (h^{-1})**	**ΔOD_{asym}**	**tc(h)**	**k (h^{-1})**	**ΔOD_{asym}**	**tc(h)**
B. infantis ATCC 15697	ND[e]	ND	ND	0.940±0.106[a]	0.066±0.008	10.3±0.6	0.801±0.077	0.093±0.008	10.3 ±0.6
B. longum UCD 401	NA[f]	NA	NA	0.632±0.120[b]	0.096±0.005[d]	12.8±0.6	0.468±0.070[d]	0.162±0.007[c]	11.0±0.0
L. plantarum ATCC BAA-793	0.890±0.158[d]	0.115±0.009[d]	2.1±0.9	NA	NA	NA	NA	NA	NA

[a]Significant difference between the growth rates of *B. infantis* ATCC 15697 in different conditioned media determined by paired t test ($p<0.05$).

[b]Significant difference between the growth rates of *B. longum* UCD401 in different conditioned media determined by paired t test ($p<0.05$).

[c]Significant difference between the asymptotic OD values of *B. longum* UCD401 in different conditioned media determined by paired t test ($p<0.05$).

[d]Significant difference in the growth kinetics of each strain in different conditioned media and its growth kinetics in xyloglucans alone (shown in Table 5.3) determined
by paired t test ($p<0.05$).

[e]ND, not determined.

[f]NA, not available.

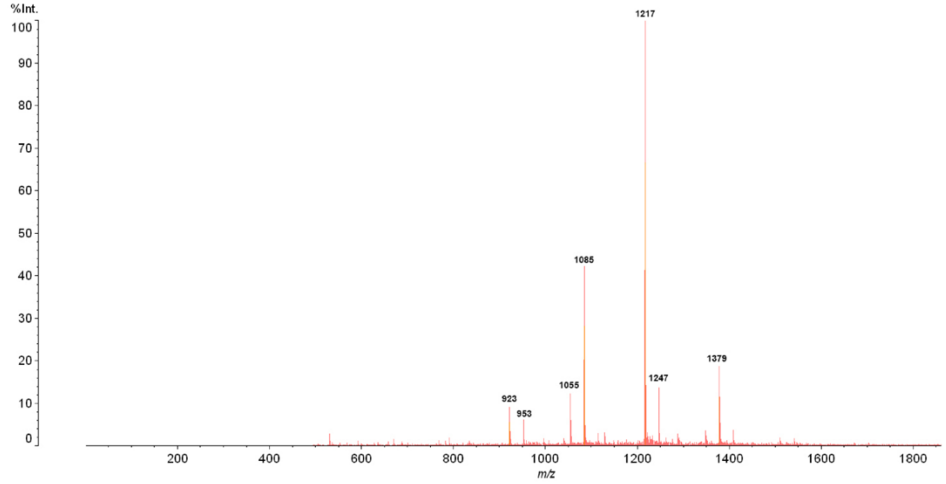

Figure 5.1 Purified cranberry xyloglucan putative structures. Positive reflectron mode MALDI-TOF-MS spectrum of cranberry xyloglucan obtained from Hiprep Sephacryl S-100 HR size exclusion column. The voltage was set at 80kV and 500 profiles were collected. Major peaks at m/z 923, 953, 1055, 1085, 1217, 1247 and 1379 represent sodium adducts ([M+Na]+) of xyloglucan with degrees of polymerization (DP) ranging from 6-9 and sugar compositions as follows: [Hexose3Pentose3+Na]+, m/z 923; [Hexose4Pentose2+Na]+, m/z 953; [Hexose3Pentose4+Na]+, m/z 1055; [Hexose4Pentose3+Na]+, m/z 1085; [Hexose4Pentose4+Na]+, m/z 1217; [Hexose5Pentose3+Na]+, m/z 1247; [Hexose5Pentose4+Na]+, m/z 1379.

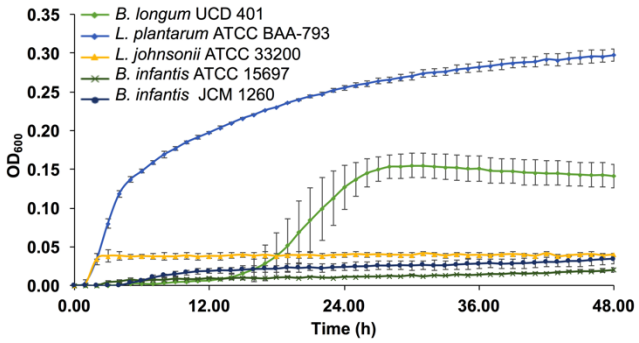

Figure 5.2 Bacterial growth while utilizing cranberry xyloglucans. Growth curves of *B. longum* subsp. *longum* UCD 401, *Lactobacillus plantarum* ATCC BAA-793, *Lactobacillus johnsonii* ATCC 33200, *B. longum* subsp. *infantis* ATCC 15697 and *B. longum* subsp. *infantis* JCM 1260 for growth on modified MRS containing 2 % (w/v) xyloglucans. The curves are drawn from average of three independent experiments.

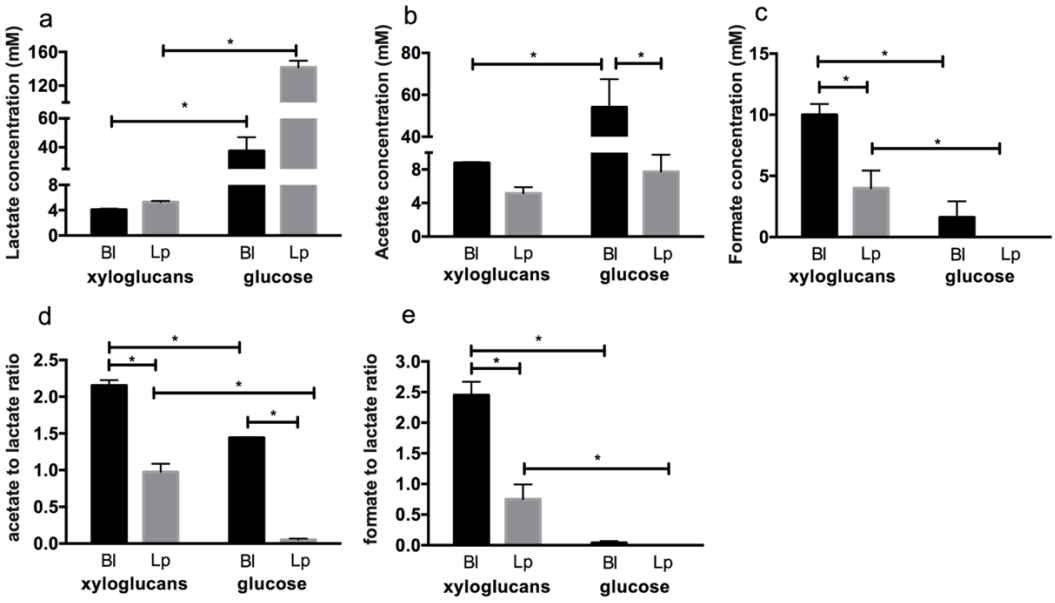

Figure 5.3 Bacterial fermentative endproducts while utilizing the cranberry xyloglucans. Production of lactate (a), acetate (b), formate (c). Acetate to lactate ratio (d), formate to lactate ratio (e). Strains are shaded as follows: *B. longum* subsp. *longum* UCD 401 (black) and *Lactobacillus plantarum* ATCC BAA-793 (grey). Averages from independent biological triplicates are shown and bars represent standard deviations of the means. The values for organic acid production are expressed in millimolar absolute concentration. Asterisks represent the significant difference evaluated by two-way ANOVA and Sidak's multiple comparison test ($p<0.05$).

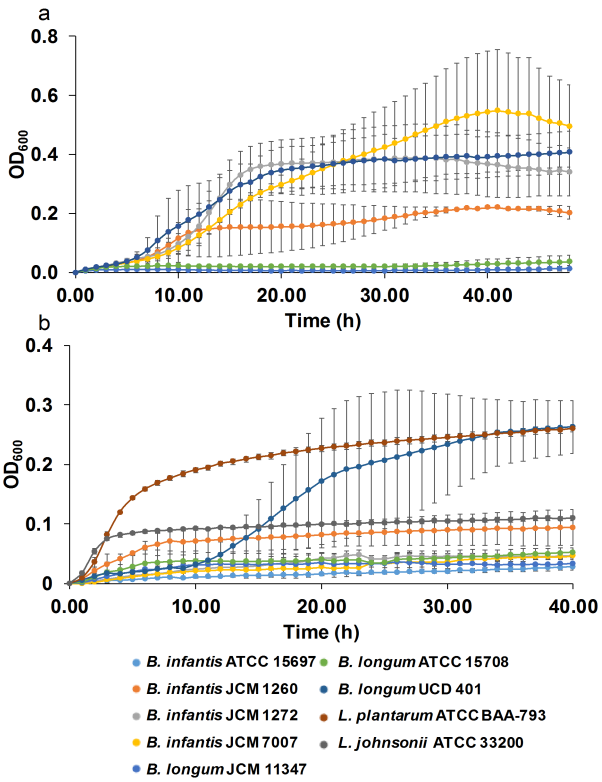

Figure 5.4 Bacterial growth on additional fractions of cranberry xyloglucans. Growth curves represent B. longum subsp. infantis ATCC 15697, *B. longum* subsp. *infantis* JCM 1260*, *B. longum* subsp. *infantis* JCM 1272, *B. longum* subsp. *infantis* JCM 7007*, *B. longum* subsp. *longum* JCM 11347*, *B. longum* subsp. *longum* ATCC 15708*, *B. longum* subsp. *longum* UCD 401, *Lactobacillus plantarum* ATCC BAA-793 and *Lactobacillus johnsonii* ATCC 33200 for growth on modified MRS containing (a) 2 % (w/v) A2 fractions xyloglucans, and (b) 2 % (w/v) A6 fractions xyloglucans. The curves are drawn from average of at least three independent experiments with the exception of strains labeled with asterisks which are based on duplicates in (a).

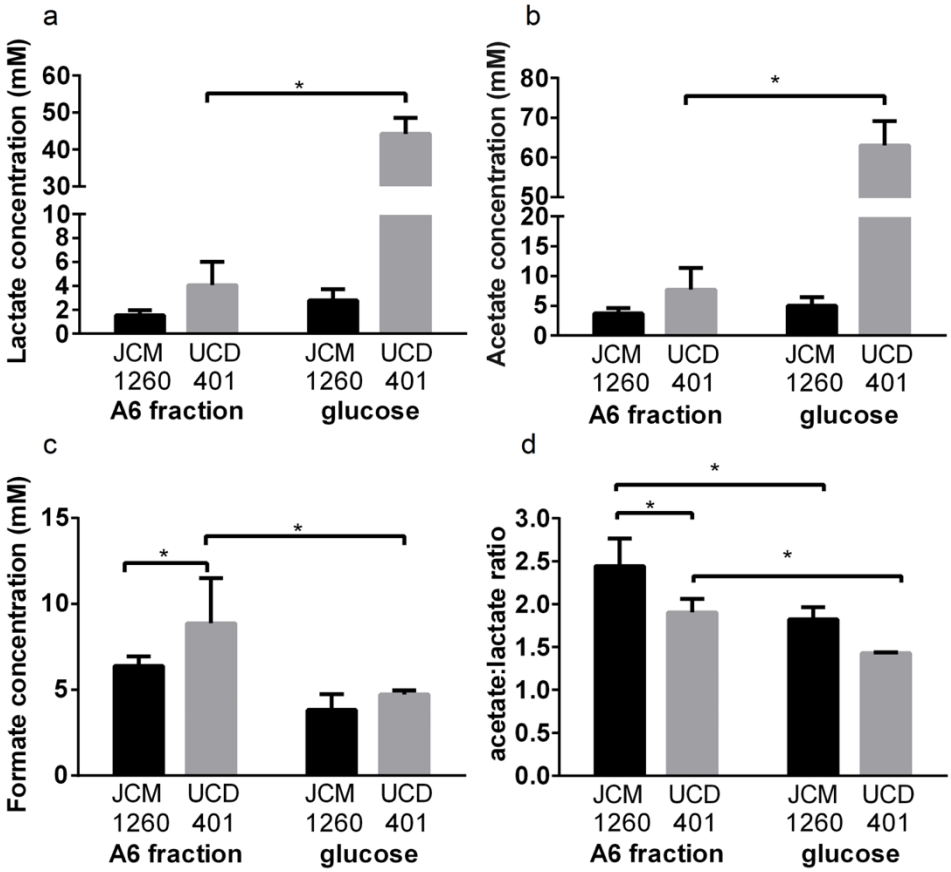

Figure 5.5 Bifidobacterial fermentative endproducts while utilizing the cranberry A6 fraction. Lactate (a), acetate (b), formate (c) production while *B. longum* subsp. *infantis* JCM 1260 and *B. longum* subsp. *longum* UCD 401 utilizes the A6 xyloglucan fraction collected at early stationary phase. Panel d also depicts the acetate to lactate ratio after fermentation. Averages from independent biological triplicates are shown and bars represent standard deviations of the means. Asterisks represent the significant difference evaluated by two-way ANOVA and Sidak's multiple comparison test ($p<0.05$).

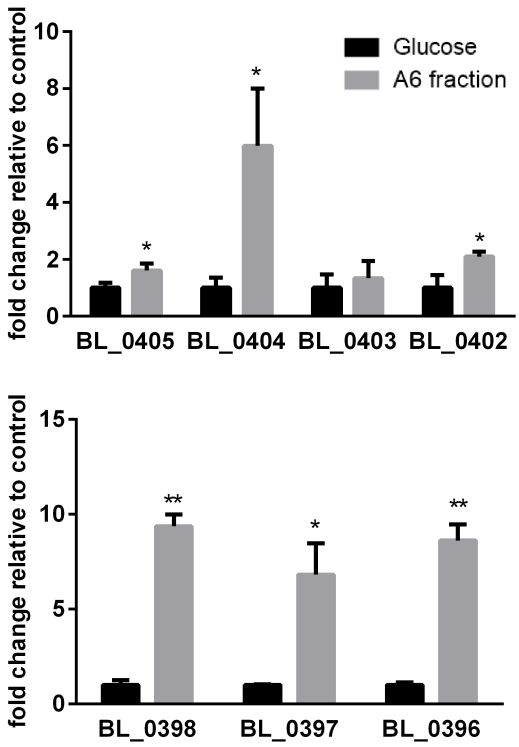

Figure 5.6 Gene expression of *B. longum* subsp. *longum* UCD 401 while utilizing the cranberry A6 fraction as a sole carbon source. Genes in arabinose cluster of *B. longum* subsp. *longum* UCD 401 predicted to participate in xyloglucan metabolism are depicted in the x-axis. The levels of expression of (a) four glycosyl hydrolase family genes, α-L-arabinofuranosidase, C-terminal (BL_0405), arabinan endo-1,5-α-L-arabinosidase (BL_0404, BL_0403), β-xylosidase (BL_0402) and (b) carbohydrate ABC transporter substrate-binding protein (BL_0398) and carbohydrate ABC transporter membrane proteins (BL_0397, BL_0396) are expressed in fold change relative to control (glucose). Averages from independent biological triplicates are shown and bars represent standard deviations of the means. Asterisks represent the significant difference evaluated by paired-t test ($p<0.05$).

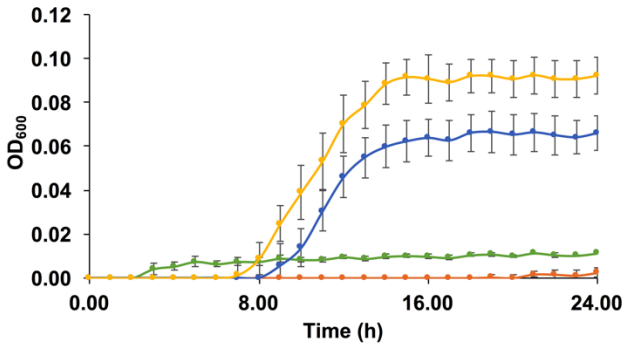

Figure 5.7 Bacterial syntrophic interactions after growth on cranberry xyloglucans. Growth curve of *B. longum* subsp. *infantis* ATCC 15697 on modified MRS containing xyloglucans (green), supernatants from *B. longum* subsp. *longum* UCD 401 (orange), *Lactobacillus plantarum* ATCC BAA-793 (blue) and *Lactobacillus johnsonii* ATCC 33200 (yellow) growth after xyloglucan fermentation. The curves are drawn from average of three independent experiments.

CHAPTER 6

THE COMBINATION OF CRANBERRY PROANTHOCYANIDINS (PACs) AND VARIOUS DIETARY OLIGOSACCHARIDES SYNERGISTICALLY PROMOTES THE GROWTH OF *LACTOBACILLUS PLANTARUM* ATCC BAA-793

Ezgi Özcan[1], Michelle Rozycki[1], and David A. Sela[1,2]

[1]Department of Food Science, University of Massachusetts Amherst, MA

[2]Department of Microbiology & Physiological Systems, University of Massachusetts Medical School, Worcester, MA

6.1 Introduction

Polyphenols are known to be bioactive antioxidant compounds with epidemiological evidence of their anti-inflammation, anti-cancer, anti-bacterial effects in both humans and animals [306–309] and *in vitro* [80]. The bioavailability of polyphenols has been found to be largely dependent on hydrolysis of polyphenols by gut microbiome such as reduction, decarboxylation, ring fussion, and demethylation [310, 311]. Cranberries contain polyphenols mainly proanthocyanidins (PACs) and anthocyanidins as well as flavanols and phenolic acids [312]. Proanthocyanidins (PACs) are condensed tannins comprised mainly of epicatechin units [313]. Polyphenol enriched cranberry products were found to be effective on obesity, inflammation and cardiovascular

disease [314–319]. The metabolism of PACs by human gut microbiome and their influence on the gut microbiome have been studied *in vitro* and *in vivo* [108, 109, 136, 319–324].

Lactic acid bacteria present in many vegetable and fruits, mostly facilitate the fermentation in fermented foods, and they have been previously studied for their association with polyphenols [325–329]. They are also probiotics and commensals in the human gut. Polyphenols might enhance the growth of intestinal microbes and probiotics due to favored sugar uptake and cell transport mechanism [330], or the degradation of PACs which provides additional energy for the cell growth (i.e., prebiotic effects)[331].

Lactobacillus plantarum IFPL935 was capable of modifying the phenolic profile of the cranberry extract, mainly due to catabolism of hydroxycinnamic and hydroxybenzoic acids not A-type or B-type dimers [325]. Adversely, catechin (100 mg/l) added to 0.5 % galactose containing media promoted the growth of *L. plantarum* RM71 by extending the sugar utilization, and sugar uptake without getting degraded by the bacteria [332]. *L. plantarum* IFPL935 was able to metabolize the polyphenols studied by means of galloyl-esterase, decarboxylase and benzyl alcohol dehydrogenase activities that led to the formation of gallic acid, pyrogallol and catechol, respectively [326]. There were also other lactobacillus strains which are capable of utilizing polyphenols. For example, grape pomace phenolic extract (1 mg/ml) induced a significant biomass of *L. acidophilus* grown in MRS broth [329]. Similarly, the mammalian intestinal commensal *L. johnsonii* N6.2 can degrade common dietary phytophenols (ferulic, caffeic, p- coumaric acid) as a mode of self-protection [333].

The synergetic effect of combination of polyphenols and probiotics are under investigation. For instance, proanthocyanidins derived from cranberries and probiotics

were tested on reducing the invasiveness of extra-intestinal pathogenic *Escherichia coli* (ExPEC) in a cell culture model [334]. Similarly, the effect of cranberry extracts on *Lactobacillus plantarum*'s anti-inflammatory activity on colon cancer cells was also investigated [335]. However, there was not much of evidence on tripartite relationship of oligosaccharides, polyphenols and gut microbes, e.g. *L. plantarum*.

We previously observed that *B. longum* UCD401 and *Lactobacillus plantarum* ATCC BAA-793 grow on xyloglucans (cranberry oligosaccharides) with a moderate biomass and produce formic acid [221]. In addition, secondary molecules in xyloglucan fractions boosted the growth of *B. infantis* and *B. longum* strains when these fractions are only carbon source in the environment [221]. Therefore, we hypothesize that oligosaccharide uptake inside the cells was favored and biomass was increased by addition of the secondary molecules. These secondary molecules are likely to be polyphenols present in cranberries. In this study, we will investigate the effect of polyphenol fractions extracted from cranberry (PACs) on the growth of *Lactobacillus plantarum* ATCC BAA-793 in the presence of different oligosaccharides such as cranberry oligosaccharides (xyloglucans, XG), fructooligosaccharides (FOS) and human milk oligosaccharides (HMOs). We will show that the mechanism underlying the effects of PACs on the *L. plantarum* physiology. We also hypothesize that *L. plantarum* deploys differential mechanism to utilize polyphenols in different fractions of cranberry PACs, depending on the carbohydrate source.

6.2 Material and Methods

6.2.1 The growth promotion assay and phenotypic response

The growth promotion assay was evaluated in a 96-well microplate. *Lactobacillus plantarum* ATCC BAA-793 was propagated in De Man Rogosa Sharp (MRS, Difco) medium supplemented with 0.05 % (wt/v) L-cysteine hydrochloride (Across Organics, New Jersey, USA) at 37 °C under anaerobic conditions (Coy Laboratory Products, Grass Lake, MI). Overnight cultures were centrifuged and resuspended in modified MRS (mMRS, without acetate and carbohydrate substrate), and then were used to inoculated (1% (v/v)) into mMRS with glucose (Sigma-Aldrich Co. St. Louis, MO), cranberry oligosaccharide fraction (xyloglucans, XG, Ocean Spray Inc, MA), fructooligosaccharides from chicory (FOS, Sigma-Aldrich Co. St. Louis, MO), pooled human milk oligosaccharides (HMOs, donated from Barile Lab at UC Davis) at a final concentration of 1% (wt/v, 10 mg/ml) as the sole carbohydrate source. Two different PAC fractions (Ocean Spray Inc, MA) were initially dissolved in absolute dimethylsulfoxide (DMSO) at 100 mg/ml concentration, then diluted in mMRS at the final concentration of 1 mg/ml for each carbohydrate source. This makes DMSO concentration 1 % (v/v) which is a concentration that does not affect the growth. The dose dependent response was conducted by diluting 1 mg/ml of PACs to 500, 250 and 125μl/ml concentrations. In addition, to investigate if PAC fractions involves in carbon metabolism, PAC fractions were also added in modified MRS as the same concentration without any carbon source. The growth assay was conducted anaerobically at 37 °C for 48 h by assessing optical density at 600 nm (OD_{600nm}) in an automated PowerWave HT microplate spectrophotometer (BioTek Instruments, Inc. Winooski, VT) placed in anaerobic chamber. Each experiment was evaluated in biological

triplicates with technical triplicates. Negative control consisted of inoculated medium in the absence of carbohydrate substrate and PAC fraction. For each carbohydrate and PAC combination, blanks were added into the respective wells and color change and degradation of polyphenols independent from bacterial fermentation were observed. The bacterial growth curves were represented by the subtraction of OD_{600nm} values of blanks of PAC fractions from respective OD_{600nm} values of bacterial growths. Growth characteristics were determined using growthcurver package in R [231], the obtained kinetics data were subjected to one-way ANOVA with Tukey's HSD test for multiple comparisons.

In addition to *L. plantarum* strain, other lactobacilli strains, *Lactobacillus johnsonii* ATCC 33200, *Lactobacillus reuteri* B-14171, *Lactobacillus pentosus* B-227, *Lactobacillus plantarum* ATCC 14914 while growing on glucose, HMOs and xyloglucans with PACs and bifidobacterial strains *Bifidobacterium longum* subsp. *infantis* ATCC 15697, *B. longum* subsp. *longum* UCD401 and ATCC 15707 while growing on lactose with PACs. The strains were acquired from ARS Culture Collection (NRRL) unless stated as ATCC. The propagation of other lactobacilli and bifidobacteria cells and microplate growth assay were performed as described above.

6.2.2 Metabolic end product determination

Cell-free supernatants from microplate growths were obtained at stationary phase and filtered through a 0.22 μm filter (Corning Costar Spin-X) following centrifugation and stored at -20 °C until further analysis. The secreted metabolites from bacterial fermentation were quantitated using an Agilent 1260 Infinity HPLC system (Agilent Technologies, Santa Clara, CA) equipped with a Wyatt Optilab T-rEX refractive-index detector (Wyatt Technology Corp., Santa Barbara, CA). Separation was carried out using an Aminex HPX-

87H column (7.8 mm ID x 300 mm, Bio Rad Laboratories, Hercules, CA) at 30 °C in a mobile phase of 5 mM H_2SO_4 at flow rate of 0.6 ml/min with 20 μl of injection volume. Standards including organic acids (i.e. acetic acid, lactic acid, formic acid), ethanol were acquired from Sigma-Aldrich Co. (St. Louis, MO). Metabolite concentrations were calculated from standard curves derived from external standards for six concentrations (0.5, 1, 5, 10, 20 and 50 mM). Metabolite profiling was carried out in triplicate and each measurement was performed in duplicate.

6.2.3 Determination of phenolic metabolites from cranberry PACs

The phenolic metabolites after *Lactobacillus plantarum* fermentation with PACs were determined using UPLC system coupled to an Acquity UV detector and an Acquity TQD tandem quadrupole mass spectrometer equipped with Z-spray electrospray interface (UPLC/Xevo TQD QQQ-MS, Waters, Milford, MA). We followed the protocol for separation as previously published [324, 325, 336]. Briefly, separation was done on a Waters BEH C18 column (100 x 1.0 mm id., Waters, Milford, MA) at 40 °C with aqueous phase A (2 % acetic acid in water (v/v) and an organic phase B (2% acetic acid in acetonitrile v/v) at a flow rate of 0.5 ml/min. The gradient was applied as: 0 min, 0.1% B; 1.5 min, 0.1% B; 11.17 min, 16.3% B; 11.5 min, 18.4% B; 14 min, 18.4% B; 14.1 min, 99.9% B; 15.5 min, 99.9% B; 15.6 min, 0.1% B with total run time 18 min. The UV was set to 280 nm wavelength. The ESI parameters were as follows: The ESI was operated in negative mode with the parameter as: capillary voltage, 3 kV; source temperature, 130 °C; desolvation temperature, 400 °C; desolvation gas (N2) flow rate, 750 l/ h; cone gas (N2) flow rate, 60 L/h. The MS/MS parameters (cone voltage and collision energy) of for analytes were optimized by direct infusion using 10 µg/ml solutions at a flow rate of 5

µl/min. The MS/MS conditions for each standard were given in Table A6.1. For quantification purposes, 3 groups of standards were prepared for separating their elusion times and mass spectra using the multiple reaction monitoring (MRM) mode. Data acquisition and processing was carried out by the MassLynx 4.1 software.

6.2.4 Preparation of transcriptome libraries of *L. plantarum* growing on PACs by RNA-seq

The cells were grown cells to their mid exponential stage in culture tubes up to 3 ml and collected approximately after 5 to 6 hours of incubation by measuring their OD in nanodrop (Thermo Scientific, Waltham, MA). The OD values differs according to their growth on each substrate measured by microplate. The pellets were obtained by centrifugation at 16,000 x g for 2 min and resuspended in 500 µl RNAlater solution after removal of supernatants. The samples were stored 4 °C overnight and transferred -80 °C. For RNA extraction, cells from -80 °C were centrifuged at 12,000 × g for 2 min to collect the cell pellet from RNAlater and the pellet washed twice with PBS buffer to remove residual RNAlater by centrifuging at 12,000 × g for 2 min. The total RNA was extracted using Ambion RNAqeous kit (LifeTechnologies, Carlsbad, CA) according to the manufacturer's instructions with slight modifications. Briefly, the cells were suspended with lysis buffer in Lysing Matrix E tubes (MP Biomedicals LLC, Solon, Ohio) to disrupt cell walls through beadbeating at 5.5 m/s for 30 s twice using FastPrep 24 bead beader (MP Biomedicals, Santa Ana, CA) with 5-min incubation on ice. Total RNA eluted in 50 μl of EB solution. After measuring RNA concentration in nanodrop, we proceeded with DNase treatment using the Ambion Turbo DNA-free (Invitrogen, Vilnius, Lithuania) using 1 μl of DNase I for 30 min. An aliquot of RNA was evaluated for genomic DNA contamination

by quantitative pcr using PowerUp Syber Green kit with primers targeted rpoD (Forward: 5'-GCT TAC GGT TCG GAC TTG ATG-3' and Reverse: 5'-GCC TTG GCT TCG ATT TGG-3') region in *L. plantarum*[19]. For samples with high levels of DNA contamination, DNase treatment repeated as same conditions. Another aliquot of RNA was quantified RNA using Qubit High Sensitivity RNA Assay Kit and RNA like integrity (RIN^e) were determined on TapeStation 2200 system using High Sensitivity RNA screen tapes and reagents (Agilent Technologies, Santa Clara, CA) following the manufacturer's protocol. The samples with RNA like integrity (RIN^e) more than 7.0 were proceeded with depletion of ribosomal RNA with Ribo-zero magnetic kit, bacteria (Illumina). Subsequently, the mRNA purification was performed using Qiagen RNaesy Minelute Cleanup according to instructions on Illumina protocol. RNA was quantified using the Qubit High Sensitivity RNA Assay (Life Technologies, Carlsbad, CA, USA) and rRNA depletion (the presence of 16S and 23S peaks) was checked on TapeStation 2200 system. The depleted RNAs (with RIN* approximately 1.0) were proceeded with NEBNext Ultra II Directional Library preparation kit (New England Biolabs, Inc, Ipswich, MA) following the instructions. The purification steps were done following the kit instructions using AmPure XP beads (Beckman Coulter, Brea, CA). The samples were indexed using NEBNext® Multiplex Oligos for Illumina (Dual Index Primers Set 1, New England Biolabs Inc, Ipswich, MA) indexes with PCR cycles of 10. The libraries were quantified using the Qubit double-stranded DNA (dsDNA) HS assay (Life Technologies, Carlsbad, CA, USA). The quality of library products was measured by DNA analysis ScreenTape assay on the TapeStation 2200 system (Agilent Technologies, Santa Clara, CA). The libraries were pooled in equimolar concentration (0.5 nM) and denatured immediately prior to sequencing

following Illumina library pool instructions. Sequencing was performed on an Illumina NextSeq platform (paired-end, NextSeq reagent kit v3, mid output, 5% Phi-X) at the Genomics Resource Laboratory, University of Massachusetts Amherst.

6.2.5 RNA-seq Analysis

Transcriptomic data (i.e. raw reads) of from Illumina BaseSpace was uploaded to the Massachusetts Green High-Performance Computing Cluster (MGHPCC) that was used for all computational/statistical analyses unless specifically noted. The RNA-seq reads were aligned to the reference *Lactobacillus plantarum* WCFS-1 genome (AL935263). Coding regions of the *L. plantarum* genome were used for alignments with bowtie 2. Total and unique gene reads aligning to a specific genomic locus (i.e. locus tag), as well as calculated raw counts (ht-seq count) was obtained for differential expression analysis.

6.2.6 Differential gene expression

In order to identify and quantify the magnitude of differentially expressed genes, the R package DESeq2 was used to analyze the raw count data [208]. Genes with a sum count < 200 was removed from analysis by pre-filtering. DESeq2 applies the Wald test for statistical analysis. Adjusted p-values ≤ 0.05 were defined as statistically significant.

6.2.7 Functional Enrichment Analysis

Gene feature fasta file of *L. plantarum* ATCC BAA793 (AL935263) was used as queries in BlastX from the National Center for Biotechnology Information (NCBI). L. plantarum protein sequencing database was used for blasting database. The resulting BlastX hits files were used to retrieve the functional annotations with OmicsBox (version 1.1.164) with default settings. For each substrate group, genes were ranked by their log2foldchange for gene expression relative to glucose. The ranked gene lists were

analyzed using Gene Set Enrichment Analysis (GSEA) for enrichment with functional annotations towards the top of the list (e.g. those most differentially expressed) using OmicsBox. Custom scripts were developed to create GSEA input files for different functional annotations as GO terms.

6.3 Results

6.3.1 High cranberry PAC fractions promotes the growth of *L. plantarum* on dietary oligosaccharides

We tested different concentrations of PAC fractions on the growth of *L. plantarum* during glucose (Figure A6.1). This showed that different doses of PAC did not significantly affect the growth on glucose. Therefore, we chose 1000 mg/ml concentration for the rest of the experiments. The growth curves for *L. plantarum* while growing on glucose, FOS, HMOs, and xyloglucans (XG) with two PAC fractions (1000 mg/ml) and PAC fractions (1000 mg/ml) alone as carbon source were shown in Figure 6.1 and the growth kinetics demonstrated as Table A6.1. While growing in glucose, PAC1 induced the growth of *L. plantarum* (OD_{600nm}=1.48±0.02) compared to glucose only (OD_{600nm}=1.21±0.03) and glucose with PAC2 (OD_{600nm}=1.07±0.01) (Figure 6.1A, $p<0.05$); however it did not grow different rate ($p>0.05$, Table A6.2). Glucose with 1 % DMSO did not show any detrimental effect on growth ($p>0.05$). While *L. plantarum* showed no growth on FOS ($p>0.05$ compared to negative control), addition of PAC1 and PAC2 significantly induced its growth (OD_{600nm}=1.02±0.01 and OD_{600nm}=0.25±0.04, Figure 6.1B, $p<0.05$) and changed their growth rate in both PACs ($p<0.05$, Table A6.2). While PAC1 elevated the *L. plantarum* growth on HMOs (OD_{600nm}=0.59±0.02, $p<0.05$), growth with PAC2 was not significantly different than the HMO only ($p>0.05$, Figure 6.1C). On the other hand, both

PAC1 and PAC2 induced the growth while growing xyloglucans (Figure 6.1D). It is also observed that PAC1 alone as carbon source promoted the growth (OD_{600}=0.40±0.02, Figure 6.1E) but PAC2 was not significantly different than the corresponding negative control ($p>0.05$). In all fermentation conditions except xyloglucans, PAC1 resulted in more biomass than PAC2 ($p<0.05$). This indicates that both PACs depending on the carbohydrate source, they enter the carbon-energy conversion in the cell metabolism and promote the growth.

6.3.2 High cranberry PAC fractions alters the fermentative end product formation during the growth on oligosaccharides

End products formed from central carbohydrate metabolism of *L. plantarum* were shown in Figure 6.2. *L. plantarum* produced mainly lactic acid (140.4±2.7 mM) and small amounts of acetic acid (16.2±0.7 mM) when growing on glucose (Figure 6.2A). It has been observed that PAC1 and PAC2 did not change both lactic acid (148.4±2.2 mM and 144.9±8.2 mM) and acetic acid (16.1±0.4 mM and 17.2±1.2 mM) concentrations in glucose fermentation ($p>0.05$, Figure 6.2A). Unlike glucose fermentation, *L. plantarum* produced formic acid, in addition to lactic and acetic acids during oligosaccharide fermentations. This phenomenon was observed previously when *L. plantarum* was growing on cranberry oligosaccharides [221]. FOS with PAC2 increased lactic acid concentration (6.2±0.3 mM) compare to FOS (4.8±0.5 mM) and FOS with PAC1 (4.5±0.6 mM) fermentations ($p<0.05$); but not formic acid and acetic acid (Figure 6.2B). It is interesting that despite the increased growth on FOS with PAC1, it did not favor the carbon metabolism. Decreased concentrations of lactic acid were observed in HMO with PAC1 (15.4±0.4 mM) compared to HMO (19.6±1.5 mM), HMO with PAC2 (18.9±0.3 mM) ($p<0.05$, Figure 6.2C) and in

PAC1 alone (5.6±0.3 mM) compared to PAC2 alone (7.9±0.9 mM) ($p<0.05$, Figure 6.2D). Similarly, XG with PAC2 significantly increased acetic acid (21.6±1.6 mM) and formic acid (4.6±0.4 mM) concentrations compared to XG alone (11.2±0.7 mM and 2.4±0.3 mM) and XG with PAC1 (10.3±0.9 mM and 2.7±0.1 mM) ($p<0.05$, Figure 6.2E). This means that PAC2 involves in the central carbon metabolism of *L. plantarum*; however, the metabolites facilitated differ between oligosaccharides fermentations.

6.3.3 *L. plantarum* involves in polyphenol degradation and produces phenolic metabolites depending on oligosaccharide type

Phenolic degradation products were profiled by mass spectrometry from the supernatants of *L. plantarum* growing on glucose, FOS, HMOs, xyloglucans (XG) with both PACs (Table 6.1). Among 13 metabolites, we observed 11 of them in our samples. The composition of two PAC fractions were displayed in Table A6.4. According to Ocean Spray method, PAC concentrations were higher in PAC1 fractions. We observed that the concentrations of procyanidin dimer B2, epicatechin and procyanidin dimer A2 in pre-fermentations varies depending on the type of oligosaccharides. It is possible that higher degree PACs might be degraded into these compounds variably due to their interaction with oligosaccharides during the set-up of the experiment. High amounts of procyanidin B2 was observed in pre-fermentations of HMO involving PAC2 and PAC2 alone. Bacterial fermentation resulted in degradation of procyanidin dimer B2 more than its simultaneous degradation over time, concomitantly production of 3-(3,4-dihydroxyphenyl) propionic acid. This metabolite was observed previously as a product of B2 bacterial metabolism [337]. This compound also observed in FOS and xyloglucans involving PAC2; however,

no B2 degradation occurred in those samples. This might be due to degradation of higher degree PACs into B2 simultaneously.

Formation of 3-(4-hydroxyphenyl) propionic acid, a product of procyanidin A2 degradation, was detected in all PAC2 fermentations. This degradation metabolite was not observed in no-fermentations. Procyanidin A2 was degraded in both bacterial and no-fermentations except HMOs. During HMOs, we did not observe degradation of A2. This means that although A2 tends to degrade over time, *L. plantarum* involves in conversion to phenolic metabolites.

Both 4-hydroxyphenylacetic acid and syringic acid were found in all fermentations and no-fermentations indicating these metabolites occurs with simultaneous degradation of PACs. In addition, there were p-coumaric acid in the pre-fermentations of PAC2; not in PAC1. This coincides with the composition of PAC fractions (Table A6.4), that PAC2 contains higher concentrations of phenolic acids. p-coumaric acid was degraded in PAC2 bacterial fermentations regardless of carbohydrate source while its concentration stayed similar in no-fermentations. This is potentially due to phenolic acid decarboxylation [338].

In pre-fermentations, epicatechin existed as trace amounts in PAC1 and relatively higher amounts in PAC2. After fermentation, we observed a degradation of epicatechin in PAC2 bacterial fermentations, but this was also observed in PAC2 no-fermentation samples. This means that this precursor compound degraded during fermentation conditions.

Catechol increased in all PAC fermentation while we have seen a decrease in protocatechuic acid in all PAC2 fermentations and HMO+PAC1 and XG+PAC1. Protocatechuic acid is precursor of catechol formation This also means that *L. plantarum*

involves in protocatechuic acid degradation with simultaneous catechol formation by means of alcohol dehydrogenase activity. Adversely, protocatechuic acid increased in PAC1 alone and FOS+PAC1. This means that the degradation of another compound resulting protocatechuic acid was faster than the conversion of protocatechuic acid to catechol formation; therefore, we observed an accumulation. These results showed that *L. plantarum* uses phenolic compounds depending on the type and carbohydrate source.

6.3.4 Whole transcriptome of *L. plantarum* differentially responds PAC fractions

To profile the transcriptional response of *L. plantarum* to major PACs with oligosaccharides, samples were extracted from duplicate cultures at mid exponential phase of their growth and glucose was used as a reference. RNAs extracted from samples were depleted of ribosomal RNA and used to quantify absolute transcript concentrations using RNA sequencing (RNA-seq). RNA-seq experiments were generated over 200 million reads in total, with each sample averaging 9.1 million reads. Reads were removed from 16S contamination using Silva 16S reference sequence, then were aligned to reference genome with NCBI accession number AL935263.

The alignment rates of reads to genome and coding genes were summarized in Table A6.3. Aligned reads to genes were counted using ht-seq count on Massachusetts Green High-Performance Computing Cluster (MGHPCC). Then, the raw counts were subjected to differential expression analysis using DESeq2 in R.

We first compared the whole transcriptomes of *L. plantarum* on every substrate with sample to sample distance matrices using hierarchical clustering (Figure 6.3). Biological replicates of samples with PACs showed dissimilarities to each other. PAC1 with oligosaccharides showed similarities with their corresponding oligosaccharide

combinations but not PAC2 samples. This might be due to *L. plantarum* switch the metabolism quickly between oligosaccharides to polyphenol.

Certain genes were highly expressed regardless of the growth conditions (Figure 6.4, Table A6.5). Genes include ribosomal proteins and elongation factors used in protein synthesis were expressed, which provides insights into lactobacillus physiology. One of the most transcribed loci across all samples was RNase P, which is a catalytic RNA that participates in post-transcriptional modification of tRNA molecules [339]. Interestingly, several key enzymes of central metabolic pathway (glycolysis), fructose-bisphosphate aldolase (lp_0330), glyceraldehyde-3-phosphate dehydrogenase (lp_0789), pyruvate kinase (lp_1897) and formate C-acetyltransferase (lp_3313) were highly expressed among all the samples.

6.3.5 Specific physiological networks are enriched during PAC metabolism

A Gene Ontology (GO) enrichment analysis was performed to determine biological processes, metabolic function, or cellular components responding to PAC fractions. The first comparison was made between cells growing on oligosaccharides with PACs and glucose as control. The most highly expressed GO terms with normalized enrichment scores for each differential expression of log2foldchange were shown in Figure 6.5. Among general GO terms nitrogen compound metabolic process was the most enriched network on both carbohydrate metabolism of HMOs (Figure A6.2G) and XGs (Figure A6.2J). *L. plantarum* differentially increased nucleic acid metabolic process, oxidoreductase activity and oxidation reduction process during both PAC1 and PAC2 metabolism (Figure 6.5A, B). PAC1 differentially increased metal ion bonding, organonitrogen compound biosynthetic process and nitrogen compound transport whereas these was not observed in

PAC2 metabolism. With HMO carbohydrate metabolism, PAC1 gene expression did not change compared to its PAC1 alone. (Figure 6.5D). HMO PAC2 increased hydrolase activity (Figure 6.5E) and FOS with PAC2 and XG with PAC2 differentially increased carboxylic acid metabolic process (Figure 6.5C, H). Decarboxylation and hydrolases are the processes involved in polyphenol metabolism.

6.3.6 High cranberry polyphenols change the growth phenotype of other lactobacilli and bifidobacterial strains on oligosaccharides

Other lactobacilli and bifidobacterial strains were tested to expand the characterization of synergistic effects of oligosaccharides with PACs. The growth curves of other lactobacilli while growing on glucose, HMOs and xyloglucans were shown in Figure 6.6 and Figure A.6.3. Among 4 additional strains, *Lactobacillus johnsonii* and *Lactobacillus plantarum* ATCC 14917 showed significant response with PACs. Addition of PAC1 significantly induced the growth of *L. johnsonii* when growing on glucose (OD_{600nm}= 0.72±0.01) and xyloglucans (OD_{600nm}= 0.48±0.02) compared to their corresponding carbohydrate source alone (Figure 6.6A, $p<0.05$). In contrast, PAC2 significantly increased the growth of *L. johnsonii* on HMO (OD_{600nm}= 0.22±0.02, $p<0.05$). Similarly, PAC2 induced the growth of ATCC 14917 on HMOs (OD_{600nm}= 0.49±0.04, $p<0.05$) whereas PAC1 promoted the growth on xyloglucans (OD_{600nm}= 0.50±0.01, $p<0.05$) (Figure 6.6B).

PACs did not significantly influence the growth of *L. reuteri* when growing on glucose, xyloglucans and HMOs (Figure A6.3A, $p>0.05$). PAC1 decreased the growth of *L. pentosus* on glucose ($p<0.05$) whereas PAC2 did not affect the growth (Figure A6.3B).

Both PACs had no impact to the growth of *L. pentosus* on HMO and xyloglucans (Figure A6.3B).

Unlike lactobacilli strains, the addition of both PACs into the growing media had detrimental effect on the growth of *Bifidobacterium longum* subsp. *longum* UCD401, ATCC 15707 while growing on lactose (Figure A6.4A, B). Only PAC2 diminished the growth of *B. longum* subsp. *infantis* ATCC 15697 while growing on lactose (Figure A6.4C).

6.4 Discussion

Both polyphenols and oligosaccharides benefit hosts through their microbiome. Commensal bacteria and probiotics use these dietary components to generate energy and release metabolites. The synergistic effect of cranberry components needs characterization to better target the benefits to host. The role of gut microflora in the catabolism of proanthocyanidins and plant oligosaccharides were separately explored using a static anaerobic incubation system with freshly collected human colonic fecal bacteria [135, 139]. A combination of xylooligosaccharides and a polyphenol blend was investigated for their effect on microbial composition and activity in a distal colon model [340]. However, the catabolic capacity of individual bacteria, that would be a probiotic candidate, is understudied. We posit the added effect of cranberry components with the oligosaccharides to contribute microbial metabolism within the human gut.

In the absence of carbohydrate, *L. plantarum* is usually unable to grow, however, both PAC1 and PAC2 increased the growth of *L. plantarum* in the absence of any carbohydrate source. This indicates that both polyphenol fractions involved in energy and carbon cycle. In addition, PAC2 increased lactic acid production compared to PAC1

metabolism and cell division functions and ATP binding were increased during PAC2 alone fermentations according to GO terms. During PAC1 fermentations, nitrogen related metabolic functions were enriched the most. This might indicate that polyphenol fractions involve not just in carbon metabolism but also nitrogen metabolism, which increase the growth of *L. plantarum*.

PAC1 addition increased the growth during all tested oligosaccharides whereas PAC2 only increased during xyloglucan growth. This means that PAC1 facilitates the cellular function. Cellular macromolecular biosynthetic processes were enriched during PAC1 alone and PAC1 with HMO (Figure 6.5), however PAC1 did not impact the metabolite production. Although growth mostly facilitated by the carbohydrate metabolism, since nitrogen compound related metabolic processes were enriched in PAC1 alone and HMO with PAC1 (Figure A6.2), this might indicate that the growth can be also facilitated by the nitrogen metabolism. Therefore, there were no carbon metabolite related enhancement.

PAC2 shows growth promotion effect during PAC2 alone, glucose, FOS and xyloglucans compared to their corresponding carbon source. In the metabolite production, we also observed that lactic acid productions with PAC2 metabolism increased compared to their corresponding FOS, HMOs and PAC2 alone. This indicates that PAC2 might extend sugar utilization. This was observed previously with catechin added to galactose during *L. plantarum* RM71 [328]. Besides, PAC2 fractions although they are rich in proanthocyanidins, it contains 15X higher total anthocyanins. Anthocyanins in plants and foods do not exist in free form, all occurring anthocyanins are O-glycosylated with sugar substitutes forms of anthocyanidins and when the sugar substitute number is higher than

three they can be attached to basic molecules with sugar and acyl linkages [341]. Therefore, these sugar linkages can be broken during *L. plantarum* growth and those sugar can become available for central metabolic pathway. This concept coincides with the increased lactic acid production. In addition, catechin addition extended sugar uptake [328] and polyphenol metabolism might favor cell transport mechanism [330]. During FOS with PAC2 metabolism, we observed that transmembrane transport activities were enriched.

During xyloglucan fermentation with PAC2, we observed an increase in formic and acetic acid production (Figure 6.2D). When the biomass is low, *L. plantarum* requires heterofermentation to produce more ATP [221]. Similarly, organic acid biosynthesis was enriched during XG+PAC2 fermentation (Figure 6.5H).

L. plantarum incorporate PAC fractions into its both carbon and nitrogen metabolism and these activities might be due to degradation of phenolic compounds in PAC fraction. Previously, the microbial metabolism of polymeric procyanidins in a static batch culture system with fresh fecal inocula resulted in products: 3-(3'hydroxyphenyl) propionic acid, 4-hydroxyphenyl acetic acid, 3-(4'-hydroxyphenyl) propionic acid, 3-pheylpropionic acid [342]. In our current study, *L. plantarum* metabolism of cranberry PACs resulted in occurrence of only 3-(4'-hydroxyphenyl) propionic acid in all PAC2 fermentations and trace amounts in PAC1 fermentations except XG+PAC1. 4-hydoxyphenyl acetic acid simultaneously occurred without fermentation except xyloglucans. 3-(3'-hydroxyphenyl) propionic acid did not appear in any fermentations. This means that *L. plantarum* is capable of deploying different pathways for degrading polyphenols. The theoretical pathway for B2 dimers microbial metabolism was demonstrated previously [68, 337] based on the findings on *in vitro* batch culture fecal

fermentations. Cleavage of the C-ring of epicatechin at C2 position or of interflavan bond to form epicatechin and oxidization of the A-ring are the initial functions. These metabolites are further degraded to valerolactone and valeric acid as intermediate metabolites and if the incubation continues, further dehydroxylation and alpha or beta oxidation occur to form various forms of phenyl propionic and acetic acids. Since we collect the samples at the stationary phase, we do not expect to see the intermediate products whereas we expect production of phenyl propionic and acetic acids. According to *in vitro* batch culture fermentations, 3-(3-4'-dihydroxyphenyl) propionic acid and 3-(3'hydroxyphenyl) propionic acid forms from microbial metabolism of epicatechin, procyanidin B2, and procyanidin A2 whereas only A2 leads to 3-(4'-hydroxyphenyl) propionic acid formation. 2-(3',4'-dihydroxyphenyl) acetic acid forms from metabolism of both B2 and A2 dimers. On the other hand, *L. plantarum* catabolized only epicatechin-O-gallate and resulting in formation of 1-(3′,4′-dihydroxyphenyl)-3-(2″,4″,6″-trihydroxyphenyl)propan-2-ol. This compound would arise from the reductive cleavage of the heterocyclic C-ring of flavan-3-ols [325]. However, in our study, we observed only catabolism of procyanidin B2. This means that depending on the type of strain *L. plantarum* deploys different mechanisms to utilize PACs.

Catabolism of cranberry extract resulted in a decrease in hydroxycinnamic acids, including p-coumaric acid as well as hydroxybenzoic acids, including protocatechuic acids, an increase in catechol fermentation but not diphenylpropan-2-ol [325]. This coincides with our findings. PAC2 fractions contains higher amounts of phenolic acids initially and pre-fermentation samples with PAC2 contains higher amounts of p-coumaric acid. The degradation of this phenolic acid contains decarboxylation and *L. plantarum* contains

decarboxylases [343, 344]. Although all PAC2 fermentations showed decrease in p-coumaric acid, only FOS with PAC2 and XG with PAC2 showed carboxylic acid metabolic process.

We observed that the synergistic *L. plantarum* metabolism on PAC fractions in presence of oligosaccharides can be extended to other lactobacilli, such as *L. johnsonii* and *L. plantarum* ATCC 14917. While PAC2 showed only increase in *L. johnsonii* growth with xyloglucans, this can be extended to HMOs in *L. plantarum* ATCC 14917. *L. johnsonii* was previously found to degrade ferulic, caffeic, p- coumaric acid as a mode of self-protection [333]. However, specific mechanisms involved in these activities for these species were not studied fully.

Although *B. infantis* strains showed promoted growth during cranberry oligosaccharide utilization when secondary molecules present, in this study, purified PAC fractions decreased their growth. This indicates that we cannot extend the synergistic metabolism of PAC with oligosaccharides to phylogenetically close neighbors of lactobacilli.

In conclusion, the development of new prebiotics, with added functionality, is one of the most serious challenges shared not only by the scientific community but also by the food industry. In this study we showed an added value of cranberry fractions within oligosaccharide fermentation of *L. plantarum*. This study provided detailed interrogation of the mechanism underlying the effects of PACs on the *L. plantarum* physiology. We observed that *L. plantarum* deploys differential mechanism to utilize polyphenols in different fractions of cranberry PAC and this is dependent on carbohydrate source.

Table 6.1 Phenolic degradation products profiled by mass spectrometry from the supernatants of *L. plantarum* growing on glucose, FOS, HMOs, xyloglucans (XG) with both PACs

	Alone					
	pre-fermentation		post-fermentation		no-fermentation	
	P1	P2	P1	P2	P1	P2
Protocatechuic acid	1.49	7.21	1.93±0.59	2.90±0.37	3.31	9.22
3,4-dihydroxyphenylacetic acid	0.12	0.12	0.00±0.00	0.09±0.09	0.12	0.18
4-hydroxyphenylacetic acid	0.46	0.46	0.37±0.17	0.46±0.17	0.53	0.66
Syringic acid	0.10	0.05	0.10±0.00	0.22±0.08	0.15	0.25
3-(4-hydroxyphenyl) propionic acid	0.06	0.06	0.12±0.12	49.06±7.34	0.06	0.00
catechol	0.00	0.00	0.36±0.31	4.61±0.92	0.00	0.00
3-(3,4-dihydroxyphenyl) propionic acid	0.00	0.00	0.00±0.00	7.93±2.98	0.00	0.00
p-coumaric acid	0.06	29.45	0.00±0.00	0.18±0.00	0.00	32.74
Procyanidin B2	0.00	6.00	0.87±1.52	2.95±2.88	1.75	3.89
epicatechin	0.66	2.69	0.72±0.09	1.84±±0.33	0.55	1.76
Procyanidin A2	8.64	6.04	2.61±0.67	4.33±0.60	1.73	3.40
	Fructo-oligosaccharides					
	pre-fermentation		post-fermentation		no-fermentation	
	P1	P2	P1	P2	P1	P2
Protocatechuic acid	1.36	6.17	2.12±0.37	2.60±0.28	7.79	9.74
3,4-dihydroxyphenylacetic acid	0.12	0.12	0.04±0.07	0.14±0.15	0.00	0.12
4-hydroxyphenylacetic acid	0.33	0.39	0.37±0.14	0.55±0.10	0.33	0.46
Syringic acid	0.10	0.00	0.10±0.05	0.19±0.03	0.40	0.66
3-(4-hydroxyphenyl) propionic acid	0.00	0.06	0.04±0.03	55.32±2.83	0.00	0.00
catechol	0.00	0.00	0.03±0.05	2.52±0.61	0.00	0.00
3-(3,4-dihydroxyphenyl) propionic acid	0.00	0.00	0.00±0.00	6.58±2.89	0.00	0.00
p-coumaric acid	0.06	30.24	0.00±0.00	0.41±0.04	0.06	31.22

Procyanidin B2	0.00	0.05	0.06±0.03	0.22±0.38	0.03	0.02
epicatechin	0.10	0.38	0.31±0.03	0.97±0.17	0.17	0.45
Procyanidin A2	0.00	0.05	0.01±0.01	0.07±0.03	0.00	0.09
	Xyloglucans (Cranberry oligosaccharides)					
	pre-fermentation		post-fermentation		no-fermentation	
	P1	P2	P1	P2	P1	P2
Protocatechuic acid	0.23	1.32	0.01±0.00	0.00±0.00	0.32	1.44
3,4-dihydroxyphenylacetic acid	0.00	0.00	0.00±0.00	0.00±0.00	0.00	0.00
4-hydroxyphenylacetic acid	0.00	0.00	0.33±0.00	0.33±0.00	0.00	0.00
Syringic acid	0.03	0.06	0.05±0.02	0.05±0.02	0.03	0.04
3-(4-hydroxyphenyl) propionic acid	0.00	0.90	0.00±0.00	1.04±0.05	0.00	0.89
catechol	0.16	0.00	0.39±0.12	1.34±0.11	0.00	0.00
3-(3,4-dihydroxyphenyl) propionic acid	0.00	0.12	0.12±0.02	1.33±0.14	0.00	0.00
p-coumaric acid	0.00	3.91	0.26±0.01	0.44±0.05	0.02	4.02
Procyanidin B2	0.41	0.44	0.18±0.16	0.35±0.03	0.14	0.28
epicatechin	0.04	0.09	0.04±0.00	0.07±0.01	0.00	0.03
Procyanidin A2	2.55	3.96	0.25±0.04	1.90±0.49	0.08	0.55
	Human milk oligosaccharides					
	pre-fermentation		post-fermentation		no-fermentation	
	P1	P2	P1	P2	P1	P2
Protocatechuic acid	1.23	7.79	0.17±0.04	0.28±0.04	2.53	11.88
3,4-dihydroxyphenylacetic acid	0.12	0.18	0.08±0.07	0.16±0.14	0.00	0.18
4-hydroxyphenylacetic acid	1.64	1.25	2.50±0.37	1.91±0.34	2.70	2.30
Syringic acid	0.05	0.05	0.07±0.03	0.27±0.03	0.20	0.20
3-(4-hydroxyphenyl) propionic acid	0.00	0.06	0.14±0.15	48.94±1.78	0.00	0.06
catechol	0.00	0.00	2.03±0.52	9.12±2.77	0.00	0.00

3-(3,4-dihydroxyphenyl) propionic acid	0.00	0.00	0.00±0.00	6.06±1.34	0.00	0.00
p-coumaric acid	0.00	24.94	0.00±0.00	0.16±0.04	0.06	28.54
Procyanidin B2	0.00	7.02	0.88+0.79	1.18±0.99	0.00	2.99
epicatechin	0.66	2.55	0.47±0.10	1.14±0.07	0.48	1.66
Procyanidin A2	5.93	6.82	4.08±0.25	5.77±0.14	7.15	6.63

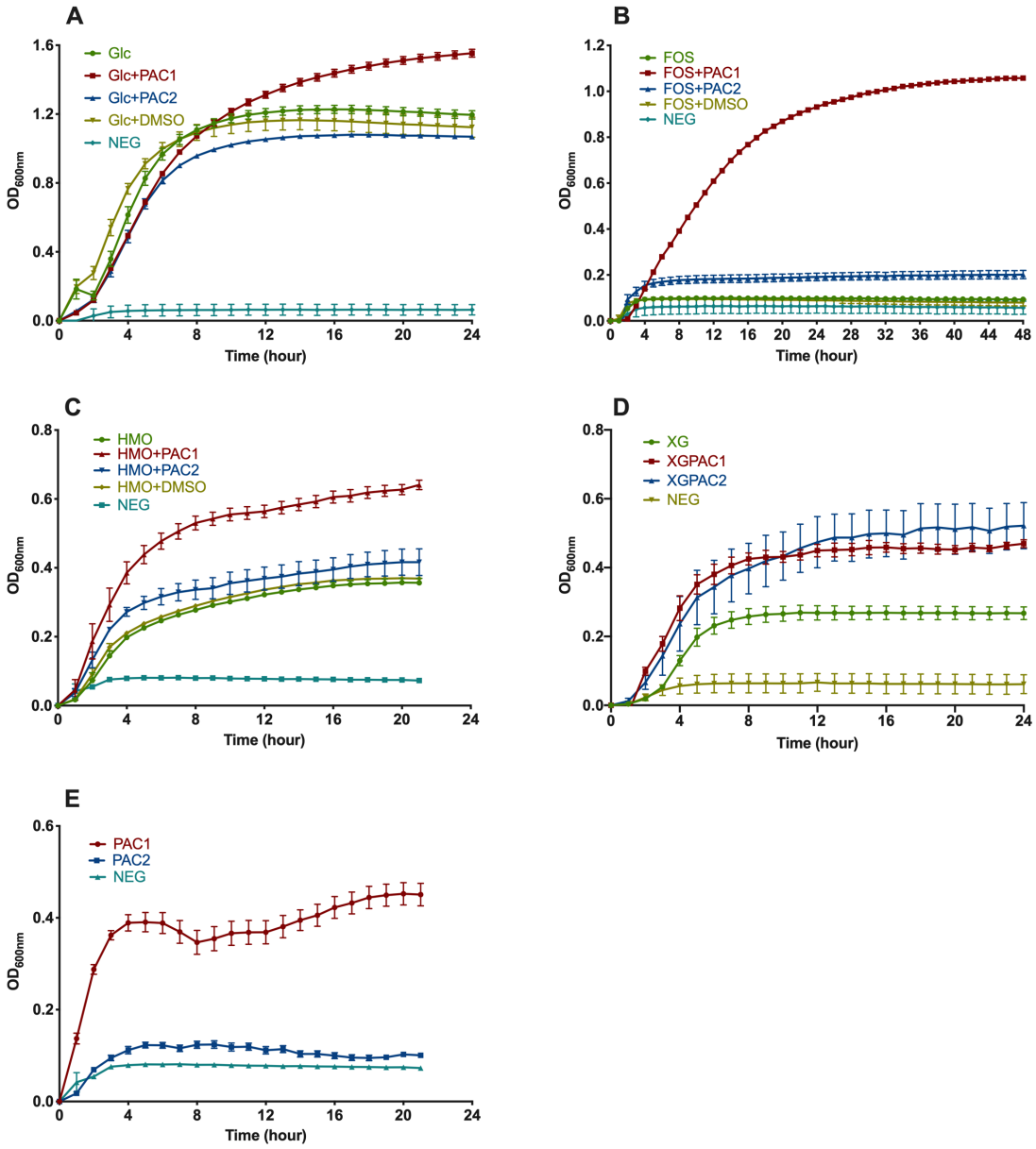

Figure 6.1 *L. plantarum* growth while utilizing cranberry PACs with oligosaccharides. Growth curves of *Lactobacillus plantarum* ATCC BAA-793 on modified MRS containing 1 % (w/v) glucose (A), fructooligosaccharides (FOS) (B), human milk oligosaccharides (HMO) (C), xyloglucans (XG) (D) and proantocyanidins (PACs) alone (D) and 1 mg/ml PAC fractions. The curves are drawn from average of three independent experiments.

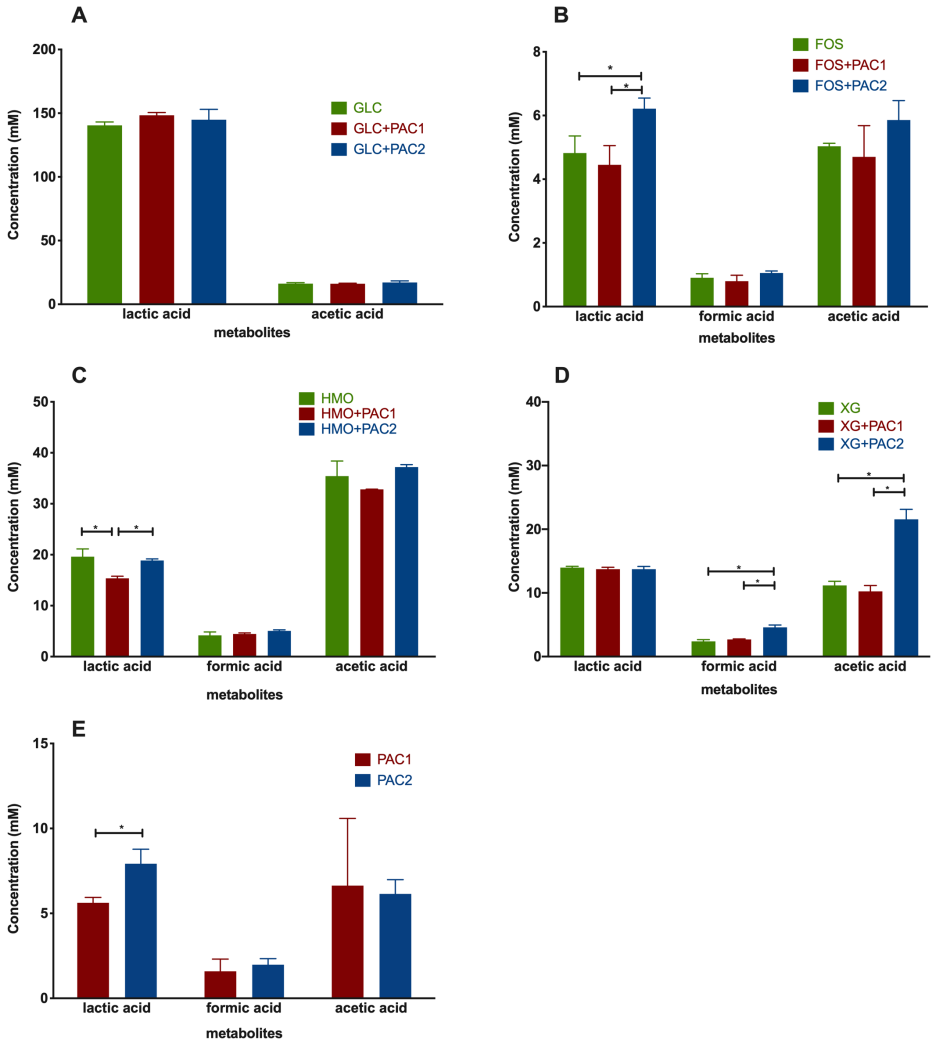

Figure 6.2 *L. plantarum* fermentative endproducts while utilizing the cranberry xyloglucans. Production of lactic acid, acetic acid, and formic acid during the growth of *L. plantarum* with PAC fractions on glucose (A), fructooligosaccharides (B), human milk oligosaccharides (C), xyloglucans (D) and PACs alone (D). Averages from independent biological triplicates are shown and bars represent standard deviations of the means. The values for organic acid production are expressed in millimolar absolute concentration. Asterisks represent the significant difference evaluated by two-way ANOVA and Sidak's multiple comparison test ($p<0.05$).

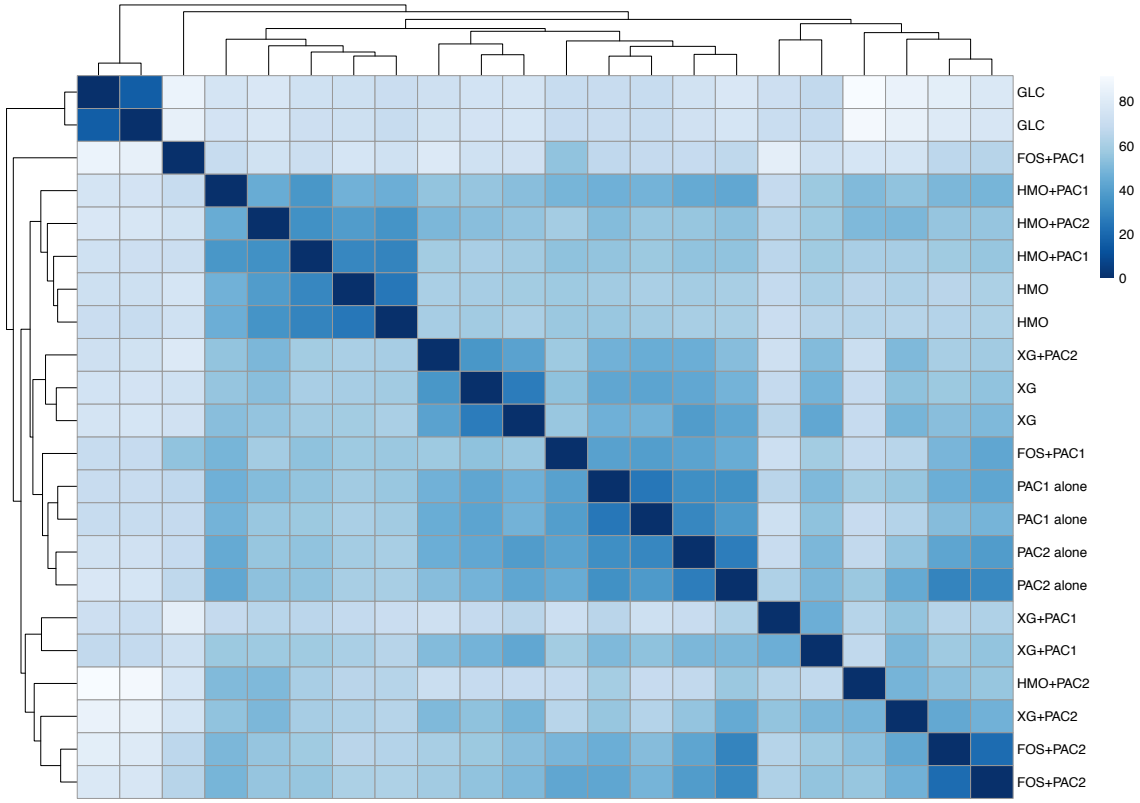

Figure 6.3 Whole transcriptome distances in substrate responses of *L. plantarum*. The heatmap shows the distances between the *L. plantarum* whole transcriptomes in response to glucose (GLC), cranberry proanthocyanidins (PACs) alone, fructooligosaccharides (FOS) with PACs, human milk oligosaccharides (HMOs) with PACs and xyloglucans (XG) with PACs The distances calculated are Euclidian distances of the regularized log transformation of counts with biological duplicates. The darkness of the blue color in the heatmap indicates the degree of similarity, from white (dissimilar) to dark blue (most similar). Likewise, the dendograms also show the distances with larger branch lengths indicating greater distances.

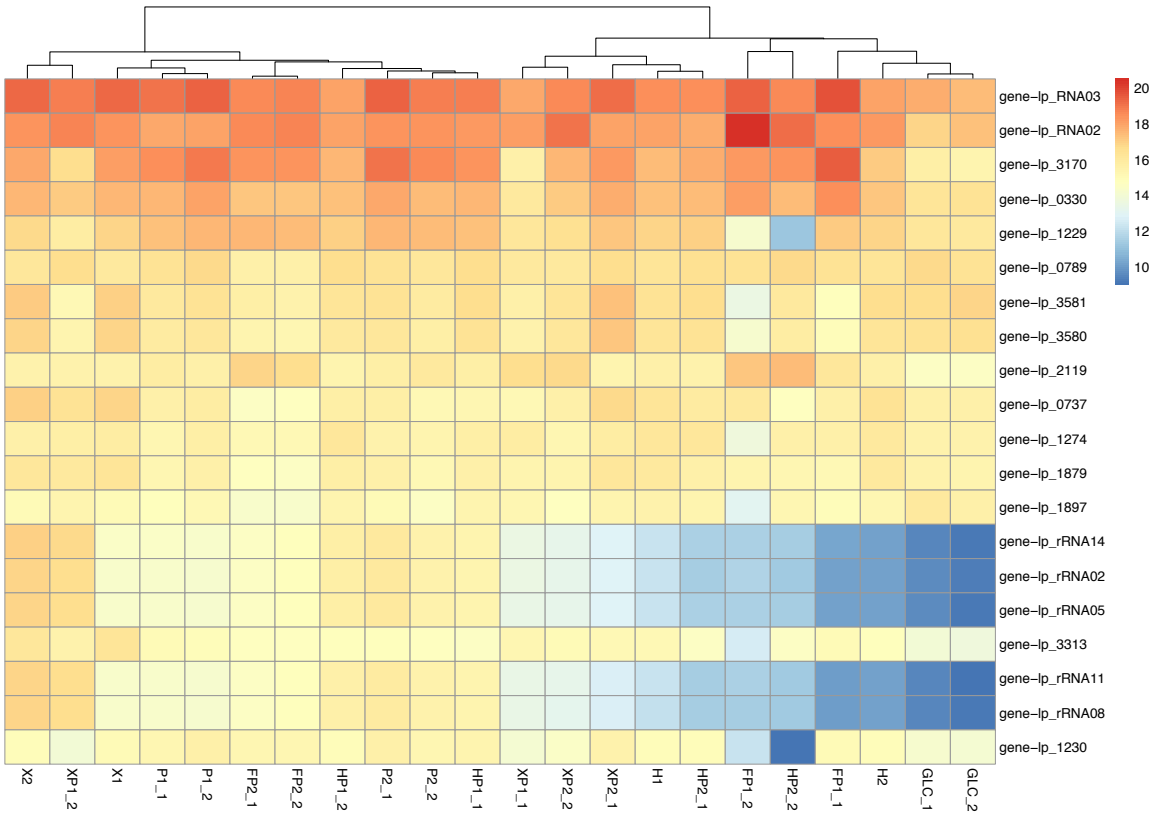

Figure 6.4 Most highly transcribed genes in all datasets in *L. plantarum*. The heatmap shows differential expressions of the *L. plantarum* whole transcriptomes in response to glucose (GLC), cranberry proanthocyanidins (PACs) alone, fructooligosaccharides (FOS) with PACs, human milk oligosaccharides (HMOs) with PACs and xyloglucans (XG) with PACs The distances calculated are Euclidian distances of the regularized log transformation of counts with biological duplicates. The darkness of the red color in the heatmap indicates the degree of highly transcribed genes. Likewise, the dendrograms also show the distances with larger branch lengths indicating greater distances between the whole transcriptomes.

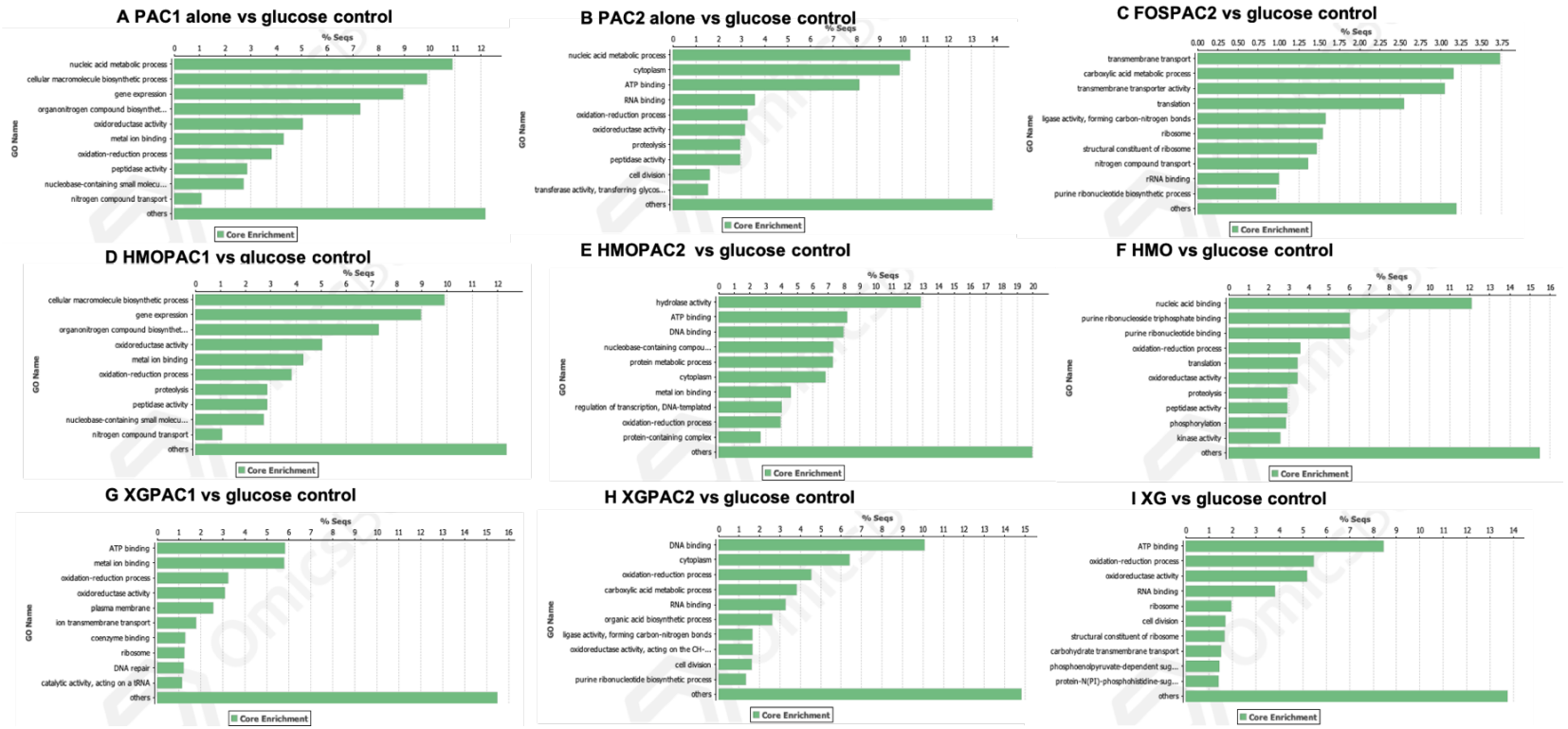

Figure 6.5 GO enrichment analysis in response to oligosaccharides with PACs. The 10 most specific GO term differential expression are considered through normalized enrichment score (NES) using OmicsBox tools. Higher scores indicate higher proportion of up-regulated genes in the pooled PAC1 alone (A), PAC2 alone (B), FOS+PAC2 (C), HMO+PAC1 (D), HMO+PAC2 (E), HMO (F), XG+PAC1 (G), XG+PAC2 (H), and XG (I) compared to the glucose control.

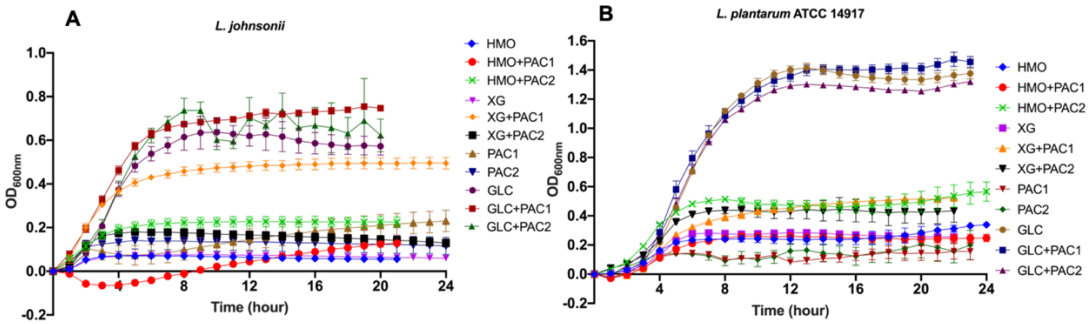

Figure 6.6 Bacterial growth while utilizing oligosaccharides with cranberry PACs. Growth curves of *Lactobacillus johnsonii* (A) and *Lactobacillus plantarum* ATCC 14917 (B) on modified MRS containing 1mg/ml PAC fractions and 1 % (w/v) glucose, human milk oligosaccharides, xyloglucans and PACs alone. The curves are drawn from average of three independent experiments.

APENDICIES

1. SUPPLEMENTARY TABLES

Table A2.1 Primers used in this study.

Primer	Sequence (5' – 3')
Blon_0393F	CCATGTCCCACCGTTACCT
Blon_0393R	CCAGCGACTTCGACATCTTC
Blon_0881F	TCGACAACGACATCAACCAG
Blon_0881R	AGTAGTCCTTGTGGCGCAGA
Blon_0882F	TGGGAGAAGAGCTTCGATGA
Blon_0882R	GAACGGGCCTTCCAGATG
Blon_0883F	TCCAAGAAGATCGAGGACGA
Blon_0883R	CGTAGGGGTTGGTGTACAGG
Blon_0884F	GTCGATCCGAACTTCATCCA
Blon_0884R	ACCGAGGGCACATAGAGGAT
Blon_0885F	GGACTTCTTCGCCTCCATTC
Blon_0885R	GGTCATGAGGGTCATGGAGA
Blon_2175F	ACCAACACGATGCTCTCGAT
Blon_2175R	CCACGAACAGGAACAGGAAG
Blon_2176F	CGTCGTGGCATCGATTATCT
Blon_2176R	TGTTGTAGCCGGTGAAGGTC
Blon_2177F	CGACTACTTCAGCGGACAGG
Blon_2177R	ACGGACAGACCGAGGTTCTT
Blon_2344F	ACCGGTGAGCACGAATACAC
Blon_2344R	TGTAGTCCTTGACGGGATCG
Blon_2345F	CTGAACTCGGTGTGGGTGTT
Blon_2345R	CCAAGCCAGTGAAGAAGTCG
Blon_2346F	GTGGACCTGTCCCTGTACGA
Blon_2346R	CCAAGCCAGTGAAGAAGTCG
Blon_2347F	GTCCCGAGGCAAGTCCTACT
Blon_2347R	AGCTGTCGAGCTTCCTGATG

Table A2.2 Function of genes described in Figure 2.5

Locus_tag	Annotation	Function
Blon_0248	alpha-L-fucosidase, GH, family 29 (EC 3.2.1.51)	Fucose metabolism
Blon_0268	GH, family 2	Enzymatic degradation
Blon_0282	GH, family 13, (EC 3.2.1.1)	Starch and sucrose metabolism
Blon_0417	glucose-6-phosphate isomerase (EC 5.3.1.9)	Sugar metabolism
Blon_0426	alpha-L-fucosidase, GH, family 29	Fucose metabolism
Blon_0459	beta-N-acetylhexosaminidase, GH, family 20	Enzymatic degradation
Blon_0538	*galE*, UDP-glucose-4-epimerase (EC 5.1.3.2)	Leloir pathway
Blon_0621	glucan 1,3-beta-glucosidase, GH family 5	Starch and sucrose metabolism
Blon_0625	beta-glucosidase, GH, family 3	Starch and sucrose metabolism
Blon_0645	*nanE* N-acylglucosamine-6-phosphate 2-epimerase (EC 5.1.3.9)	Amino sugar metabolism
Blon_0732	beta-N-acetylhexosaminidase, GH, family 20	Enzymatic degradation
Blon_0840	*ldh*, lactate dehydrogenase, (EC 1.1.1.37)	F6PPK pathway
Blon_0881	*nagB*, glucosamine-6-P isomerase (EC 3.5.99.6)	Amino sugar metabolism
Blon_0882	*nagA*, GlcNAc-6-P deacetylase (EC 3.5.1.25)	Amino sugar metabolism
Blon_0883	extracellular solute-binding protein, family 1	ABC transporter
Blon_0884	binding-protein-dependent transport systems inner membrane component	ABC transporter
Blon_0885	binding-protein-dependent transport systems inner membrane component	ABC transporter
Blon_0900	type I glyceraldehyde-3-phosphate dehydrogenase (EC 1.2.1.12)	F6PPK pathway
Blon_1095	*tal*, transaldolase (EC 2.2.1.2)	F6PPK pathway
Blon_1096	*tkt*, transketolase (EC 2.2.1.1)	F6PPK pathway
Blon_1100	GH, family 25	Enzymatic degradation
Blon_1368	ribulose phosphate-3 epimerase (EC 5.1.3.1)	F6PPK pathway
Blon_1654	GH, family 25	Enzymatic degradation
Blon_1714	*pfl*, pyruvate formate lyase (EC 1.97.1.4)	F6PPK pathway
Blon_1715	*pfl,* formate acetyl transferase (EC 2.3.1.54)	F6PPK pathway
Blon_1722	*xfp*, fructose-6-phosphoketolase (EC 4.1.2.22)	F6PPK pathway
Blon_1731	*ack*, acetate kinase (EC 2.7.2.1)	F6PPK pathway
Blon_1740	GH, family 13	Starch and sucrose metabolism
Blon_1745	*pyk*, pyruvate kinase (EC 2.7.1.40)	F6PPK pathway
Blon_1836	*eno*, enolase (EC 4.2.1.11)	F6PPK pathway
Blon_1843	beta-N-acetylhexosaminidase, GH, family 3	Amino sugar metabolism
Blon_1905	beta-glucosidase, GH, family 1	Starch and sucrose metabolism
Blon_2016	beta-galactosidase, GH, family 42	Galactose metabolism
Blon_2062	*galK*, galactokinase (EC 2.7.1.6)	Leloir pathway
Blon_2063	*galT*, galactose-1-phosphate uridyltransferase (EC:2.7.7.12)	Leloir pathway
Blon_2123	beta-galactosidase, GH, family 42	Galactose metabolism
Blon_2171	*galE*, UDP-glucose-4-epimerase (EC 5.1.3.2)	Leloir pathway
Blon_2172	*galT*, galactose-1-phosphate uridyltransferase (EC 2.7.7.10)	Leloir pathway
Blon_2173	*nahK*, N-acetylhexosamine-1-kinase (EC:2.7.1.162)	LNB metabolism

Blon_2174	1,3-galactosyl N-acetylhexosamine phosphorylase (EC 2.4.1.211)	LNB metabolism
Blon_2175	binding-protein-dependent transport systems inner membrane component	ABC transporter
Blon_2176	binding-protein-dependent transport systems inner membrane component	ABC transporter
Blon_2177	extracellular solute-binding protein, family 1	ABC transporter
Blon_2184	pgm, phosphoglucomutase, alpha-D-glucose phosphate-specific (EC 5.4.2.2)	Amino sugar metabolism Galactose metabolism
Blon_2191	*rpi*, ribose-5-phosphate isomerase EC 5.3.1.6)	F6PPK pathway
Blon_2334	*lacZ,* beta-galactosidase, GH, family 2	Galactose metabolism
Blon_2335	alpha-L-fucosidase 2, GH, family 65	Other glycan degradation
Blon_2336	alpha-L-fucosidase, GH, family 29	Other glycan degradation
Blon_2342	binding-protein-dependent transport systems inner membrane component	ABC transporter
Blon_2344	extracellular solute-binding protein, family 1	ABC transporter
Blon_2347	extracellular solute-binding protein, family 1	ABC transporter
Blon_2348	exo-alpha-sialidase	Other glycan degradation
Blon_2350	extracellular solute-binding protein, family 1	ABC transporter
Blon_2351	extracellular solute-binding protein, family 1	ABC transporter
Blon_2352	extracellular solute-binding protein, family 1	ABC transporter
Blon_2354	extracellular solute-binding protein, family 1	ABC transporter
Blon_2355	beta-N-acetylhexosaminidase, GH, family 20	Enzymatic degradation
Blon_2411	GH, family 43	Enzymatic degradation
Blon_2416	beta-galactosidase, GH, family 42	Galactose metabolism
Blon_2453	GH, family 13	Galactose metabolism
Blon_2460	GH, family 36	Galactose metabolism
Blon_2468	endo-beta-N-acetylglucosaminidase, GH, family 20	Enzymatic degradation

Table A2.3. Growth kinetics of *B. infantis* strains while utilizing milk carbohydrates calculated with Wolfram Mathematica 10.3[a]

Strains/ Carbohydrate source	UMA299		UMA300		UMA301	
	$OD_{600nm, asym}$	**k (h^{-1})**	**$OD_{600nm, asym}$**	**k (h^{-1})**	**$OD_{600nm, asym}$**	**k (h^{-1})**
Glucose	0.955 ± 0.083^{B}	0.553 ± 0.005^{B}	0.949 ± 0.055^{A}	0.580 ± 0.026^{B}	0.779 ± 0.066^{C}	0.301 ± 0.038^{C}
Galactose	1.033 ± 0.021^{AB}	0.590 ± 0.021^{B}	1.184 ± 0.209^{A}	0.753 ± 0.056^{A}	1.224 ± 0.045^{AB}	0.625 ± 0.060^{A}
GlcNAc	0.423 ± 0.092^{D}	0.160 ± 0.007^{C}	0.293 ± 0.080^{B}	0.154 ± 0.006^{C}	ND	ND
Lactose	1.161 ± 0.024^{A}	0.513 ± 0.009^{B}	0.525 ± 0.161^{B}	0.503 ± 0.110^{B}	1.285 ± 0.050^{A}	0.561 ± 0.054^{AB}
LNT	0.693 ± 0.091^{C}	0.567 ± 0.053^{B}	0.998 ± 0.196^{A}	0.719 ± 0.083^{A}	1.006 ± 0.167^{BC}	0.443 ± 0.057^{AB}
LNnT	0.708 ± 0.060^{C}	0.680 ± 0.057^{A}	1.300 ± 0.118^{A}	0.507 ± 0.049^{B}	0.861 ± 0.042^{C}	0.395 ± 0.138^{BC}

[a]The letters indicate significant differences observed between carbohydrates using one-way ANOVA and Tukey's test ($p<0.05$). ND - not determined.

Table A3.1. Growth kinetics of *B. infantis* strains while utilizing milk carbohydrates calculated with growthcurver package in R.

	pooled HMO		lactose		2´FL	
	$OD_{600nm, asym}$	Rate (k, h^{-1})	$OD_{600nm, asym}$	Rate (k, h^{-1})	$OD_{600nm, asym}$	Rate (k, h^{-1})
ATCC 15697	0.55±0.06a	0.76±0.05a	1.33±0.03	0.34±0.03c	0.41±0.11b	0.38±0.06
UMA299	0.49±0.04a	0.46±0.02c	1.31±0.04	0.35±0.01bc	0.79±0.08a	0.29±0.06
UMA300	0.34±0.05b	0.23±0.03d	1.14±0.14	0.53±0.03a	0.62±0.06ac	0.32±0.03
UMA301	0.62±0.08a	0.63±0.01b	1.15±0.28	0.40±0.01b	0.54±0.07bc	0.35±0.00

*The letters represent the significant difference between strains within the same column ($p<0.05$)

Table A5.1 MALDI-TOF Mass Spectrometry of cranberry xyloglucans with sodium adduct ions, composition and tentative assignments[a]

$[M+Na]^+$	Composition	Assigned structure
923	H_3P_3	SXG, XSG
953	H_4P_2	SGGG
1055	H_3P_4	SSG, GSS
1085	H_4P_3	GSXG
1217	H_4P_4	SSGG
1247	H_5P_3	SXGGG
1379	H_5P_4	SSGGG

[a]H: hexose, P: pentose, G: β-D-glucopyranosyl (β-D-Glc*p*), X: β-D-Glc*p* substituted at O-6 position with α-D-xylopyranosyl (α-D-Xyl*p*), S: X substituted at O-2 position of α-D-xyl*p* with α-D-arabinofuranosyl (α-D-Ara*f*).

Table A6.1 MS/MS conditions for phenolic metabolites detection[336]

Compound	Retention time (min)	[M-H]- (m/z)	m/z	Cone voltage	Collision Energy (V)
Pyrogallol	1.1	125	79	36	16
Protocatechuic acid	1.8	153	109	30	12
Catechol/pyrocatechol	2.6	109	81	44	14
3,4-dihydroxyphenylacetic acid	2.7	167	123	20	12
4-hydroxyphenylacetic acid	4.3	151	107	24	6
3-(3,4-Dihydroxyphenyl)-propionic acid	4.4	181	137	32	12
3-hydroxybenzoic acid	4.5	137	93	30	18
3-hydroxyphenyl acetic acid	5.0	151	197	25	16
Syringic acid	5.7	197	182	30	12
3-(4-hydroxyphenyl)-propionic acid	6.3	165	121	33	12
p-coumaric acid	6.7	163	119	30	14
3-(3-hydroxyphenyl)-propionic acid	7.6	165	121	32	12
Epicatechin	6.31	289	245	34	16
Procyanidin A2	10.17	575	285	44	24
Procyanidin A2	10.17	575	449	44	20
Procyanidin B2	5.26	577	289	36	22
Procyanidin B2	5.26	577	425	36	12

Table A6.2. Growth kinetics of L. plantarum in response to carbohydrates with PACs calculated with growthcurver package in R.

	$OD_{600nm, asym}$	RATE
Glucose	1.21±0.03	0.74±0.03
Glucose+PAC1	1.48±0.02abc	0.44±0.00b
Glucose+PAC2	1.07±0.01ab	0.73±0.01b
FOS	0.10±0.00	2.77±0.26
FOS+PAC1	1.02±0.01abc	0.23±0.00abc
FOS+PAC2	0.25±0.04ab	1.05±0.14ab
HMO	0.34±0.01	0.51±0.01
HMO+PAC1	0.59±0.02abc	0.66±0.01b
HMO+PAC2	0.38±0.04b	0.70±0.07b
XG	0.27±0.02	1.12±0.11
XG+PAC1	0.48±0.04a	0.83±0.12b
XG+PAC2	0.50±0.06ab	0.55±0.10ab
PAC1 alone	0.40±0.02cd	1.78±0.18
PAC2 alone	0.11±0.01	1.99±0.25

*The letters indicate significant differences observed between carbohydrates using one-way ANOVA and Tukey's test ($p<0.05$).
a: if it is different than corresponding carbon source
b: if it is different than corresponding PAC alone
c: if it is different between the two pac within same carbon source
d: if PAC alone different than negative control

Table A6.3. General features of the RNA-seq experiments

Sample	Number of reads*	% reads aligning to genome	% counts mapped to genes	number of no feature reads	% counts unmapped to genes
LP_GLC_1	9221438	98.79	84.9	1445048	15.7
LP_GLC_2	12093346	98.77	85.4	1849639	15.3
LP_PAC1_1	8624612	97.14	63.2	3010386	34.9
LP_PAC1_2	6599974	96.42	60.9	2399896	36.4
LP_PAC2_1	6588582	91.35	55.0	2437166	37.0
LP_PAC2_2	7572692	96.68	62.2	2676866	35.3
LP_FOSP1_1	6596108	98.43	49.0	3287733	49.8
LP_FOSP1_2	10096652	99.24	29.6	7214820	71.5
LP_FOSP2_1	9920768	96.85	57.9	3950811	39.8
LP_FOSP2_2	7836120	82.17	48.7	2671105	34.1
LP_HMO_1	2924134	96.4	70.5	786543	26.9
LP_HMO_2	8705044	99	72.1	2449899	28.1
LP_HMOP1_1	7736134	93.15	65.2	2249911	29.1
LP_HMOP1_2	8763882	90.77	67.2	2159683	24.6
LP_HMOP2_1	8963566	98.55	76.0	2210053	24.7
LP_HMOP2_2	9104024	98.55	72.4	2496786	27.4
LP_XG_1	8440096	96.82	62.9	2946760	34.9
LP_XG_2	8055766	82.13	54.0	2321634	28.8
LP_XGP1_1	8364220	82.97	71.7	1077865	12.9
LP_XGP1_2	6524084	55.62	36.3	1290991	19.8
LP_XGP2_1	8609078	98.17	66.8	2793281	32.4
LP_XGP2_2	9826372	93.66	66.3	2800076	28.5

*After 16S cleanup

Table A6.4. The composition of Cranberry PAC fractions obtained from Ocean Spray, Inc.

Test	Unit	8498 (PAC2)	120814 (PAC1)	Note
Total Organic Acid	%	2.9	ND	
Total Sugar	%	7	2	
Total Phenolic acid	mg/kg	134,600	2,500	HPLC method
Total flavonol	mg/kg	60,300	59,200	HPLC method
PACs-BL DMAC	mg/kg	190,500	194,000	with A2 Dimer as standard
PACs -OSC DMAC*	mg/kg	535,000	832,000	Ocean Spray internal method
Total Anthocyanin	mg/kg	16,300	1,300	HPLC method

* use PAC from whole fruit as standard

Table A6.5. Function of genes associated to highly expressed genes in *L. plantarum* described in Figure 6.4

Locus_tag	Annotation
lp_RNA03	misc_RNA
lp_RNA02	Rnase P RNA
lp_3170	pm9, phosphoglycerate mutase family protein, EC_number 5.4.2.1
lp_0330	fba, fructose-bisphosphate aldolase, EC_number 4.1.2.13
lp_1229	msa, mannose-specific adhesin, LPXTG-motif cell wall anchor
lp_0789	gapB, glyceraldehyde 3-phosphate dehydrogenase
lp_3581	lamC, two-component system histidine protein kinase; sensor, EC_number 2.7.3.-
lp_3580	lamA, two-component system response regulator; accesory gene
lp_2119	tuf, translation elongation factor Tu
lp_0737	sigma 54 modulation protein/ribosomal protein S30EA
lp_1274	ptsI, phosphoenolpyruvate-protein phosphotransferase
lp_1879	hbsU, DNA-binding protein
lp_1897	pyk, pyruvate kinase
lp_rRNA14	23S ribosomal RNA
lp_rRNA02	23S ribosomal RNA
lp_rRNA05	23S ribosomal RNA
lp_3313	pflB, formate C-acetyltransferase
lp_rRNA11	23S ribosomal RNA
lp_rRNA08	23S ribosomal RNA
lp_1230	transcription regulator, MarR family

2. SUPPLEMENTARY FIGURES

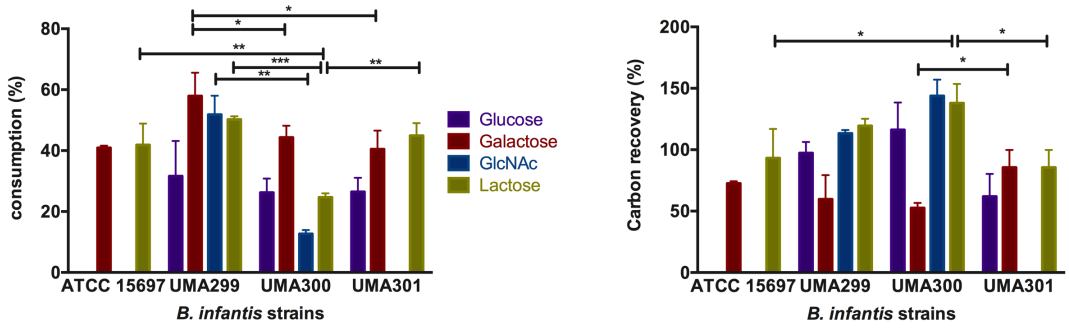

Figure A2.1 Consumption of mono- and di-saccharides by *B. longum* subsp. *infantis* strains. The mono- and di-saccharides consumption in percentages (A) and amount of carbon recovered in metabolites in percentages (B) of *B. infantis* strains subsisting on mMRS medium containing 2% (wt/v), glucose (purple), galactose (red), *N*-acetylglucosamine (GlcNAc, blue) and lactose (yellow). The data depicts mean ±SD of three independent experiments. The asterisks indicate the significant differences between strains evaluated by one-way ANOVA and Tukey's multiple comparison. Single asterisk (*) indicates $p<0.05$, double asterisks (**) $p<0.005$, triple asterisks (***) $p<0.0005$. For glucose and GlcNAc, the comparison was made between strains consuming those carbohydrate sources.

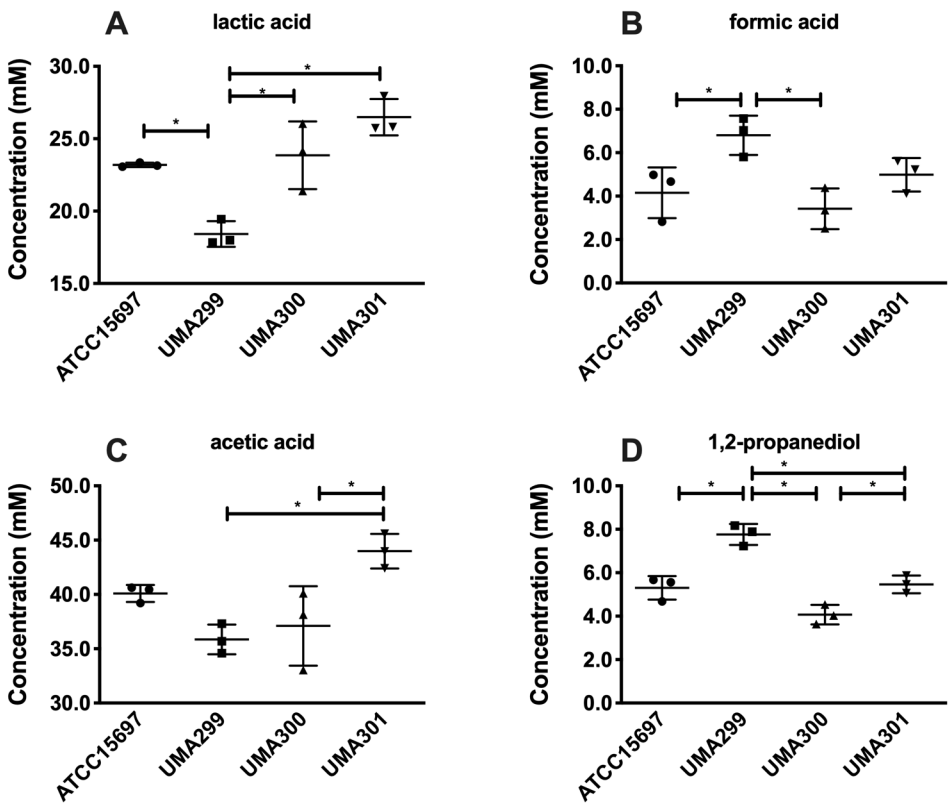

Figure A3.1 *B. longum* subsp. *infantis* strains fermentative end products while utilizing HMOs through the F6PPK pathway. Absolute concentrations of lactic acid (A), formic acid (B), acetic acid (C), and 1, 2-propanediol (D). All panels represent *B. infantis* ATCC15697 growing on mMRS medium containing 2% (wt/v) human milk oligosaccharides. Averages from independent biological triplicates are shown with bars representing standard deviations of the means. The values for organic acid production are expressed in millimolar (mM) absolute concentrations. A single asterisk (*) denotes significant differences between strain evaluated by one-way ANOVA and Tukey's multiple comparison test ($p<0.05$).

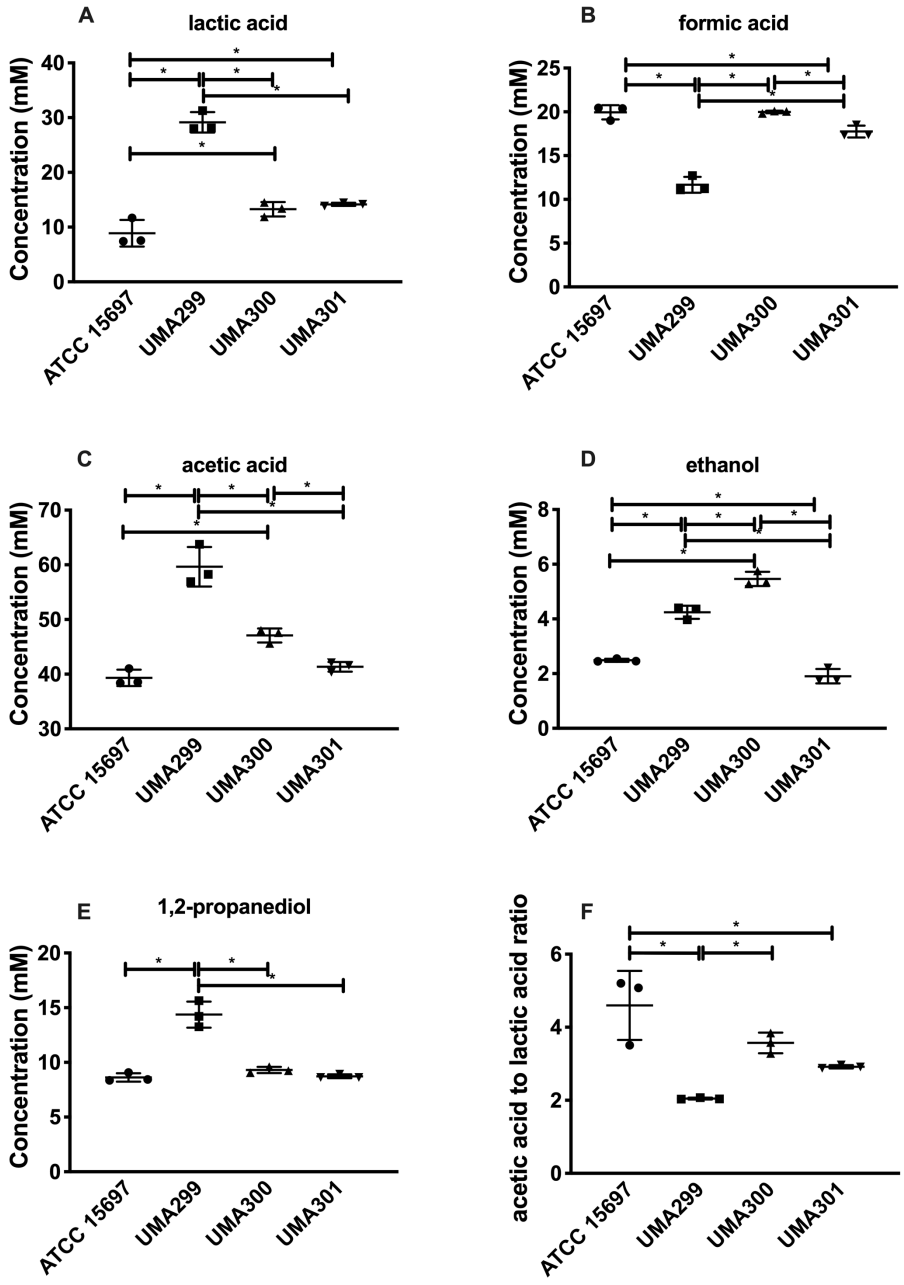

Figure A3.2 *B. longum* subsp. *infantis* strainsfermentative end products while utilizing HMOs through the F6PPK pathway. Absolute concentrations of lactic acid (A), formic acid (B), acetic acid (C), ethanol (D), and 1, 2-propanediol (E) and acetic acid to lactic acid ratio (F). All panels represent *B. infantis* ATCC15697 growing on mMRS medium containing 2% (wt/v) 2'fucosyllactose. Averages from independent biological triplicates are shown with bars representing standard deviations of the means. The values for organic acid production are expressed in millimolar (mM) absolute concentrations. A single asterisk (*) denotes significant differences between strains evaluated by one-way ANOVA and Tukey's multiple comparison test ($p<0.05$).

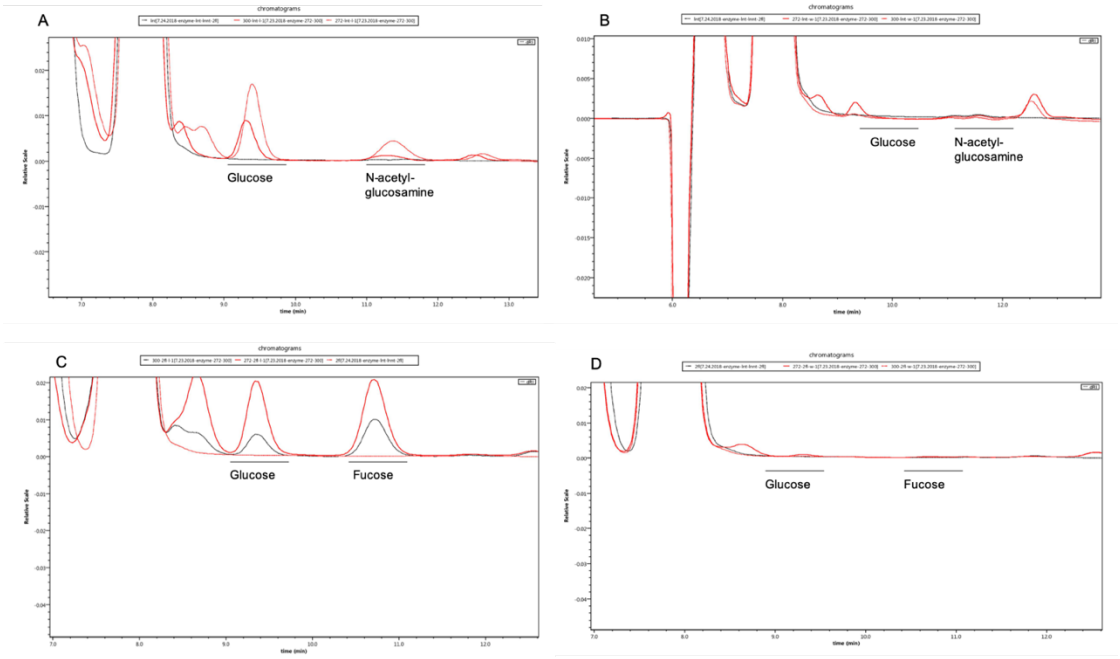

Figure A3.3 HPLC chromatograms of monosaccharides produced after whole cells and cell free lysates fermentations of *B. infantis* strains on LNT and 2 fucosyllactose. (A) peaks of glucose and N-acetylglucosamine after LNT fermentation of cell free lysates of ATCC 15697 (UMA272) and UMA300. (B) peaks of glucose and N-acetylglucosamine after LNT fermentation of whole cells of ATCC 15697 (UMA272) and UMA300. (C) peaks of glucose and fucose after 2'fucosyllactose fermentation of cell free lysates of ATCC 15697 (UMA272) and UMA300. (D) peaks of glucose and fucose after 2'fucosyllactose fermentation of whole cells of ATCC 15697 (UMA272) and UMA300.

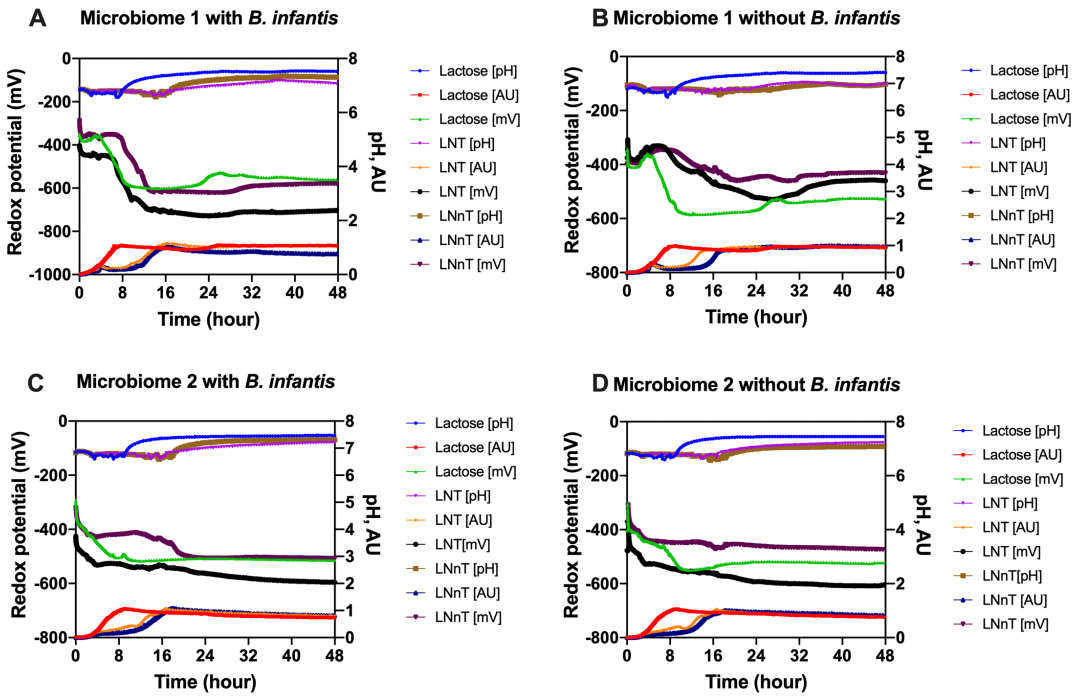

Figure A4.1 Fermentation parameters (redox potential (mV), pH and absorbance unit (AU) monitored over time. Parameters for each set of bioreactors inoculated with 1st microbiomes derived from baby fecal samples with *B. infantis* (A) and without *B. infantis* (B) and with 2nd microbiomes derived from baby fecal with *B. infantis* (C) and without *B. infantis* (D).

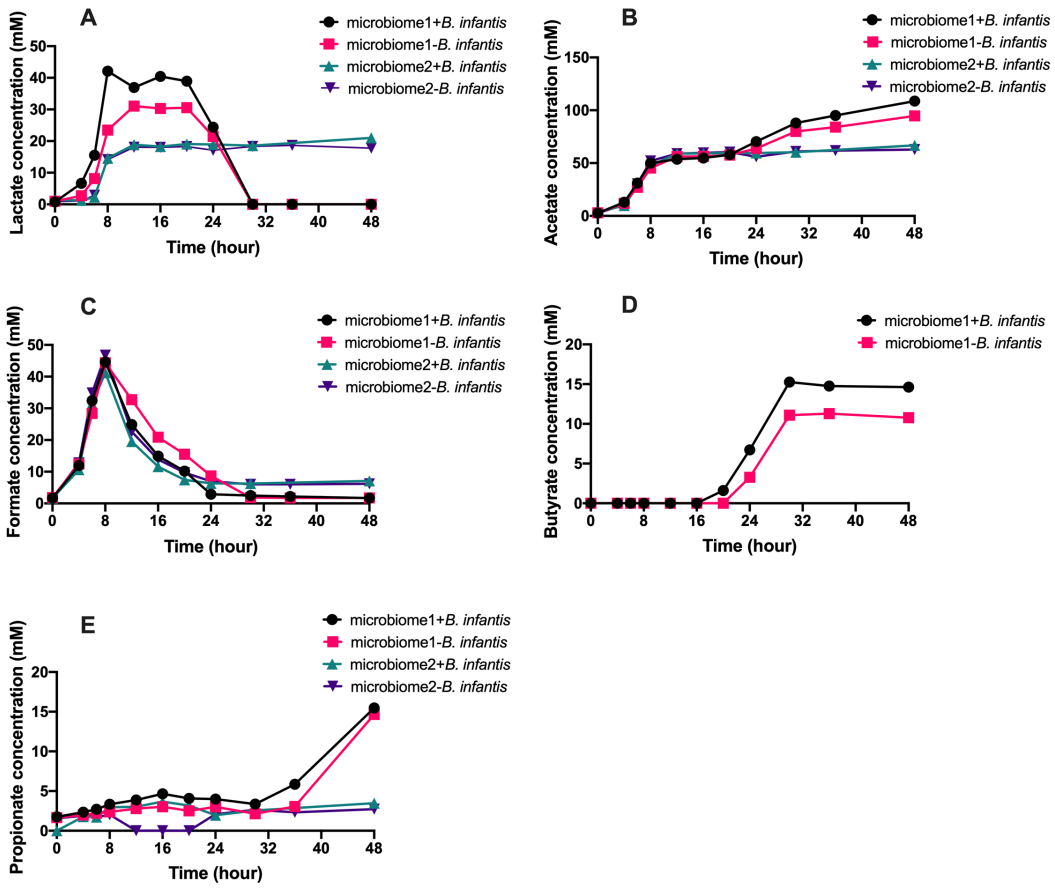

Figure A4.2 Microbial metabolites produced during the growth of infant fecal inoculated microbiomes with and without *B. infantis* addition on lactose as control within a modeled system. Absolute concentrations of **(A)** lactate, **(B)** acetate, **(C)** formate, **(D)** butyrate and **(E)** propionate in millimolar (mM).

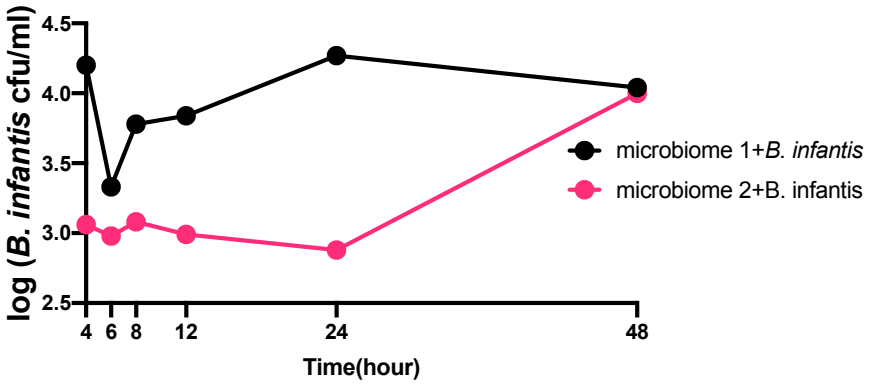

Figure A4.3 *B. infantis* levels during the lactose fermentations. The levels were determined by qPCR represented as log (cfu/ml) on microbiomes derived from 1st baby fecal and from 2nd baby fecal. B. infantis initially inoculated at 104 cfu/ml at time 0.

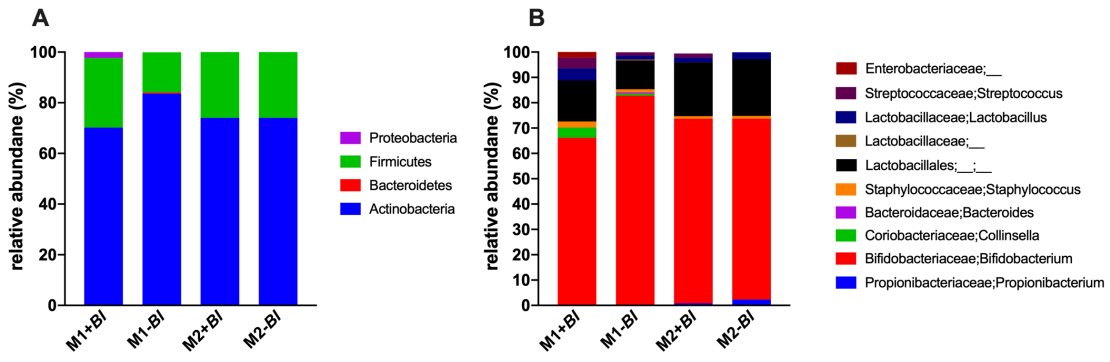

Figure A4.4 Relative abundances of bacterial phyla (A) and genera (B) of microbiomes derived from baby fecal samples which are inoculated into bioreactors before *B. infantis* addition. M1+BI: 1st microbiomes that inoculated into bioreactors with *B. infantis* M1-BI: 1st microbiomes that inoculated into bioreactors without *B. infantis* M2+BI: 2nd microbiomes that inoculated into bioreactors with *B. infantis* M2-BI: 2nd microbiomes that inoculated into bioreactors without *B. infantis*.

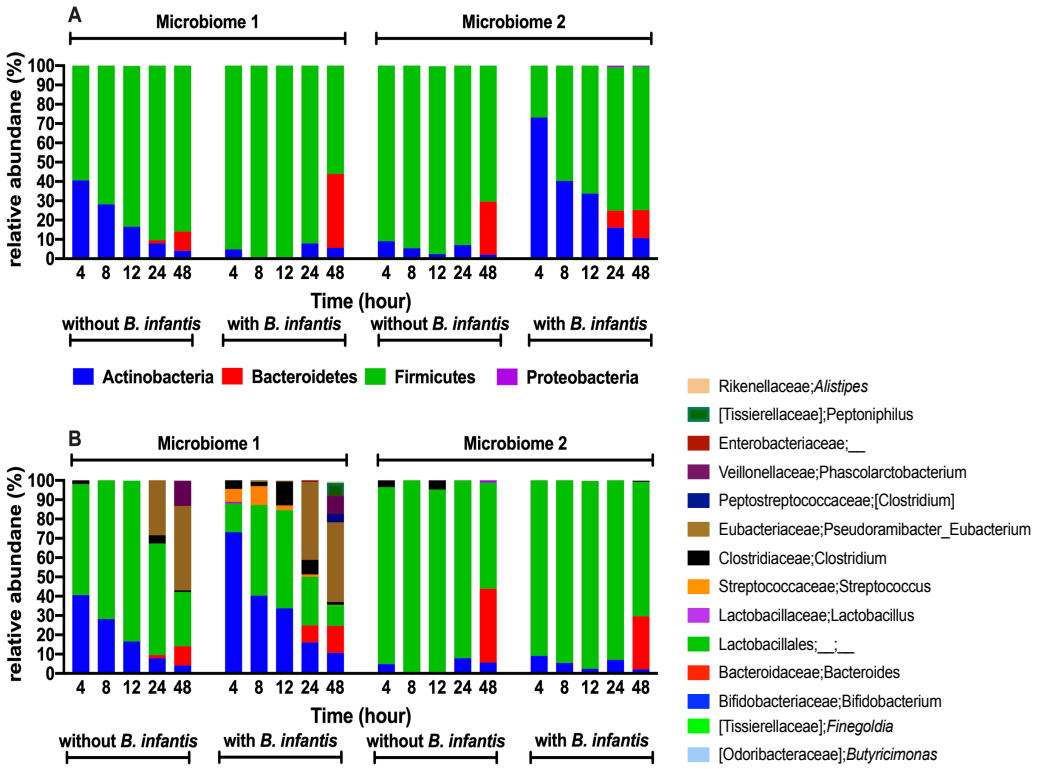

Figure A4.5 Relative abundances of bacterial phyla (A) and genera (B) during lactose fermentations of in vitro modeled microbiomes with and without addition of *B. infantis*.

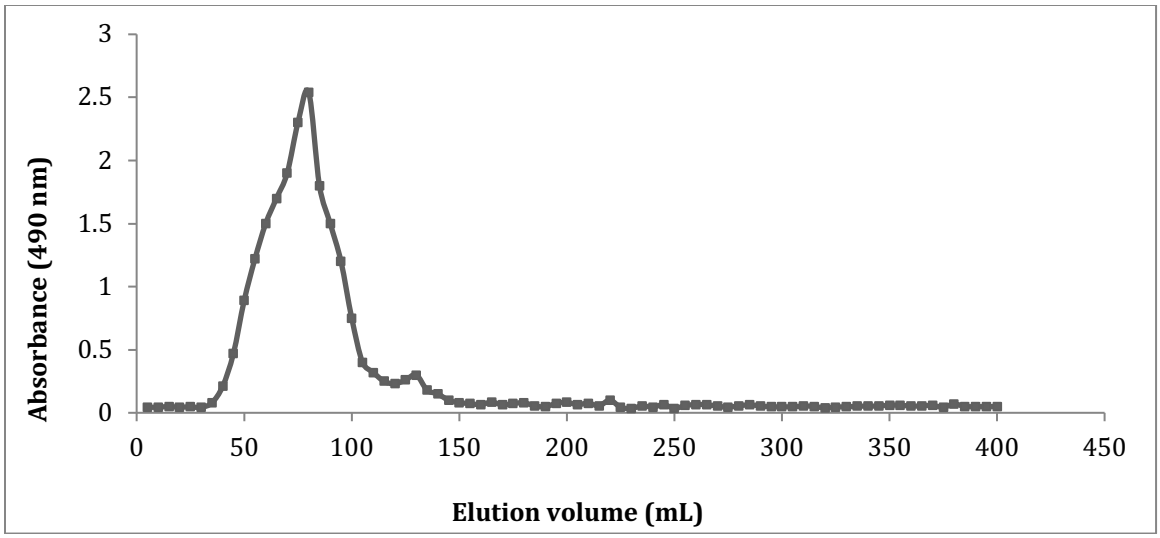

Figure A5.1 Elution profile of cranberry xyloglucans on a sephacryl S-100 HR 16/60 column, eluted with deionized water.

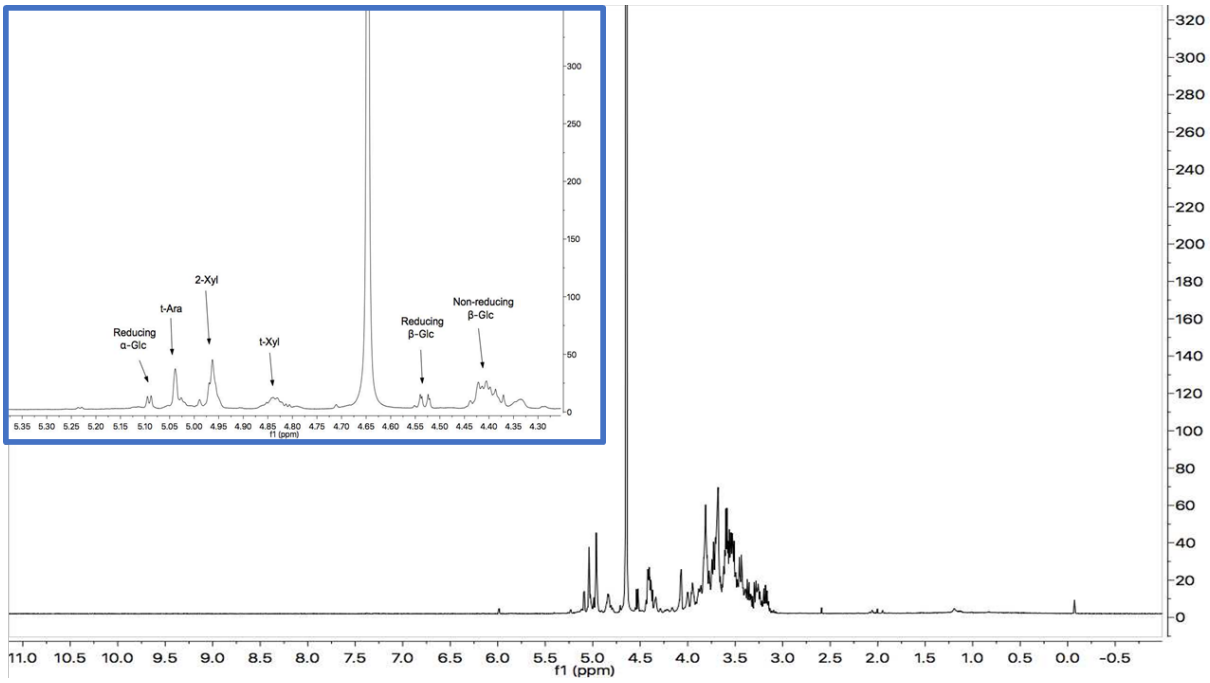

Figure A5.2 ^{1}H NMR spectra of cranberry xyloglucan (500 MHz, D_2O). The inset blue box shows an expanded anomeric region of the ^{1}H NMR spectrum.

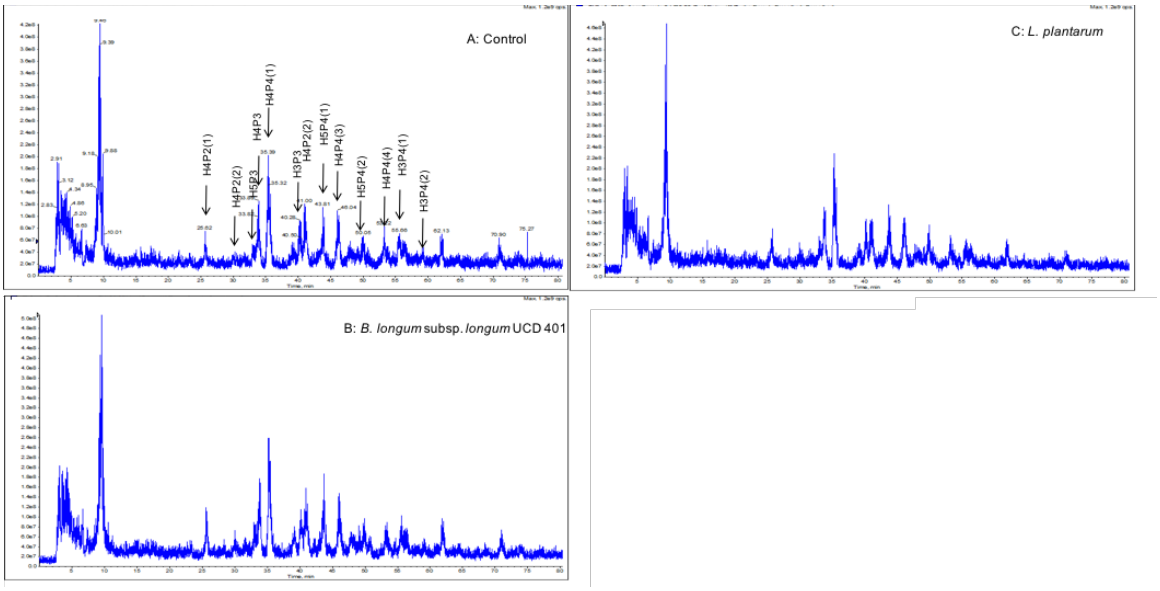

Figure A5.3 LC-MS analysis of xyloglucans (A) before fermentation and remaining post-fermentation by (B) *B. longum* subsp. *longum* UCD 401 and (C) *Lactobacillus plantarum* ATCC BAA-793. Shown in the upper left section are the full scan MS of the blank control along with the corresponding xyloglucan structures between DP=6-9.

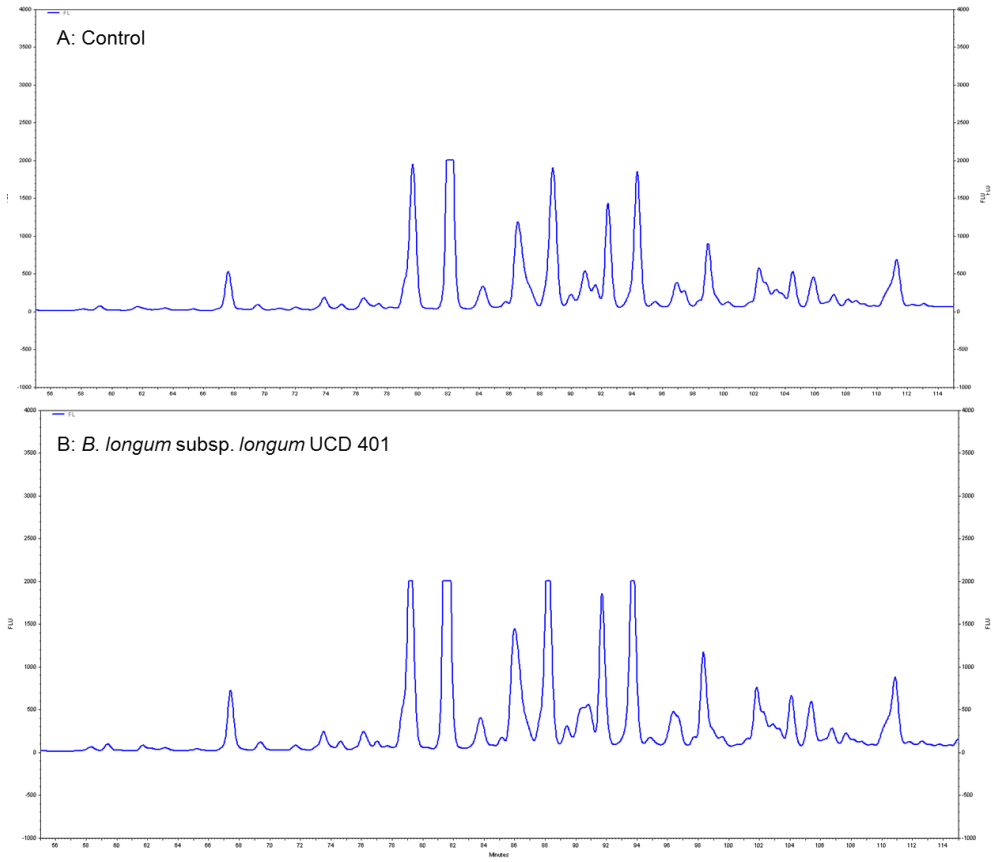

Figure A5.4 FL-HPLC chromatograms of xyloglucans (A) before fermentation (control) and remaining post fermentation by (B) *B. longum* subsp. *longum* UCD 401.

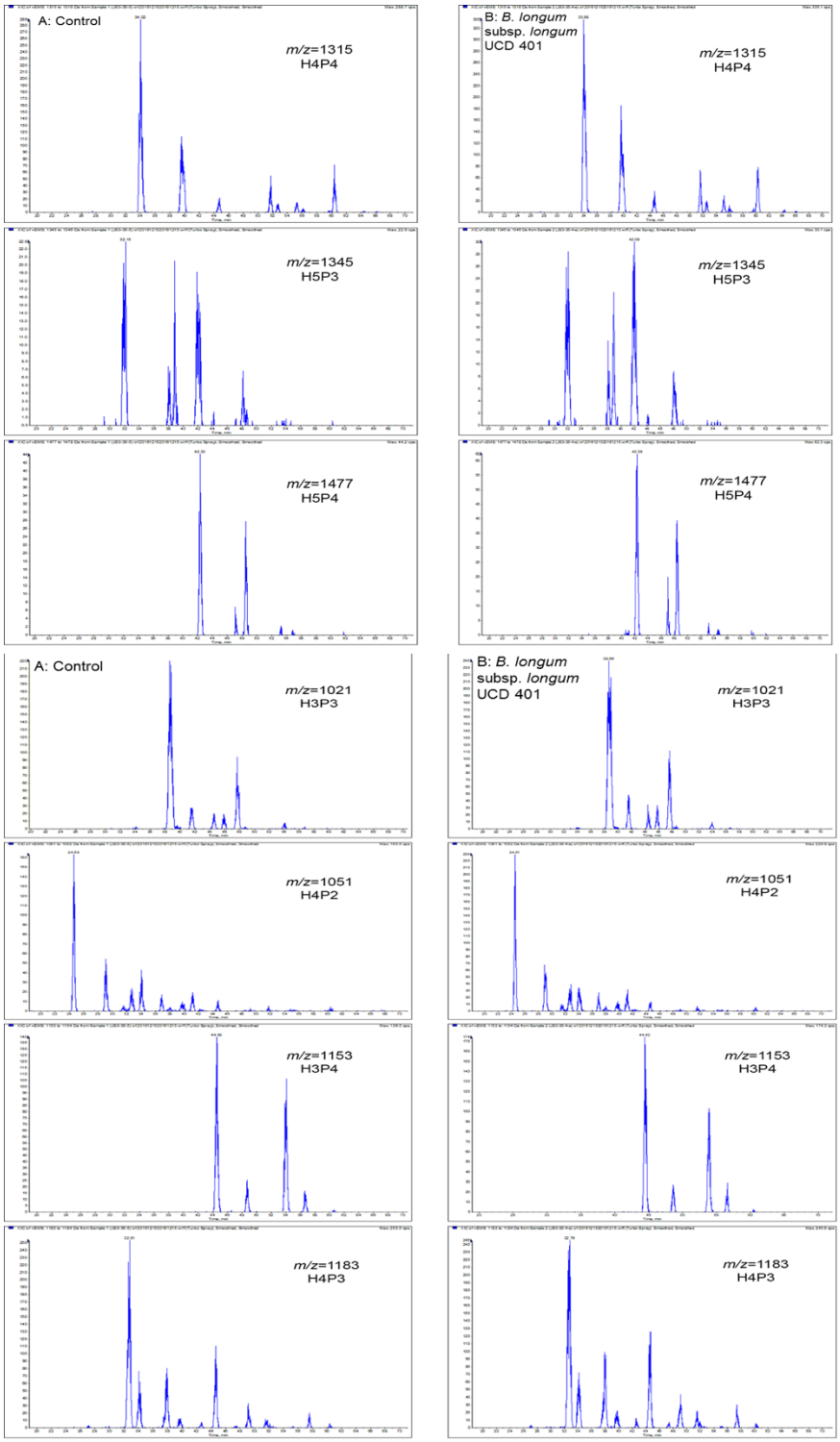

Figure A5.5 LC-MS analysis for specific xyloglucan structures by *B. longum* subsp. *longum* UCD 401 fermentation. The extracted ion chromatograms (EIC) of xyloglucans (A) before incubation (control) and (B) after incubation with *B. longum* subsp. *longum* UCD 401.

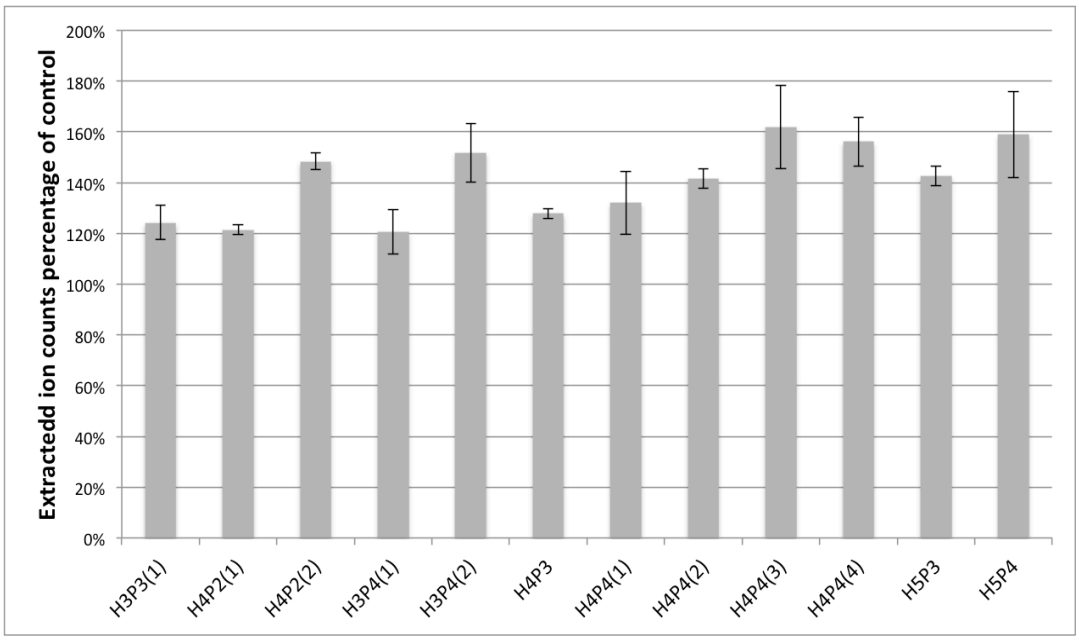

Figure A5.6 Abundance of xyloglucan glycoprofiles LC-MS analysis of *B. longum* subsp. *longum* UCD 401 grown on a medium supplemented with 2 % (w/v) cranberry xyloglucans. The quantity of xyloglucans is represented as the percentage of extracted ion counts compared to control (t=0) (see Figure A5.5 and Table A5.1 for full scan MS and detailed structure of xyloglucans)

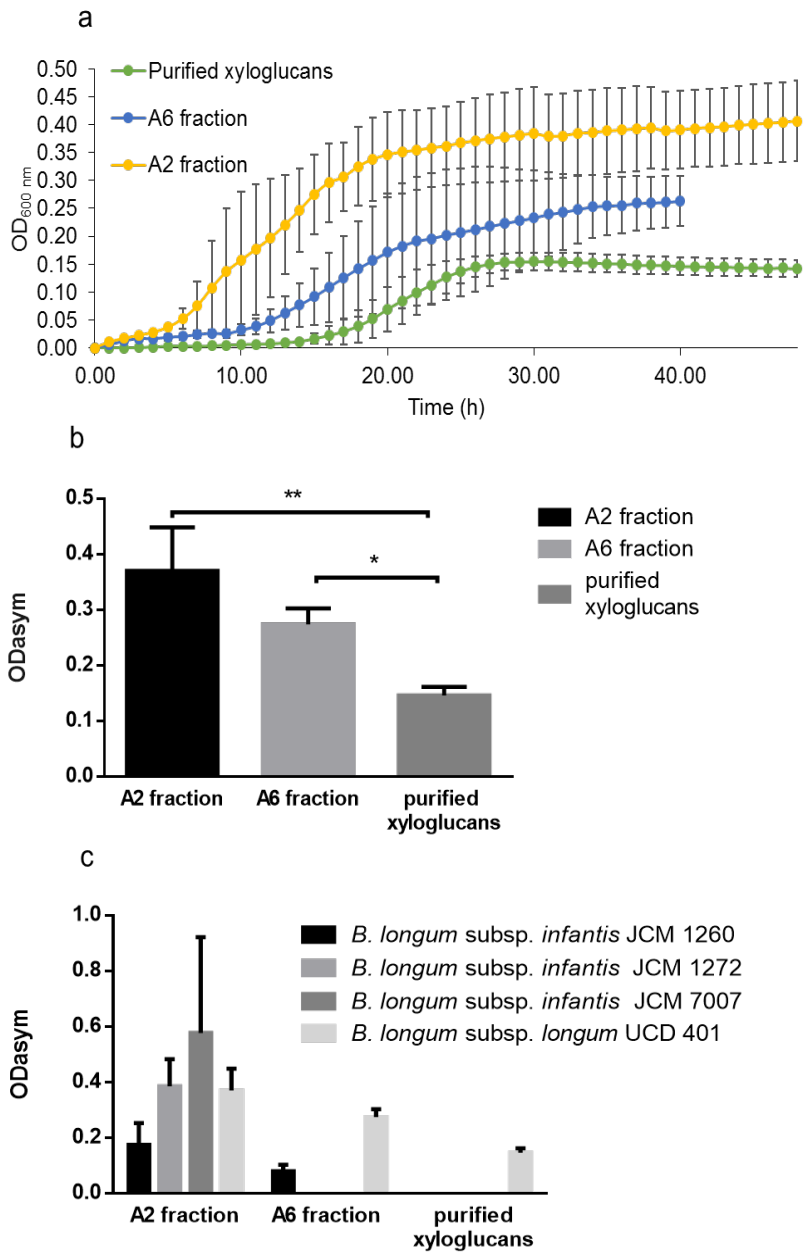

Figure A5.7 Comparison of utilization of different xyloglucan fractions. (a) the growth curve of *B. longum* subsp. *longum* UCD 401 on modified MRS containing 2% (w/v) A2 fraction (yellow), A6 fraction (blue), purified xyloglucans (green). (b) Asymptotic OD (OD600 nm at the stationary level) of *B. longum* subsp. *longum* UCD 401 on A2 and A6 fractions and purified xyloglucans. (c) Asymptotic OD (OD600 nm at the stationary level) of *B. longum* subsp. *infantis* JCM 1260, *B. longum* subsp. *infantis* JCM 1272, *B. longum* subsp. *infantis* JCM 7007 and *B. longum* subsp. *longum* UCD 401 on A2 and A6 fractions and purified xyloglucans.

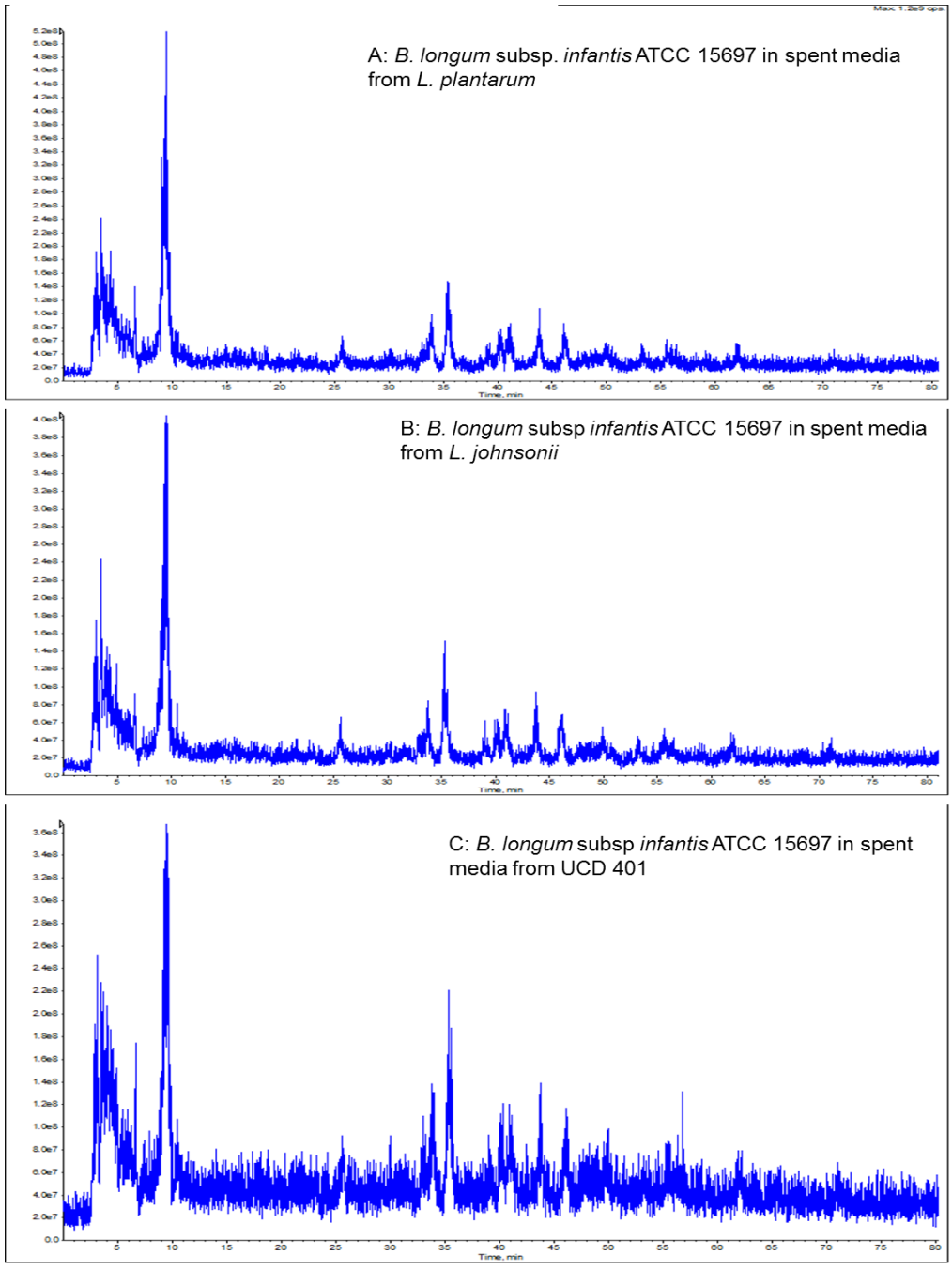

Figure A5.8. LC-MS analysis of xyloglucans remaining after syntropic interactions of *B. longum* subsp. *infantis* ATCC 15697 between (A) *Lactobacillus plantarum* ATCC BAA-793, (B) *Lactobacillus plantarum* ATCC BAA-793 and (C) *B. longum* subsp. *longum* UCD 401. (see Figure A5.5 for full scan MS and detailed structure of xyloglucans remaining after fermentation of three strains).

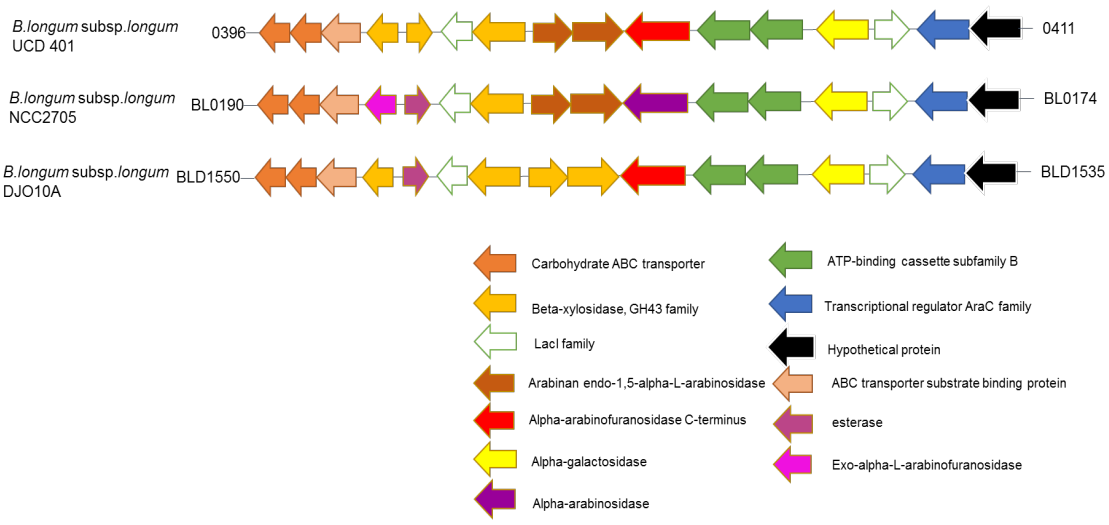

Figure A5.9 Genomic regions putatively linked with xyloglucan/arabinoxylose utilization in *B. longum* strains. Gene orthologous annotations for *B. longum* subsp. *longum* UCD 401 were obtained from genomic sequence available as draft in the Joint Genome Institute Integrated Microbiome Genomes and Microbiome platform (IMG). Genes are represented by arrows and are colored according to predicted function (not depicted according to scale).

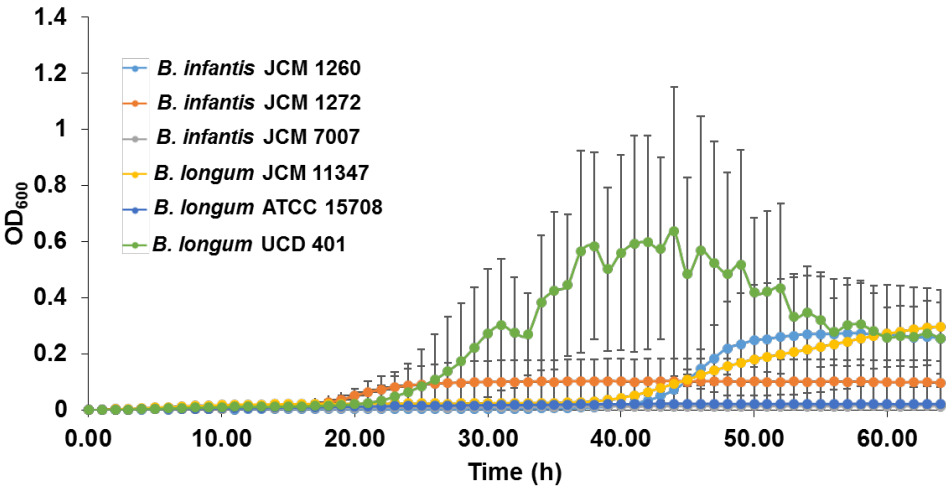

Figure A5.10 Growth curves of *B. longum* subsp. *infantis* JCM 1260, *B. longum* subsp. *infantis* JCM 1272, *B. longum* subsp. *infantis* JCM 7007, *B. longum* subsp. *longum* JCM 11347, *B. longum* subsp. *longum* ATCC 15708, *B. longum* subsp. *longum* UCD 401 on modified MRS containing 2 % (w/v) arabinose with triplicates.

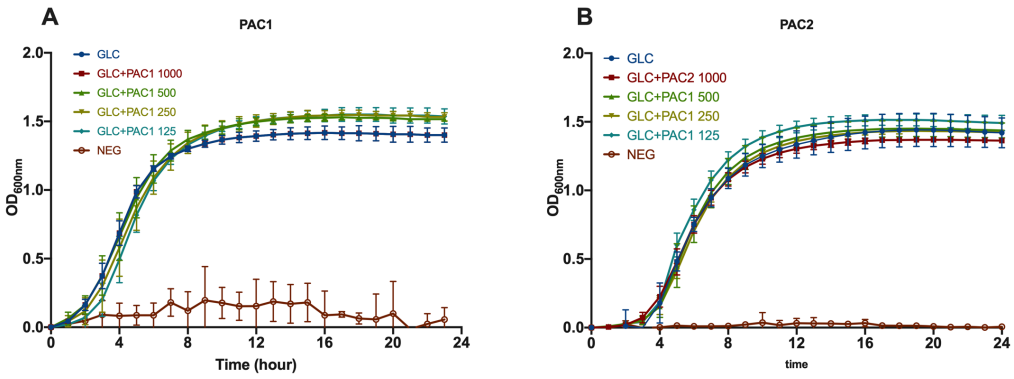

Figure A6.1 Dose-dependent *L. plantarum* growth while utilizing glucose with cranberry PACs. Growth curves of *Lactobacillus plantarum* ATCC 1BAA793 on modified MRS containing 1000-0.125 mg/ml PAC1 (A) and PAC2 (B) fractions with 1 % (w/v) glucose. The curves are drawn from average of three independent experiments.

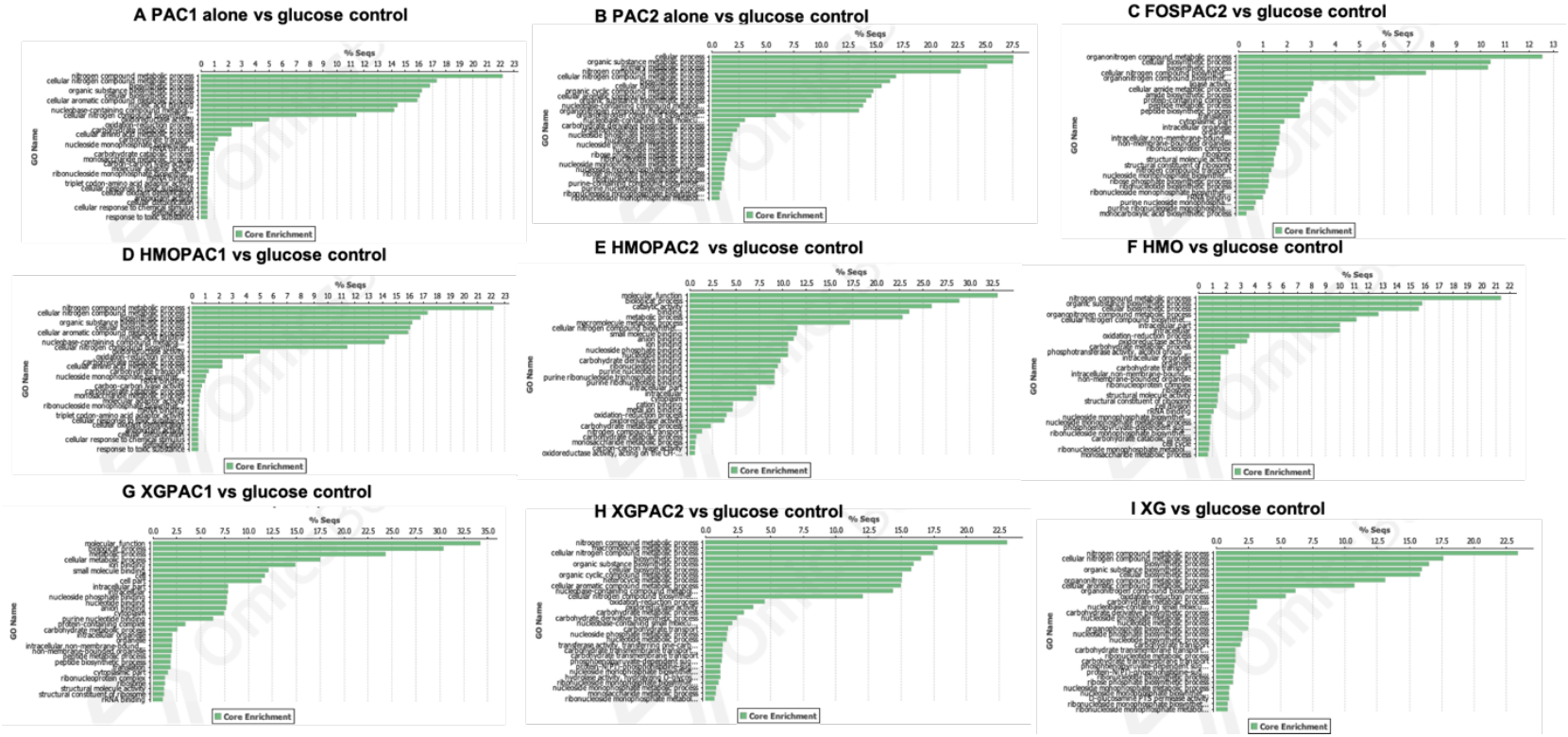

Figure A6.2 GO enrichment analysis in response to oligosaccharides with PACs. The GO term differential expression is considered through normalized enrichment score (NES) using OmicsBox tools. Higher score indicates higher proportion of up-regulated genes in the pooled PAC1 alone (A), PAC2 alone (B), FOS+PAC2 (C) HMO+PAC1 (D). HMO+PAC2 (E), HMO (F), XG+PAC1 (G), XG+PAC2 (H), and XG (I) compared to the glucose control.

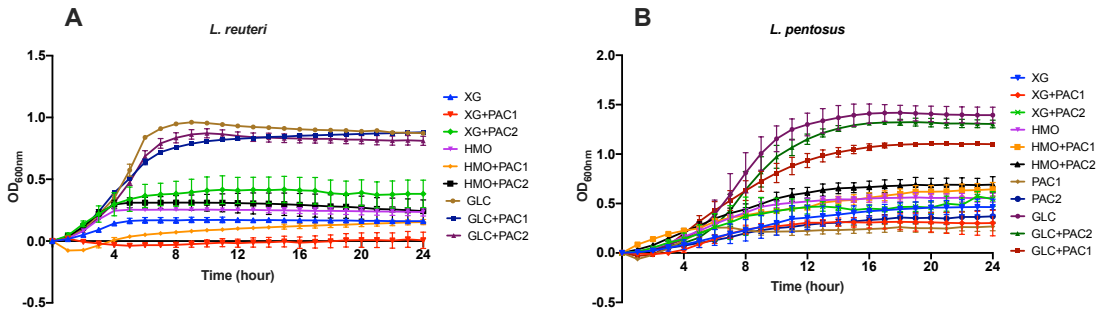

Figure A6.3 Bacterial growth while utilizing oligosaccharides with cranberry PACs. Growth curves of *Lactobacillus reuteri* (A) and *Lactobacillus pentosus* (B) on modified MRS containing 1000mg/ml PAC fractions and 1 % (w/v) glucose, human milk oligosaccharides, xyloglucans and PACs alone. The curves are drawn from average of three independent experiments.

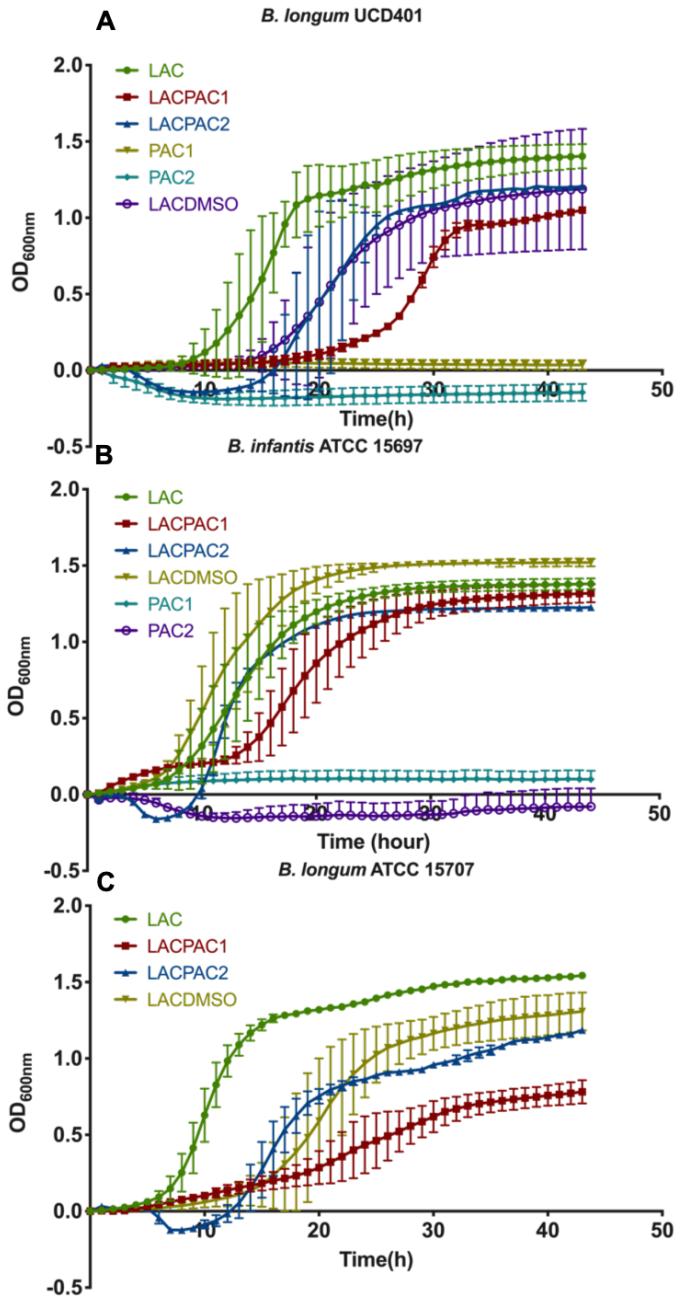

Figure A6.4 Bacterial growth while utilizing lactose with cranberry PACs. Growth curves of *Bifidobacterium longum* UCD401 (A) and *Bifidobacterium longum subsp. infantis* (B) and *Bifidobacterium longum* ATCC 15707 on modified MRS containing 1000mg/ml PAC fractions and 1 % (w/v) lactose. The curves are drawn from average of three independent experiments.

BIBLIOGRAPHY

[1] Macfarlane, G., McBain, A.J., The human colonic microbiota, in: Gibson, G., Roberfroid, M. (Eds.), *Colonic Microbiota, Nutrition and Health*, Kluwer Academic, Dordrecht ;;Boston 1999, pp. 1–25.

[2] Power, S.E., O'Toole, P.W., Stanton, C., Ross, R.P., et al., Intestinal microbiota, diet and health. *Br. J. Nutr.* 2013, *111*, 387–402.

[3] Payne, A.N., Zihler, A., Chassard, C., Lacroix, C., Advances and perspectives in in vitro human gut fermentation modeling. *Trends Biotechnol.* 2012, *30*, 17–25.

[4] Olano-Martin, E., Mountzouris, K.C., Gibson, G.R., Rastall, R.A., In vitro fermentability of dextran, oligodextran and maltodextrin by human gut bacteria. *Br. J. Nutr.* 2000, *83*, 247–55.

[5] Macfarlane, G.T., Gibson, G., Cummings, J.H., Comparison of fermentation reactions in different regions of the human colon. *J. Appl. Bacteriol.* 1992, *72*, 57–64.

[6] Macfarlane, S., Macfarlane, G., Proteolysis and amino acid fermentation, in: Gibson, G., Macfarlane, G. (Eds.), *Human Colonic Bacteria: Role in Nutrition, Physiology and Pathology*, Boca Raton: CRC Press, 1995, pp. 75–100.

[7] Macfarlane, G., Macfarlane, S., Gibson, G., Validation of a three-stage compound continuous culture system for investigating the effect of retention time on the ecology and metabolism of bacteria in the human colon. *Microb. Ecol.* 1998, *35*, 180–7.

[8] Ventura, M, Turroni, F, Canchaya, C, Vaughan, EE, O'Toole, PW, van Sinderen, D., Microbial diversity in the human intestine and novel insights from metagenomics. *Front. Biosci.* 2009, *14*, 3214–3863.

[9] Sela, D.A., Bifidobacterial utilization of human milk oligosaccharides. *Int. J. Food Microbiol.* 2011, *149*, 58–64.

[10] Turroni, F., Peano, C., Pass, D.A., Foroni, E., et al., Diversity of bifidobacteria within the infant gut microbiota. *PLoS One* 2012, *7*, e36957.

[11] Sela, D.A., Chapman, J., Adeuya, A., Kim, J.H., et al., The genome sequence of *Bifidobacterium longum* subsp. *infantis* reveals adaptations for milk utilization within the infant microbiome. *Proc. Natl. Acad. Sci. U. S. A.* 2008, *105*, 18964–9.

[12] Marcobal, A., Sonnenburg, J.L., Human milk oligosaccharide consumption by intestinal microbiota. *Clin. Microbiol. Infect.* 2012, *18*, 12–15.

[13] Li, M., Bauer, L.L., Chen, X., Wang, M., et al., Microbial Composition and In Vitro Fermentation Patterns of Human Milk Oligosaccharides and Prebiotics Differ between Formula-Fed and Sow-Reared Piglets. *J. Nutr.* 2012, *142*, 681–689.

[14] Guaraldi, F., Salvatori, G., Effect of breast and formula feeding on gut microbiota shaping in newborns. *Front. Cell. Infect. Microbiol.* 2012, *2*, 94.

[15] Fan, W., Huo, G., Li, X., Yang, L., et al., Diversity of the intestinal microbiota in different patterns of feeding infants by Illumina high-throughput sequencing. *World J. Microbiol. Biotechnol.* 2013, *29*, 2365–72.

[16] De Filippo, C., Cavalieri, D., Di Paola, M., Ramazzotti, M., et al., Impact of diet in shaping gut microbiota revealed by a comparative study in children from Europe and rural Africa. *Proc. Natl. Acad. Sci. U. S. A.* 2010, *107*, 14691–6.

[17] Claesson, M.J., Jeffery, I.B., Conde, S., Power, S.E., et al., Gut microbiota composition correlates with diet and health in the elderly. *Nature* 2012, *488*, 178–84.

[18] Kabeerdoss, J., Devi, R.S., Mary, R.R., Ramakrishna, B.S., Faecal microbiota composition in vegetarians: comparison with omnivores in a cohort of young women in southern India. *Br. J. Nutr.* 2012, *108*, 953–7.

[19] Wu, G.D., Chen, J., Hoffmann, C., Bittinger, K., et al., Linking long-term dietary patterns with gut microbial enterotypes. *Science* 2011, *334*, 105–8.

[20] Zimmer, J., Lange, B., Frick, J.-S., Sauer, H., et al., A vegan or vegetarian diet substantially alters the human colonic faecal microbiota. *Eur. J. Clin. Nutr.* 2012, *66*, 53–60.

[21] Wu, M., McNulty, N.P., Rodionov, D.A., Khoroshkin, M.S., et al., Genetic determinants of in vivo fitness and diet responsiveness in multiple human gut Bacteroides. *Science (80-.).* 2015, *350*, aac5992.

[22] Kang, S.S., Jeraldo, P.R., Kurti, A., Miller, M.E.B., et al., Diet and exercise orthogonally alter the gut microbiome and reveal independent associations with anxiety and cognition. *Mol. Neurodegener.* 2014, *9*, 36.

[23] Claesson, M.J., O'Sullivan, O., Wang, Q., Nikkila, J., et al., Comparative analysis of pyrosequencing and a phylogenetic microarray for exploring microbial community structures in the human distal intestine. *PLoS One* 2009, *4*.

[24] Rajilic-Stojanovic, M., Smidt, H., De Vos, W.M., Diversity of the human gastrointestinal tract microbiota revisited. *Environ. Microbiol.* 2007, *9*, 2125–2136.

[25] Dethlefsen, L., Eckburg, P.B., Bik, E.M., Relman, D.A., Assembly of the human intestinal microbiota. *Trends Ecol. Evol.* 2006, *21*, 517–23.

[26] Dethlefsen, L., McFall-Ngai, M., Relman, D.A., An ecological and evolutionary perspective on human-microbe mutualism and disease. *Nature* 2007, *449*, 811–8.

[27] Tap, J., Mondot, S., Levenez, F., Pelletier, E., et al., Towards the human intestinal microbiota phylogenetic core. *Environ. Microbiol.* 2009, *11*, 2574–84.

[28] Eckburg, P.B., Diversity of the Human Intestinal Microbial Flora. *Science (80-.).* 2005, *308*, 1635–1638.

[29] Turnbaugh, P.J., Hamady, M., Yatsunenko, T., Cantarel, B.L., et al., A core gut microbiome in obese and lean twins. *Nature* 2009, *457*, 480–484.

[30] Finegold, M., Attebery, R., Sutter, V.L., Effect of diet on human fecal flora: comparison of Japanese American diets. *Am. J. Clin. Nutr.* 1974, *27*, 1456–1469.

[31] Macfarlane, S., Macfarlane, G.T., Bacterial Diversity in the Human Gut. *Adv. Appl. Microbiol.* 2004, *54*, 261–289.

[32] Staley, J.T., Konopka, A., Measurement of in situ activities of nonphotosynthetic microorganisms in aquatic and terrestrial habitats. *Annu. Rev. Microbiol.* 1985, *39*, 321–346.

[33] Franks, A.H., Harmsen, H.J.M., Gerwin, C., Jansen, G.J., et al., Variations of bacterial populations in human feces measured by fluorescent in situ hybridization with group-specific 16S rRNA-targeted oligonucleotide probes. *Appl. Environ. Microbiol.* 1998, *64*, 3336–3345.

[34] Wang, X., Heazlewood, S.P., Krause, D.O., Florin, T.H.J., Molecular characterization of the microbial species that colonize human ileal and colonic mucosa by using 16S rDNA sequence analysis. *J. Appl. Microbiol.* 2003, *95*, 508–520.

[35] Rajilić-Stojanović, M., Heilig, H.G.H.J., Molenaar, D., Kajander, K., et al., Development and application of the human intestinal tract chip, a phylogenetic microarray: analysis of universally conserved phylotypes in the abundant microbiota of young and elderly adults. *Environ. Microbiol.* 2009, *11*, 1736–51.

[36] Kurokawa, K., Itoh, T., Kuwahara, T., Oshima, K., et al., Comparative metagenomics revealed commonly enriched gene sets in human gut microbiomes. *DNA Res.* 2007, *14*, 169–181.

[37] Blottière, H.M., de Vos, W.M., Ehrlich, S.D., Doré, J., Human intestinal metagenomics: state of the art and future. *Curr. Opin. Microbiol.* 2013, *16*, 232–9.

[38] Jansson, J., Willing, B., Lucio, M., Fekete, A., et al., Metabolomics reveals metabolic biomarkers of Crohn's disease. *PLoS One* 2009, *4*.

[39] Verberkmoes, N.C., Russell, A.L., Shah, M., Godzik, A., et al., Shotgun

metaproteomics of the human distal gut microbiota. *ISME J*. 2009, *3*, 179–89.

[40] Van Baarlen, P., Kleerebezem, M., Wells, J.M., Omics approaches to study host-microbiota interactions. *Curr. Opin. Microbiol*. 2013, *16*, 270–7.

[41] Lozupone, C.A., Stombaugh, J.I., Gordon, J.I., Jansson, J.K., et al., Diversity, stability and resilience of the human gut microbiota. *Nature* 2012, *489*, 220–30.

[42] The Human Microbiome Project Consortium, Structure, function and diversity of the healthy human microbiome. *Nature* 2012, *486*, 207–14.

[43] Qin, J., Li, R., Raes, J., Arumugam, M., et al., A human gut microbial gene catalogue established by metagenomic sequencing. *Nature* 2010, *464*, 59–65.

[44] Turnbaugh, P.J., Ley, R.E., Hamady, M., Fraser-Liggett, C.M., et al., The human microbiome project. *Nature* 2007, *449*, 804–10.

[45] Garrido, D., Ruiz-Moyano, S., Lemay, D.G., Sela, D.A., et al., Comperative transcriptomics reveals key differences in the response to milk oligosaccharides of infant gut-associated bifidobacteria. *Sci. Rep*. 2015, *5*, 13517.

[46] Gonzalez, R., Klaassens, E.S., Malinen, E., de Vos, W.M., et al., Differential transcriptional response of Bifidobacterium longum to human milk, formula milk, and galactooligosaccharide. *Appl. Environ. Microbiol*. 2008, *74*, 4686–4694.

[47] Adamberg, S., Sumeri, I., Uusna, R., Ambalam, P., et al., Survival and synergistic growth of mixed cultures of bifidobacteria and lactobacilli combined with prebiotic oligosaccharides in a gastrointestinal tract simulator. *Microb. Ecol. Heal. Dis*. 2014, *25*, 23062.

[48] Han, K.H., Kobayashi, Y., Nakamura, Y., Shimada, K.I., et al., Comparison of the effects of longer chain inulins with different degrees of polymerization on colonic fermentation in a mixed culture of swine fecal bacteria. *J. Nutr. Sci. Vitaminol. (Tokyo)*. 2014, *60*, 206–212.

[49] Martens, E.C., Lowe, E.C., Chiang, H., Pudlo, N.A., et al., Recognition and degradation of plant cell wall polysaccharides by two human gut symbionts. *PLoS Biol*. 2011, *9*, e1001221.

[50] Rossi, M., Corradini, C., Amaretti, A., Nicolini, M., et al., Fermentation of fructooligosaccharides and inulin by bifidobacteria : a comparative study of pure and fecal cultures. *Appl. Environ. Microbiol*. 2005, *71*, 6150–6158.

[51] Shen, Q., Tuohy, K.M., Gibson, G.R., Ward, R.E., In vitro measurement of the impact of human milk oligosaccharides on the faecal microbiota of weaned formula-fed infants compared to a mixture of prebiotic fructooligosaccharides and galactooligosaccharides. *Lett. Appl. Microbiol*. 2011, *52*, 337–343.

[52] Stiverson, J., Williams, T., Chen, J., Adams, S., et al., Prebiotic Oligosaccharides: Comparative Evaluation Using In Vitro Cultures of Infants' Fecal Microbiomes. *Appl. Environ. Microbiol*. 2014, *80*, 7388–7397.

[53] Ze, X., Duncan, S.H., Louis, P., Flint, H.J., Ruminococcus bromii is a keystone species for the degradation of resistant starch in the human colon. *ISME J*. 2012, *6*, 1535–1543.

[54] Duncan, S.H., Scott, K.P., Ramsay, A.G., Harmsen, J.M., et al., Effects of alternative dietary substrates on competition between human colonic bacteria in an anaerobic fermentor system. *Society* 2003.

[55] Richardson, A.J., Mckain, N., Wallace, R.J., Ammonia production by human faecal bacteria , and the enumeration , isolation and characterization of bacteria capable of growth on peptides and amino acids. 2013.

[56] Davila, A., Blachier, F., Gotteland, M., Andriamihaja, M., et al., Re-print of "Intestinal luminal nitrogen metabolism: Role of the gut microbiota and consequences for the host." *Pharmacol. Res*. 2013, *69*, 114–126.

[57] Walker, A.W., Duncan, S.H., McWilliam Leitch, E.C., Child, M.W., et al., pH and peptide supply can radically alter bacterial populations and short-chain fatty acid ratios within microbial communities from the human colon. *Appl. Environ. Microbiol*. 2005, *71*, 3692–700.

[58] Ozdal, T., Sela, D.A., Xiao, J., Boyacioglu, D., et al., The reciprocal interactions between polyphenols and gut microbiota and effects on bioaccessibility. *Nutrients* 2016, *8*, 1–36.

[59] Landete, J.M., Updated knowledge about polyphenols: functions, bioavailability, metabolism, and health. *Crit. Rev. Food Sci. Nutr.* 2012, *52*, 936–48.

[60] Kemperman, R.A., Bolca, S., Roger, L.C., Vaughan, E.E., Novel approaches for analysing gut microbes and dietary polyphenols: challenges and opportunities. *Microbiology* 2010, *156*, 3224–31.

[61] Hervert-Hernández, D., Goñi, I., Dietary polyphenols and human gut microbiota: a review. *Food Rev. Int.* 2011, *27*, 154–169.

[62] Crozier, A., Jaganath, I.B., Clifford, M.N., Dietary phenolics: chemistry, bioavailability and effects on health. *Nat. Prod. Rep.* 2009, *26*, 1001.

[63] D'Archivio, M., Filesi, C., Benedetto, R. Di, Gargiulo, R., et al., Polyphenols, dietary sources and bioavailability. *Ann Ist Super Sanita* 2007, *43*, 348–361.

[64] Etxeberria, U., Fernández-Quintela, A., Milagro, F.I., Aguirre, L., et al., Impact of polyphenols and polyphenol-rich dietary sources on gut microbiota composition. *J. Agric. Food Chem.* 2013, *61*, 9517–33.

[65] Van Dorsten, F.A., Peters, S., Gross, G., Roldan, V.G., et al., Gut microbial metabolism of polyphenols from black tea and red wine/grape juice is source-specific and colon-region dependent. *J. Agric. Food Chem.* 2012, *60*, 11331–11342.

[66] Van der Hooft, J.J.J., de Vos, R.C.H., Mihaleva, V., Bino, R.J., et al., Structural elucidation and quantification of phenolic conjugates present in human urine after tea Intake. *Anal. Chem.* 2012, *84*, 7263–7271.

[67] Tzounis, X., Rodriguez-Mateos, A., Vulevic, J., Gibson, G.R., et al., Prebiotic evaluation of cocoa-derived flavanols in healthy humans by using a randomized, controlled, double-blind, crossover intervention study. *Am. J. Clin. Nutr.* 2011, *93*,

62–72.

[68] Stoupi, S., Williamson, G., Drynan, J.W., Barron, D., et al., Procyanidin B2 catabolism by human fecal microflora: partial characterization of “dimeric” intermediates. *Arch. Biochem. Biophys.* 2010, *501*, 73–8.

[69] Manach, C., Williamson, G., Morand, C., Scalbert, A., et al., Bioavailability and bioefficacy of polyphenols in humans. I. Review of 97 bioavailability studies. *Am. J. Clin. Nutr.* 2005, *81*, 230S-242S.

[70] Flint, H.J., Bayer, E.A., Rincon, M.T., Lamed, R., et al., Polysaccharide utilization by gut bacteria: potential for new insights from genomic analysis. *Nat. Rev. Microbiol.* 2008, *6*, 121–31.

[71] Flint, H.J., Scott, K.P., Duncan, S.H., Louis, P., et al., Microbial degradation of complex carbohydrates in the gut. *Gut Microbes* 2012, *3*, 289–306.

[72] Andreasen, M.F., Kroon, P.A., Williamson, G., Esterase activity able to hydrolyze dietary antioxidant hydroxycinnamates is distributed along the intestine of mammals. *J. Agircultural Food Chem.* 2001, *49*, 5679–5684.

[73] Turroni, F., Strati, F., Foroni, E., Serafini, F., et al., Analysis of predicted carbohydrate transport systems encoded by *Bifidobacterium bifidum* PRL2010. *Appl. Environ. Microbiol.* 2012, *78*, 5002–5012.

[74] Belenguer, A., Duncan, S.H., Calder, A.G., Holtrop, G., et al., Two routes of metabolic cross-feeding between *Bifidobacterium adolescentis* and butyrate-producing anaerobes from the human gut. *Appl. Enviromental Microbiol.* 2006, *72*, 3593–3599.

[75] den Besten, G., van Eunen, K., Groen, A.K., Venema, K., et al., The role of short-chain fatty acids in the interplay between diet, gut microbiota, and host energy metabolism. *J. Lipid Res.* 2013, *54*, 2325–40.

[76] Canani, R.B., Costanzo, M. Di, Leone, L., Pedata, M., et al., Potential beneficial effects of butyrate in intestinal and extraintestinal diseases. *World J.*

Gastroenterol. 2011, *17*, 1519–28.

[77] Puertollano, E., Kolida, S., Yaqoob, P., Biological significance of short-chain fatty acid metabolism by the intestinal microbiome. *Curr. Opin. Clin. Nutr. Metab. Care* 2014, *17*, 139–44.

[78] Huda-Faujan, N., Abdulamir, A.S., Fatimah, A.B., Anas, O.M., et al., The Impact of the Level of the Intestinal Short Chain Fatty Acids in Inflammatory Bowel Disease Patients Versus Healthy Subjects. *Open Biochem. J*. 2010, *4*, 53–58.

[79] Sang, S., Lambert, J.D., Tian, S., Hong, J., et al., Enzymatic synthesis of tea theaflavin derivatives and their anti-inflammatory and cytotoxic activities. *Bioorg. Med. Chem*. 2004, *12*, 459–467.

[80] Crouvezier, S., Powell, B., Keir, D., Yaqoob, P., The effects of phenolic components of tea on the production of pro- and anti-inflammatory cytokines by human leukocytes in vitro. *Cytokine* 2001, *13*, 280–6.

[81] Russell, W.R., Labat, A., Scobbie, L., Duncan, S.H., Availability of blueberry phenolics for microbial metabolism in the colon and the potential inflammatory implications. *Mol. Nutr. Food Res*. 2007, *51*, 726–31.

[82] Hughes, R., Magee, E.A., Bingham, S., Protein degradation in the large intestine: relevance to colorectal cancer. *Curr. Issues Intest. Microbiol*. 2000, *1*, 51–8.

[83] Auchtung, J.M., Robinson, C.D., Britton, R.A., Cultivation of stable, reproducible microbial communities from different fecal donors using minibioreactor arrays (MBRAs). *Microbiome* 2015, *3*, 42.

[84] Child, M.W., Kennedy, A., Walker, A.W., Bahrami, B., et al., Studies on the effect of system retention time on bacterial populations colonizing a three-stage continuous culture model of the human large gut using FISH techniques. *FEMS Microbiol. Ecol*. 2006, *55*, 299–310.

[85] Macfarlane, S., Woodmansey, E.J., George, T., Macfarlane, G.T., Colonization of mucin by human intestinal bacteria and establishment of biofilm communities in a

two-stage continuous culture system. *Society* 2005, *71*, 7483–7492.

[86] Minekus, M., Smeets-Peeters, M., Bernalier, A., Marol-Bonnin, S., et al., A computer-controlled system to simulate conditions of the large intestine with peristaltic mixing, water absorption and absorption of fermentation products. *Appl. Microbiol. Biotechnol.* 1999, *53*, 108–14.

[87] Possemiers, S., Verthé, K., Uyttendaele, S., Verstraete, W., PCR-DGGE-based quantification of stability of the microbial community in a simulator of the human intestinal microbial ecosystem. *FEMS Microbiol. Ecol.* 2004, *49*, 495–507.

[88] Probert, H.M., Gibson, G.R., Development of a fermentation system to model sessile bacterial populations in the human colon. *Biofilms* 2004, *1*, 13–19.

[89] Rajilić-Stojanović, M., Maathuis, A., Heilig, H.G.H.J., Venema, K., et al., Evaluating the microbial diversity of an in vitro model of the human large intestine by phylogenetic microarray analysis. *Microbiology* 2010, *156*, 3270–81.

[90] Van de Wiele, T., Boon, N., Possemiers, S., Jacobs, H., et al., Prebiotic effects of chicory inulin in the simulator of the human intestinal microbial ecosystem. *FEMS Microbiol. Ecol.* 2004, *51*, 143–153.

[91] Venema, K., Van Nuenen, M., M, S.-P., M, M., et al., TNO's in vitro large intestinal model: an excellent screening tool for functional food and pharmaceutical research. *Nutrition* 2000, *24*, 558–564.

[92] Venema, K., van Nuenen, M.H.M.C., van den Heuvel, E.G., Pool, W., et al., The Effect of lactulose on the composition of the intestinal microbiota and short-chain fatty acid production in human volunteers and a computer-controlled model of the proximal large intestine. *Microb. Ecol. Health Dis.* 2003, *15*, 94–105.

[93] Bonten, M.J.M., Nathan, C., Weinstein, R.A., Recovery of nosocomial fecal flora from frozen stool specimens and rectal swabs: Comparison of preservatives for epidemiological studies. *Diagn. Microbiol. Infect. Dis.* 1997, *27*, 103–106.

[94] Macfarlane, G.T., Macfarlane, S., Models for intestinal fermentation : association

between food components, delivery systems, bioavailability and functional interactions in the gut. *Curr. Opin. Biotechnol.* 2007, *18*, 156–162.

[95] Williams, C.F., Walton, G.E., Jiang, L., Plummer, S., et al., Comparative analysis of intestinal tract models. *Annu. Rev. Food Sci. Technol.* 2014, *6*, 150223151639004.

[96] Gross, G., van Duynhoven, J., Vaughan, E.E., van Dewiele, T., et al., In vitro bioconversion of polyphenols from black tea and red wine/grape juice by human intestinal microbiota displays strong interindividual variability. *J. Agric. Food Chem.* 2010, *58*, 10236–10246.

[97] Oufir, L.E., Barry, J.L., Flourié, B., Cherbut, C., et al., Relationships between transit time in man and in vitro fermentation of dietary fiber by fecal bacteria. *Eur. J. Clin. Nutr.* 2000, *54*, 603–609.

[98] Pompei, A., Cordisco, L., Raimondi, S., Amaretti, A., et al., In vitro comparison of the prebiotic effects of two inulin-type fructans. *Anaerobe* 2008, *14*, 280–286.

[99] Barry, J.L., Hoebler, C., Macfarlane, G.T., Macfarlane, S., et al., Estimation of the fermentability of dietary fibre in vitro: a European interlaboratory study. *Br. J. Nutr.* 1995, *74*, 303–322.

[100] Gietl, E., Mengerink, W., de Slegte, J., Gibson, G., et al., Factors involved in the in vitro fermentability of short carbohydrates in static faecal batch cultures. *Int. J. Carbohydr. Chem.* 2012, *2012*, 1–10.

[101] Likotrafiti, E., Tuohy, K.M., Gibson, G.R., Rastall, R. a., An invitro study of the effect of probiotics, prebiotics and synbiotics on the elderly faecal microbiota. *Anaerobe* 2014, *27*, 50–55.

[102] Wang, X., Gibson, G.R., Effects of the in vitro fermentation of oligofructose and inulin by bacteria in the large human intestine. *J. Pplied Bacteriol.* 1993, *75*, 373–380.

[103] Macfarlane, G.T., Allison, C., Gibson, S.A.W., Cummings, J.H., Contribution of

the microflora to proteolysis in the human large intestine. *J. Appl. Bacteriol.* 1988, *64*, 37–46.

[104] Wang, X., Gibson, G.R., Effects of the in vitro fermentation of oligofructose and inulin by bacteria growing in the human large intestine. *J. Appl. Bacteriol.* 1993, *75*, 373–80.

[105] Aura, A.-M., Martin-Lopez, P., O'Leary, K.A., Williamson, G., et al., In vitro metabolism of anthocyanins by human gut microflora. *Eur. J. Nutr.* 2005, *44*, 133–42.

[106] Aura, A.-M., O'Leary, K.A., Williamson, G., Ojala, M., et al., Quercetin derivatives are deconjugated and converted to hydroxyphenylacetic acids but not methylated by human fecal flora in vitro. *J. Agric. Food Chem.* 2002, *50*, 1725–30.

[107] Tzounis, X., Vulevic, J., Kuhnle, G.G.C., Trevor, G., et al., Flavanol monomer -induced changes to the human faecal microflora. *Br. J. Nutr.* 2008, *99*, 782–792.

[108] Cueva, C., Sánchez-Patán, F., Monagas, M., Walton, G.E., et al., In vitro fermentation of grape seed flavan-3-ol fractions by human faecal microbiota: changes in microbial groups and phenolic metabolites. *FEMS Microbiol. Ecol.* 2013, *83*, 792–805.

[109] Sánchez-Patán, F., Cueva, C., Monagas, M., Walton, G.E., et al., In Vitro Fermentation of a Red Wine Extract by Human Gut Microbiota: Changes in Microbial Groups and Formation of Phenolic Metabolites. *J. Agric. Food Chem.* 2012, *60*, 2136–2147.

[110] Hidalgo, M., Oruna-Concha, M.J., Kolida, S., Walton, G.E., et al., Metabolism of anthocyanins by human gut microflora and their influence on gut bacterial growth. *J. Agric. Food Chem.* 2012, *60*, 3882–90.

[111] Serra, A., Macià, A., Romero, M.-P., Reguant, J., et al., Metabolic pathways of the colonic metabolism of flavonoids (flavonols, flavones and flavanones) and phenolic acids. *Food Chem.* 2012, *130*, 383–393.

[112] Serra, A., Macià, A., Romero, M.-P., Anglés, N., et al., Metabolic pathways of the colonic metabolism of procyanidins (monomers and dimers) and alkaloids. *Food Chem*. 2011, *126*, 1127–1137.

[113] Appeldoorn, M.M., Vincken, J.-P., Aura, A.-M., Hollman, P.C.H., et al., Procyanidin Dimers Are Metabolized by Human Microbiota with 2-(3,4-Dihydroxyphenyl)acetic Acid and 5-(3,4-Dihydroxyphenyl)-γ-valerolactone as the Major Metabolites. *J. Agric. Food Chem*. 2009, *57*, 1084–1092.

[114] Long, W., Xue, Z., Zhang, Q., Feng, Z., et al., Differential responses of gut microbiota to the same prebiotic formula in oligotrophic and eutrophic batch fermentation systems. *Sci. Rep*. 2015, *5*, 13469.

[115] Macfarlane, G.T., Gibson, G.R., Cummings, J.H., Comparison of fermentation reactions in different regions of the human colon. *J. Appl. Bacteriol*. 1992, *72*, 57–64.

[116] Miller, T.L., Wolin, M.J., Fermentation by the human large intestine microbial community in an in vitro semicontinuous culture system. *Appl. Environ. Microbiol*. 1981, *42*, 400–7.

[117] Veilleux, B.G., Rowland, I., Simulation of the rat intestinal ecosystem using a two-stage continuous culture system. *J. Gen. Microbiol*. 1981, *123*, 103–115.

[118] Gibson, G.R., Cummings, J.H., Macfarlane, G.T., Use of a three-stage continuous culture system to study the effect of mucin on dissimilatory sulfate reduction and methanogenesis by mixed populations of human gut bacteria. *Appl. Environ. Microbiol*. 1988, *54*, 2750–2755.

[119] Maccaferri, S., Vitali, B., Klinder, A., Kolida, S., et al., Rifaximin modulates the colonic microbiota of patients with Crohn's disease: An in vitro approach using a continuous culture colonic model system. *J. Antimicrob. Chemother*. 2010, *65*, 2556–2565.

[120] Hobden, M.R., Martin-Morales, A., Guérin-Deremaux, L., Wils, D., et al., In vitro fermentation of NUTRIOSE® FB06, a wheat dextrin soluble fibre, in a continuous culture human colonic model system. *PLoS One* 2013, *8*, 1–7.

[121] Vamanu, E., Sarbu, I., Nedelcu, I., Pelinescu, D., Study of PROEXO product influence on infant microbiota in an in vitro colonic fermentation system. *Ann. Microbiol.* 2014, 1189–1193.

[122] Mäkivuokko, H. a, Saarinen, M.T., Ouwehand, A.C., Rautonen, N.E., Effects of lactose on colon microbial community structure and function in a four-stage semi-continuous culture system. *Biosci. Biotechnol. Biochem.* 2006, *70*, 2056–2063.

[123] Mäkeläinen, H.S., Mäkivuokko, H.A., Salminen, S.J., Rautonen, N.E., et al., The effects of polydextrose and xylitol on microbial community and activity in a 4-stage colon simulator. *J. Food Sci.* 2007, *72*, M153–M159.

[124] Mäkeläinen, H., Forssten, S., Saarinen, M., Stowell, J., et al., Xylo-oligosaccharides enhance the growth of bifidobacteria and *Bifidobacterium lactis* in a simulated colon model. *Benef. Microbes* 2010, *1*, 81–91.

[125] Molly, K., Woestyne, M., Verstraete, W., Development of a 5-step multi-chamber reactor as a simulation of the human intestinal microbial ecosystem. *Appl. Microbiol. Biotechnol.* 1993, *39*.

[126] Molly, K., Woestyne, M. Vande, Smet, I. De, Verstraete, W., Validation of the simulator of the human intestinal microbial ecosystem (SHIME) reactor using microorganism-associated activities. *Microb. Ecol. Health Dis.* 1994, *7*, 191–200.

[127] Alander, M., De Smet, I., Nollet, L., Verstraete, W., et al., The effect of probiotic strains on the microbiota of the Simulator of the Human Intestinal Microbial Ecosystem (SHIME). *Int. J. Food Microbiol.* 1999, *46*, 71–79.

[128] Gmeiner, M., Kneifel, W., Kulbe, K.D., Wouters, R., et al., Influence of a synbiotic mixture consisting of Lactobacillus acidophilus 74-2 and a fructooligosaccharide preparation on the microbial ecology sustained in a simulation of the human intestinal microbial ecosystem (SHIME reactor). *Appl. Microbiol. Biotechnol.* 2000, *53*, 219–223.

[129] Kontula, P., Jaskari, J., Nollet, L., De Smet, I., et al., The colonization of a simulator of the human intestinal microbial ecosystem by a probiotic strain fed on a fermented oat bran product: effects on the gastrointestinal microbiota. *Appl Microbiol Biotechnol* 1998, *50*, 246–252.

[130] Van De Wiele, T., Boon, N., Possemiers, S., Jacobs, H., et al., Inulin-type fructans of longer degree of polymerization exert more pronounced in vitro prebiotic effects. *J. Appl. Microbiol.* 2007, *102*, 452–460.

[131] De Boever, P., Deplancke, B., Verstraete, W., Fermentation by gut microbiota cultured in a simulator of the human intestinal microbial ecosystem is improved by supplementing a soygerm powder. *J. Nutr.* 2000, *130*, 2599–606.

[132] Decroos, K., Eeckhaut, E., Possemiers, S., Verstraete, W., Administration of equol-producing bacteria alters the equol production status in the simulator of the gastrointestinal microbial ecosystem (SHIME). *J. Nutr.* 2006, *136*, 946–952.

[133] Grootaert, C., Van den Abbeele, P., Marzorati, M., Broekaert, W.F., et al., Comparison of prebiotic effects of arabinoxylan oligosaccharides and inulin in a simulator of the human intestinal microbial ecosystem. *FEMS Microbiol. Ecol.* 2009, *69*, 231–42.

[134] Van den Abbeele, P., Grootaert, C., Marzorati, M., Possemiers, S., et al., Microbial community development in a dynamic gut model is reproducible, colon region specific, and selective for Bacteroidetes and Clostridium Cluster IX. *Appl. Environ. Microbiol.* 2010, *76*, 5237–5246.

[135] Kemperman, R.A., Gross, G., Mondot, S., Possemiers, S., et al., Impact of polyphenols from black tea and red wine/grape juice on a gut model microbiome. *Food Res. Int.* 2013, *53*, 659–669.

[136] Sánchez-Patán, F., Barroso, E., van de Wiele, T., Jiménez-Girón, A., et al., Comparative in vitro fermentations of cranberry and grape seed polyphenols with colonic microbiota. *Food Chem.* 2015, *183*, 273–282.

[137] Barroso, E., Sánchez-Patán, F., Martín-Alvarez, P.J., Bartolomé, B., et al., Lactobacillus plantarum IFPL935 favors the initial metabolism of red wine polyphenols when added to a colonic microbiota. *J. Agric. Food Chem.* 2013, *61*, 10163–72.

[138] Finegold, S.M., Li, Z., Summanen, P.H., Downes, J., et al., Xylooligosaccharide increases bifidobacteria but not lactobacilli in human gut microbiota. *Food Funct.* 2014, *5*, 436–45.

[139] Marzorati, M., Qin, B., Hildebrand, F., Klosterbuer, A., et al., Addition of acacia gum to a FOS/inulin blend improves its fermentation profile in the Simulator of the Human Intestinal Microbial Ecosystem (SHIME®). *J. Funct. Foods* 2015, *16*, 211–222.

[140] Minekus, M., Marteaul, P., Havenaarl, R., Huis in't Veld, J.H.J., A multicompartmental dynamic computer- controlled model simulating the stomach and small intestine. *ATLA* 1995, *23*, 197–209.

[141] Gao, K., Xu, A., Krul, C., Venema, K., et al., Of the major phenolic acids formed during human microbial fermentation of tea, citrus, and soy flavonoid supplements, only 3,4-dihydroxyphenylacetic acid has antiproliferative activity. *J. Nutr.* 2006, 52–57.

[142] Egert, M., De Graaf, A. a., Maathuis, A., De Waard, P., et al., Identification of glucose-fermenting bacteria present in an in vitro model of the human intestine by RNA-stable isotope probing. *FEMS Microbiol. Ecol.* 2007, *60*, 126–135.

[143] Kovatcheva-Datchary, P., Egert, M., Maathuis, A., Rajilić-Stojanović, M., et al., Linking phylogenetic identities of bacteria to starch fermentation in an in vitro model of the large intestine by RNA-based stable isotope probing. *Environ. Microbiol.* 2009, *11*, 914–926.

[144] van Nuenen, M.H.M.C., Diederick Meyer, P., Venema, K., The effect of various inulins and Clostridium difficile on the metabolic activity of the human colonic microbiota in vitro. *Microb. Ecol. Health Dis.* 2003, *15*, 137–144.

[145] Van Den Abbeele, P., Venema, K., Van De Wiele, T., Verstraete, W., et al., Different human gut models reveal the distinct fermentation patterns of arabinoxylan versus inulin. *J. Agric. Food Chem.* 2013, *61*, 9819–9827.

[146] Barroso, E., Cueva, C., Peláez, C., Martínez-Cuesta, M.C., et al., Development of human colonic microbiota in the computer-controlled dynamic SIMulator of the GastroIntestinal tract SIMGI. *LWT - Food Sci. Technol.* 2015, *61*, 283–289.

[147] Robinson, C.D., Auchtung, J.M., Collins, J., Britton, R.A., Epidemic Clostridium difficile strains demonstrate increased competitive fitness compared to nonepidemic isolates. *Infect. Immun.* 2014, *82*, 2815–2825.

[148] Moal, V.L.-L., Servin, A.L., The front line of enteric host defense against unwelcome intrusion of harmful microorgansims: mucins, antimicrobial peptides and microbiota. *Clin. Microbiol. Rev.* 2006, *19*, 315–337.

[149] Macfarlane, S., Dillon, J.F., Microbial biofilms in the human gastrointestinal tract. *J. Appl. Microbiol.* 2007, *102*, 1187–1196.

[150] Van den Abbeele, P., Van de Wiele, T., Verstraete, W., Possemiers, S., The host selects mucosal and luminal associations of coevolved gut microorganisms: A novel concept. *FEMS Microbiol. Rev.* 2011, *35*, 681–704.

[151] Zoetendal, E.G., Wright, A. Von, Ben-amor, K., Antoon, D.L., et al., Mucosa-associated bacteria in the human gastrointestinal tract are uniformly distributed along the colon and differ from the community recovered from feces. *Appl. Environ. Microbiol.* 2002, *68*, 3401–3407.

[152] Lacroix, C., LeBlay, G., Cinquin, C., Fliss, S.-F., United States patent application publication in vitro gastrointestinal model system and uses thereof, 2004.

[153] Cinquin, C., Le Blay, G., Fliss, I., Lacroix, C., Immobilization of infant fecal microbiota and utilization in an in vitro colonic fermentation model. *Microb. Ecol.* 2004, *48*, 128–138.

[154] Lamboley, L., Lacroix, C., Champagne, C.P., Vuillemard, J.C., Continuous mixed strain mesophilic lactic starter production in supplemented whey permeate medium using immobilized cell technology. *Biotechnol. Bioeng.* 1997, *56*, 502–516.

[155] Le Blay, G., Rytka, J., Zihler, A., Lacroix, C., New in vitro colonic fermentation model for Salmonella infection in the child gut. *FEMS Microbiol. Ecol.* 2009, *67*, 198–207.

[156] Crowther, G.S., Chilton, C.H., Todhunter, S.L., Nicholson, S., et al., Development and validation of a chemostat gut model to study both planktonic and biofilm modes of growth of Clostridium difficile and human microbiota. *PLoS One* 2014, *9*, 1–11.

[157] Van den Abbeele, P., Roos, S., Eeckhaut, V., MacKenzie, D.A., et al., Incorporating a mucosal environment in a dynamic gut model results in a more representative colonization by lactobacilli. *Microb. Biotechnol.* 2012, *5*, 106–115.

[158] Berner, Z.A., Fuentes, S., Dostal, A., Payne, A.N., et al., Novel Polyfermentor intestinal model (PolyFermS) for controlled ecological studies: validation and effect of pH. *PLoS One* 2013, *8*, e77772.

[159] Fehlbaum, S., Chassard, C., Haug, M.C., Fourmestraux, C., et al., Design and Investigation of PolyFermS In Vitro Continuous Fermentation Models Inoculated with Immobilized Fecal Microbiota Mimicking the Elderly Colon. *PLoS One* 2015, *10*, e0142793.

[160] Tanner, S. a, Zihler Berner, A., Rigozzi, E., Grattepanche, F., et al., In vitro continuous fermentation model (PolyFermS) of the swine proximal colon for simultaneous testing on the same gut microbiota. *PLoS One* 2014, *9*, e94123.

[161] Kim, H.J., Huh, D., Hamilton, G., Ingber, D.E., Human gut-on-a-chip inhabited by microbial flora that experiences intestinal peristalsis-like motions and flow. *Lab Chip* 2012, *12*, 2165.

[162] Tottey, W., Denonfoux, J., Jaziri, F., Parisot, N., et al., The human gut chip "HuGChip", an explorative phylogenetic microarray for determining gut microbiome diversity at family level. *PLoS One* 2013, *8*, 1–12.

[163] Chen, J., Gaikwad, V., Holmes, M., Murray, B., et al., Development of a simple model device for in vitro gastric digestion investigation. *Food Funct.* 2011, *2*, 174–182.

[164] Vardakou, M., Mercuri, A., Barker, S. a, Craig, D.Q.M., et al., Achieving antral grinding forces in biorelevant in vitro models: comparing the USP Dissolution Apparatus II and the Dynamic Gastric Model with human in vivo data. *AAPS PharmSciTech* 2011, *12*, 620–626.

[165] Mackie, A., Bajka, B., Rigby, N., Roles for dietary fibre in the upper GI tract: The importance of viscosity. *Food Res. Int.* 2015.

[166] Maathuis, A.J.H., Keller, D., Farmer, S., Survival and metabolic activity of the GanedenBC30 strain of Bacillus coagulans in a dynamic in vitro model of the stomach and small intestine. *Benef. Microbes* 2010, *1*, 31–36.

[167] Kong, F., Singh, R.P., A human gastric simulator (HGS) to study food digestion in human stomach. *J. Food Sci*. 2010, *75*.

[168] Guerra, A., Etienne-Mesmin, L., Livrelli, V., Denis, S., et al., Relevance and challenges in modeling human gastric and small intestinal digestion. *Trends Biotechnol*. 2012, *30*, 591–600.

[169] Mainville, I., Arcand, Y., Farnworth, E.R., A dynamic model that simulates the human upper gastrointestinal tract for the study of probiotics. *Int. J. Food Microbiol*. 2005, *99*, 287–296.

[170] Marteau, P., Minekus, M., Havenaar, R., Huis in't Veld, J.H., Survival of lactic acid bacteria in a dynamic model of the stomach and small intestine: validation and the effects of bile. *J. Dairy Sci*. 1997, *80*, 1031–1037.

[171] Gabrielli, O., Zampini, L., Galeazzi, T., Padella, L., et al., Preterm Milk Oligosaccharides During the First Month of Lactation. *Pediatrics* 2011, *128*, e1520–e1531.

[172] Coppa, G., Pierani, P., Zampini, L., Carloni, I., et al., Oligosaccharides in human milk during different phases of lactation. *Acta Paediatr*. 1999, *88*, 89–94.

[173] Saarela, T., Kokkonen, J., Koivisto, M., Macronutrient and energy contents of human milk fractions during the first six months of lactation. *Acta Paediatr*. 2005, *94*, 1176–1181.

[174] Sumiyoshi, W., Urashima, T., Nakamura, T., Arai, I., et al., Determination of each neutral oligosaccharide in the milk of Japanese women during the course of lactation. *Br. J. Nutr*. 2003, *89*, 61.

[175] Bode, L., Human milk oligosaccharides: every baby needs a sugar mama. *Glycobiology* 2012, *22*, 1147–62.

[176] Thurl, S., Mü Ller-Werner, B., Sawatzki, G.N., Quantification of Individual Oligosaccharide Compounds from Human Milk Using High-pH Anion-Exchange Chromatography. *Anal. Biochem.* 1996, *235*, 202–206.

[177] Wu, S., Tao, N., German, J.B., Grimm, R., et al., Development of an Annotated Library of Neutral Human Milk Oligosaccharides. *J. Proteome Res.* 2010, *9*, 4138–4151.

[178] Charlwood, J., Tolson, D., Dwek, M., Camilleri, P., A Detailed Analysis of Neutral and Acidic Carbohydrates in Human Milk. *Anal. Biochem.* 1999, *273*, 261–277.

[179] Stahl, B., Thurl, S., Zeng, J.R., Karas, M., et al., Oligosaccharides from Human Milk as Revealed by Matrix-Assisted Laser Desorption/Ionization Mass Spectrometry. *Anal. Biochem.* 1994, *223*, 218–226.

[180] Underwood, M.A., German, J.B., Lebrilla, C.B., Mills, D.A., Bifidobacterium longum subspecies infantis: champion colonizer of the infant gut. *Pediatr. Res.* 2015, *77*, 229–35.

[181] Klaassens, E.S., Boesten, R.J., Haarman, M., Knol, J., et al., Mixed-species genomic microarray analysis of fecal samples reveals differential transcriptional responses of bifidobacteria in breast- and formula-fed infants. *Appl. Environ. Microbiol.* 2009, *75*, 2668–76.

[182] Roger, L.C., Costabile, A., Holland, D.T., Hoyles, L., et al., Examination of faecal Bifidobacterium populations in breast- and formula-fed infants during the first 18 months of life. *Microbiology* 2010, *156*, 3329–41.

[183] Sela, D.A., Mills, D.A., Nursing our microbiota: Molecular linkages between bifidobacteria and milk oligosaccharides. *Trends Microbiol.* 2010, *18*, 298–307.

[184] Garrido, D., Kim, J.H., German, J.B., Raybould, H.E., et al., Oligosaccharide Binding Proteins from *Bifidobacterium longum* subsp. *infantis* Reveal a Preference for Host Glycans. *PLoS One* 2011, *6*, e17315.

[185] Garrido, D., Ruiz-Moyano, S., Mills, D.A., Release and utilization of N-acetyl-d-glucosamine from human milk oligosaccharides by Bifidobacterium longum subsp. infantis. *Anaerobe* 2012, *18*, 430–435.

[186] Sela, D.A., Li, Y., Lerno, L., Wu, S., et al., An infant-associated bacterial commensal utilizes breast milk sialyloligosaccharides. *J. Biol. Chem.* 2011, *286*, 11909–11918.

[187] Sela, D.A., Garrido, D., Lerno, L., Wu, S., et al., *Bifidobacterium longum* subsp. *infantis* ATCC 15697 α-fucosidases are active on fucosylated human milk oligosaccharides. *Appl. Environ. Microbiol.* 2012, *78*, 795–803.

[188] Palframan, R.J., Gibson, G.R., Rastall, R.A., Carbohydrate preferences of Bifidobacterium species isolated from the human gut. *Curr. Issues Intest. Microbiol.* 2003, *4*, 71–5.

[189] Fushinobu, S., Unique sugar metabolic pathways of bifidobacteria. *Biosci. Biotechnol. Biochem.* 2010, *74*, 2374–84.

[190] Pokusaeva, K., Fitzgerald, G.F., Van Sinderen, D., Carbohydrate metabolism in Bifidobacteria. *Genes Nutr.* 2011, *6*, 285–306.

[191] De Vuyst, L., Moens, F., Selak, M., Rivière, A., et al., Summer Meeting 2013: growth and physiology of bifidobacteria. *J. Appl. Microbiol.* 2014, *116*, 477–491.

[192] Rivière, A., Selak, M., Lantin, D., Leroy, F., et al., Bifidobacteria and Butyrate-Producing Colon Bacteria: Importance and Strategies for Their Stimulation in the Human Gut. *Front. Microbiol.* 2016, *7*, 979.

[193] Van Der Meulen, R., Adriany, T., Verbrugghe, K., De Vuyst, L., Kinetic analysis of bifidobacterial metabolism reveals a minor role for succinic acid in the regeneration of NAD+ through its growth-associated production. *Appl. Environ. Microbiol.* 2006, *72*, 5204–5210.

[194] Bridgman, S.L., Azad, M.B., Field, C.J., Haqq, A.M., et al., Fecal Short-Chain Fatty Acid Variations by Breastfeeding Status in Infants at 4 Months: Differences

in Relative versus Absolute Concentrations. *Front. Nutr.* 2017, *4*, 11.

[195] Chow, J., Panasevich, M.R., Alexander, D., Vester Boler, B.M., et al., Fecal Metabolomics of Healthy Breast-Fed versus Formula-Fed Infants before and during In Vitro Batch Culture Fermentation. *J. Proteome Res.* 2014, *13*, 2534–2542.

[196] Asakuma, S., Hatakeyama, E., Urashima, T., Yoshida, E., et al., Physiology of Consumption of Human Milk Oligosaccharides by Infant Gut-associated Bifidobacteria. *J. Biol. Chem.* 2011, *286*, 34583–34592.

[197] LoCascio, R.G., Desai, P., Sela, D.A., Weimer, B., et al., Broad conservation of milk utilization genes in *Bifidobacterium longum* subsp. *infantis* as revealed by comparative genomic hybridization. *Appl. Environ. Microbiol.* 2010, *76*, 7373–7381.

[198] LoCascio, R.G., Niñonuevo, M.R., Kronewitter, S.R., Freeman, S.L., et al., A versatile and scalable strategy for glycoprofiling bifidobacterial consumption of human milk oligosaccharides. *Microb. Biotechnol.* 2009, *2*, 333–342.

[199] LoCascio, R.G., Ninonuevo, M.R., Freeman, S.L., Sela, D.A., et al., Glycoprofiling of Bifidobacterial Consumption of Human Milk Oligosaccharides Demonstrates Strain Specific, Preferential Consumption of Small Chain Glycans Secreted in Early Human Lactation. *J. Agric. Food Chem.* 2007, *55*, 8914–8919.

[200] Marcobal, A., Barboza, M., Froehlich, J.W., Block, D.E., et al., Consumption of Human Milk Oligosaccharides by Gut-Related Microbes. *J. Agric. Food Chem.* 2010, *58*, 5334–5340.

[201] Turroni, F., Foroni, E., Pizzetti, P., Giubellini, V., et al., Exploring the diversity of the bifidobacterial population in the human intestinal tract. *Appl. Environ. Microbiol.* 2009, *75*, 1534–1545.

[202] Orban, J.I., Patterson, J.A., Modification of the phosphoketolase assay for rapid identification of bifidobacteria. *J. Microbiol. Methods* 2000, *40*, 221–224.

[203] Satokari, R.M., Vaughan, E.E., Akkermans, A.D., Saarela, M., et al., Bifidobacterial diversity in human feces detected by genus-specific PCR and denaturing gradient gel electrophoresis. *Appl. Environ. Microbiol.* 2001, *67*, 504–13.

[204] Lewis, Z.T., Shani, G., Masarweh, C.F., Popovic, M., et al., Validating bifidobacterial species and subspecies identity in commercial probiotic products. *Pediatr. Res.* 2016, *79*, 445–52.

[205] Dai, Y., McLandsborough, L.A., Weiss, J., Peleg, M., Concentration and application order effects of sodium benzoate and eugenol mixtures on the growth inhibition of *Saccharomyces cerevisiae* and *Zygosaccharomyces bailii*. *J. Food Sci.* 2010, *75*, 482–488.

[206] Xia, J., Wishart, D.S., Using MetaboAnalyst 3.0 for Comprehensive Metabolomics Data Analysis, in: *Current Protocols in Bioinformatics*, John Wiley & Sons, Inc., Hoboken, NJ, USA 2016, pp. 14.10.1-14.10.91.

[207] Parche, S., Beleut, M., Rezzonico, E., Jacobs, D., et al., Lactose-over-Glucose Preference in Bifidobacterium longum NCC2705: glcP, Encoding a Glucose Transporter, Is Subject to Lactose Repression. *J. Bacteriol.* 2006, *188*, 1260–1265.

[208] Love, M.I., Huber, W., Anders, S., Moderated estimation of fold change and dispersion for RNA-seq data with DESeq2. *Genome Biol.* 2014, *15*, 550.

[209] Lin, C.-H., Wang, Y.-H., Chen, Y.-W., Lin, Y.-L., et al., Transcriptional and posttranscriptional regulation of CXCL8/IL-8 gene expression induced by connective tissue growth factor. *Immunol. Res.* 2016, *64*, 369–384.

[210] Takaishi, K., Komohara, Y., Tashiro, H., Ohtake, H., et al., Involvement of M2-polarized macrophages in the ascites from advanced epithelial ovarian carcinoma in tumor progression via Stat3 activation. *Cancer Sci.* 2010, *101*, 2128–2136.

[211] Romieu-Mourez, R., Solis, M., Nardin, A., Goubau, D., et al., Distinct Roles for IFN Regulatory Factor (IRF)-3 and IRF-7 in the Activation of Antitumor Properties of Human Macrophages. *Cancer Res* 2006, *66*, 10576–85.

[212] Ruiz-Moyano, S., Totten, S.M., Garrido, D.A., Smilowitz, J.T., et al., Variation in Consumption of Human Milk Oligosaccharides by Infant Gut-Associated Strains of Bifidobacterium breve. *Appl. Environ. Microbiol.* 2013, *79*, 6040–6049.

[213] Garrido, D., Ruiz-Moyano, S., Jimenez-Espinoza, R., Eom, H.-J., et al., Utilization of galactooligosaccharides by Bifidobacterium longum subsp. infantis isolates. *Food Microbiol.* 2013, *33*, 262–270.

[214] Falony, G., Lazidou, K., Verschaeren, A., Weckx, S., et al., *In vitro* kinetic analysis of fermentation of prebiotic inulin-type fructans by Bifidobacterium species reveals four different phenotypes. *Appl. Environ. Microbiol.* 2009, *75*, 454–461.

[215] Milani, C., Andrea Lugli, G., Duranti, S., Turroni, F., et al., Bifidobacteria exhibit social behavior through carbohydrate resource sharing in the gut. *Sci. Rep.* 2015, *5*, 15782.

[216] Van Der Meulen, R., Avonts, L., De Vuyst, L., Short fractions of oligofructose are preferentially metabolized by *Bifidobacterium animalis* DN-173 010. *Appl. Environ. Microbiol.* 2004, *70*, 1923–1930.

[217] Kim, J.-H., An, H.J., Garrido, D., German, J.B., et al., Proteomic Analysis of Bifidobacterium longum subsp. infantis Reveals the Metabolic Insight on Consumption of Prebiotics and Host Glycans. *PLoS One* 2013, *8*, e57535.

[218] Yoshida, E., Sakurama, H., Kiyohara, M., Nakajima, M., et al., Bifidobacterium longum subsp. infantis uses two different-galactosidases for selectively degrading type-1 and type-2 human milk oligosaccharides. *Glycobiology* 2012, *22*, 361–368.

[219] Wickramasinghe, S., Pacheco, A.R., Lemay, D.G., Mills, D.A., Bifidobacteria grown on human milk oligosaccharides downregulate the expression of inflammation-related genes in Caco-2 cells. *BMC Microbiol.* 2015, *15*, 172.

[220] Chichlowski, M., De Lartigue, G., German, J.B., Raybould, H.E., et al., Bifidobacteria Isolated From Infants and Cultured on Human Milk Oligosaccharides Affect Intestinal Epithelial Function. *J. Pediatr. Gastroenterol. Nutr.* 2012, *55*, 321–327.

[221] Özcan, E., Sun, J., Rowley, D.C., Sela, D.A., A Human Gut Commensal Ferments Cranberry Carbohydrates To Produce Formate. *Appl. Environ. Microbiol.* 2017, *83*, e01097-17.

[222] Van der Meulen, R., Makras, L., Verbrugghe, K., Adriany, T., et al., In vitro kinetic analysis of oligofructose consumption by Bacteroides and Bifidobacterium spp. indicates different degradation mechanisms. *Appl. Environ. Microbiol.* 2006, *72*, 1006–1012.

[223] Amaretti, A., Bernardi, T., Tamburini, E., Zanoni, S., et al., Kinetics and metabolism of Bifidobacterium adolescentis MB 239 growing on glucose, galactose, lactose, and galactooligosaccharides. *Appl. Environ. Microbiol.* 2007, *73*, 3637–3644.

[224] James, K., Motherway, M.O., Bottacini, F., van Sinderen, D., et al., Bifidobacterium breve UCC2003 metabolises the human milk oligosaccharides lacto-N-tetraose and lacto-N-neo-tetraose through overlapping, yet distinct pathways. *Sci. Rep.* 2016, *6*, 38560.

[225] Schwab, C., Gänzle, M., Lactic acid bacteria fermentation of human milk oligosaccharide components, human milk oligosaccharides and galactooligosaccharides. *FEMS Microbiol. Lett.* 2011, *315*, 141–8.

[226] Rudloff, S., Pohlentz, G., Borsch, C., Lentze, M.J., et al., Urinary excretion of in vivo 13 C-labelled milk oligosaccharides in breastfed infants. *Br. J. Nutr.* 2012, *107*, 957–963.

[227] Kim, J.-H., An, H.J., Garrido, D., German, J.B., et al., Proteomic Analysis of Bifidobacterium longum subsp. infantis Reveals the Metabolic Insight on Consumption of Prebiotics and Host Glycans. *PLoS One* 2013, *8*, e57535.

[228] Garrido, D., Nwosu, C., Ruiz-Moyano, S., Aldredge, D., et al., Endo-β-N-acetylglucosaminidases from infant gut-associated bifidobacteria release complex N-glycans from human milk glycoproteins. *Mol. Cell. Proteomics* 2012, *11*, 775–85.

[229] Özcan, E., Sela, D.A., Inefficient Metabolism of the Human Milk Oligosaccharides Lacto-N-tetraose and Lacto-N-neotetraose Shifts

Bifidobacterium longum subsp. infantis Physiology. *Front. Nutr.* 2018, *5*, 46.

[230] James, K., Motherway, M.O., Penno, C., O'Brien, R.L., et al., Bifidobacterium breve UCC2003 employs multiple transcriptional regulators to control metabolism of particular human milk oligosaccharides. *Appl. Environ. Microbiol.* 2018, *84*, e02774-17.

[231] Sprouffske, K., Wagner, A., Growthcurver: an R package for obtaining interpretable metrics from microbial growth curves. *BMC Bioinformatics* 2016, *17*, 172.

[232] Wu, S., Grimm, R., German, J.B., Lebrilla, C.B., Annotation and Structural Analysis of Sialylated Human Milk Oligosaccharides. *J. Proteome Res.* 2011, *10*, 856–868.

[233] Roger, L.C., Costabile, A., Holland, D.T., Hoyles, L., et al., Examination of faecal Bifidobacterium populations in breast- and formula-fed infants during the first 18 months of life. *Microbiology* 2010, *156*, 3329–3341.

[234] Kwak, M.-J., Kwon, S.-K., Yoon, J.-K., Song, J.Y., et al., Evolutionary architecture of the infant-adapted group of Bifidobacterium species associated with the probiotic function. *Syst. Appl. Microbiol.* 2016, *39*, 429–439.

[235] McGuire, M.K., Meehan, C.L., McGuire, M.A., Williams, J.E., et al., What's normal? Oligosaccharide concentrations and profiles in milk produced by healthy women vary geographically. *Am. J. Clin. Nutr.* 2017, *105*, 1086–1100.

[236] Azad, M.B., Robertson, B., Atakora, F., Becker, A.B., et al., Human Milk Oligosaccharide Concentrations Are Associated with Multiple Fixed and Modifiable Maternal Characteristics, Environmental Factors, and Feeding Practices. *J. Nutr.* 2018, *148*, 1733–1742.

[237] Wang, M., Li, M., Wu, S., Lebrilla, C.B., et al., Fecal microbiota composition of breast-fed infants is correlated with human milk oligosaccharides consumed. *J. Pediatr. Gastroenterol. Nutr.* 2015, *60*, 825–33.

[238] Arboleya, S., Bottacini, F., O'Connell-Motherway, M., Ryan, C.A., et al., Gene-trait matching across the Bifidobacterium longum pan-genome reveals considerable diversity in carbohydrate catabolism among human infant strains. *BMC Genomics* 2018, *19*, 33.

[239] Bunesova, V., Lacroix, C., Schwab, C., Fucosyllactose and L-fucose utilization of infant Bifidobacterium longum and Bifidobacterium kashiwanohense. *BMC Microbiol*. 2016, *16*, 248.

[240] Egan, M., O'Connell Motherway, M., Kilcoyne, M., Kane, M., et al., Cross-feeding by Bifidobacterium breve UCC2003 during co-cultivation with Bifidobacterium bifidum PRL2010 in a mucin-based medium. *BMC Microbiol*. 2014, *14*, 282.

[241] Marcobal, A., Barboza, M., Sonnenburg, E.D., Pudlo, N., et al., Bacteroides in the Infant Gut Consume Milk Oligosaccharides via Mucus-Utilization Pathways. *Cell Host Microbe* 2011, *10*, 507–514.

[242] Ward, R.E., Niñonuevo, M., Mills, D. a, Lebrilla, C.B., et al., In vitro fermentation of breast milk oligosaccharides by Bifidobacterium infantis and Lactobacillus gasseri. *Appl. Environ. Microbiol*. 2006, *72*, 4497–9.

[243] Sonnenburg, J.L., Xu, J., Leip, D.D., Chen, C.-H., et al., Glycan foraging in vivo by an intestine-adapted bacterial symbiont. *Science* 2005, *307*, 1955–9.

[244] Rey, F.E., Faith, J.J., Bain, J., Muehlbauer, M.J., et al., Dissecting the in vivo metabolic potential of two human gut acetogens. *J. Biol. Chem*. 2010, *285*, 22082–90.

[245] Duncan, S.H., Louis, P., Flint, H.J., Lactate-utilizing bacteria, isolated from human feces, that produce butyrate as a major fermentation product. *Appl. Environ. Microbiol*. 2004, *70*, 5810–7.

[246] Falony, G., Vlachou, A., Verbrugghe, K., De Vuyst, L., Cross-feeding between *Bifidobacterium longum* BB536 and acetate-converting, butyrate-producing colon bacteria during growth on oligofructose. *Appl. Environ. Microbiol*. 2006, *72*, 7835–7841.

[247] Turroni, F., Özcan, E., Milani, C., Mancabelli, L., et al., Glycan cross-feeding activities between bifidobacteria under in vitro conditions. *Front. Microbiol.* 2015, *6*.

[248] Moens, F., Weckx, S., De Vuyst, L., Bifidobacterial inulin-type fructan degradation capacity determines cross-feeding interactions between bifidobacteria and Faecalibacterium prausnitzii. *Int. J. Food Microbiol.* 2016.

[249] Moens, F., Verce, M., De Vuyst, L., Lactate- and acetate-based cross-feeding interactions between selected strains of lactobacilli, bifidobacteria and colon bacteria in the presence of inulin-type fructans. 2017.

[250] Moens, F., Rivière, A., Selak, M., De Vuyst, L., Inulin-type fructan degradation capacity of interesting butyrate-producing colon bacteria and cross-feeding interactions of Faecalibacterium prausnitzii DSM 17677T with bifidobacteria. *Arch. Public Heal.* 2014, *72*, O6.

[251] Vester Boler, B.M., Rossoni Serao, M.C., Faber, T.A., Bauer, L.L., et al., In Vitro Fermentation Characteristics of Select Nondigestible Oligosaccharides by Infant Fecal Inocula. *J. Agric. Food Chem.* 2013, *61*, 2109–2119.

[252] Wiese, M., Khakimov, B., Nielsen, S., Sørensen, H., et al., CoMiniGut—a small volume *in vitro* colon model for the screening of gut microbial fermentation processes. *PeerJ* 2018, *6*, e4268.

[253] Gotoh, A., Katoh, T., Sakanaka, M., Ling, Y., et al., Sharing of human milk oligosaccharides degradants within bifidobacterial communities in faecal cultures supplemented with Bifidobacterium bifidum. *Sci. Rep.* 2018, *8*, 13958.

[254] Chow, J., Panasevich, M.R., Alexander, D., Vester Boler, B.M., et al., Fecal Metabolomics of Healthy Breast-Fed versus Formula-Fed Infants before and during In Vitro Batch Culture Fermentation. *J. Proteome Res.* 2014, *13*, 2534–2542.

[255] Hughes, E.R., Winter, M.G., Duerkop, B.A., Spiga, L., et al., Microbial Respiration and Formate Oxidation as Metabolic Signatures of Inflammation-Associated Dysbiosis. *Cell Host Microbe* 2017, *21*, 208–219.

[256] Bolyen, E., Rideout, J.R., Dillon, M.R., Bokulich, N.A., et al., QIIME 2: Reproducible, interactive, scalable, and extensible microbiome data science. 2018.

[257] Edgar, R.C., Flyvbjerg, H., Error filtering, pair assembly and error correction for next-generation sequencing reads. *Bioinformatics* 2015, *31*, 3476–3482.

[258] Callahan, B.J., McMurdie, P.J., Rosen, M.J., Han, A.W., et al., DADA2: High-resolution sample inference from Illumina amplicon data. *Nat. Methods* 2016, *13*, 581–583.

[259] Pedregosa, F., Varoquaux, G., Gramfort, A., Michel, V., et al., Scikit-learn: Machine Learning in Python. *J. Mach. Learn. Res.* 2012.

[260] McDonald, D., Price, M.N., Goodrich, J., Nawrocki, E.P., et al., An improved Greengenes taxonomy with explicit ranks for ecological and evolutionary analyses of bacteria and archaea. *ISME J.* 2012, *6*, 610–8.

[261] Bokulich, N.A., Kaehler, B.D., Rideout, J.R., Dillon, M., et al., Optimizing taxonomic classification of marker-gene amplicon sequences with QIIME 2's q2-feature-classifier plugin. *Microbiome* 2018, *6*, 90.

[262] McDonald, D., Clemente, J.C., Kuczynski, J., Rideout, J.R., et al., The Biological Observation Matrix (BIOM) format or: how I learned to stop worrying and love the ome-ome. *Gigascience* 2012, *1*, 7.

[263] Mckinney, W., Data Structures for Statistical Computing in Python, 2010.

[264] Price, M.N., Dehal, P.S., Arkin, A.P., FastTree 2 – Approximately Maximum-Likelihood Trees for Large Alignments. *PLoS One* 2010, *5*, e9490.

[265] Katoh, K., Standley, D.M., MAFFT Multiple Sequence Alignment Software Version 7: Improvements in Performance and Usability. *Mol. Biol. Evol.* 2013, *30*, 772–780.

[266] Weiss, S., Xu, Z.Z., Peddada, S., Amir, A., et al., Normalization and microbial

differential abundance strategies depend upon data characteristics. *Microbiome* 2017, *5*, 27.

[267] Laverde Gomez, J.A., Mukhopadhya, I., Duncan, S.H., Louis, P., et al., Formate cross-feeding and cooperative metabolic interactions revealed by transcriptomics in co-cultures of acetogenic and amylolytic human colonic bacteria. *Environ. Microbiol.* 2019, *21*, 259–271.

[268] Wu, F., Guo, X., Zhang, J., Zhang, M., et al., Phascolarctobacterium faecium abundant colonization in human gastrointestinal tract. *Exp. Ther. Med.* 2017, *14*, 3122.

[269] Shimizu, J., Kubota, T., Takada, E., Takai, K., et al., Propionate-producing bacteria in the intestine may associate with skewed responses of IL10-producing regulatory T cells in patients with relapsing polychondritis. 2018.

[270] Dolfing, J., Jiang, B., Henstra, A.M., Stams, A.J.M., et al., Syntrophic Growth on Formate: a New Microbial Niche in Anoxic Environments. *Appl. Environ. Microbiol.* 2008, *74*, 6126–6131.

[271] D'hoe, K., Vet, S., Faust, K., Moens, F., et al., Integrated culturing, modeling and transcriptomics uncovers complex interactions and emergent behavior in a three-species synthetic gut community. *Elife* 2018, *7*.

[272] Lorna, M., De Leoz, A., Kalanetra, K.M., Bokulich, N.A., et al., Human Milk Glycomics and Gut Microbial Genomics in Infant Feces Show a Correlation between Human Milk Oligosaccharides and Gut Microbiota: A Proof-of-Concept Study. 2014.

[273] Schwab, C., Ruscheweyh, H.-J., Bunesova, V., Pham, V.T., et al., Trophic Interactions of Infant Bifidobacteria and Eubacterium hallii during L-Fucose and Fucosyllactose Degradation. *Front. Microbiol.* 2017, *8*, 95.

[274] Pham, V.T., Lacroix, C., Braegger, C.P., Chassard, C., Lactate-utilizing community is associated with gut microbiota dysbiosis in colicky infants. *Sci. Rep.* 2017, *7*, 11176.

[275] Smith, P.M., Howitt, M.R., Panikov, N., Michaud, M., et al., The microbial metabolites, short-chain fatty acids, regulate colonic Treg cell homeostasis. *Science* 2013, *341*, 569–73.

[276] Zindel, U., Freudenberg, W., Rieth, M., Andreesen, J.R., et al., Eubacterium acidaminophilum sp. nov., a versatile amino acid-degrading anaerobe producing or utilizing H2 or formate. *Arch. Microbiol.* 1988, *150*, 254–266.

[277] Sharak Genthner, B.R., Bryant, M.P., Additional characteristics of one-carbon-compound utilization by Eubacterium limosum and Acetobacterium woodii. *Appl. Environ. Microbiol.* 1987, *53*, 471–6.

[278] Hehemann, J.-H., Kelly, A.G., Pudlo, N.A., Martens, E.C., et al., Bacteria of the human gut microbiome catabolize red seaweed glycans with carbohydrate-active enzyme updates from extrinsic microbes. *Proc. Natl. Acad. Sci. U. S. A.* 2012, *109*, 19786–91.

[279] Van den Broek, L.A.M., Hinz, S.W.A., Beldman, G., Vincken, J.-P., et al., *Bifidobacterium* carbohydrases-their role in breakdown and synthesis of (potential) prebiotics. *Mol. Nutr. Food Res.* 2008, *52*, 146–63.

[280] Odamaki, T., Horigome, A., Sugahara, H., Hashikura, N., et al., Comparative genomics revealed genetic diversity and species/strain-level differences in carbohydrate metabolism of three probiotic bifidobacterial species. *Int. J. Genomics* 2015, *2015*, 567809.

[281] Carpita, N.C., Gibeaut, D.M., Structural models of primary cell walls in flowering plants: consistency of molecular structure with the physical properties of the walls during growth. *Plant J.* 1993, *3*, 1–30.

[282] Hsieh, Y.S.Y., Harris, P.J., Xyloglucans of monocotyledons have diverse structures. *Mol. Plant* 2009, *2*, 943–965.

[283] Brennan, M., Harris, P.J., Distribution of fucosylated xyloglucans among the walls of different cell types in monocotyledons determined by immunofluorescence microscopy. *Mol. Plant* 2011, *4*, 144–156.

[284] Hotchkiss, A.T., Nunez, A., Strahan, G.D., Chau, H., et al., Cranberry xyloglucan structure and inhibition of *Escherichia coli* adhesion to epithelial cells. *J. Agric. Food Chem.* 2015, *63*, 5622–5633.

[285] Coleman, C.M., Ferreira, Daneel Amy B. Howell, A.B., Reed, J.D., Krueger, C.G., et al., Isolation and identification of antiadhesive urinary metabolites produced as a result cranberry juice consumption, in: *2010 Joint Annual Meeting of the American Society of Pharmacognosy & the Phytochemical Society of North America Natural Solutions to 21st Century Problems – from Discovery to Commercialization*, 2010, p. O-47.

[286] Sun, J., Marais, J.P.J., Khoo, C., LaPlante, K., et al., Cranberry (*Vaccinium macrocarpon*) oligosaccharides decrease biofilm formation by uropathogenic *Escherichia coli*. *J. Funct. Foods* 2015, *17*, 235–242.

[287] Hartemink, R., Laere, K. Van, Mertens, A., Rombouts, F., Fermentation of xyloglucan by intestinal bacteria. *Anaerobe* 1996, *2*, 223–30.

[288] Holzapfel, W.H., Haberer, P., Snel, J., Schillinger, U., et al., Overview of gut flora and probiotics. *Int. J. Food Microbiol.* 1998, *41*, 85–101.

[289] Masuko, T., Minami, A., Iwasaki, N., Majima, T., et al., Carbohydrate analysis by a phenol–sulfuric acid method in microplate format. *Anal. Biochem.* 2005, *339*, 69–72.

[290] McLaughlin, H.P., Motherway, M.O., Lakshminarayanan, B., Stanton, C., et al., Carbohydrate catabolic diversity of bifidobacteria and lactobacilli of human origin. *Int. J. Food Microbiol.* 2015, *203*, 109–121.

[291] Borch, E., Berg, H., Holst, O., Heterolactic fermentation by a homofermentative *Lactobacillus* sp. during glucose limitation in anaerobic continuous culture with complete cell recycle. *J. Appl. Bacteriol.* 1991, *71*, 265–269.

[292] Kontula, P., von Wright, A., Mattila-Sandholm, T., Oat bran β-gluco- and xylo-oligosaccharides as fermentative substrates for lactic acid bacteria. *Int. J. Food Microbiol.* 1998, *45*, 163–169.

[293] Milani, C., Lugli, G.A., Duranti, S., Turroni, F., et al., Genomic encyclopedia of type strains of the genus *Bifidobacterium*. *Appl*. *Environ*. *Microbiol*. 2014, *80*, 6290–6302.

[294] Pastell, H., Westermann, P., Meyer, A.S., Päivi, T., et al., *In vitro* fermentation of arabinoxylan-derived carbohydrates by bifidobacteria and mixed fecal microbiota. *J*. *Agric*. *Food Chem*. 2009, *57*, 8598–8606.

[295] Rivière, A., Moens, F., Selak, M., Maes, D., et al., The ability of bifidobacteria to degrade arabinoxylan oligosaccharide constituents and derived oligosaccharides is strain dependent. *Appl*. *Environ*. *Microbiol*. 2014, *80*, 204–217.

[296] Thum, C., Roy, N.C., McNabb, W.C., Otter, D.E., et al., *In vitro* fermentation of caprine milk oligosaccharides by bifidobacteria isolated from breast-fed infants. *Gut Microbes* 2015, *6*, 352–363.

[297] Blumberg, J.B., Camesano, T.A., Cassidy, A., Kris-Etherton, P., et al., Cranberries and their bioactive constituents in human health. *Adv*. *Nutr*. 2013, *4*, 618–32.

[298] Rossi, M., Corradini, C., Amaretti, A., Nicolini, M., et al., Fermentation of fructooligosaccharides and inulin by bifidobacteria: a comparative study of pure and fecal cultures. *Appl*. *Environ*. *Microbiol*. 2005, *71*, 6150–8.

[299] Gibson, G., Roberfroid, M.B., Dietary modulation of the human colonic microbiota: introducing the concept of prebiotics. *J*. *Nutr*. 1995, *125*, 1401–1412.

[300] Watson, D., O'Connell Motherway, M., Schoterman, M.H.C., van Neerven, R.J.J., et al., Selective carbohydrate utilization by lactobacilli and bifidobacteria. *J*. *Appl*. *Microbiol*. 2013, *114*, 1132–1146.

[301] Arsköld, E., Lohmeier-Vogel, E., Cao, R., Roos, S., et al., Phosphoketolase pathway dominates in *Lactobacillus reuteri* ATCC 55730 containing dual pathways for glycolysis. *J*. *Bacteriol*. 2008, *190*, 206–12.

[302] Okano, K., Yoshida, S., Tanaka, T., Ogino, C., et al., Homo D-Lactic acid fermentation from arabinose by redirection of phosphoketolase pathway to pentose

phosphate pathway in L-Lactate dehydrogenase gene-deficient *Lactobacillus plantarum*. *Appl*. *Environ*. *Microbiol*. 2009, *75*, AEM.00573-09.

[303] Pfeiffer, T., Bonhoeffer, S., Evolution of cross-feeding in microbial populations. *Am*. *Nat*. 2004, *163*, E126-135.

[304] Turroni, F., Milani, C., Duranti, S., Mancabelli, L., et al., Deciphering bifidobacterial-mediated metabolic interactions and their impact on gut microbiota by a multi-omics approach. *ISME J*. 2016, *10*, 1656–1668.

[305] Lee, J.-H., Karamychev, V.N., Kozyavkin, S.A., Mills, D., et al., Comparative genomic analysis of the gut bacterium *Bifidobacterium longum* reveals loci susceptible to deletion during pure culture growth. *BMC Genomics* 2008, *9*, 247.

[306] Schroeter, H., Heiss, C., Balzer, J., Kleinbongard, P., et al., (-)-Epicatechin mediates beneficial effects of flavanol-rich cocoa on vascular function in humans. *Proc*. *Natl*. *Acad*. *Sci*. *U*. *S*. *A*. 2006, *103*, 1024–9.

[307] Cerdá, B., Tomás-Barberán, F. a, Espín, J.C., Metabolism of antioxidant and chemopreventive ellagitannins from strawberries, raspberries, walnuts, and oak-aged wine in humans: identification of biomarkers and individual variability. *J*. *Agric*. *Food Chem*. 2005, *53*, 227–35.

[308] Kaur, S., Greaves, P., Cooke, D.N., Edwards, R., et al., Breast cancer prevention by green tea catechins and black tea theaflavins in the C3(1) SV40 T,t antigen transgenic mouse model is accompanied by increased apoptosis and a decrease in oxidative DNA adducts. *J*. *Agric*. *Food Chem*. 2007, *55*, 3378–85.

[309] Femia, A. Pietro, Caderni, G., Vignali, F., Salvadori, M., et al., Effect of polyphenolic extracts from red wine and 4-OH-coumaric acid on 1,2-dimethylhydrazine-induced colon carcinogenesis in rats. *Eur*. *J*. *Nutr*. 2005, *44*, 79–84.

[310] Gonthier, M.-P., Remesy, C., Scalbert, A., Cheynier, V., et al., Microbial metabolism of caffeic acid and its esters chlorogenic and caftaric acids by human faecal microbiota in vitro. *Biomed*. *Pharmacother*. 2006, *60*, 536–40.

[311] Cardona, F., Andrés-Lacueva, C., Tulipani, S., Tinahones, F.J., et al., Benefits of Polyphenols on Gut Microbiota and Implications in Human Health. *J. Nutr. Biochem*. 2013, *24*, 1415–22.

[312] Biswas, N., Balac, P., Narlakanti, S.K., Haque, E., et al., Identification of Phenolic Compounds in Processed Cranberries by HPLC Method. *J. Nutr. Food Sci*. 2013, *3*, 1–6.

[313] Santos-Buelga, C., Scalbert, A., Proanthocyanidins and tannin-like compounds – nature , occurrence , dietary intake and effects on nutrition and health. *J. Sci. Food Agric*. 2000, *1117*, 1094–1117.

[314] Novotny, J.A., Baer, D.J., Khoo, C., Gebauer, S.K., et al., Cranberry Juice Consumption Lowers Markers of Cardiometabolic Risk , Including Blood Pressure and Circulating C-Reactive Protein , Triglyceride , and Glucose Concentrations. 2015, 1–9.

[315] Yan, X., Murphy, B.T., Hammond, G.B., Vinson, J. a, et al., Antioxidant activities and antitumor screening of extracts from cranberry fruit (Vaccinium macrocarpon). *J. Agric. Food Chem*. 2002, *50*, 5844–9.

[316] Anhê, F.F., Roy, D., Pilon, G., Dudonné, S., et al., A polyphenol-rich cranberry extract protects from diet-induced obesity, insulin resistance and intestinal inflammation in association with increased Akkermansia spp. population in the gut microbiota of mice. *Gut* 2015, *64*, 872–83.

[317] Bodet, C., Chandad, F., Grenier, D., Anti-inflammatory activity of a high-molecular-weight cranberry fraction on macrophages stimulated by lipopolysaccharides from periodontopathogens. *J. Dent. Res*. 2006, *85*, 235–9.

[318] Howell, A.B., Reed, J.D., Krueger, C.G., Winterbottom, R., et al., A-type cranberry proanthocyanidins and uropathogenic bacterial anti-adhesion activity. *Phytochemistry* 2005, *66*, 2281–2291.

[319] Foo, L.Y., Lu, Y., Howell, A.B., Vorsa, N., A-Type Proanthocyanidin Trimers from Cranberry that Inhibit Adherence of Uropathogenic P-Fimbriated Escherichia coli. *J. Nat. Prod*. 2000, *63*, 1225–1228.

[320] Déprez, S., Brezillon, C., Rabot, S., Philippe, C., et al., Polymeric proanthocyanidins are catabolized by human colonic microflora into low-molecular-weight phenolic acids. *J. Nutr.* 2000, *130*, 2733–8.

[321] Choy, Y.Y., Jaggers, G.K., Oteiza, P.I., Waterhouse, A.L., Bioavailability of Intact Proanthocyanidins in the Rat Colon after Ingestion of Grape Seed Extract. *J. Agric. Food Chem.* 2013, *61*, 121–127.

[322] Zhang, L., Carmody, R.N., Kalariya, H.M., Duran, R.M., et al., Grape proanthocyanidin-induced intestinal bloom of Akkermansia muciniphila is dependent on its baseline abundance and precedes activation of host genes related to metabolic health. *J. Nutr. Biochem.* 2018, *56*, 142–151.

[323] Casanova-Martí, À., Serrano, J., Portune, K.J., Sanz, Y., et al., Grape seed proanthocyanidins influence gut microbiota and enteroendocrine secretions in female rats. *Food Funct.* 2018, *9*, 1672–1682.

[324] Jiménez-Girón, A., Queipo-Ortuño, M.I., Boto-Ordóñez, M., Muñoz-González, I., et al., Comparative Study of Microbial-Derived Phenolic Metabolites in Human Feces after Intake of Gin, Red Wine, and Dealcoholized Red Wine. *J. Agric. Food Chem.* 2013, *61*, 3909–3915.

[325] Sánchez-Patán, F., Tabasco, R., Monagas, M., Requena, T., et al., Capability of lactobacillus plantarum IFPL935 to catabolize flavan-3-ol compounds and complex phenolic extracts. *J. Agric. Food Chem.* 2012, *60*, 7142–7151.

[326] Tabasco, R., Sánchez-Patán, F., Monagas, M., Bartolomé, B., et al., Effect of grape polyphenols on lactic acid bacteria and bifidobacteria growth: Resistance and metabolism. *Food Microbiol.* 2011, *28*, 1345–1352.

[327] Knockaert, D., Raes, K., Wille, C., Struijs, K., et al., Metabolism of ferulic acid during growth of Lactobacillus plantarum and Lactobacillus collinoides. *J. Sci. Food Agric.* 2012, *92*, 2291–6.

[328] López de Felipe, F., Curiel, J.A., Muñoz, R., Improvement of the fermentation performance of *Lactobacillus plantarum* by the flavanol catechin is uncoupled from its degradation. *J. Appl. Microbiol.* 2010, *109*, 687–697.

[329] Hervert-Hernández, D., Pintado, C., Rotger, R., Goñi, I., Stimulatory role of grape pomace polyphenols on Lactobacillus acidophilus growth. *Int. J. Food Microbiol.* 2009, *136*, 119–22.

[330] Özcan, E., Ekinci, Y.F., Mechanisms underlying the Effects of Lactic Acid Bacteria (LAB) on Phenolic Compounds. *Int. J. Food Biosyst. Eng.* 2016, *1*, 7–15.

[331] Rodríguez-Costa, S., Cardelle-Cobas, A., Roca-Saavedra, P., Porto-Arias, J.J., et al., In vitro evaluation of the prebiotic effect of red and white grape polyphenolic extracts. *J. Physiol. Biochem.* 2018, *74*, 101–110.

[332] López de Felipe, F., Curiel, J.A., Muñoz, R., Improvement of the fermentation performance of Lactobacillus plantarum by the flavanol catechin is uncoupled from its degradation. *J. Appl. Microbiol.* 2010, *109*, 687–97.

[333] Birs, A., Identification of key enzymes in the phenolic degradation pathway of Lactobacillus johnsonii N6.2, University of Florida, n.d.

[334] Polewski, M.A., Krueger, C.G., Reed, J.D., Leyer, G., Ability of cranberry proanthocyanidins in combination with a probiotic formulation to inhibit in vitro invasion of gut epithelial cells by extra-intestinal pathogenic E. coli. *J. Funct. Foods* 2016, *25*, 123–134.

[335] Nguyen, T., Kimble, L., Mathison, B., Chew, B., Cranberry extract promotes anti-inflammatory activity of Lactobacillus plantarum on HT-29 human colon cancer cells (647.35). *FASEB J.* 2014, *28*, 647.35.

[336] Sánchez-Patán, F., Monagas, M., Moreno-Arribas, M.V., Bartolomé, B., Determination of Microbial Phenolic Acids in Human Faeces by UPLC-ESI-TQ MS. *J. Agric. Food Chem.* 2011, *59*, 2241–2247.

[337] Ou, K., Gu, L., Absorption and metabolism of proanthocyanidins. *J. Funct. Foods* 2014, *7*, 43–53.

[338] Rodríguez, H., Landete, J.M., Curiel, J.A., de las Rivas, B., et al., Characterization of the *p* -Coumaric Acid Decarboxylase from Lactobacillus plantarum CECT 748

T. *J. Agric. Food Chem.* 2008, *56*, 3068–3072.

[339] Kazantsev, A. V., Pace, N.R., Bacterial RNase P: a new view of an ancient enzyme. *Nat. Rev. Microbiol.* 2006, *4*, 729–740.

[340] Van den Abbeele, P., Duysburgh, C., Jiang, T.A., Rebaza, M., et al., A combination of xylooligosaccharides and a polyphenol blend affect microbial composition and activity in the distal colon exerting immunomodulating properties on human cells. *J. Funct. Foods* 2018, *47*, 163–171.

[341] Francis, F.J., Markakis, P.C., Food colorants : Anthocyanins. *Crit. Rev. Food Sci. Nutr.* 1989, *28*, 273–314.

[342] Appeldoorn, M.M., Vincken, J.-P., Aura, A.-M., Hollman, P.C.H., et al., Procyanidin Dimers Are Metabolized by Human Microbiota with 2-(3,4-Dihydroxyphenyl)acetic Acid and 5-(3,4-Dihydroxyphenyl)-γ-valerolactone as the Major Metabolites. *J. Agric. Food Chem.* 2009, *57*, 1084–1092.

[343] Rodríguez, H., Landete, J.M., Curiel, J.A., de las Rivas, B., et al., Characterization of the *p* -Coumaric Acid Decarboxylase from Lactobacillus plantarum CECT 748 T. *J. Agric. Food Chem.* 2008, *56*, 3068–3072.

[344] Reverón, I., de las Rivas, B., Muñoz, R., López de Felipe, F., Genome-wide transcriptomic responses of a human isolate of Lactobacillus plantarum exposed to p -coumaric acid stress. *Mol. Nutr. Food Res.* 2012, *56*, 1848–1859.